Western University
Scholarship@Western

Digitized Theses | Digitized Special Collections

1977

Petrogenesis Of Al Hadah Plutonic Rocks, Kingdom Of Saudi Arabia

Fouad Mohammed Marzouki

Follow this and additional works at: https://ir.lib.uwo.ca/digitizedtheses

Recommended Citation
Marzouki, Fouad Mohammed, "Petrogenesis Of Al Hadah Plutonic Rocks, Kingdom Of Saudi Arabia" (1977). *Digitized Theses*. 1015.
https://ir.lib.uwo.ca/digitizedtheses/1015

This Dissertation is brought to you for free and open access by the Digitized Special Collections at Scholarship@Western. It has been accepted for inclusion in Digitized Theses by an authorized administrator of Scholarship@Western. For more information, please contact tadam@uwo.ca, wlswadmin@uwo.ca.

National Library of Canada

Cataloguing Branch
Canadian Theses Division

Ottawa, Canada
K1A 0N4

Bibliothèque nationale du Canada

Direction du catalogage
Division des thèses canadiennes

NOTICE

The quality of this microfiche is heavily dependent upon the quality of the original thesis submitted for microfilming. Every effort has been made to ensure the highest quality of reproduction possible.

If pages are missing, contact the university which granted the degree.

Some pages may have indistinct print especially if the original pages were typed with a poor typewriter ribbon or if the university sent us a poor photocopy.

Previously copyrighted materials (journal articles, published tests, etc.) are not filmed.

Reproduction in full or in part of this film is governed by the Canadian Copyright Act, R.S.C. 1970, c. C-30. Please read the authorization forms which accompany this thesis.

THIS DISSERTATION HAS BEEN MICROFILMED EXACTLY AS RECEIVED

AVIS

La qualité de cette microfiche dépend grandement de la qualité de la thèse soumise au microfilmage. Nous avons tout fait pour assurer une qualité supérieure de reproduction.

S'il manque des pages, veuillez communiquer avec l'université qui a conféré le grade.

La qualité d'impression de certaines pages peut laisser à désirer, surtout si les pages originales ont été dactylographiées à l'aide d'un ruban usé ou si l'université nous a fait parvenir une photocopie de mauvaise qualité.

Les documents qui font déjà l'objet d'un droit d'auteur (articles de revue, examens publiés, etc.) ne sont pas microfilmés.

La reproduction, même partielle, de ce microfilm est soumise à la Loi canadienne sur le droit d'auteur, SRC 1970, c. C-30. Veuillez prendre connaissance des formules d'autorisation qui accompagnent cette thèse.

LA THÈSE A ÉTÉ MICROFILMÉE TELLE QUE NOUS L'AVONS REÇUE

PETROGENESIS OF AL HADAH PLUTONIC ROCKS KINGDOM OF SAUDI ARABIA

by

Fouad Mohammed Hamid Marzouki
Department of Geology

Submitted in partial fulfillment
of the requirements for the degree of
Doctor of Philosophy

Faculty of Graduate Studies
The University of Western Ontario
London, Ontario
September, 1977

© Fouad M.H. Marzouki 1977.

FRONTVIEW

A view, looking southeast, of the biotite monzogranite intrusion of Al Hadah Pluton.

ABSTRACT

The Al Hadah igneous complex of the western Arabian Shield is intrusions of gabbro, diorite, granodiorite, monzogranite and dikes of basalt-andesite to rhyolite in composition intruded in that order during the Pan African orogeny (≈ 600 my) into a Precambrian basement of amphibolite and quartz feldspathic gneiss. Epidote replacing plagioclase is common in the dioritic rocks and mainly concentrated at dike walls. Similar plutonic sequences occur in parallel linear features eastward across the Arabian Shield.

The Al Hadah igneous complex is comparable to that of Sierra Nevada of western United States and some of the continental subduction environments and probably related to magma generation along a subduction zone. The pervasive epidote is indicative of infiltration of oxygenated surface water during emplacement and hence is a general guide to water flow into undersaturated magmas. Repetition of plutonic suites similar to Al Hadah across the Arabian Shield suggest three subduction zones with minor continental collision involving closely spaced ocean basin.

ACKNOWLEDGEMENTS

I would like to gratefully acknowledge the support of the Directorate General for Mineral Resources of Saudi Arabia who generously provided field and financial support for this thesis. I am also grateful to Sheikh A.Z. Yamani and Mr Gazi H. Sultan who gave me the opportunity to carry out this work. Without their help and encouragement this work would not have been possible. I am also greatly indebted to my chief supervisor, Dr W.S. Fyfe for giving me a lot of helpful suggestions and criticisms during the course of research and writing. I would like, also, to thank Mr D. Meloche, Mr R.L. Barnett and Dr H. Hunter and also Dr R. Kerrich for their assistance in the analytical work; John Forth for preparation of thin-sections.

TABLE OF CONTENTS

page

CERTIFICATE OF EXAMINATION..... ii

FRONTVIEW..... iii

ABSTRACT..... iv

ACKNOWLEDGEMENTS..... v

TABLE OF CONTENTS..... vi

LIST OF FIGURES..... x

LIST OF TABLES..... xvii

CHAPTER 1 - INTRODUCTION..... 1

1.1 Statement of the Problem..... 1

1.2 General Geology of the Arabian Shield..... 3

CHAPTER 2 - AL HADAH AREA..... 15

2.1 General Statement..... 15

2.2 Location of Thesis Area..... 15

2.3 Physiographic Provinces..... 17

2.4 Field Studies..... 19

2.5 Previous Work..... 19

CHAPTER 3 - GEOLOGIC SETTING..... 22

3.1 General Statement..... 22

3.2 Rock Units of Al Hadah Area..... 23

3.2.1 Amphibolite Schist..... 26

3.2.2 Dioritic Rocks..... 26

Page

3.2.2.1 Meta-Quartz-Bearing Diorite and Monzodiorite..... 27
3.2.2.2 Hornblende Gabbro and Monzogabbro..... 30
3.2.3 Granodiorite..... 30
3.2.4 Biotite Monzogranite..... 33
3.2.5 Dikes..... 42
3.2.5.1 Felsic Dikes..... 42
3.2.5.2 Mafic Dikes..... 46
3.2.6 Quaternary Deposits..... 54
CHAPTER 4- PETROGRAPHY..... 58
4.1 General Statement..... 58
4.2 Methods of Study..... 58
4.3 Amphibolite..... 59
4.4 Meta-Quartz-Bearing Diorites and Monzodiorites..... 61
4.4.1 Epidotized Diorite..... 72
4.4.2 Hornblende Gabbro..... 76
4.5 Granodiorite..... 83
4.6 Biotite Monzogranite..... 91
4.7 Dikes..... 103
4.7.1 Felsic Dikes..... 103
4.7.2 Mafic Dikes..... 104
CHAPTER 5 - PETROCHEMISTRY..... 106
5.1 General Statement..... 106

page

5.2 Classification..... 107

5.3 Comagmatic Relationships..... 107

5.3.1 Major Element Abundances..... 111

5.3.2 Trace Element Abundances..... 122

5.4 A Comparison of the Element Abundances in the Al Hadah Plutonic Rocks and Other Orogenic Suites..... 138

5.5. Summary and Discussion 147

CHAPTER 6 - EPIDOTIZATION PROCESS..... 150

6.1 General Statement..... 150

6.2 Whole-Rock Chemistry..... 151

6.3 Mineral Chemistry..... 155

6.4 Composition-Volume Changes..... 160

6.5 Oxygen Isotope Relations..... 162

6.6 Conclusions on the Process..... 173

CHAPTER 7 - PETROGENESIS AND TECTONICS..... 176

7.1 General Statement..... 176

7.2 Origin of Calc-Alkaline Andesite (=Diorite)..... 177

7.3 Origin of Granite..... 186

7.4 Al Hadah Granite in the Light of Granite Hypotheses..... 194

7.5 Some Quantitative Aspects of Granitic Magmas.... 194

7.6 Tectonics of the Arabian Shield..... 200

7.7 Discussion..... 207

CHAPTER 8 - CONCLUSIONS..... 211

page

APPENDIX A - METHODS..... 214

APPENDIX B - ELEMENT ABUNDANCES..... 217

APPENDIX C - MICROPROBE ANALYSES..... 227

REFERENCES..... 244

VITA..... 267

LIST OF FIGURES

Figure	Description	Page
1	Distribution of Plutonic Rocks in the Arabian Shield..	11
2	Location Map of the Studied Area.....	16
3	Index map of west Saudi Arabia showing major topographic features.....	18
4	Generalized geologic map of NW part of Southern Hijaz Quadrangle.....	20
5	Amphibolite intruded by quartz feldspathic gneiss.....	29
6	Pegmatitic patches in diorites.....	29
7	Irregular patterns of pegmatitic patches.....	29
8	Close view of pegmatitic patch.....	29
9	Epidote veins.....	32
10	View of an epidotized outcrop.....	32
11	Irregular felsic veins enclosing dioritic patches.....	32
12	Rhythmic banding in the diorites.....	32
13	Rhythmic banding in the diorites.....	35
14	Xenoliths of fine-grained mafic rocks enclosed in the diorites.....	35
15	View showing the approximate contact between the diorite and the granodiorite.....	35
16	Andesitic-basaltic dikes filling vertical fractures..	35
17	Contact between biotite monzogranite and the diorite.	38

Figure	Description	Page
18	Contact between biotite monzogranite and the dioritic rocks	38
19	Small xenolith of the dioritic rocks enclosed within the monzogranite	38
20	Biotite bands at the contact between the biotite monzogranite and the dioritic rocks	38
21	Massive non-structural pegmatite dike	39
22	Pegmatite dike truncated by graded layers	40
23	Graded layers in the monzogranite	44
24	Cross-bedded features in the graded layers	44
25	Truncated graded layers	44
26	Truncated graded layers	44
27	Sharp contact between the monzogranite and the diorite	48
28	Diorite intruded by Granodiorite	48
29	Brittle behavior of a felsic dike	48
30	Diorites intruded by both mafic and felsic dikes	48
31	Felsic material enclosing slabs of dioritic rocks	50
32	Andesitic dike cutting a felsic dike	50
33	Felsic dike cutting the dioritic rocks	50
34	Conjugate set of felsic dikes	50
35	Felsic dike cutting the diorite	52
36	Felsic dike cutting the diorite	52

Figure	Description	Page
37	Pegmatite dike cutting the monzogranite.....	52
38	Criss-cross relationships between three sets of dikes.....	52
39	Felsic dike cutting an andesitic dike.....	56
40	Basaltic dike filling vertical fractures.....	56
41	Felsic dike cutting vertical basaltic dike.....	56
42	Close view at the intersection between the felsic and basaltic dike.....	56
43	Basaltic dike cutting another basaltic dike.....	56
45	A handspecimen of amphibolite.....	63
46	Thin-section of amphibolite.....	63
47	A handspecimen of diorite.....	63
48	Porphyritic diorite.....	63
49	Biotite replacing plagioclase.....	68
50	Polysynthetic twinning in hornblende.....	68
51	Ophitic and subophitic texture in hornblende.....	68
52	Pyroxene remnants in hornblende.....	68
53	Biotite replacing plagioclase.....	70
54	Hornblende altered to biotite.....	70
55	Hornblende altered to biotite.....	70
56	Hornblende altered to chlorite.....	70
57	Remnants of pyroxene in hornblende.....	75
58	Plagioclase crystals enclosed within biotite.....	75

Figure	Description	Page
59	Epidote crystals in epidotized diorite.....	75
60	Epidote pseudomorphs after plagioclase.....	75
61	Ilmenite crystal rimmed by sphene.....	78
62	Quartz associated with epidote.....	78
63	Hornblende altered to tremolite-actinolite.....	78
64	Hornblende altered to tremolite.....	78
65	Hornblende partially altered to epidote.....	82
66	Hornblende partially altered to epidote.....	82
67	Hornblende altered to tremolite-actinolite.....	82
68	Hornblende partially altered to tremolite.....	82
69	Remnants of pyroxene in hornblende.....	87
70	A handspecimen of granodiorite.....	87
71	Zoned plagioclase.....	87
72	Microcline perthite replacing plagioclase.....	87
73	Microcline perthite replacing plagioclase.....	90
74	Polysynthetic twinning in microcline perthite.....	90
75	Microcline perthite.....	90
76	A handspecimen of biotite monzogranite.....	97
77	Albite and pericline twinning in plagioclase.....	97
78	Microcline perthite enclosing laths of plagioclase.	97
79	Myrmekitic inclusions.....	99
80	Polysynthetically twinned microcline perthite.....	99
81	Microcline perthite rimmed by plagioclase.....	99

Figure	Description	Page
82	Microcline perthite replacing plagioclase.....	99
83	Normative classification of the rock types of Al Hadah Pluton.....	108
84	Modal classification of the rock types of Al Hadah Pluton.....	109
85	The division between Tholeiitic and Calc-alkaline fields.....	110
86	Harker variation diagram for the dioritic rocks..	
87	Ca and Mg plotted against the mafic index (M)....	114
88	The Differentiation Index plotted against alkalies, CaO and Fe_2O_3t/MgO.....	115
89	SiO_2 plotted against the differentiation index (DI).....	118
90	Harker variation diagrams for the granitic group.	120
91	Na, K, Mg and Ca are plotted against the felsic index (F).....	121
92	The trace-elements Rb, Ni, Ba, and Cr plotted against SiO_2.....	124
93	The trace-elements Sr, Ni and Cr plotted against the mafic index (M).....	125
94	Ba/Sr and K/Rb ratios plotted against DI.....	127
95	Ba/Rb ratio plotted against DI.....	128
96	The trace-elements Sr, Zr and Pb plotted against SiO_2.....	130

Figure	Description	Page
97	Zr, Ba/Sr and K/Rb plotted against the felsic index (F).....	134
98	Sr plotted against the K_2O content.....	136
99	Rb plotted against the K_2O content.....	137
100	AFM diagram for the plutonic rocks of Al Hadah....	142
101	Comparison between the plutonic trends of Al Hadah Pluton with the trends of various plutons from the United States and Canada.....	145
102	Composition-volume diagram for the samples 57→58A.	164
103	Composition-volume diagram for the samples 69→68..	165
104	Composition-volume diagram for the samples 7535→ 7534.....	166
105	Schematic diagram showing the early and later phases of development of island arcs.....	183
106	A diagram showing the region for maximum magma generation.....	189
107	Schematic diagram of the formation of a pluton....	193
108	Schematic diagram showing the ascent of granitic magma.....	196
109	The Pan African domains.....	202
110	Distribution of ultramafic rocks in the Arabian Shield and east and northeast Africa.....	206
111	A schematic model explaining the parallel suture zones.....	208

Figure Description Page

112 A schematic model for the generation of Al Hadah igneous rocks..... 209

LIST OF TABLES

Table	Description	Page
1	Summary of Precambrian formation, tectonism, plutonism and volcanism in the Arabian Shield.....	4
2	Stratigraphy, orogenic events and plutonic rocks in the southern part of the Arabian Shield.....	9
3	Comparison between calc-alkaline island-arc rock and the metavolcanic rocks of the Arabian Shield..	13
4	Comparison between graded layering in the monzo-granite of Al Hadah Pluton and other types of layering described in the literature.....	41
5	Summary of the dike features.....	45
6	Summary of the petrographic features of the amphibolite.....	60
7	Summary of the petrographic features of the diorites.....	64
8	Modal analysis of the dioritic rocks.....	65
9	Summary of the petrographic features of the epidotized diorites.....	73
10	Summary of the petrographic features of the hornblende gabbro.....	77
11	Summary of the petrographic features of the granodiorite.....	84

Table	Description	Page
12	Modal analysis of the granodiorite.....	85
13	Summary of the petrographic features of the biotite monzogranite.....	92
14	Modal analysis of the biotite monzogranite.....	93
15	Modal analysis of samples from non-layered parts of the biotite monzogranite.....	94
16	Average composition of the diorites and gabbros..	112
17	Average composition of the granodiorite and monzogranite.....	119
18	Average trace-element abundances in the diorites and gabbros.....	123
19	Average trace-element abundances in the granodiorite and monzogranite.....	132
20	Trace element abundance in the Al Hadah Plutonic rocks and other similar igneous rocks.....	133
21	Comparison between the composition of Al Hadah diorites and various andesites.....	140
22	Comparison between the trace-element abundances in the dioritic rocks of Al Hadah Pluton and various orogenic suites.....	141
23	Generalized differences between calc-alkaline volcanic rocks of island-arcs and those of continental margins.....	143

Table	Description	Page
24	Comparison between the composition of the Al Hadah granitic rocks and the plutonic rocks in orogenic suites	146
25	Chemical analysis of unepidotized, partially epidotized and epidotized rocks	152
26	FeO, ΣFe and $Fe^{2+}/\Sigma Fe$ in the unepidotized, and completely epidotized diorites	153
27	Average compositions of plagioclases	157
28	Average compositions of amphiboles	158
29	Average compositions of epidotes	159
30	Chemical analysis of three sets altered-unaltered examples	162
31	The actual gains and losses that took place in the epidotization process	167
32	Oxygen isotope data for primary and altered rocks	170

The author of this thesis has granted The University of Western Ontario a non-exclusive license to reproduce and distribute copies of this thesis to users of Western Libraries. Copyright remains with the author.

Electronic theses and dissertations available in The University of Western Ontario's institutional repository (Scholarship@Western) are solely for the purpose of private study and research. They may not be copied or reproduced, except as permitted by copyright laws, without written authority of the copyright owner. Any commercial use or publication is strictly prohibited.

The original copyright license attesting to these terms and signed by the author of this thesis may be found in the original print version of the thesis, held by Western Libraries.

The thesis approval page signed by the examining committee may also be found in the original print version of the thesis held in Western Libraries.

Please contact Western Libraries for further information:
E-mail: libadmin@uwo.ca
Telephone: (519) 661-2111 Ext. 84796
Web site: http://www.lib.uwo.ca/

CHAPTER 1

INTRODUCTION

1.1 Statement of the Problem

This thesis deals with two problems in the field of igneous geology and tries to cast some light on possible explanations. The first deals mainly with the petrochemistry of Al Hadah igneous complex and the application of plate tectonic models to Proterozoic igneous events in the studied area. Although the application of present day geological processes at plate boundaries to Precambrian rocks is still controversial, recent work carried out in the Arabian Shield and the surrounding areas, has provided some evidence for the applicability of these models during late Precambrian time. Gass and Neary (1976) found that the granites which constitute more than 60% of the crystalline basement of NE Sudan, mostly carry an isotopic age of $\leq$ 600 my; secondly, they suggest that these granitic rocks represent cratonization of an island arc. Al-Shanti and Mitchell (1975) found that 'the thick volcanic, volcanoclastic and sedimentary succession of the proterozoic Halaban group in the east of the Arabian Shield is intruded by syntectonic to late tectonic plutons, and

resembles Cenozoic subduction-related magmatic areas'. Greenwood et al. (1975) concluded that the southern part of the Arabian Shield represents cratonized intra-oceanic island arcs. Similar studies, in the northern part of the Arabian Shield (Rexworthy, 1971; Bakor, 1973; Neary, 1974), and in the eastern desert of Egypt (Garson and Shalaby, 1974) all invoke the cratonization of oceanic island arc systems. Nasseef and Gass (1976) proposed that the At Taif granites suite (which include the granitic rocks of the area studied) were produced during the last phase of cratonization* of an island arc system which occupied a period of 75 my (595-520 my).

Along the lines of these previously mentioned studies, the author, by means of geochemical, mineralogical and petrographical data, has attempted to give a possible petrogenetic explanation for the magmatic igneous events which took place in the studied area in terms of a plate-tectonic model.

---

* Cratonization is here taken to imply a series of orogenic events which involved volcanic and sedimentary deposition accompanied by tectonism, metamorphism and plutonism during that certain period of time (1050-550 my) which led to the stabilization of the Shield.

The second problem, that was examined involves the process of epidote formation which has been found in many rocks of the area studied. In these altered rocks plagioclase is often completely altered to epidote near contact regions.

1.2 General Geology of Arabian Shield

The Kingdom of Saudi Arabia has an area of 2,1[illegible]000 km^2 of which approximately a quarter is occupied by the Arabian Shield. The Arabian Shield extends from the coast for distances ranging from 50 to 700 km inland. It consists of Precambrian to early Palaeozoic rocks, partly overlain by younger sedimentary rocks, Tertiary to Quaternary basalt and alluvium. In general, the effort to map and understand this region began only in the 1950's.

The Precambrian Arabian Shield covers an area of about 541,060 km^2, and has a pseudotrapizoidal plane-section. There are eight major stratigraphic Precambrian units recognized in the Arabian Shield overlying a basement gneiss complex called the "Khamis Mushayt Gneiss", (see Table 1). Six of these units were identified and described by Schmidt and others (1972) in the Southern part of the Arabian Shield. The chronological order of these units from oldest to youngest is: "Hali Group", "Baish Group", "Bahah Group", "Jiddah Formation", "Halaban Group", "Murdama Group" (in the southern part), "Shammar Group" and "Jubaylah Group" (in the northern part).

Table 1 - Summary of Precambrian Formations, Tectonism, Plutonism and Volcanism in the Arabian Shield Modified by Greenwood et al. (1974).

ASSEMBLAGES	UNITS	MAJOR ROCK TYPES	VOLCANIC ROCKS		TECTONIC EPISODES	PLUTONIC EPISODES	RADIO-METRIC AGES (my)
Nonmetamorphosed	Jubaylah Group	Clastic rocks, minor volcanic rocks, and marine marble and shale	Andesitic basalt		Najd orogeny Left-lateral wrench faulting	Granite to granodiorite	520-540
Nonmetamorphosed	Shammar Group	Rhyolite and minor clastic rocks	Mostly rhyolite		Shammar subsidence	Granite to granodiorite	570
	Murdama Group	Clastic and volcanic rocks, minor marine marble, and shale	Andesite and rhyolite		Bishah orogeny North-south folding	Granite to granodiorite and gabbro	600
		Upper: silicic volcanic rocks	Dacite and rhyolite	HIJAZ TECTONIC CYCLE		Granite to granodiorite	720-800+
	Halaban Group	Middle: andesite and basalt	Andesite and basalt		Ranyah orogeny North-south folding and wrench faulting	Gabbro and diorite	
		Lower: clastic rocks and minor volcanic rocks	Andesite				
	Jiddah Group	Andesitic volcanic rocks and minor clastic rocks	Andesite, dacite, and basalt		Aqiq orogeny North-south folding	Major dioritic magmatism. Gabbro	1000
Metabasalt, metagray-wacke, and metachert	Bahah Group	Greenschist, minor marble, and clastic rocks			Tihama orogeny North-south folding and greenschist metamorphism	Minor quartz porphyry ortho-schist	>1000
	Baish Group	Mafic volcanic rocks	Basalt				
Biotite schist, amphibolite and orthogneiss	Hali Group	Biotite-garnet schist, quartzite, amphibolite and marble	Basalt		Asir orogeny Folding and metamorphism to amphibolite facies	Tonalite ortho-gneiss	>1000
	Khamis Mushayt Gneiss	Orthogneiss, para-gneiss, schist and amphibolite	Basalt		Inferred orogeny and metamorphism	Quartz diorite to quartz monzonite orthogneiss	>1000

The "Khamis Mushayt Gneiss" is considered to be the basement of the Arabian Shield. It consists of "coarse grained banded orthogneiss and migmatite that is regionally metamorphosed to the amphibolite facies". Fyfe (personal communication) has suggested that some of these rocks may even be retrograde granulites.

1. The "Hali Group" consists of several thick units of quartz-biotite-garnet schist interlayered with amphibolite, metamorphosed at amphibolite facies. This group has been intensively tectonized.

2. The "Baish Group" overlies "Hali Group", and is characteristically greenstone, consisting mainly of mafic metavolcanic rocks intercalated by agglomerates and tuffs and detrital beds with concordant bodies of quartz porphyry and subvolcanic sills. The metamorphic grade is greenschist facies, and most of the rock units have been highly deformed.

3. The "Bahah Group" overlies "Baish Group" and is characterized by a thick metasedimentary section consisting mostly of quartz-chlorite-sericite schists representing well bedded, commonly thinly bedded, siltstone, mudstone, siliceous slate and fine grained sandstone. They are also regionally metamorphosed to the greenschist facies.

4. The "Jiddah Formation" or "Jiddah Greenstone" follows the Bahah Group and consists mainly of red and green andesitic agglomerates, flow breccias, tuffs and trachytes.

They are regionally metamorphosed to the greenschist facies.

5. The "Ablah Group" consists essentially of andesitic and dacitic volcanic rocks. It is regarded as a separate unit between the "Jiddah Group" and the overlying "Halaban Group".

6. The "Halaban Group" includes metavolcanic and metasedimentary rocks. It is subdivided into three main groups: clastic lower part, predominently andesitic middle part and an upper part of silicic flows and pyroclastic rocks. The base of Halaban or the lower group consists of thick green conglomerate, sandstone and siltstone of largely andesitic volcanic derivation. The middle group consists of green massive and commonly deuterically altered flows, agglomerates, extrusive breccias, tuffs and detrital rocks of andesitic composition.

The upper Halaban group is characterized by green to buff rhyolitic and trachytic flows and pyroclastic rocks including ignimbritic flows. The Halaban group is metamorphosed to the greenschist facies. It must represent a major volcanic event.

The Halaban Group is estimated to be at least 10 km thick near Halaban in the central part of the Shield (Brown and Jackson, 1960). The Group is characterized by rapid lateral and vertical facies variations of the types

that are typical of environments near volcanic sources (Greenwood et al., 1975). Very limited chemical data (G.F. Brown, unpublished data) suggests that the rocks of Halaban Group in the central and northern part of the Shield resemble rocks of the basalt-andesite-dacite series of Cascade Mountains in the United States (Greenwood, et al., 1975).

7. The "Murdama Group" is characterized by metasedimentary rocks and consists of gray to greenish-gray, well bedded to massive, thick bedded sandstone, siltstone and subordinate shale that are largely derived from underlying andesitic and granitic rocks.

8. The "Shammar and Jubaylah Group" are the youngest groups recognized in the Precambrian Arabian Shield; they are non-metamorphosed. The "Shammar Group" consists mainly of rhyolite and minor clastic rocks and the "Jubaylah Group" consists mainly of clastic rocks with minor volcanic rocks.

Deformation of the Shield:

There are four major tectonic episodes that affected the Arabian Shield indicated by the presence of observed angular unconformities in the southern part of the Arabian Shield. The tectonic cycles that took place in the Shield were the following: the "Asir Orogeny", the "Tihama Orogeny", the "Hijaz Tectonic Cycle" and the "Najd Orogeny" (Table 1).

The "Asir Orogeny" is considered to be the oldest tectonic episode. It is assumed to be the cause for the intensive deformation and metamorphism of the "Khamis Mushayt Gneiss" and "Hali Group". The younger Baish and Bahah Groups are considered by Greenwood et al. (1974) to have been metamorphosed and deformed during the "Tihama Orogeny." The extrusion of huge volumes of basaltic lavas of the "Baish Group" is considered (loc. cit.) to signify an abrupt change in the evolution of the Arabian Shield and possibly it marks the beginning of the "Tihama Orogeny". The shift from basaltic volcanism, which took place during the Baish times, to andesitic volcanism and dioritic plutonism of Jiddah-Halaban Groups marks a significant change in the crustal processes and it probably indicates the beginning of the "Hijaz Tectonic Cycle". The "Hijaz Tectonic Cycle" has been divided into three episodes, (Greenwood, et al., 1975). The stratigraphy, orogenic events and the plutonic rocks associated with these episodes are summerized in Table 2. The fourth tectonic movement which affected the Shield is the "Najd Orogeny" which is mainly a fault system consisting of prominent northwest trending shear zones with left lateral movement. This deformation affects rocks of upper Proterozoic to early Palaeozoic age. It cuts across the southern part

Table 2 - Stratigraphy, orogenic events, and plutonic rocks in the southern part of the Arabian Shield. (After Greenwood, et al., 1975.)

		UNITS	PRINCIPAL LAYERED ROCKS	OROGENIC EVENTS	PLUTONIC ROCKS
HIJAZ TECTONIC CYCLE	THIRD EPISODE	Murdama Group	Conglomerate Graywacke Andesite Rholite Marble	BISHAH - Folds and faults; northerly trends; greenschist metamorphism	Granite and quartz monzonite (570-550 Ma)
		UNCONFORMITY			
	SECOND EPISODE	Halaban Group	Conglomerate Graywacke Rhyolite Dacite Andesite Marble	YAFIKH - Folds and faults; northerly trends; greenschist metamorphism	Quartz monzonite (650-600 Ma)
		UNCONFORMITY-?-			
		Ablah Group		RANYAH - Folds and faults; northerly and northeasterly trends; late transverse shears; greenschist, amphibolite, and granulite metamorphism	Injection gneiss (785 Ma) Second dioritic series (800 Ma)
		UNCONFORMITY			
	FIRST EPISODE	Jiddah Group Bahah Group Baish Group	Conglomerate Graywacke Dacite Andesite Basalt	AQIA - Folds and faults; northerly trends; greenschist metamorphism	First dioritic series (960 Ma)

of the Shield and truncates the older north trending structures produced by the Hijaz-Tectonic Cycle.

Igneous Events in the Shield:

Some of the orogenies that affected the Shield were accompanied by plutonism. Plutonic rocks crop out over 218,000 km^2, or 40% of the exposed part of the Arabian Shield (Greenwood et al., 1973). There are two major intrusive series: an older calcic series ranging from diorite to trondhjemite and a younger calc-alkaline series of granodiorite and granite. The diorites are commonly deformed. Granitic plutons, which range from large irregular stocks to small batholiths, circular plugs, and cone sheets, ring structures, are most abundant in the northeast part of the Shield. Dioritic plutons are concentrated in the southwestern part of the Shield (Fig. 1).

The Precambrian to early Palaeozoic evolution of the Shield has been divided in its southern part into three phases. The early and middle phases are represented by the rock groups of "Hali", "Baish" and "Bahah" and are interpreted by Greenwood et al. (1975) as having been formed in an oceanic environment. These give way to a meta-andesitic assemblage in the "Jiddah", "Halaban" and "Murdama" Groups which were formed during a later phase of the orogenic cycle and may appear to be continental. The unmetamorphosed assemblages of the "Shammar" and "Jubaylah"

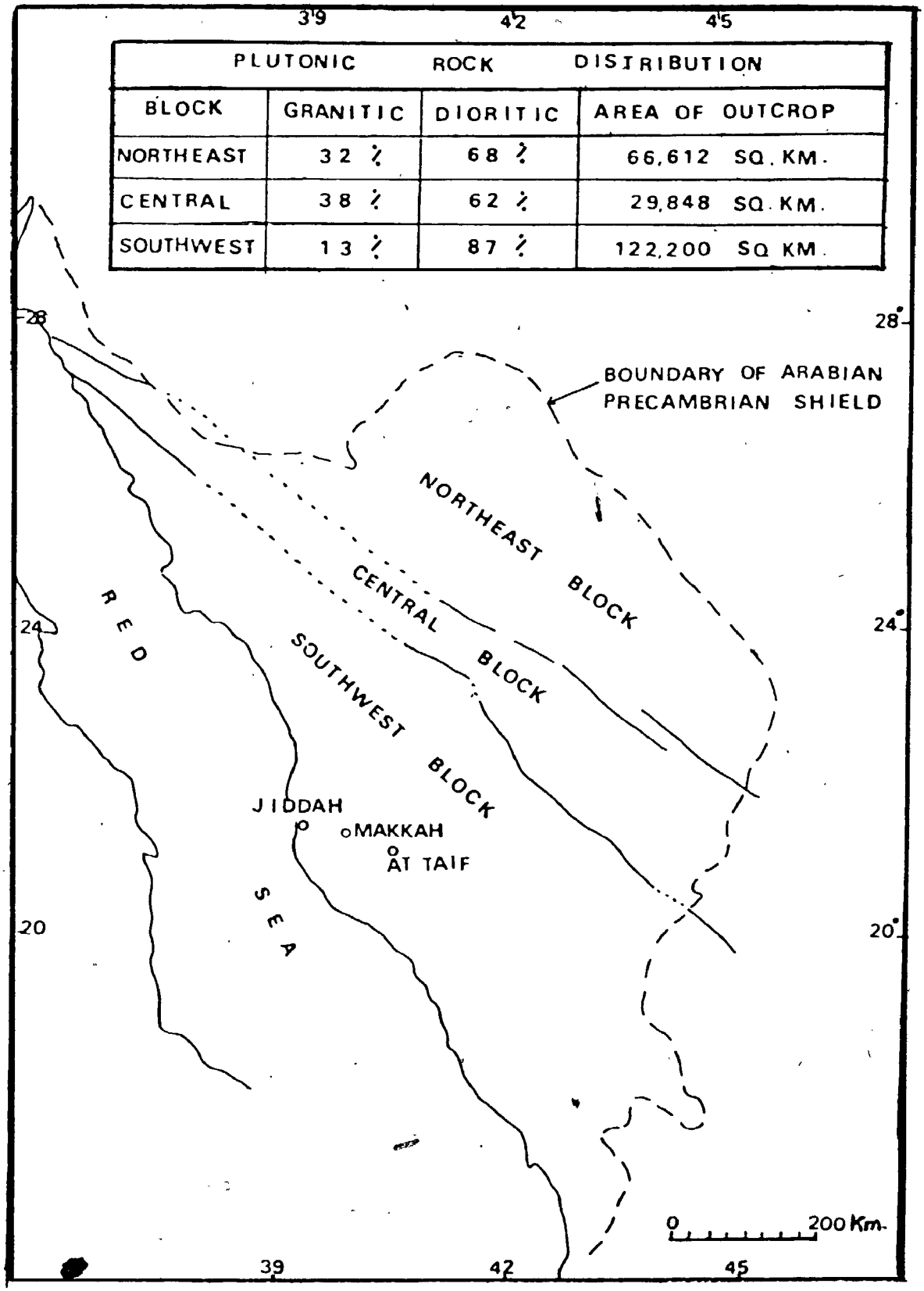

PLUTONIC ROCK DISTRIBUTION			
BLOCK	GRANITIC	DIORITIC	AREA OF OUTCROP
NORTHEAST	32 %	68 %	66,612 SQ. KM.
CENTRAL	38 %	62 %	29,848 SQ. KM.
SOUTHWEST	13 %	87 %	122,200 SQ KM.

Fig.1 . The distribution of plutonic rocks in the Arabian Shield(after Greenwood and Brown,1973).

Groups represent a late phase, formed in a post-orgenic environment. The petrography of the igneous rocks of the Shield and their evolution in composition from tholeiitic to calc-alkaline are similar to those of island arcs elsewhere in the world (Mitchell and Reading, 1971). Limited chemical data also show similarity to island-arc volcanism, especially in the evolutionary trend from early tholeiitic, iron-fractionated volcanic rocks to the later calc-alkaline volcanic rocks (Gill, 1970; Jakes and Gill, 1970). In Table 3 a comparison is drawn between the chemistry of the metavolcanic rocks of the Arabian Shield with some representative major element analyses of calc-alkaline rocks, island-arc tholeiite, and continental tholeiite. Greenwood and others (1975), on the basis of limited information, suggested a northwest trend for an island-arc. This trend was based on contoured K_2O/Na_2O+K_2O ratios for granodiorites to granites in the southern part of the Shield (Greenwood and Brown, 1973). Furthermore, the suggested northwest trend is also supported by outcrop patterns in which the oldest (tholeiitic) volcanic rocks are exposed in the southwest and the youngest (calc-alkalic) rocks in the northeast (USGS-ARAMCO, 1963), and by an increase in the proportion of granitic to dioritic rocks toward the northeast.

Table 3 - Comparison of some major element geochemistry of calc-alkaline rocks, island-arc tholeitte, abyssal tholeiite, and continental tholeiite with Arabian Shield metavolcanic rocks. (After Greenwood, et al., 1975).

	Calc-alkaline series (1)	Island arc tholeiitic series (1)	Abyssal tholeiitic series (1)	Continental tholeiites (2)
SiO_2 range %	53-70	45-70	47-62	51.5
SiO_2 mode %	59	53	49	-
TiO_2 %	0.5-1.2	0.5-1.5	1.0-2.5	1.2
Al_2O_3 %	16-19	14-19	14-19	16.3
Na_2O/K_2O	2-3	4-6	10-15	2.9

ARABIAN SHIELD VOLCANIC ROCKS

	Baish Group (3)		Jiddah Group (4)		Halaban Group (5)	
	range	mode	range	mode	range	mode
SiO_2 %	42-56	47	44-68	58	58-76	68
TiO_2 %	0.6-0.7	0.6	0.4-1.3	0.9	0.3-1.4	0.5
Al_2O_3 %	9-18	15	14-19	17	12-18	14
Na_2O/K_2O	1-23	5	0.2-4.4	1.7	0.2-5.6	1.6
Ferric-femic index	90		76		69	

(1) from Anhaeusser 1973, table 4
(2) from Anhaeusser 1973, table 4
(3) 11 flow rocks, from Jackaman 1972
(4) 13 flow rocks from Jackaman 1972
(5) 6 flow rocks, G.F. Brown, unpub. data

In summary, the geology of the Arabian Shield is dominated by igneous products. The old metamorphic basement complex (> 1 Gy) is covered by successions of basaltic, andesitic and rhyolitic rocks. The final events of the entire cratonization process involve the intrusion of granites. The volcanic-tectonic evolution leading to stability, involved a time interval of some 300 my. Almost everything observed today, with the exception of the basement pushed up by doming of the Red Sea rift, exhibits rather low-grade metamorphism. Thus, the present exposure of the Shield must represent a rather shallow section through this region of crustal modification.

CHAPTER 2

AL HADAH AREA

2.1 General Statement

A major part of this thesis resulted from the desire to study in detail a section through the later igneous activity associated with the tectonic cycle. Because of the lack of chemical data on rocks of the Arabian Shield, the Al Hadah region of considerable relief and with fresh exposure created by road construction, seemed ideal for study. Desert terrain may present problems for collecting fresh rocks inasmuch as chemical weathering is often intensive.

2.2 Location of Thesis Area

The Jabal Al-Hadah escarpment is a well exposed Precambrian igneous plutonic complex in the southern part of the Arabian Shield. It lies about 20 km NW of At-Taif city and 150 km SE of the city of Jeddah on the Red Sea. The area studied lies between the lat. 21°18'52"N and 21°21'15"N and long. 40°11'22"E and 40°16'15"E (location map, Fig. 2). The area is in very rugged mountainous

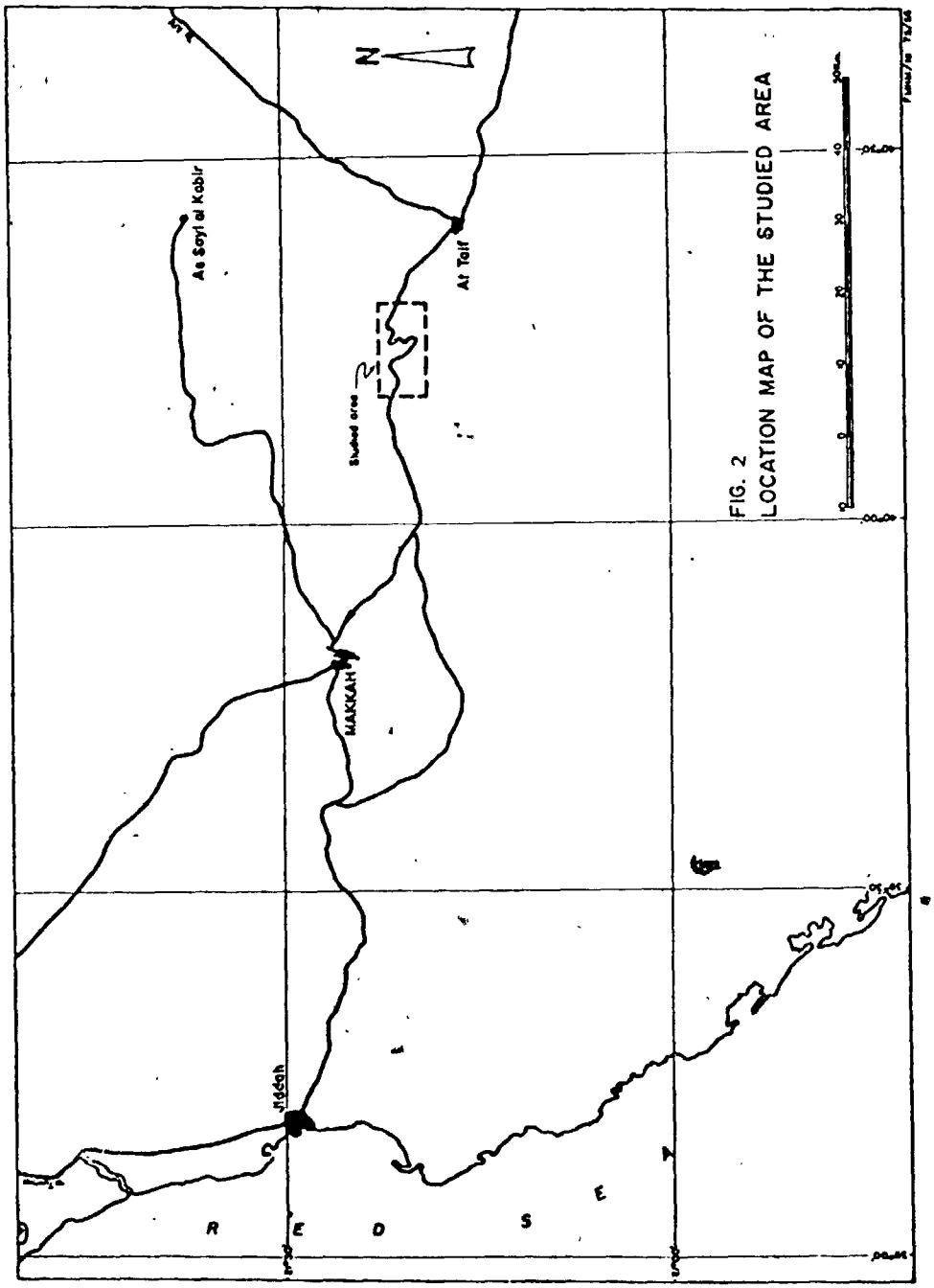

FIG. 2
LOCATION MAP OF THE STUDIED AREA

country with a range of elevation of 2000 m. The escarpment is cut by a zig-zag highway which runs between the cities of Jeddah and At-Taif; otherwise accessibility is very difficult.

2.3 Physiographic Provinces of the Arabian Shield

The Arabian Shield can be divided into four main geomorphological provinces: The Tihama, Scarp Mountains, Hijaz plateau and Najd pediplain (Brown, 1960); (Fig. 3). The Tihama or the coastal plain extends from the coral reefs along the Red Sea to the foothills of the Scarp Mountains ranging from 5 to 25 km in width.

The Scarp Mountains are a magnificent erosional escarpment extending from the most southern part of the Shield northward subparallel to the coastline. It is characterized by sharp peaks and deep wadies, some of which extend right back to the scarp producing a considerable local relief and spectacular scenery. The height and ruggedness tend to decrease from the southern and northward sides. The crest of the scarp has an average altitude of about 2000 m above sea level. Jabal Al Hadah is one of these scarp mountains and has an average altitude of about 2500 m above sea level. The Hijaz plateau is a highly elevated and tilted peneplain lying south of At-Taif. Its surface is deeply dissected by wadies that drain north and northeast.

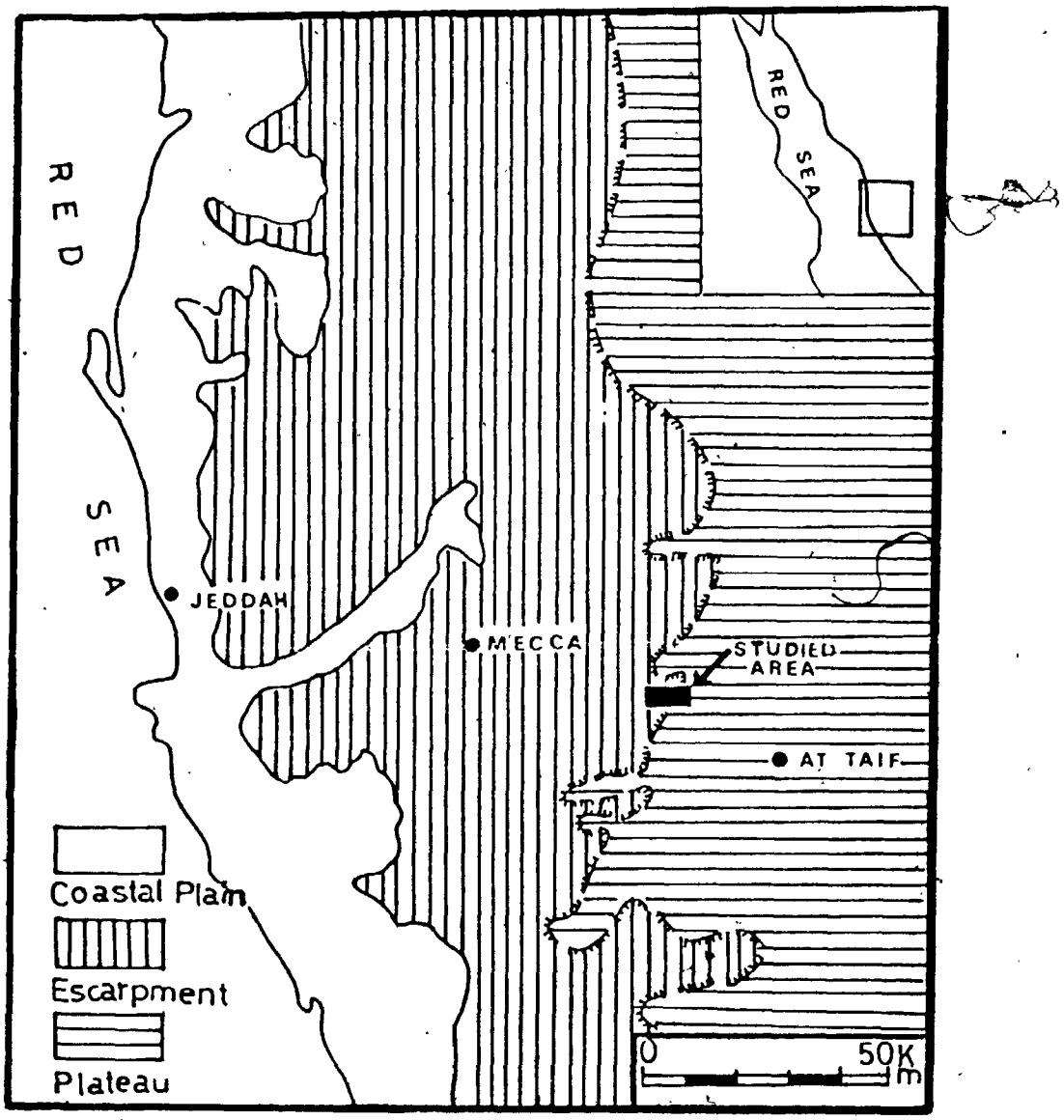

Fig. 3. Index map of west Saudi Arabia showing major topographic features. The location of the studied area is also shown. (After Nassef, 1973).

The Najd pediplain lies north of At-Taif and is characterized by an irregular upland surface which slopes gently northeastward from the escarpment into the large desert plain of Najd.

Drainage is from east to west. The main wadi channels disappear in the sand of the coastal plain and rarely reach the Red Sea. Such wadis are vital to the local water supply.

2.4 Field Studies

The field work has been carried out in the period 1974-75. During this field work, about 200 samples were collected, mostly along the section of highway running across the escarpment.

2.5 Previous Work

In 1962, G.F. Brown, R.O. Jackson, R.G. Bogue and W.H. Maclean of the United States Geological Survey published the first geological map of the Southern Hijaz quadrangle (map I-210A) at the scale of 1:500,000. The area studied is included in this region (see Fig. 4). In 1963, a geologic map of the Arabian peninsula was published at a scale of 1:2,000,000 (USGS-ARAMCO, 1963). In 1971, the Directorate General of Mineral Resources (DGMR) in Jiddah-Saudi Arabia,

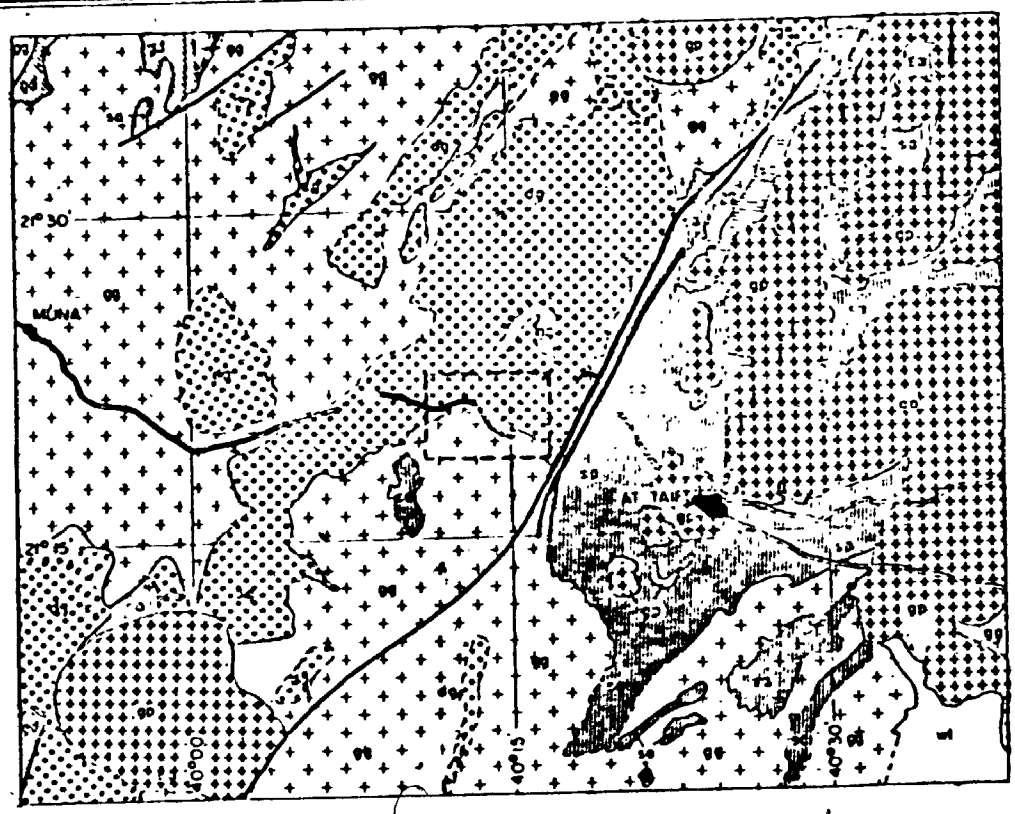

FIG. 4 GENERALIZED GEOLOGIC MAP SURROUNDING THE STUDIED AREA.

(AFTER G. F BROWN AND OTHERS)

FMMM/IR 75/42

published a bulletin (Bulletin No. 5), on the mineral resources of the southern Hijaz quadrangle by R. Goldsmith. In 1972, G.F. Brown of the USGS published the first tectonic map of the Arabian peninsula at a scale of 1:4,000,000 (Map AP-2). Schmidt and others (1973) published a report on the stratigraphy and tectonism of the southern part of the Precambrian Shield of Saudi Arabia (Bulletin No. 8). In 1973, DGMR published a bulletin on the petrology and chemical analysis of selected plutonic rock from the Arabian Shield by W.R. Greenwood and G.F. Brown (Bulletin No. 9). This bulletin was one of the first major petrochemical contributions. W.R. Greenwood and others (1975), submitted a report on late Proterozoic cratonization in southwestern Saudi Arabia which represented one of the first modern attempts at a tectonic synthesis. All these above mentioned works cover the general region with no detail concerning the studied area investigated in this thesis.

CHAPTER 3

GEOLOGIC SETTING

3.1 General Statement

The area studied is a small part of the west-southern Hijaz Mountains; covering an area of about 20 km^2 of the prominent westerly-facing erosional escarpment that separates the coastal plain of the Red Sea from the elevated peneplain of the Hijaz Plateau. The crystalline rocks of the Arabian Shield range in age from c.1100 to c.500 my and belong to two major subdivisions: (a) sequences of sedimentary and volcanic rocks which were metamorphosed to the greenschist facies and (b) granitic rocks of variable ages that were intruded into the metamorphosed sedimentary and volcanic sequences. Five plutonic phases at 966, 800, 785, 650-600 and 570-550 my respectively have been identified (Greenwood and others, 1975; Fleck and others, 1975). Earlier phases consist of calcic diorite, while the later ones are mostly calc-alkali granites and quartz monzonites. There seems to be a gradual increase in alkalinity with time. The tectonism, metamorphism, and plutonism which took place in this area belongs to the "Hijaz Tectonic Cycle" which has been divided into three episodes, all of which are

considered to be stages in late Proterozoic evolution of an intraoceanic island arc system (Greenwood and others, 1975).

3.2 Rock Units of the Al Hadah Area

The mass of rocks mapped in the Al Hadah area consist of a series of granitic intrusions emplaced into an amphibolite schist and quartzofeldspathic gneiss basement. All these granitic intrusions belong to the younger granites of Brown and others (1962). This complex consists of the following rock types listed in their chronological order from oldest to youngest according to their field relationship (Geologic Maps I and II):

The Host Rock:

- Amphibolite schist

The Intrusive Rocks:

- Dioritic rocks (meta-quartz bearing diorite, monzodiorite, with hornblendic and gabbroic patches)
- Granodiorite
- Biotite monzogranite
- Felsic and Mafic dikes
- Quaternary deposits

1 of 1

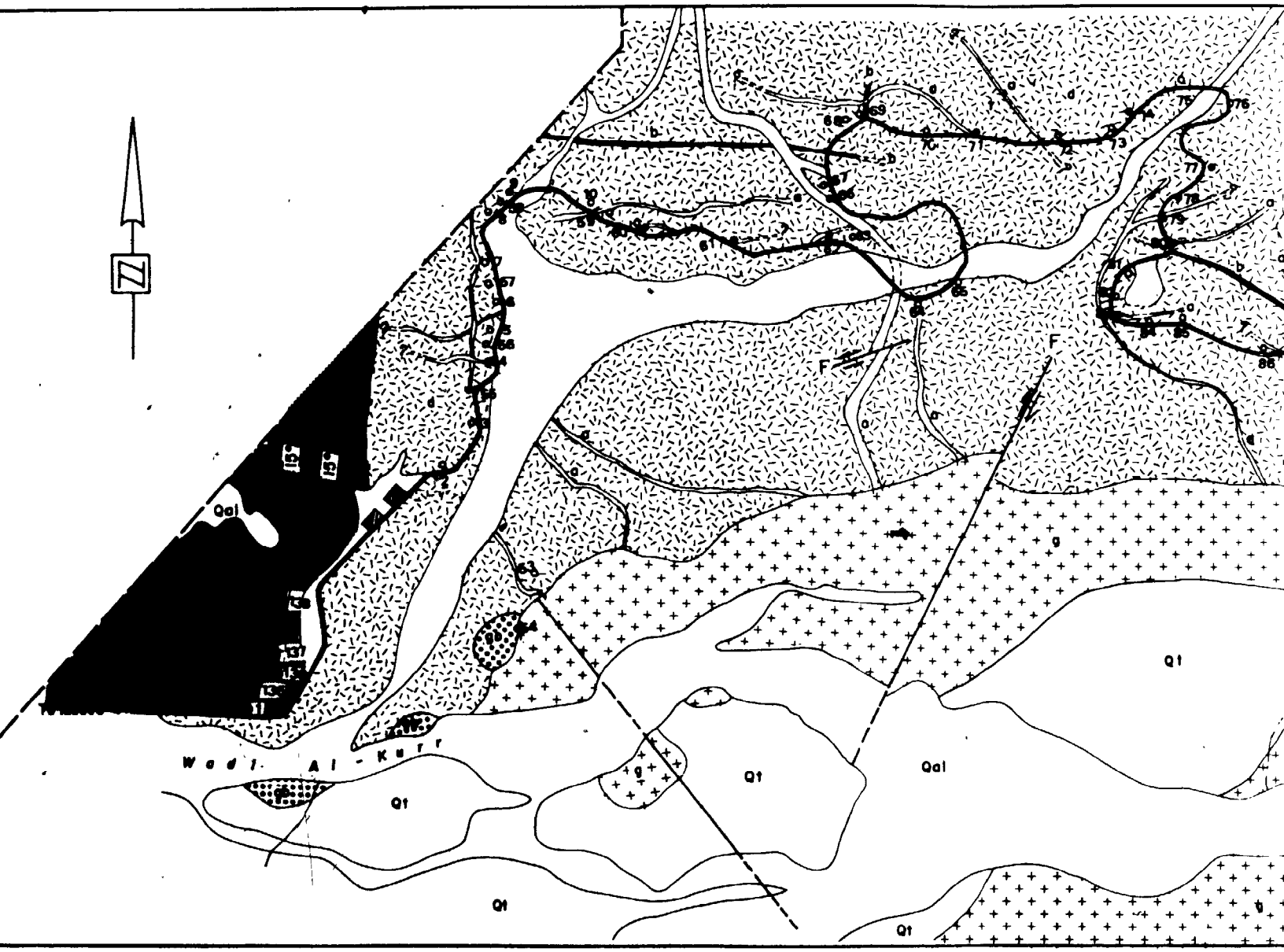

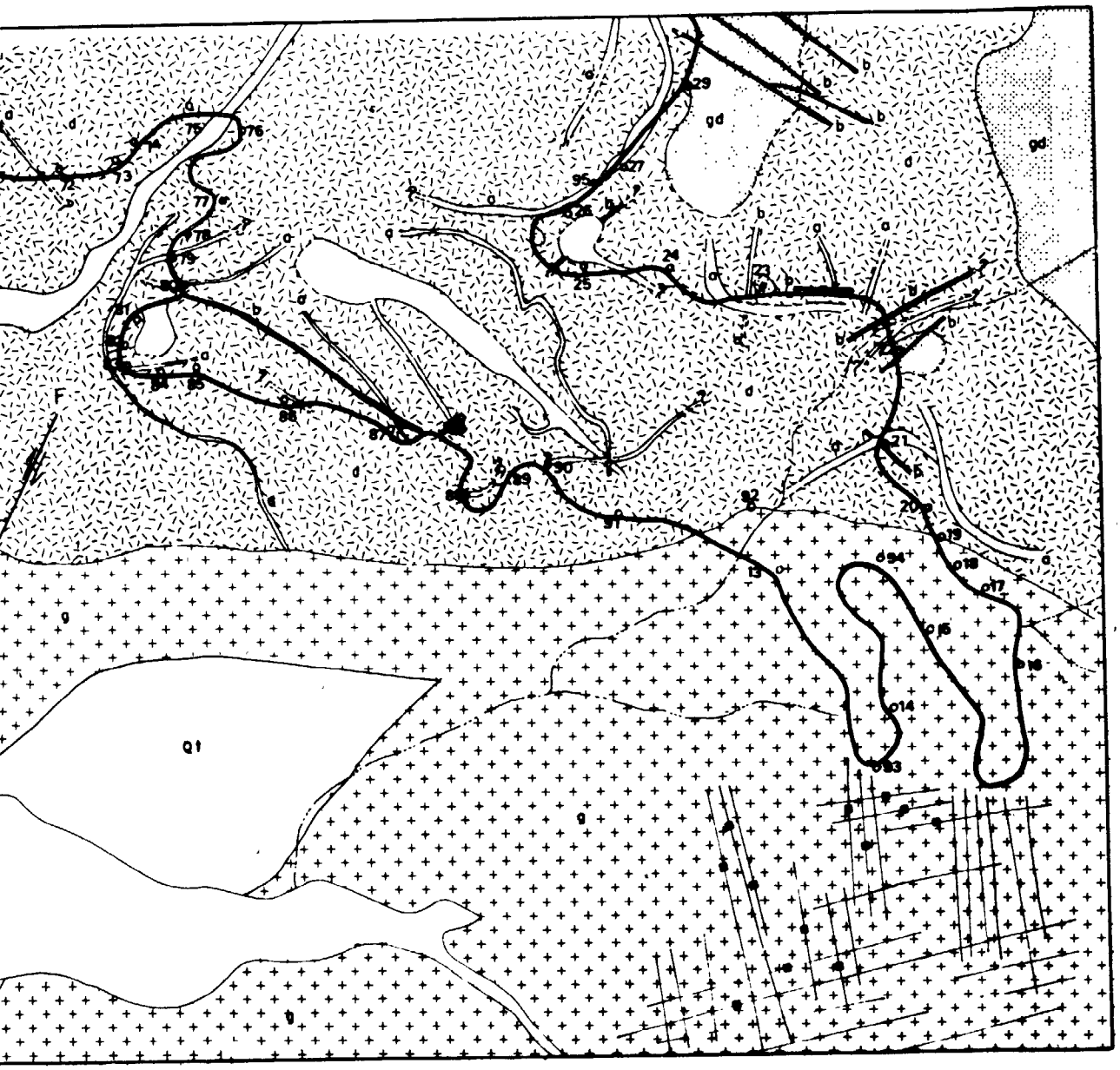

EXPLAN

Qal Quaternary

Q1 Quaternary

DIKES

a
b

PLUTONIC

Biotite gra
equigranula

Granodiorit
and equigr

Diorite, Qtz
light to dar
with the ex

METAMARP

Amphibolite
equigranula

SYMBOLS

Contact, d
Fault, d
Vertical Fr
15° Lineation
Coffee sh
Highway b
Drainage s
o22 Sample Lo

22°00
21°00
39°00

Road Map Across t
between Mecca an

To Mecca

Part (1)

GEO
JABAL AL
NORT

3 of 1

EXPLANATION

Qal — Quaternary alluvial and aeolian

Qt — Quaternary fan deposits

DIKES

a
b

PLUTONIC ROCKS

Biotite granite, light pinkish, coarse-grained massive and equigranular, contains bands of biotite

Granodiorite, light greyish, medium to coarse grained massive and equigranular

Diorite, Qtz. diorite & meta qtz. diorite with local patches of gabbro light to dark greyish, medium grained, massive and equigranular with the exception of some few porphyritic patches

METAMARPHIC ROCKS

Amphibolite, slightly shistosed dark greenish grey, fine-grained equigranular with the exception of porphyroblastic patches

SYMBOLS

Contact, dashed where inferred

Fault, dashed where inferred

Vertical Fractures and Joints

15° Lineation direction

Coffee shops

Highway between MECCA and AT-TAIF

Drainage system

o22 Sample Location

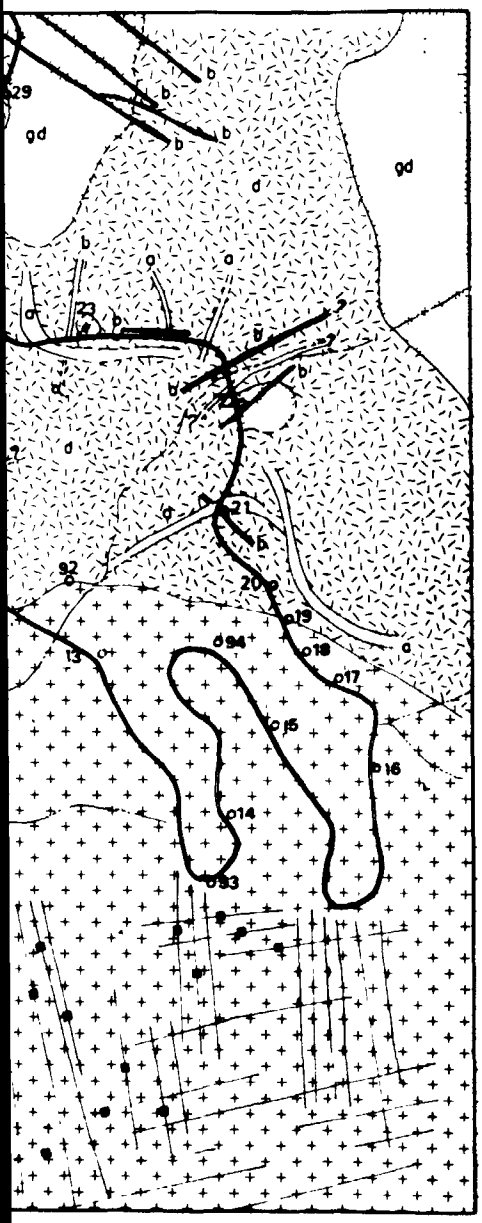

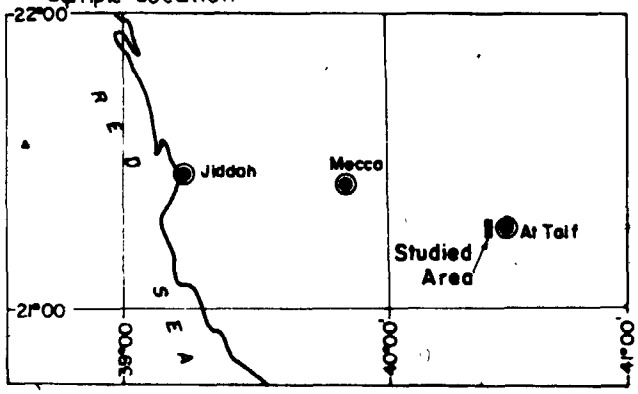

LOCATION MAP
Scale: 1 : 2,000,000

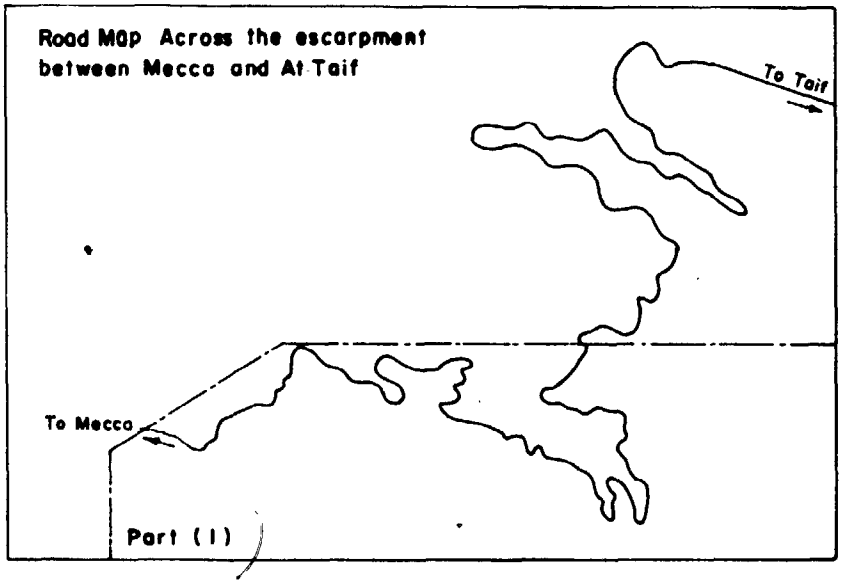

GEOLOGIC MAP ACROSS JABAL AL-HADA ESCARPMENT (PART-1)

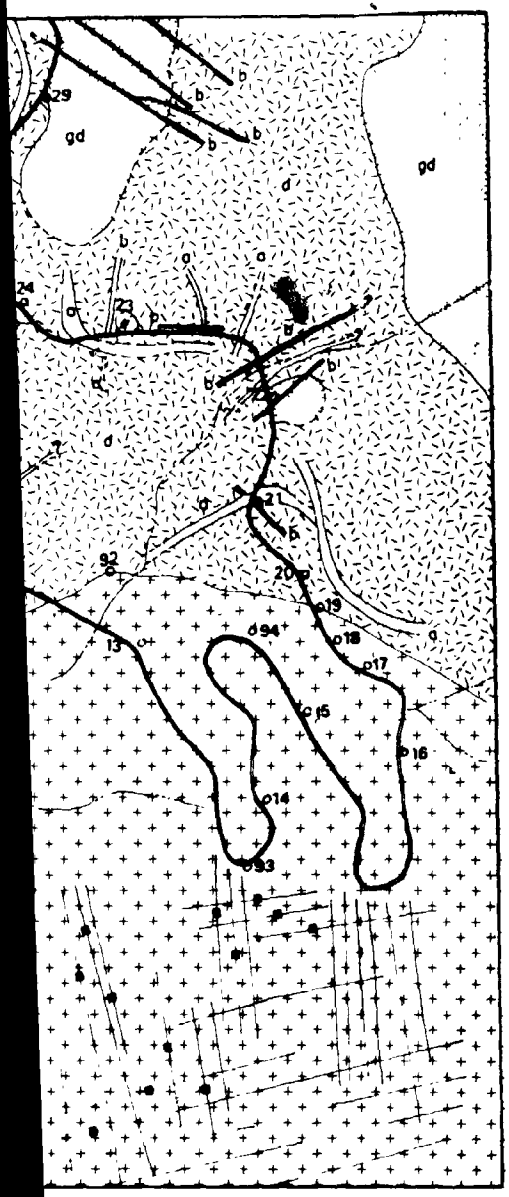

+g+ Biotite granite, light pinkish, coarse-grained massive and equigranular, contains bands of biotite.

gd Granodiorite, light greyish, medium to coarse grained massive and equigranular

Diorite, Qtz. diorite & meta qtz. diorite with local patches of gabbro light to dark greyish, medium grained, massive and equigranular with the exception of some few porphyritic patches

METAMARPHIC ROCKS

Amphibolite, slightly shistosed dark greenish grey, fine-grained equigranular with the exception of porphyroblastic patches

SYMBOLS

- Contact, dashed where inferred
- Fault, dashed where inferred
- Vertical Fractures and Joints
- 15° Lineation direction
- Coffee shops
- Highway between MECCA and AT-TAIF
- Drainage system
- o22 Sample Location

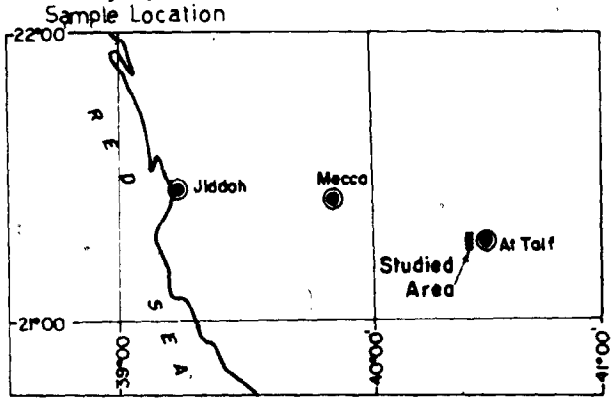

LOCATION MAP
Scale. 1 : 2,000,000

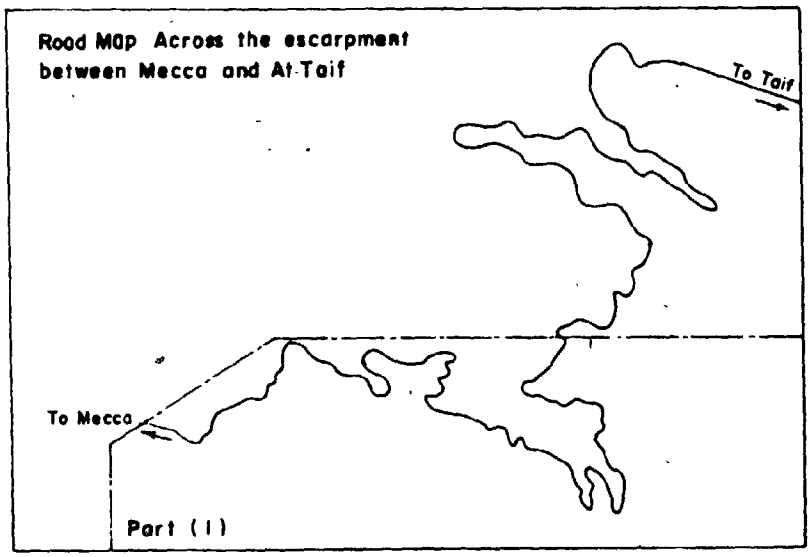

GEOLOGIC MAP ACROSS JABAL AL-HADA ESCARPMENT (PART-I) NORTH WEST OF AT TAIF CITY

BY

FOUAD M. H. MARZOUKI

0 500 1000 Meters

1 of 1

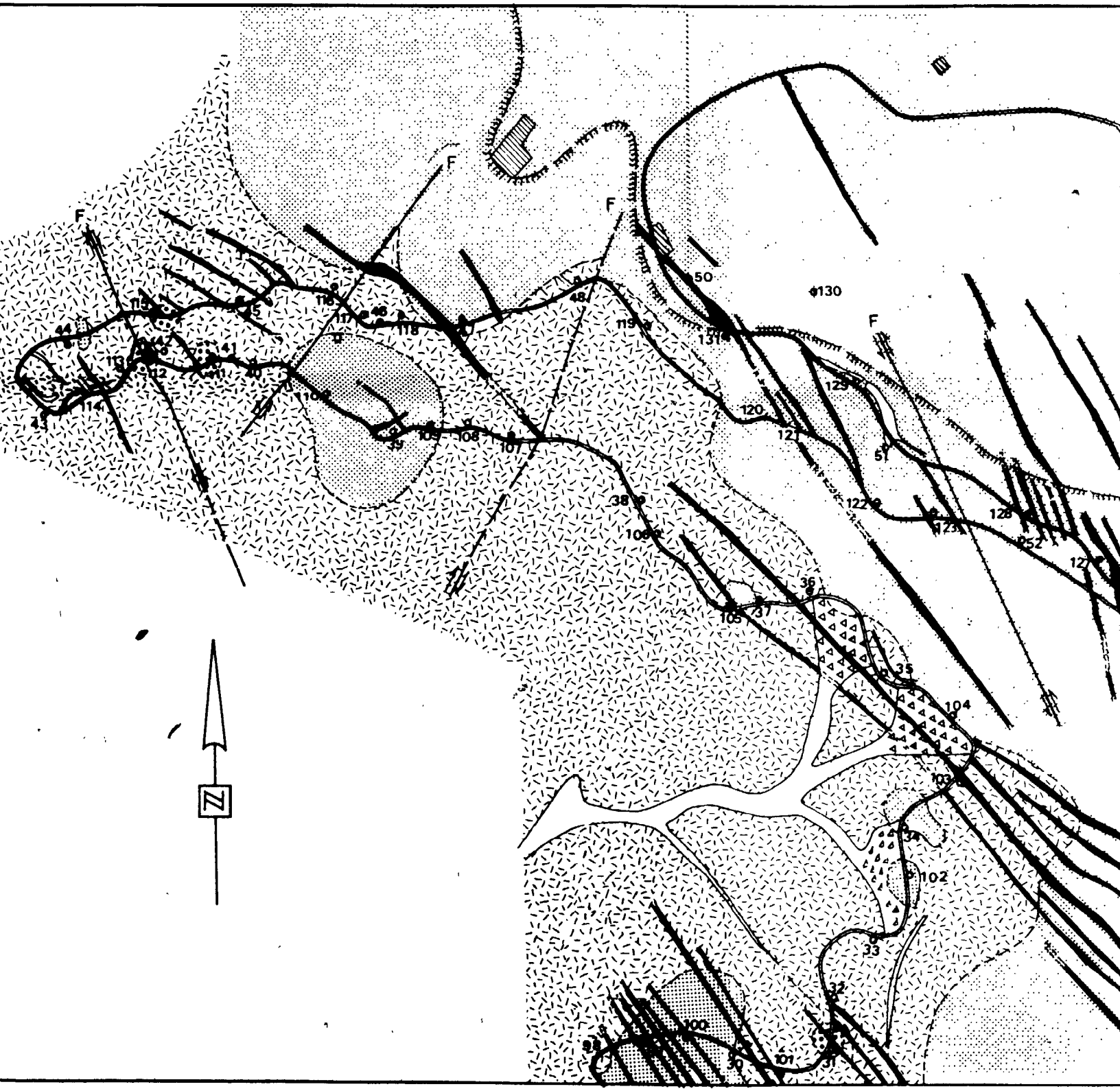
F
F
F
F
50
130
131
129
120
121
51
122
123
128
127
36
105
37
35
104
103
34
102
33
32
100
101
31
30
38
108
107
N

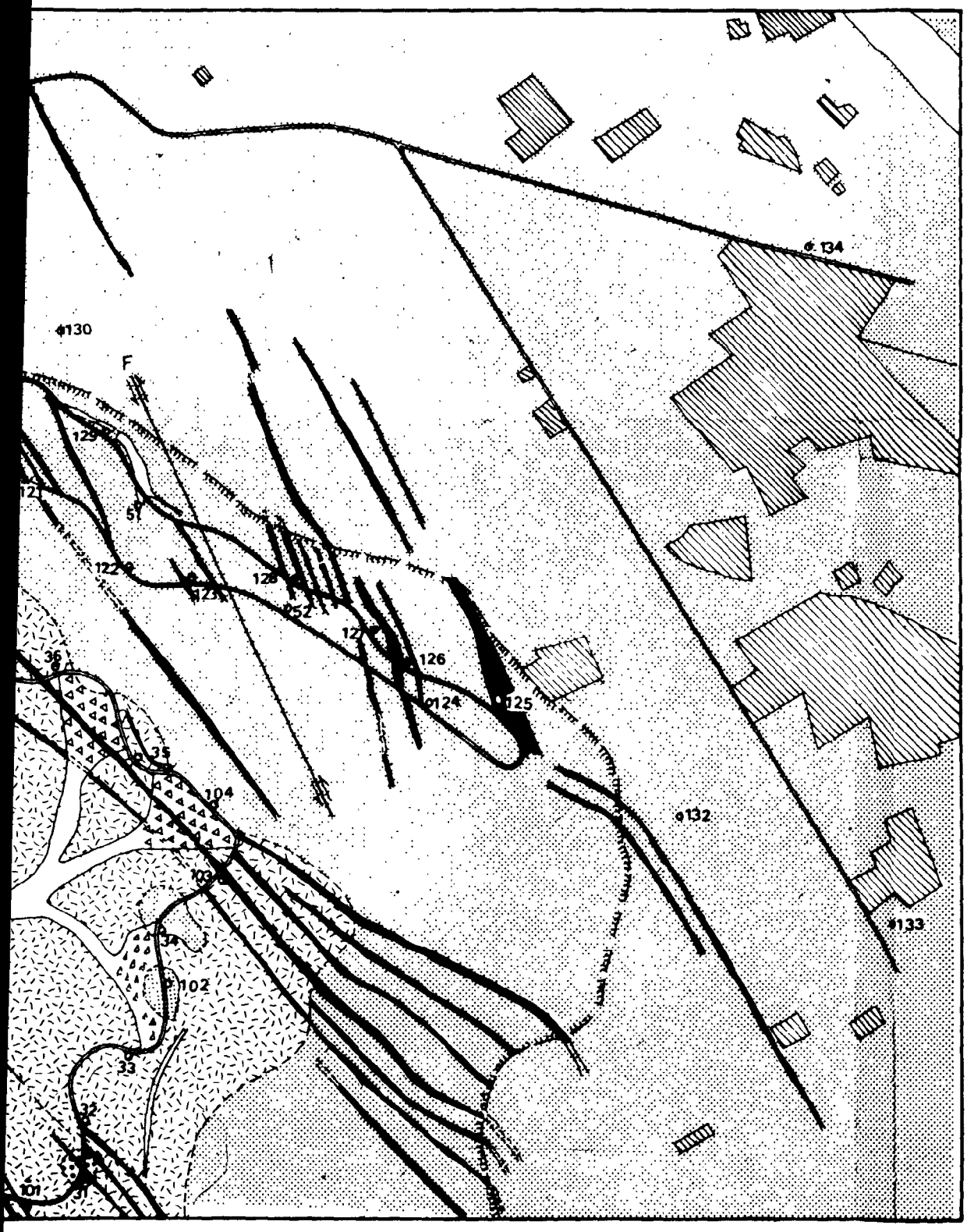

EXPLAN

Quaternary

Scree

DIKES

Acidic (mos
Intermediat

PLUTONIC

Granodiorit
massive an

Diorite, Qu
of gabbro
equigranula

SYMBOLS

Contact, da

F Fault, dash

House and

Escarpmen

Highway

032 Sample

22°00

21°00

Road Map Across th
between Mecca and

To Mecca

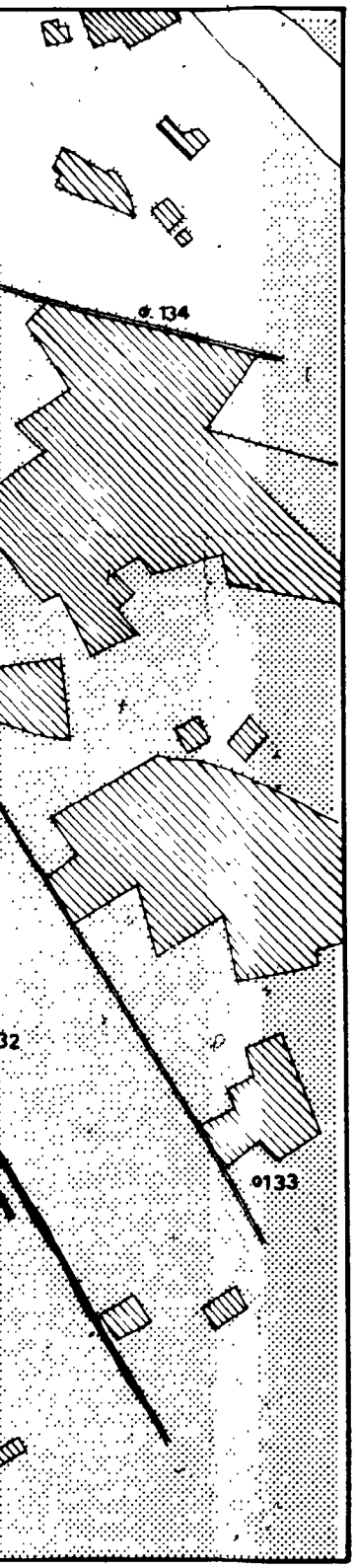

EXPLANATION

13 of

Quaternary alluvial and eolian sand

Scree

DIKES

Acidic (mostly rhyolite and microgranite) dikes (a)
Intermediate to basic dikes. (b)

PLUTONIC ROCKS

Granodiorite, light greyish, medium to coarse grained massive and equigranular

Diorite, Quartz diorite and meta qtz. diorite with local patches of gabbro light to dark greyish, medium grained, massive and equigranular with the exception of some few porphyritic patches

SYMBOLS

Contact, dashed where inferred

F Fault, dashed where inferred

House and cultivated fields

Escarpment edge

Highway

032 Sample Location

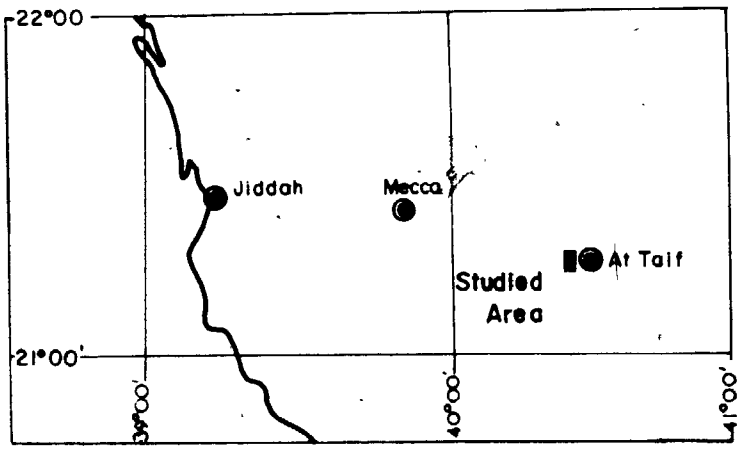

LOCATION MAP
Scale: 1 : 2,000,000

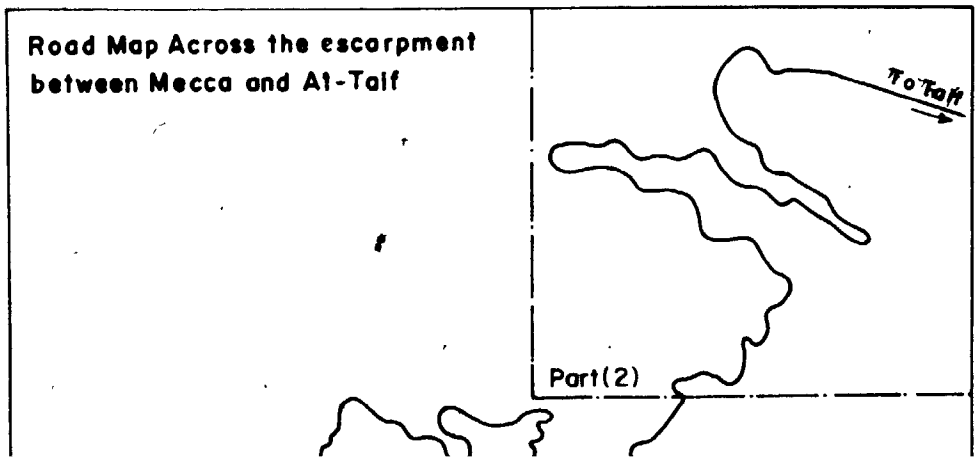

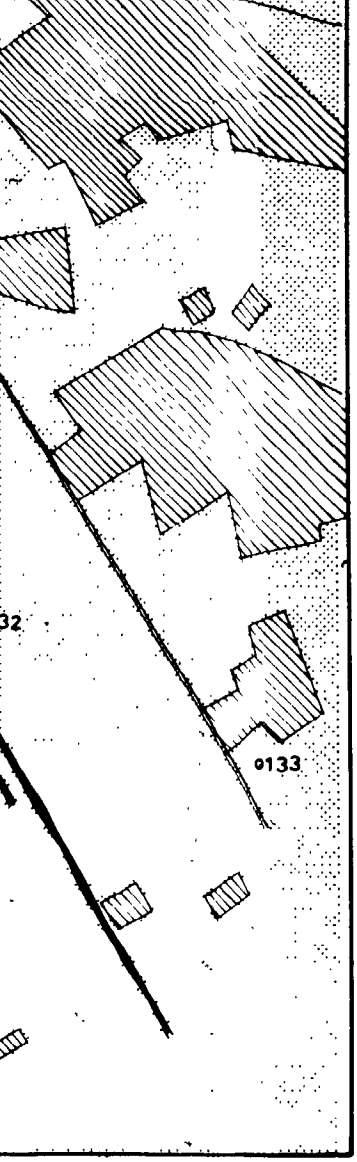

Escarpment edge

Highway

032 Sample Location

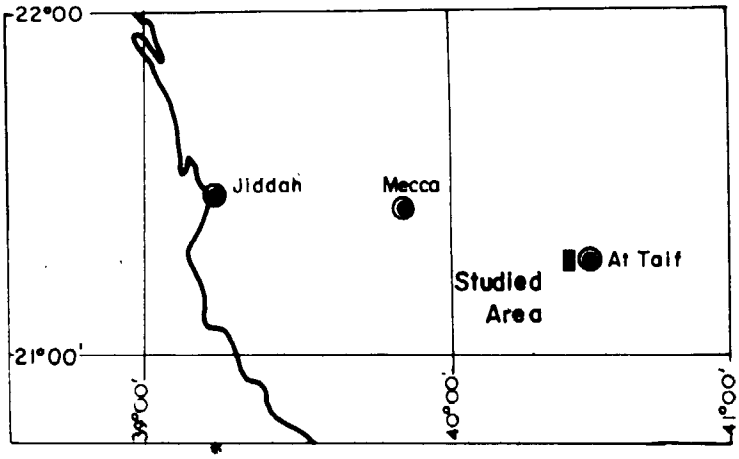

LOCATION MAP

Scale 1 : 2,000,000

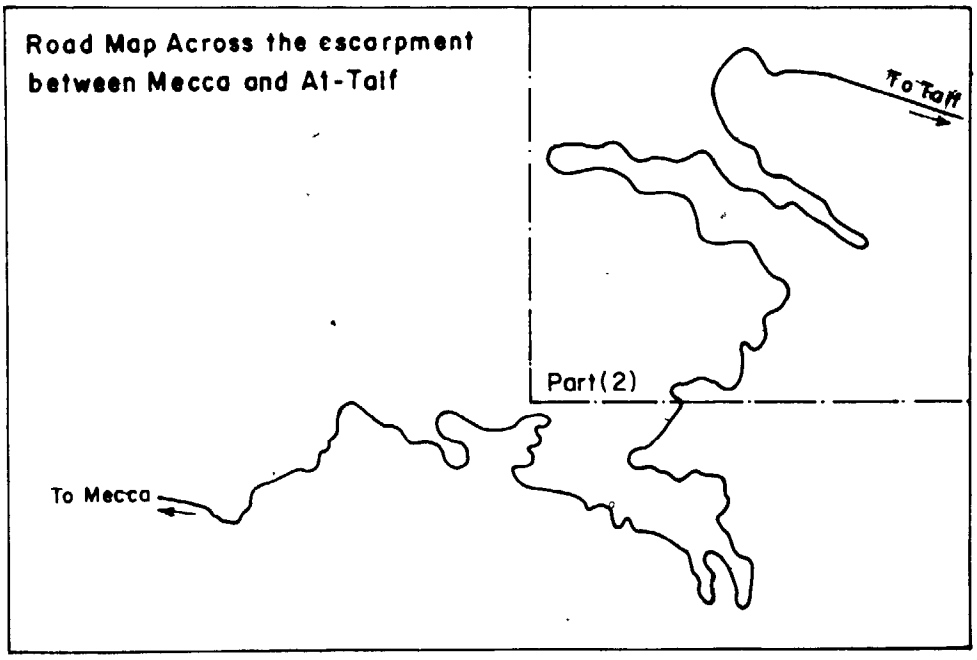

GEOLOGIC MAP ACROSS JABAL AL-HADA ESCARPMENT (PART-2) NORTH WEST OF AT TAIF CITY

BY

FOUAD M. H. MARZOUKI

0 500 1000 Meters

[redacted]

3.2.1 Amphibolite Schist

The amphibolite schist and the quartzfeldspathic gneiss are the oldest rocks in the area and they act as the host rock to all the granitic intrusions. They occur in the most southern part of the area (Geologic Map I), and they occupy about 1% of the mapped area. The amphibolites are intruded and occasionally interlayered by the quartzfeldspathic gneiss (Fig. 5). The contact between the amphibolite and the quartzfeldspathic gneiss is everywhere sharp and clear and is concordant with the schistosity. The schistosity has a steep dip, trending 010°-015°.

3.2.2 Dioritic Rocks

The dioritic rocks represent the earliest intrusion that was emplaced in the amphibolite schist. The diorites cover about 70% of the area and constitute most of the escarpment rocks. Intrusive contact with the amphibolites are sharp. These rocks display a great variation in texture and composition. Most of the observed variations are gradational. The whole dioritic mass is cut frequently by mafic and felsic dikes. They also contain xenoliths of mafic rocks. These xenoliths vary in shape, size and texture (Fig. 14). The dioritic rocks can be subdivided into two distinct groups:

3.2.2.1 Meta-quartz-bearing diorite and monzodiorite

3.2.2.2 Gabbro and monzogabbro

3.2.2.1 Meta-quartz-bearing diorite and monzodiorite

This group constitutes about 90% of the dioritic rocks. They show a wide textural and composition variation. During the course of investigation the following characteristic features were observed in this group:

(a) Pegmatitic patches: these are composed of very coarse hornblende and plagioclase. This feature is observed throughout all dioritic rocks across the escarpment, showing a very great irregularity in geometry and size (Figs. 6, 7, 8). Their occurrence may be due to late residual magmatic pulses, or due to local recrystallization.

(b) Epidotization: the second characteristic feature is epidotization. Epidotization occurs in three forms: as epidote veins (Fig. 9), as fracture coatings, but mainly as an extensive replacement of plagioclase. The first two occurrences are very common and often seen in the various localities in the escarpment. The third form of occurrence is restricted to fewer localities associated with felsic dikes. In these localities the diorites are extensively epidotized, and the plagioclase is completely replaced by epidote, giving the rock a greenish colour (Fig. 10).

(c) A third feature which is not uncommon, is the local occurrence of patches of granite. In some localities replacement of mafic rocks by medium-grained felsic granitic rock is suggested by the presence of irregular embayed

Fig. 5. The amphibolite intruded and interlayered by the quartz feldspathic gneiss. (Field St. #1).

Fig. 6. Pegmatitic patches composed of coarse plagioclase and hornblende in the diorites occurring at the contact of a rhyolitic dike. (Field St. #5).

Fig. 7. The same pegmatitic patches as in Fig. 6 showing irregular patterns also showing a concentration of hornblende crystals on one side and plagioclase crystals on the other side. (Horizontal field of view is 10 m). (Field St. #64).

Fig. 8. A close view of the pegmatitic patches. (Field St. #8).

5

7

8

contacts (Fig. 11). It is not impossible that some workers might even think of liquid immiscibility!

(d) The fourth and least common feature is rhythmic banding. In a few localities, rhythmic bands of hornblende alternating with bands of plagioclase have been observed (Figs. 12, 13). The thickness of these bands is in the order of a few centimeters.

3.2.2.2 Hornblende Gabbro and Monzogabbro

The occurrence of gabbro is restricted to small areas and isolated patches within the dioritic rocks at various localities in the escarpment (Geologic Map I & II). Some of these gabbroic patches have sharp contact with the dioritic rocks and others have gradational contact.

3.2.3 Granodiorite

This forms the uppermost part of the escarpment and covers most of Al-Hadah plateau. It constitutes about 20% of the mapped area (Geologic Map I & II). It intrudes the dioritic complex and has, generally, a sharp clean cut boundary with it (Fig. 15). This boundary is almost vertical. There is no field evidence of any chemical reaction between the two types of rocks. No chilling has been observed. The granodiorite exhibits a slight variation

Fig. 9. Epidote veins of varying thickness found within the diorites; they fill and run parallel to major fractures. (Field St. #115).

Fig. 10. An outcrop of highly epidotized diorite having a greenish colour. This outcrop is cut by a main pinkish rhyolite dike having numerous branches coming out of it. (Horizontal field of view is 50 m.) (Field St. #5.)

Fig. 11. Irregular coarse felsic granitic rock patches having embayed contacts found within fine to medium grained mafic dioritic rock (Field St. #78).

Fig. 12. Rhythmic banding found within the diorite composed of alternating hornblende and plagioclase bands (bands a few centimeters in thickness).

9

11

10

12

in texture: near the contact with the diorite the rocks tend to be more or less, medium-grained while those that outcrop on the plateau, are more coarse-grained. The granodiorites contain numerous xenoliths of variable size (5-50 cm), composition (intermediate to mafic) and texture (medium to fine-grained). These inclusions are commonly spheroids or discoid in shape. The granodiorites are cut by felsic (rhyolitic and granitic) and mafic (andesitic to basaltic)dikes. Towards the top of the escarpment, in particular, at the edge of the escarpment, the mafic dikes form a prominent set, filling vertical fractures and running 320°-330° (Fig. 16).

3.2.4 Biotite Monzogranite

The biotite monzogranite forms the youngest intrusion in the area, and is probably late Precambrian to early Palaeozoic in age by comparison to other monzogranite plutons in the Arabian Shield (Fleck and others, 1975; Schmidt and others, 1973). It forms a roughly circular intrusion measuring 11.5 km east-west and 9.5 km north-south (Hadley and Greenwood, 1976). Only a small portion (10%) of this circular pluton outcrops in the studied area covering its southern part. Contacts with the country rocks are very steep (dipping 70°-80° outward), sharp, clear cut (Figs. 17, 18) and in numerous places are offset as much as

Fig. 13. Similar rhythmic banding to those in Fig. 12 composed also of alternating hornblende and plagioclase (Field St. #64).

Fig. 14. Xenoliths of fine-grained mafic rock of various sizes enclosed within the diorite. (Field St. #46).

Fig. 15. Showing an approximate contact between the granodiorite (GD) towards the top of the escarpment and the dioritic rocks (D). (Looking SE on Field St. #103, 34).

Fig. 16. Numerous andesitic-basaltic dikes filling vertical fractures in the granodiorite and having a trend of about N30-40W. These dikes become very common near the top of the escarpment. (Near Field St. #124.)

13

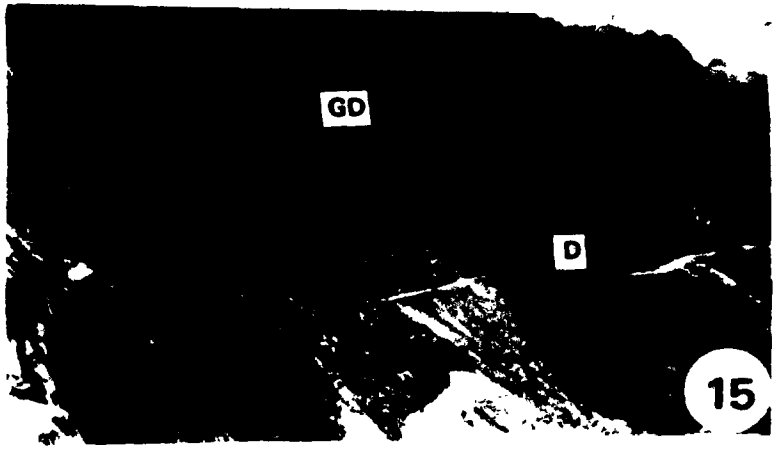

15

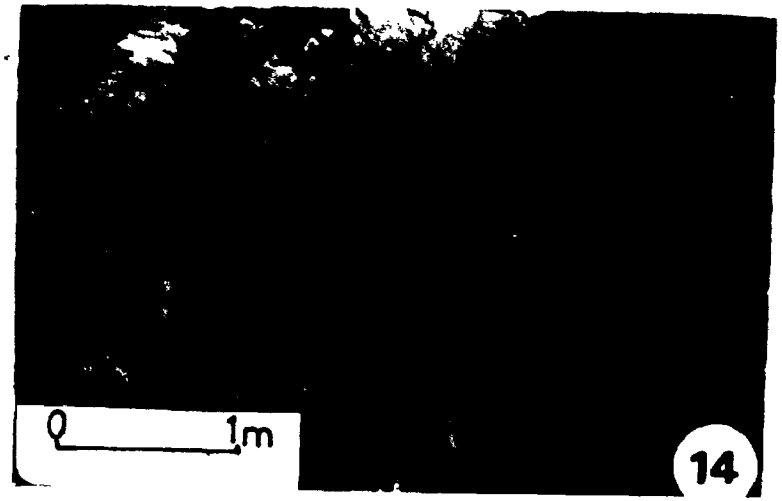

14

16

3 meters by small faults. The pluton is cut by a prominent system of vertical joints running east-west, through the entire intrusion. Mafic inclusions are very rare; only a few occurrences are observed in the immediate vicinity of the contact between the dioritic rock and the granite. These inclusions are generally spherical, relatively small (10 cm in diameter), (Fig. 19), fine-grained and mafic. In one of the localities (Field station #92) bands of mafic minerals, mainly biotite (5-10 cm thick) running parallel to the contact are observed (Fig. 20). Another feature which has been commonly seen in some localities in the biotite monzogranite (field station numbers 14, 17, 18) is the presence of igneous layering consisting of disrupted layers and a zone of generally non-deformed uniformly bedded layers 2-7 cm in thickness. Pegmatitic and aplitic dikes related to the pluton are of two ages: pre-layering and post-layering (Figs. 21, 22). The layering of this biotite monzogranite has been studied and described in detail by Hadley and Greenwood (1976). Table 4 shows a comparison of graded layering in the biotite monzogranite of Al Hadah with other types of layering described in the literature. The main layering occurs near the contact with the diorite and is exposed for a distance of about 200 m. The layering consists of uniform bedded and cross-bedded graded units. The main layered zone ranges

Fig. 17. The contact between the youngest rock type in Al Hadah Pluton (biotite monzogranite = MG) and the diorite (D). The contact is sharp and steep. It also shows a rhyolite dike offshooting out of the monzogranite and cutting the diorite. (Field St. #19).

Fig. 18. Shows the sharp contact between the monzogranite (MG) and the diorite (D) rocks (Field St. #54).

Fig. 19. A small xenolith (about 7 cm in diameter) of the dioritic rocks found near the contact between the monzogranite and the dioritic rocks. (Field St. #54).

Fig. 20. A close view at the contact between the monzogranite and the diorite. The contact is sharp and steep. A few centimeters from the contact biotite bands are present having various widths and run roughly parallel to the contact. (Field St. #92).

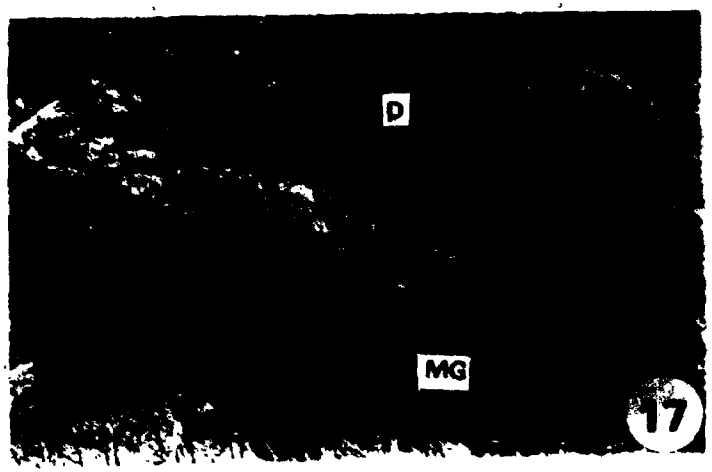
D
MG
17

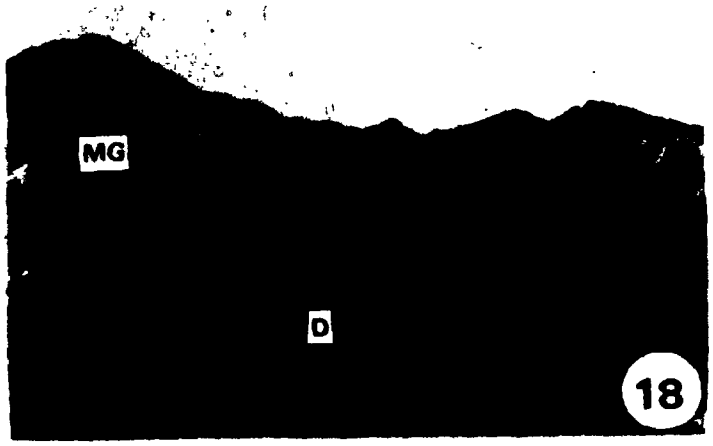
MG
D
18

19

20

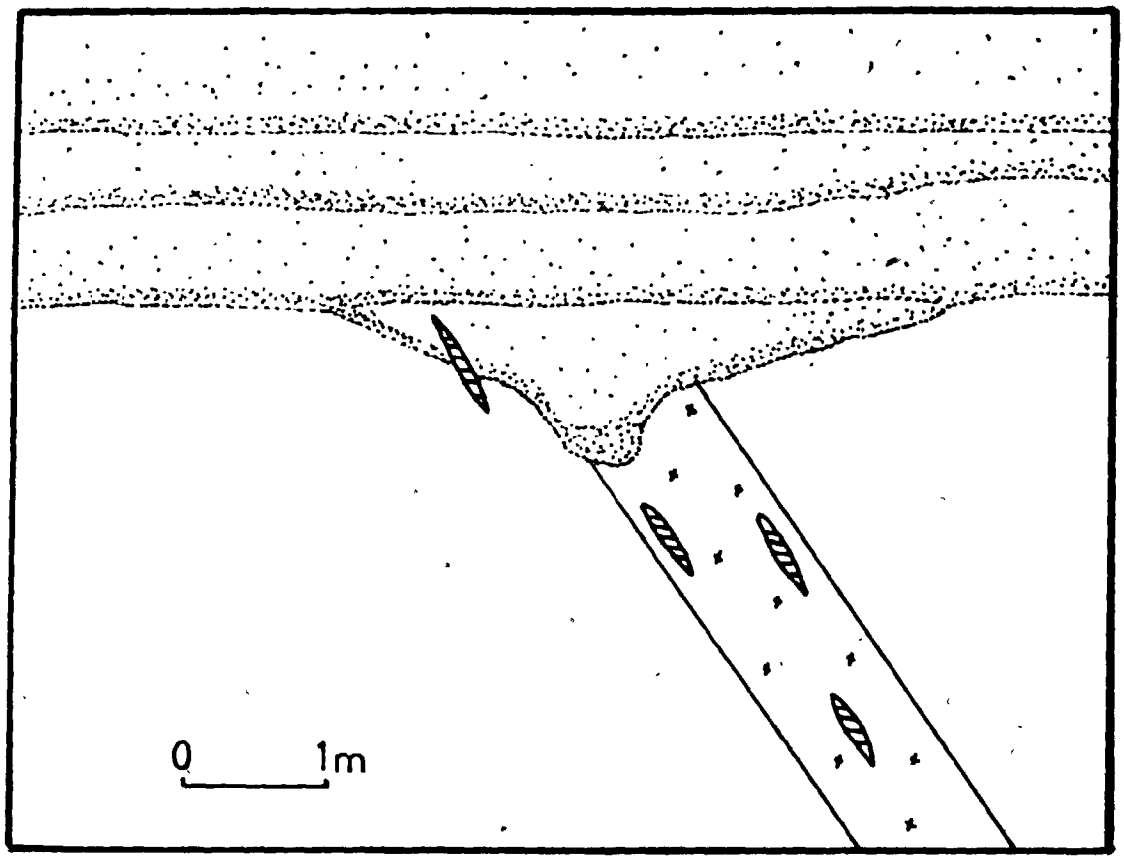

Fig. 21. Drawing of a plane section of massive non-structured pegmatite dike truncated by graded layers. The pegmatite dike encloses mafic blebs. Some of these blebs cut across the lower boundary of one layer indicating growth of the blebs in place. (After Hadley and Greenwood, 1976.)

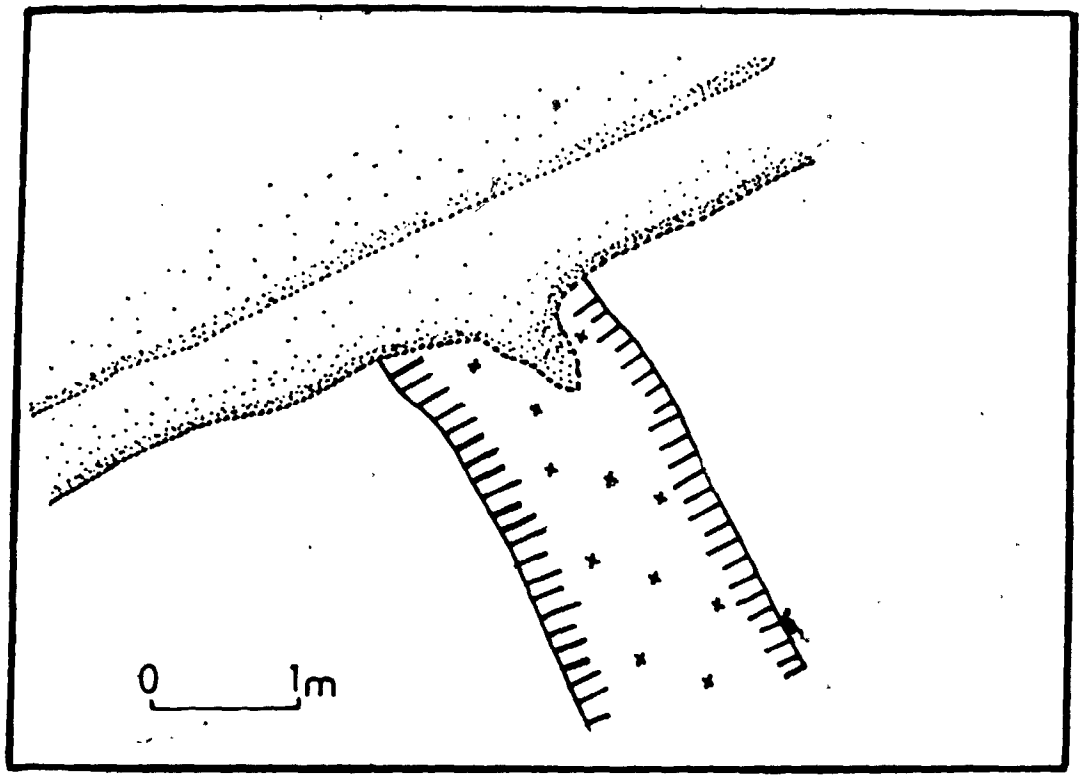

Fig. 22. Drawing of a plane section of a pegmatite dike truncated by graded layers. Hornblende crystals in the dike (shown schematically as heavy bars) have grown in a comb-structured arrangement similar to that described by Moore and Lockwood (1973). (After Hadley and Greenwood, 1976.)

Table 4 - Comparison and contrast of layering in the Twin Lakes Granodiorite, Colorado, Sierra Nevada Batholith, California, and the Al Hadah pluton (After Hadley and Greenwood, 1976).

Formation	Layering Type	Layer Description	Location of Layering	Attitude of Layers	Mafic Minerals	Mineral Orientation	Mineral Concentration	Layer Compositional Changes	Individual Layer Composition	Direction of Layer Deposition	Depositing Mechanism
Sierra Nevada Batholith	Comb Schlieren	Comb: Granitoid layers in which the constituent minerals (primarily plagioclase and hornblende) are oriented about perpendicular to the plane of layering. Schlieren: Granitoid layers alternately enriched or depleted in mafic minerals elongated parallel to the plane of layering.	At or near contact with country rock	Vertical to steeply dipping (commonly overhanging)	Hornblende	Perpendicular and parallel to plane of layering	None	Mafic mineral rich and mafic mineral poor layers commonly alternate	Uniform	Toward intrusion	By aqueous fluid currents; no suspended minerals
Twin Lakes Colorado	No term given	Granitoid layers consisting of minerals segregated into bands and lenses of contrasting colour and grain size	At or near contact with country rock	Mostly vertical	Biotite and minor hornblende	Irregular	Graded from base to top	Layers may be enriched in mafic minerals, orthoclase, or plagioclase.	Commonly graded with respect to mafic minerals and feldspar	Toward intrusion	By flow differentiated currents; mafic minerals and feldspars in suspension
Al Hadah Pluton Saudi Arabia	Graded	Granitoid layers, each layer of which is normally of reversely graded from bottom to top in terms of modal concentration with respect to the constituent minerals	At or near contact with country rock	Moderately dipping	Biotite and sparse hornblende	Irregular	Graded from base to top	Layers are uniform in composition	Invariably graded from mafic and plagioclase rich bases to mafic poor and K-spar rich tops	Toward country rock	By flow differentiation currents; mafic minerals and feldspar in suspension

from 2.0 m to 6.7 m in thickness. The individual layers range in thickness from 2 to 30 cm, and they have a general strike of 290° and a dip of 34°NE. Various layering structures are observed such as regular bedding (Fig. 23), cross bedding (Fig. 24), and channelling and thinning of layers (Figs. 25, 26). The origin of this layering has been discussed in detail elsewhere (Hadley and Greenwood, 1976).

3.2.5 Dikes

The Al Hadah region is intensively traversed by felsic and mafic dikes. In many localities they often form complex patterns. These dikes were classified into two main groups according to their composition. A summary of the main features of the different types of dikes is presented in Table 5.

3.2.5.1 Felsic Dikes

The felsic dikes occur throughout the whole area. Their width varies from a few centimeters up to 15 m. They vary in texture from very fine-grained through aplitic to pegmatitic. On the basis of chemical compositions, (Appendix B, Table 5) it appears that some of the felsic dikes precede the latest granite event while some are

Fig. 23. Graded layers composed of biotite, K-feldspar, plagioclase and quartz found in the monzogranite. The layers range in thickness from 2.2 cm to 30.4 cm and the average is 9.8 cm. They have a general trend N55-80W and a moderate dip of about 30NE. (Field St. #18.)

Fig. 24. The graded layers described in Fig. 23 show here cross-bedding features. (Field St. #17.)

Fig. 25. Shows truncated graded layers. (Field St. #17.)

Fig. 26. Shows also the truncation in these graded layers and also the sharp intrusive contact between the layers and the host rock. (Field St. #14.)

23

24

25

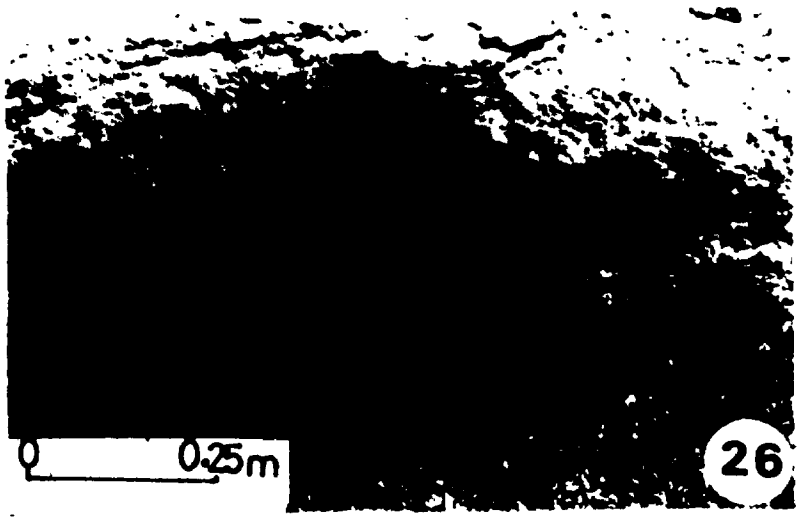
0
0.25m
26

TABLE 5. A summary of the main features of the different dikes in Al Hadah igneous complex.

Trends	Description	Composition
	M A F I C D I K E S	
EW	Blackish, fine-grained, equigranular	Basaltic
(310°-330°)	Blackish, mostly fine-grained, equigranular to porphyritic	Basaltic
(020°-030°)	Dark greyish, fine to medium grained, equigranular to porphyritic	Andesitic
NS	Dark greyish, fine-grained, equigranular	Andesitic
	F E L S I C D I K E S	
(290°-320°)	Light pinkish, aplitic	Granitic
(050°-070°)	Pinkish, fine-grained	Granitic
EW	Reddish, very fine-grained	Granitic

directly related to the biotite monzogranite intrusion. In some localities it is clearly seen that these dikes are branching out of the parent intrusion and root in the pluton (Figs. 17, 27). Most of the felsic dikes appear to fill fractures in the country rocks (Figs. 16, 28) which are probably created by the rising pluton (Figs. 29, 30). At a later stage different blocks or pieces of the country rocks are completely enclosed and appear as islands within these felsic veins (Fig. 31). Matching irregularities in the opposing walls of some dikes indicate that they were emplaced by dilation of their walls (Fig. 32). Furthermore, some of these felsic dikes show narrow shear zones along their borders with the country rock (Fig. 33), and some conjugate sets (Fig. 34). In some of these dikes zones of mafic mineral, the same as those found in the country rock, are observed in their margins (Fig. 36) or sometimes form a central band (Fig. 35). The cores of some pegmatite dikes are very coarse-grained compared to their edges (Fig. 37).

3.2.5.2 Mafic Dikes

These occur through the whole area and especially towards the top of the escarpment, where they form a very prominent set striking 210°-230° and filling vertical fractures

Fig. 27. Showing the sharp contact between the monzogranite and the diorite, also showing numerous rhyolite dikes branching from the monzogranite intrusion.

Fig. 28. The diorite host is intruded by granodiorite, a dike of the granodiorite is shown penetrating the diorite in a brittle fashion.

Fig. 29. Brittle behaviour in a felsic dike cutting the diorite and enclosing fragments of the host rock. (Field St. #12.)

Fig. 30. The dioritic host is intruded by a mafic dike and both are intruded by two felsic dikes.

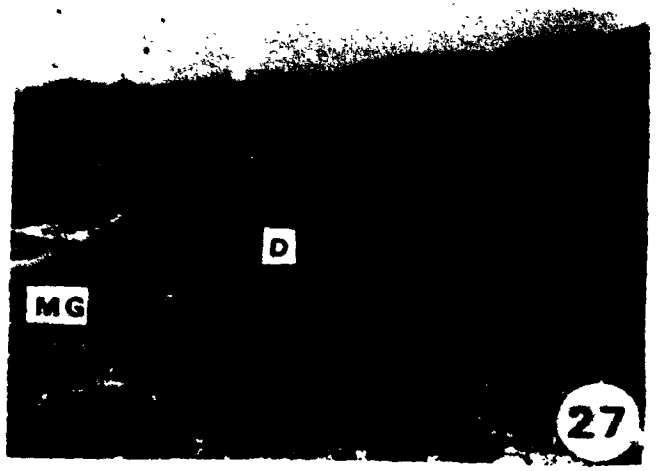
D
MG
27

28

29

30

Fig. 31. Felsic material replacing and enclosing slabs of the dioritic rocks. (Field St. #108.)

Fig. 32. Andesitic dike cutting a felsic dike and dilating it. (Horizontal field of view 20 m.)

Fig. 33. A felsic dike cutting the diorite; the contact is marked by a strong foliation zone. (Field St. #65.)

Fig. 34. Showing a conjugate set of felsic dikes. (Between Field St. #60 and #61.)

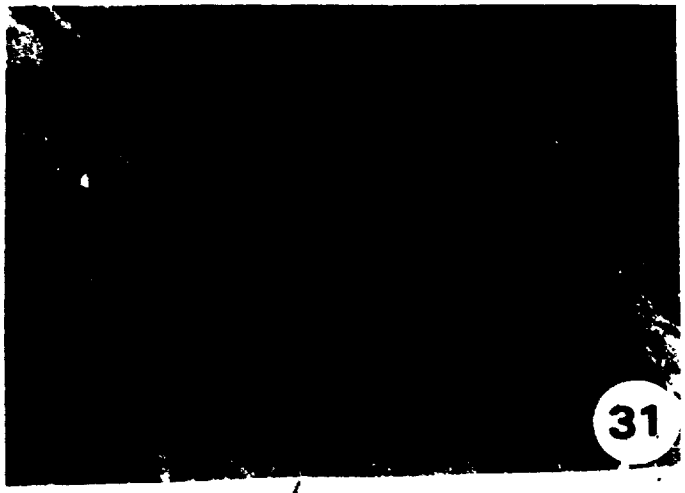
31

32

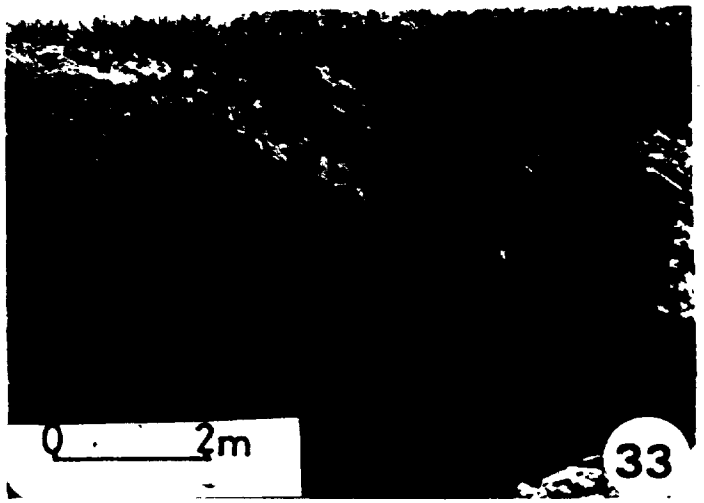
0
2m
33

34

Fig. 35. A felsic dike cutting the diorite. The felsic dike shows a band of hornblende, in the middle of the dike.

Fig. 36. A felsic dike cutting the diorite. The borders of the dike are enriched in hornblende indicating assimilation of the diorite by the felsic dike.

Fig. 37. A pegmatite dike with very coarse core. (Field St. #17).

Fig. 38. Shows criss-cross relationship between the three sets of dikes: andesitic dike cut by a felsic dike and both are cut by a younger basaltic dike. (Field St. #111).

35

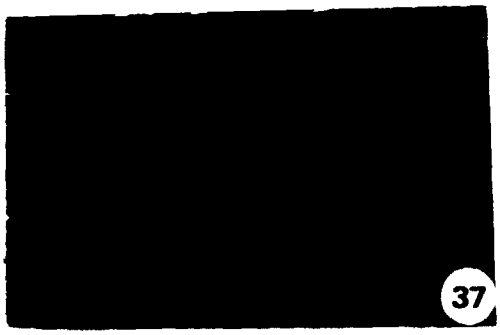
37

36

38

(Fig. 16, 40). Compositionally, they range from andesitic to basaltic and texturally they range from fine-grained equigranular to porphyritic with plagioclase phenocrysts up to 5 cm in diameter. They vary in width from 30 cm up to 5 m. Many have been strongly sheared parallel to their walls. According to their trend four subgroups could be identified:

EW trending group

310°-330° trending group (most common)

020°-030° trending group

NS trending group

Correlation between the different trending groups and their composition is difficult because of great similarities in the bulk composition.

Understanding the age relationships between the different trending groups of the felsic and mafic dikes was a difficult task to accomplish due to the complexity of these dikes and their numerous occurrences with very few cross-cutting relationships. On the basis of the information gathered from the few localities where such relationships occur, one could say that there are at least two generations of felsic dikes and also at least two generations of mafic dikes. Fortunately, in one locality (Field Station #111) the relation between three of these

generations was apparent (Fig. 38, 39) in which one could observe a felsic dike cutting a mafic one, while both are cut by a third mafic dike. In another locality, towards the top of the escarpment, felsic dikes are observed cutting the prominent set of mafic dikes (Figs. 41, 42). Furthermore, this set of mafic dikes is cut by another younger mafic dike (Fig. 43). It is clear that there is a complex set of dikes which may be synchronous with the various members of the intrusive sequence. As there is considerable evidence of Tertiary basaltic activity along the western part of the Shield, it is possible that the latest basaltic dikes could be related to such activity. But these basaltic dikes do not seem to cut the youngest granites. Without dating techniques and very detailed field study, it is difficult to solve the age relationship problem of these complex dikes.

3.2.6 Quaternary Deposits

The Quaternary deposits consist of unconsolidated deposits including fan deposits, fluviatile terraces, and alluvial wadi fillings and eolian sand. The fan deposits surround the mountains of the area and form unsorted accumulations, spherical to angular fragments of all sizes ranging from pebbles up to blocks. These fragments are

Fig. 39. Shows a felsic dike cutting and enclosing a basaltic-andesite dike. (Horizontal field of view 15 m). (Field St. #35).

Fig. 40. Basaltic dikes filling vertical fractures trending 320°-330°. These are most prominent toward the top of the escarpment. (Horizontal field of view 35 m).

Fig. 41. The set of basaltic dikes shown in Fig. 40 and Fig. 16 are cut by a younger felsic dike.

Fig. 42. A close view showing one of the set of these basaltic dikes cut by the felsic dikes. (Across the highway from Field St. #129).

Fig. 43. The set of basaltic dikes are also cut by another set of basaltic dikes. (Horizontal field of view 15 m).

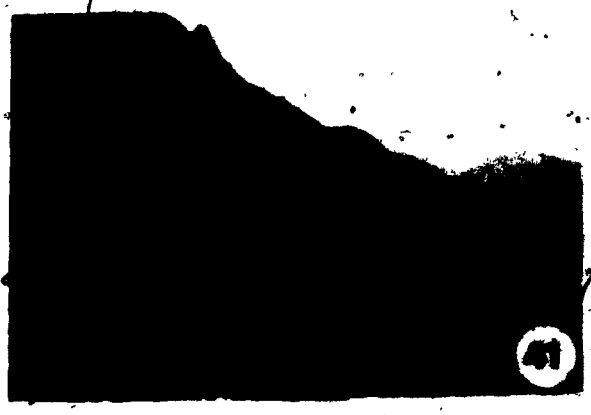

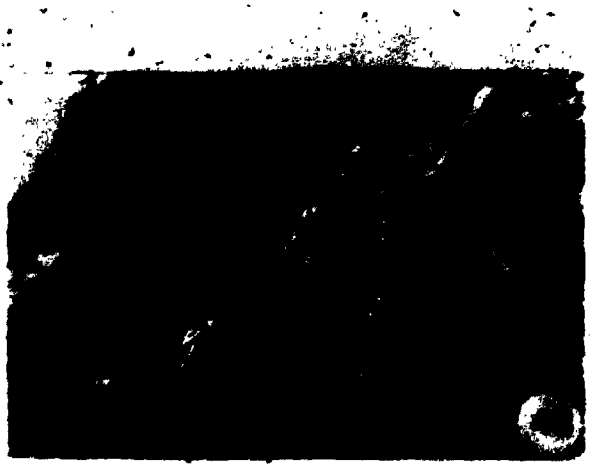

derived mostly from the granitic rocks of the area. The fluviatile terraces are exposed at the foot of the Escarp Mountains and form low hills composed of poorly stratified and poorly sorted clastic material of fragments embedded in a loose sandy matrix. The alluvial wadi fillings consist of sand and gravel, transported mainly by occasional floods during heavy rainfall. The Quaternary eolian sand mainly covers the flat plains and wadis.

CHAPTER 4

PETROGRAPHY

4.1 General Statement

This chapter deals with the study of the principal mineralogical composition of the major rock groups of the Al-Hadah igneous complex. The methods of study and the detailed petrographic descriptions of the different rock units are given, and then used to establish the crystallization history of these magmas.

4.2 Methods of Study

During the course of this investigation, over 100 thin-sections were selected from representative samples for detailed petrographic study. Mineral percentages (modes) were determined for about 30 of these sections by counting; an average of 600 counts per section were taken. The plagioclase composition was determined by two methods: 1) by measuring the extinction angle of the albite twinning in sections of plagioclase cut perpendicular to both 001 and 010 cleavages, 2) by the microprobe analysis.

4.3 Amphibolites

Macroscopically, the amphibolites are dark greenish grey in colour, mostly massive, fine to medium-grained, and occasionally show a porphyroblastic texture with hornblende porphyroblasts of 3-5 mm in diameter (Fig. 45). The mineralogy of the amphibolite is dominantly composed of hornblende + plagioclase + quartz. The principal petrographic features of this rock group are presented in Table 6. The major mineral phases are described in decreasing order of abundance.

Hornblende:

Hornblende (65%) is the major mineral component. Generally, coarse hornblende grains form bands; between these bands finer grained hornblende, plagioclase and quartz crystals occur (Fig. 46).

Plagioclase:

The average composition of plagioclase is andesine (An_{32}): albite twinning and zoning are common. Plagioclase grains typically show partial alteration, particularly in the cores; sericite and epidote are the main alteration products.

Quartz:

Quartz is a minor mineral constituent (3%); mostly associated with plagioclase.

TABLE 6. A summary of the principal petrographic features of the Al-Hadah amphibolites.

	%	Grain Size	Colour	Remarks
Major Constituents				
Hornblende	65%	0.7 mm	olive green	subhedral to euhedral prismatic crystals, form bands, within the bands finer hornblende grains occur (0.1-0.2 mm), polysythetically twinned, show poikilitic texture.
Plagioclase	30%	0.1-0.3 mm	colour-less	euhedral, tabular crystals albite twinning and normal zoning are very common. Partially altered to sericite and epidote.
Minor Constituent				
Quartz	3%	0.1 mm	colour-less	anhedral, interstitial.
Accessory Minerals				
Magnetite	2%	0.1 mm	opaque	subhedral grains, commonly enclosed with the hornblende.

Accessory Minerals:

The principal accessory mineral is magnetite.

Interpretation of Mineral Data:

The occurrence of plagioclase and hornblende, both in major amounts is characteristic of the amphibolite facies (Hyndman, 1972). Furthermore, the calcic composition of plagioclase An>15 (An_{32}) is also a characteristic of the amphibolite facies (Hyndman, 1972; Winkler, 1967) in contrast to the greenschist facies in which the composition of the plagioclase is An_{0-7}. Zoning and twinning, both albite and carlsbad, are indicative of igneous origin, rather than a sedimentary origin. The parent rock of equivalent chemical composition is most likely to be basaltic andesite which has been subjected to medium to high grade regional metamorphism.

4.4 Meta-Quartz-Bearing Diorite and Monzodiorite

The dioritic rocks vary in colour from light to dark greyish. These rocks are mostly massive, fine to medium grained and mainly equigranular, but exceptionally porphyritic, in some localities (Fig. 48). Mineralogically, the major components are plagioclase and hornblende with biotite and quartz as minor constituents. The principal petrographic features of this rock type are presented in Table 7. The modal analyses are presented in Table 8.

Fig. 45. A handspecimen of amphibolite composed mainly of hornblende and plagioclase. It is fine to medium grained (FM137B).

Fig. 46. A thin-section of the amphibolite showing relatively coarse and fine prismatic crystals of hornblende. The relatively coarse hornblende forms bands; between them there are fine to medium euhedral plagioclase, few quartz, and hornblende too (FM 137B).

Fig. 47. A handspecimen of the diorite composed mainly of hornblende and plagioclase. It is medium grained (FM5).

Fig. 48. A patch of porphyritic diorite with plagioclase phenocrysts enclosed within equigranular diorite. (Field St. #45.)

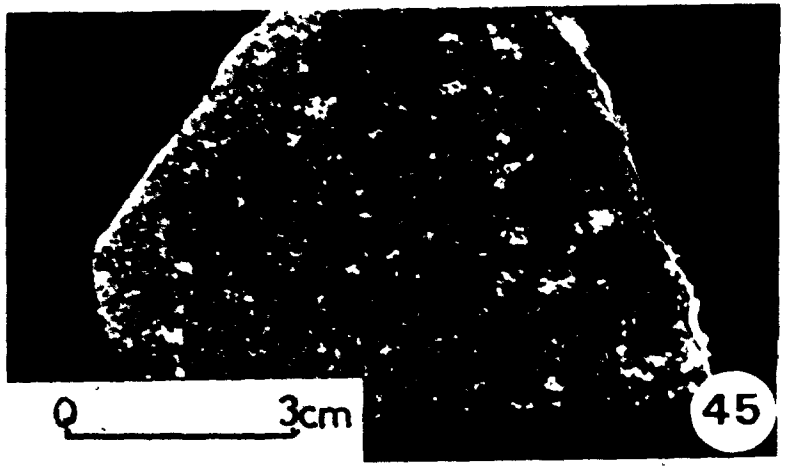
0
3cm
45

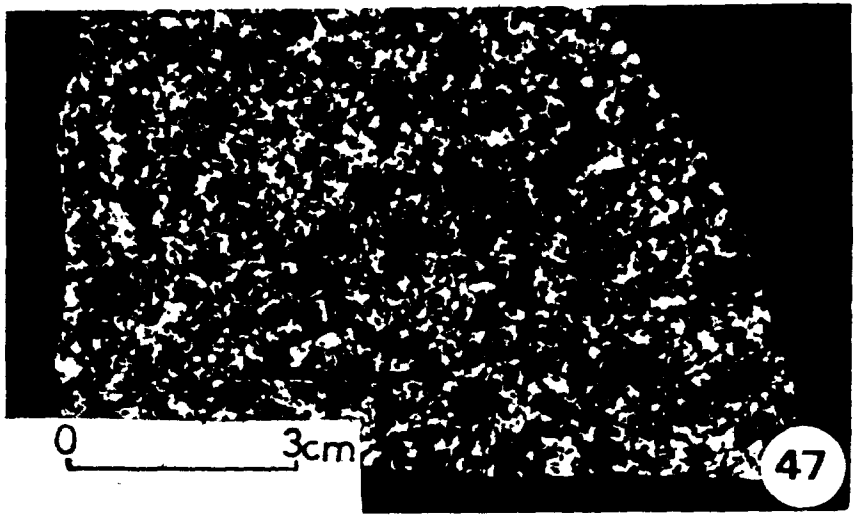
0
3cm
47

H
H
H
0
1mm
46

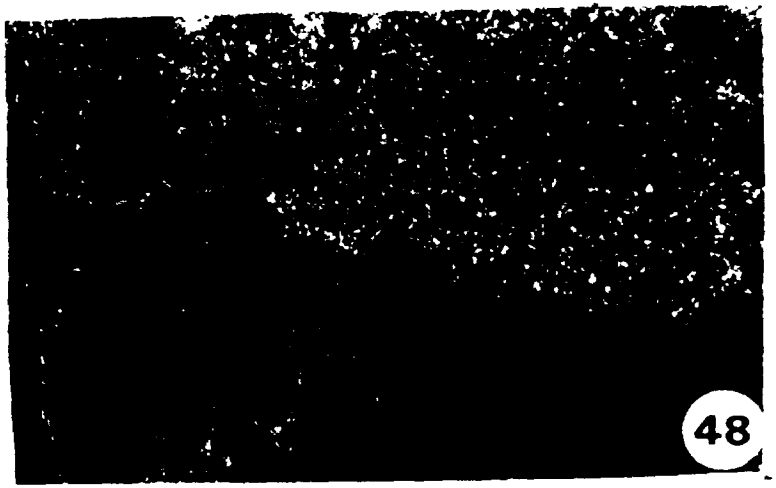
48

TABLE 7. A summary of the principal petrographic features of the Al-Hadah diorites

	%	Grain Size	Colour	Remarks
Major Constituents				
Plagioclase	54%	1.5 mm length 0.7 mm width	colourless	Subhedral to euhedral tabular and columnar grains, twinned and zoned, slightly altered to sericite and epidote.
Hornblende	26%	0.5-2 mm	olive green	subhedral to euhedral prismatic crystals, polysynthetically twinned, show ophitic to subophitic texture.
Minor Constituent				
Biotite	8%	0.8 mm	brown	subhedral to euhedral columnar and flaky grains.
Quartz	7%	0.5 mm	colourless	anhedral and interstitial, show undulatory extinction
Accessory Minerals				
Magnetite		0.25 mm	opaque	subhedral to euhedral grains, some reach up to 1 mm in diameter.
Apatite		<0.1 mm	colourless	prismatic and acicular grains often show six-sided cross section.
Sphene		<0.3 mm		subhedral to euhedral prismatic crystals
Zircon		0.1 mm		euhedral prismatic crystals

TABLE 8. Modal analyses (in percent) for some of the dioritic rocks

	FM7	FM11	FM48	FM66	FM26	FM42A	FM68	FM108	FM39	FM84
Plagioclase	54	59	50	55	60	50	55	52	50	55
Hornblende	40.5	39	22	35	20	35	35	25	25	30
Biotite	1	-	10	-	6	-	-	15	10	7
Quartz	1.5	1	15	-	10	10	4	7	10	3
Access.	2.5	2	3	5	4	5	6	2	5	5
An. Content			34	42	32	31	40	34	34	36

The major mineral phases are described in decreasing order of abundance.

Plagioclase:

Plagioclase (54%) crystals often show albite, carlsbad and occasional pericline twinning. Most crystals show normal zoning. The average composition is andesine (An_{36}). Partial to complete alteration, particularly the core of the grains, is characteristic. The alteration products are mainly sericite, epidote and sometimes biotite or chlorite (Fig. 49). Inclusions of hornblende, biotite and some of the accessory minerals are common in the plagioclase grains.

Hornblende:

Most of the hornblende (26%) grains are polysynthetically twinned (Fig. 50), and often show ophitic to subophitic texture where plagioclase crystals are partially to completely enclosed within the hornblende crystals (Figs. 51, 52). Alteration to biotite and chlorite (Figs. 53, 54, 55), and sometimes to epidote (Fig. 56) is a common feature in some of the hornblende grains. Furthermore, some hornblende grains contain remnants of clinopyroxene (Figs. 51, 57).

Biotite:

Biotite (8%) occurs both as a primary mineral and also as an alteration product of hornblende (Figs. 53, 54).

Fig. 49. Biotite (B) replacing plagioclse (P), a remnant of the plagioclase still exists; anhedral quartz (Q) grains and prismatic hornblende (H) crystals are observed (FM 26).

Fig. 50. Polysynthetic twinning observed in hornblende prismatic crystals (H); altered plagioclase crystals (P) are also observed (FM 65).

Fig. 51. A hornblende crystal (H) with its outline corroded by plagioclase; the hornblende crystal shows ophitic to subophitic texture by enclosing completely to partly plagioclase crystals (P), which are altered to sericite (FM 42A).

Fig. 52. Hornblende crystals (H) enclosing plagioclase (P) and remnants of pyroxene (Px). (In plane light.) (FM 84A).

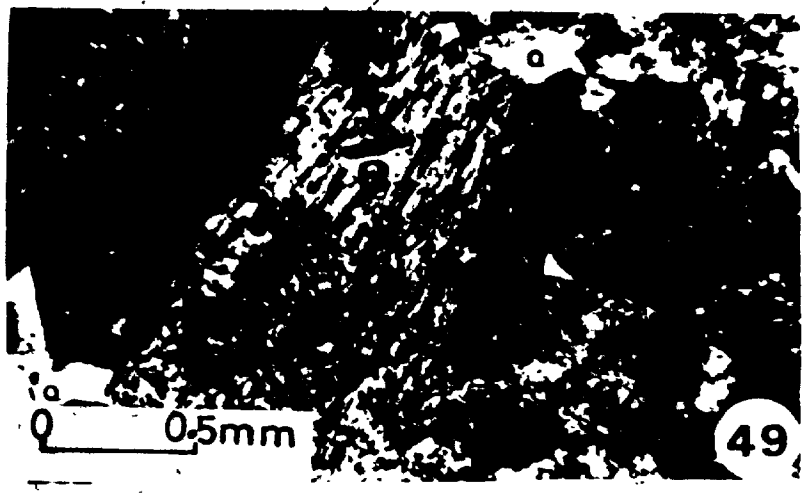
Q
0 0.5mm
49

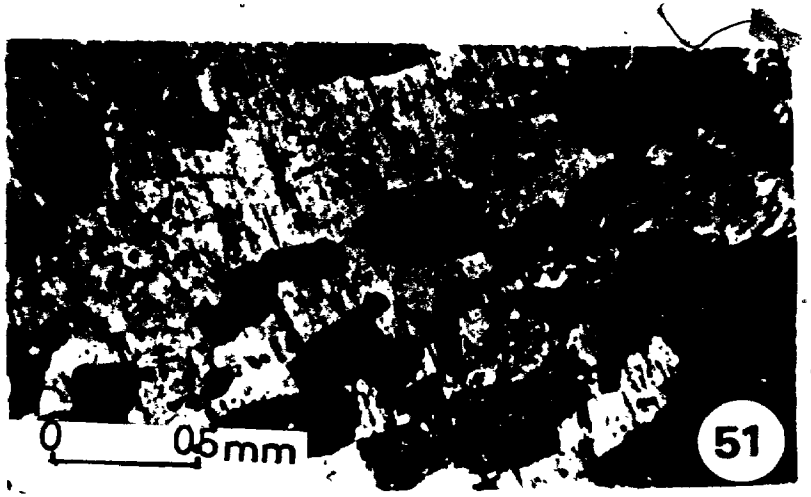
0 0.5mm
51

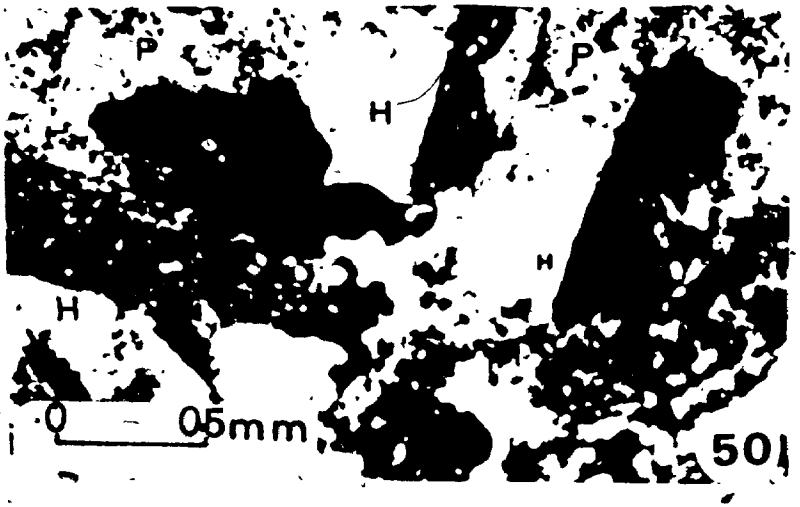
P
H
P
H
H
0 0.5mm
50

0 1mm
52

Fig. 53. The plagioclase (P) is altered to sericite and biotite (B). Anhedral quartz (Q) and prismatic hornblende (H) are also observed. (FM 26).

Fig. 54. Hornblende (H) altered to biotite (B). Anhedral quartz (Q) and plagioclase (P) altered to sericite showing albitized rims are also observed. (FM 19).

Fig. 55. Hornblende (H) altered to biotite (B); a remnant of the hornblende is still existing within the biotite. Anhedral quartz (Q) and zoned plagioclase (P) are observed too. (FM 33).

Fig. 56. Hornblende (H) altered to chlorite (Ch) and epidote (E).

2

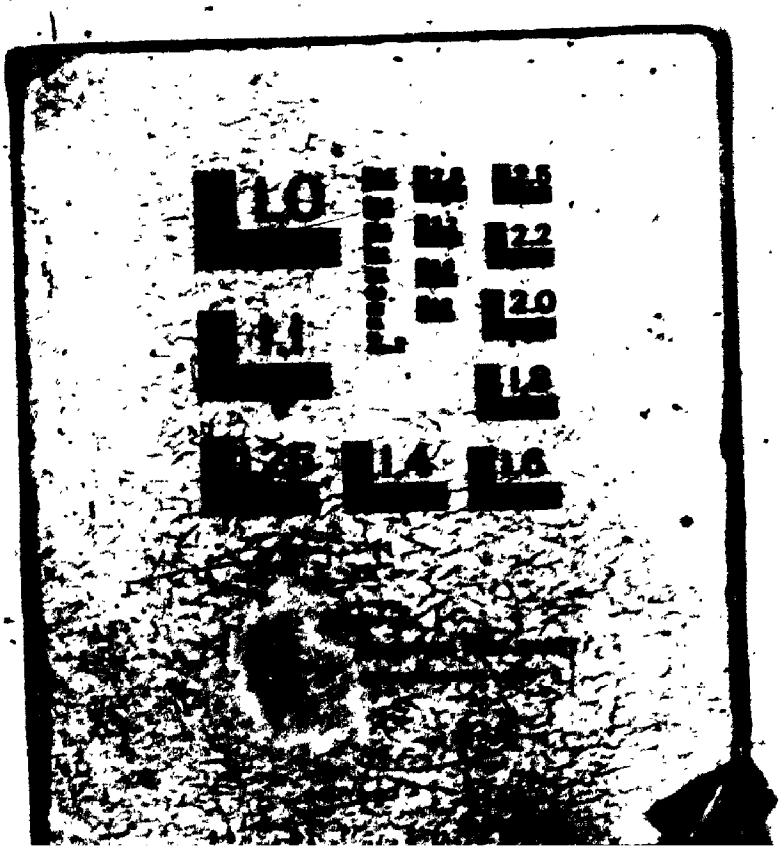

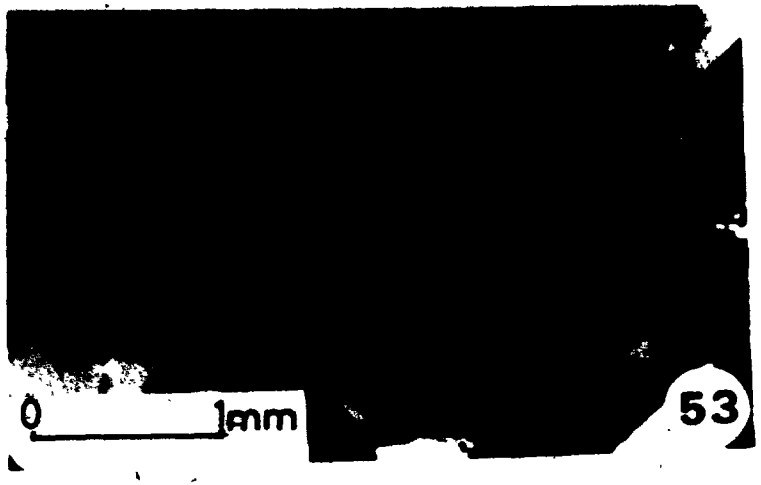
0 1mm
53

0 05mm
55

0 05mm
54

0 05mm
56

Biotite grains generally contain various amounts of inclusions of plagioclase (Fig. 58), quartz and accessory minerals.

Quartz:

The quartz (7%) grains are interstitial and contain inclusions of apatite and zircon.

Accessory Minerals:

The principal accessory minerals in decreasing order of abundance are magnetite, apatite, sphene and zircon. Sphene exhibits extensive fracturing. Zircon is commonly present as inclusions in biotite.

Interpretation of Mineral Data:

The order of crystallization, determined by the conventional method involving relative crystallization and enclosure of one mineral by another, seems to be in the following order: pyroxene, hornblende, and plagioclase, with some degree of overlap. Biotite crystallized over a wide range extending to the termination of plagioclase formation. Quartz was the latest phase to crystallize. The abundance of amphibole replacing pyroxene and crystallizing over a greatly extended range of temperature is almost certainly due to crystallization of a water rich magma at a high vapor pressure (Pitcher and Berger, 1972).

4.4.1 Epidotized Diorite

The epidotized diorites are characterized by extensive alteration, involving the complete replacement of plagioclase by epidote. These altered rocks were recognized in several localities within the Al Hadah igneous complex, generally covering an area up to a few hundred square meters. Macroscopically, these rocks are greenish in colour, equigranular, medium to fine-grained and mainly composed of epidote and amphiboles. The principal petrographic features of these rocks are presented in Table 9. The major mineral phases are described in decreasing order of abundance.

Epidote:

Epidotes (60%) occur as fine-grained aggregates and also as prismatic grains (Fig. 59). Patchy twinning and zoning are characteristic features. Most of the epidotes occur as pseudomorphs after the plagioclase (Fig. 60). Inclusions of ilmenite intergrowing with sphene, magnetite and apatite are common (Fig. 61).

Hornblende:

Hornblende (15%) grains are partially to completely altered to tremolite-actinolite (Figs. 63-64) and occasionally to epidote (Figs. 65, 66). Some grains contain inclusions of sphene, ilmenite, magnetite (Fig. 66), apatite and epidote.

TABLE 9. A summary of the principal petrographic features of the Al Hadah epidotized diorite.

	%	grain size	colour	Remarks
Major Constituents				
Epidote	60%	0.1-0.5 mm	light yellowish-green	anhedral to subhedral prismatic grains, sometimes form veins (0.1-0.3 mm).
Hornblende	15%	1.5-3 mm in length 0.5-1 mm in width	dark green	subhedral to euhedral prismatic grains
Tremolite-actinolite	15%	1.5 mm	colourless to light green	subhedral to euhedral, fibrous
Minor Constituents				
Quartz	7%	0.2 mm	colourless	anhedral, interstitial
Accessory Minerals				
Ilmenite		0.1-0.5 mm	opaque	subhedral to euhedral
Sphene		0.1-0.3 mm	colourless	subhedral to euhedral
Magnetite		0.1-0.3 mm	opaque	subhedral to euhedral
Apatite		0.1 mm	colourless	euhedral, some grain reach up to 1.7 mm.

Fig. 57. Remnants of pyroxene (Px) are enclosed within the hornblende (H). Plagioclase (P) having albite twinning is observed too. (FM 66).

Fig. 58. Biotite grains (B) are enclosing ophitically to subophitically plagioclase crystals. Plagioclase are partially altered to sericite and some still have albite and/or carlsbad twinning. (FM 99).

Fig. 59. A completely epidotized diorite having fine and coarse prismatic epidote crystals (E). Anhedral quartz grains (Q) are seen in association with epidote. (FM 67).

Fig. 60 Epidote (E) grains growing pseudomorphously in place of plagioclase enclosed in a hornblende crystal. (FM 5A).

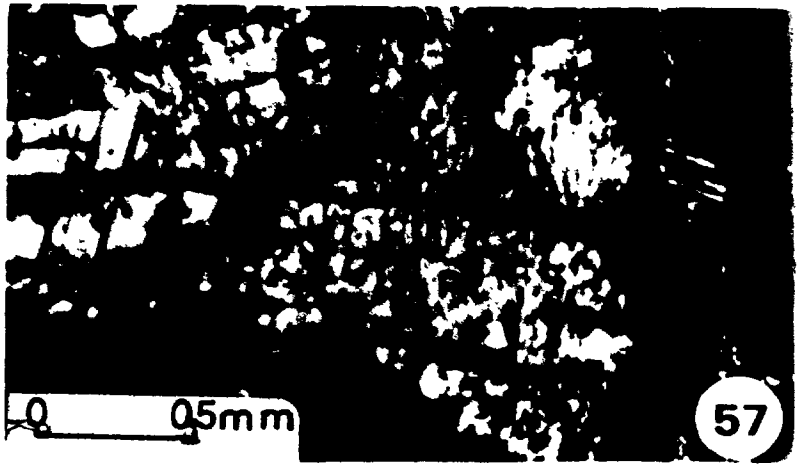
0 0.5mm
57

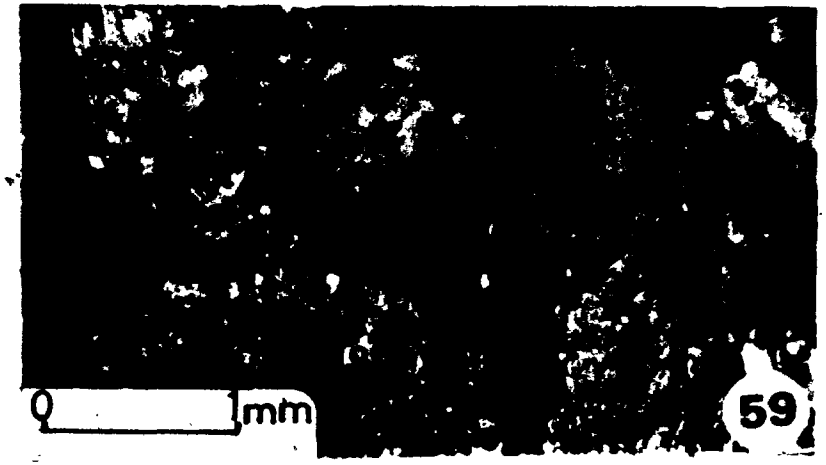
0 1mm
59

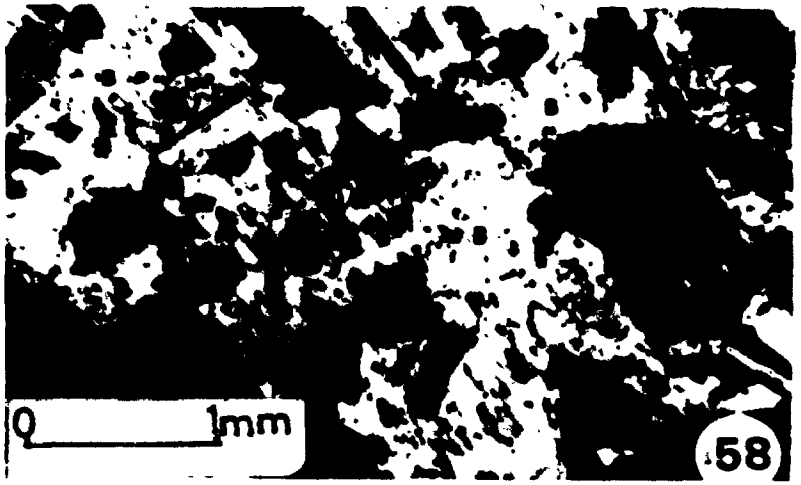
0 1mm
58

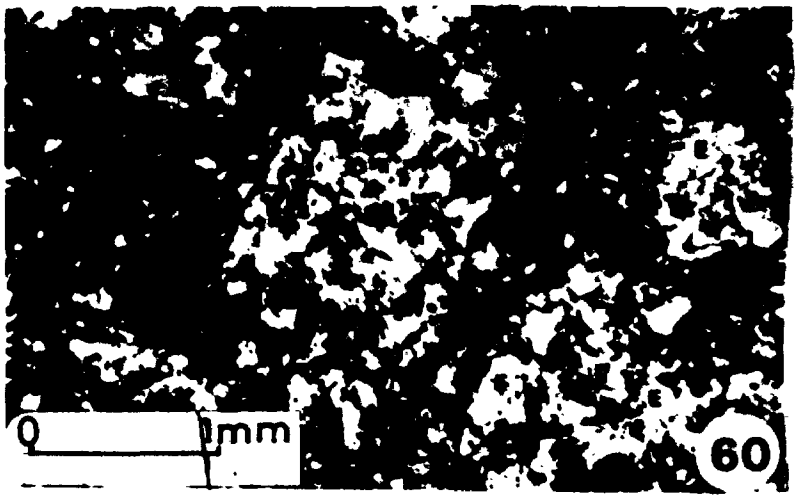
0 1mm
60

Tremolite-Actinolite:

Tremolite-actinolite (15%) grains are well developed as a major alteration product of hornblende and mostly pseudomorphously replacing them (Fig. 64). Furthermore, the tremolite-actinolite grains sometimes occur as a rim, or form an intergrowth with hornblende (Figs. 63, 64).

Minor Constituents:

Quartz:

Quartz (7%) commonly contains inclusions of epidote (Fig. 62).

Accessory Minerals:

The principal accessory minerals in decreasing order of abundance are ilmenite, sphene, magnetite and apatite. Ilmenite exhibits partial alteration to sphene (Fig. 61). Sphene occurs as inclusions within ilmenite, or forms a rim around ilmenite grains.

4.4.2 Hornblende Gabbros

The hornblende gabbros occur as patches within the diorites. They are dark green rocks, generally medium to coarse-grained and equigranular. Plagioclase and hornblende are the major mineral constituents. Their principal petrographic features are presented in Table 10.

Fig. 61. Ilmenite crystals are rimmed by sphene (S); it is also partially altered to sphene and rutile (R). (FM 67).

Fig. 62. Anhedral quartz (Q), containing inclusions of epidote (E). (FM 68).

Fig. 63. Hornblende (H) crystal is partially altered to tremolite-actinolite (T) and slightly to epidote (E). Quartz grains are also developed (Q). (FM 67).

Fig. 64. Hornblende (H) is partially altered to fibrous tremolite (T) and also slightly to epidote (E). (FM 67).

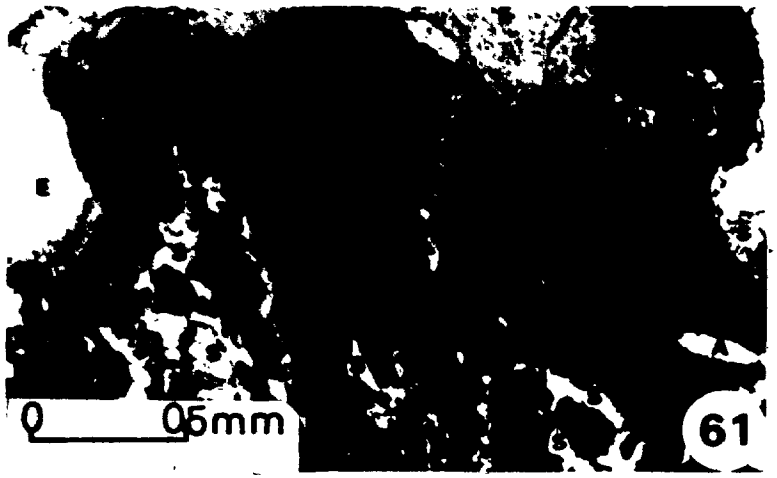
0 0.5mm
61

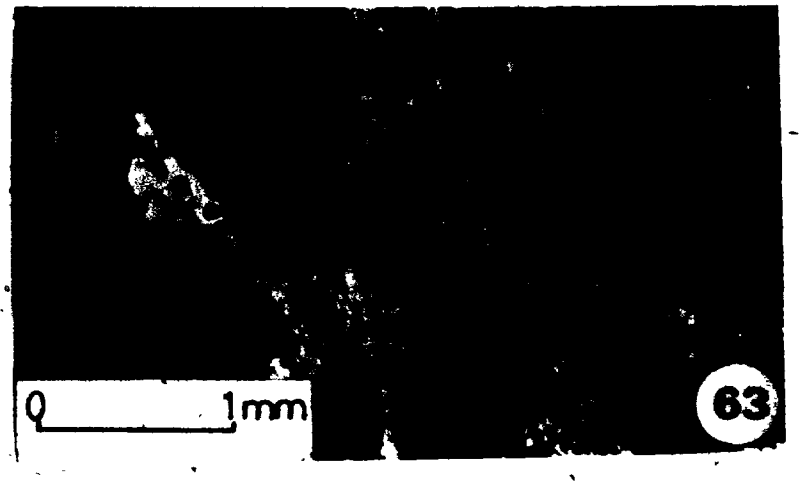
0 1mm
63

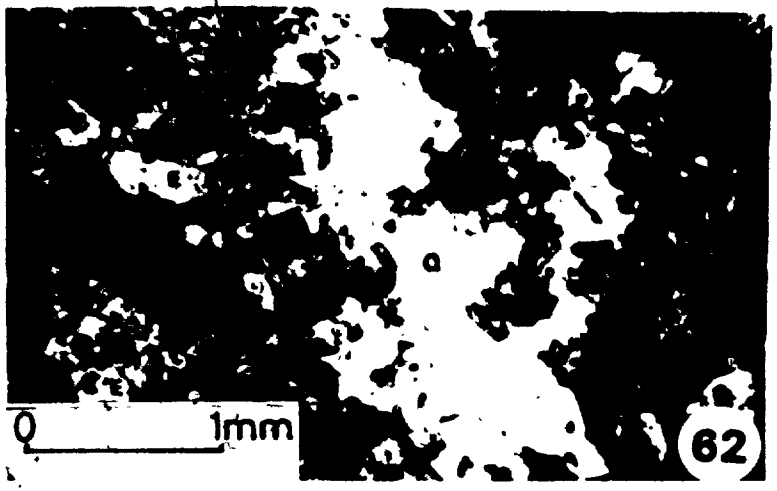
0 1mm
62

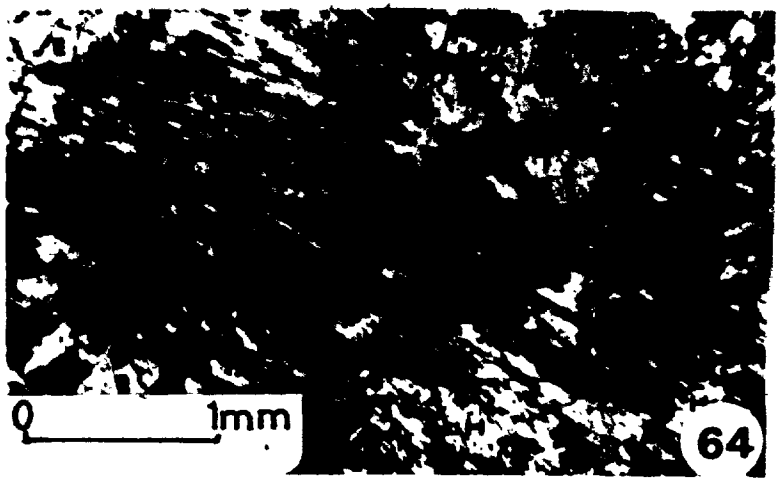
0 1mm
64

TABLE 10. A summary of the principal petrographic features of the Al Hadah hornblende gabbros.

	%	Grain size	Colour	Remarks
Major Constituent				
Plagioclase (An_{46}-An_{52})	60%	1-2.5 mm in length 0.3 mm in width	Colour-less	Subhedral to euhedral columnar and tabular crystals, mostly alter-ed to sericite.
Hornblende	30%	0.5-3.5 mm in length 0.4 mm in width	green	subhedral to euhedral pris-matic crystals, mostly altered to tremolite-actinolite.
Minor Constituent				
Clinopyroxene	5%	0.5-1.5 mm	colour-less	subhedral to euhedral pris-matic crystals.
Accessory Minerals				
Magnetite		0.1-0.4 mm	opaque	subhedral to euhedral, mostly occur as in-clusions in the hornblende.

Plagioclase:

Plagioclase (60%), displays albite, carlsbad and occasional pericline twinning. Their average anorthite content is An_{46}-An_{52} (Andesine-Labradorite). Partial to complete alteration to sericite is characteristic, and sometimes epidote. Inclusions of some major and accessory minerals are common in some of the plagioclase grains.

Hornblende:

Hornblende (30%) is the second major mineral phase. Most of the hornblende grains show ophitic to subophitic texture. Clinopyroxene remnants are observed in a number of hornblende crystals indicating that some of the hornblendes are not primary. Hornblende is commonly altered to fibrous crystals of tremolite-actinolite (Figs. 67, 68), biotite and sometimes chlorite. Inclusions of plagioclase, magnetite and apatite are common.

Minor constituents:

Clinopyroxene:

Clinopyroxene (5%) occurs mostly as remnants or relicts enclosed within the hornblende grains (Fig. 69) or tremolite-actinolite. Inclusions of magnetite are common in the clinopyroxene grains.

Accessory Minerals:

The main accessory mineral is magnetite which

Fig. 65 & Fig. 66. Hornblende (H) partially altered to epidote (E), ilmenite (black) and sphene. (FM 67).

Fig. 67. Hornblende completely altered to tremolite-actinolite (T-A). The altered hornblende crystal encloses ophitically euhedral plagioclase crystal which is completely altered to sericite. (FM 64).

Fig. 68. Hornblende (H) partially altered to tremolite (T). (FM 112).

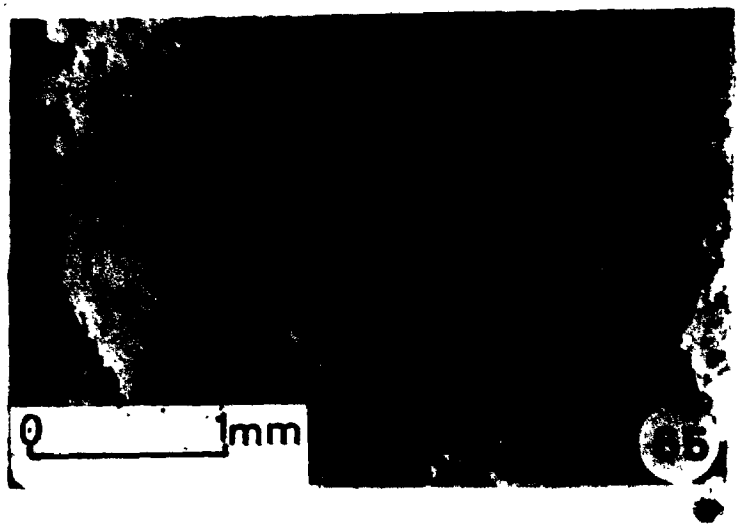
0
1mm
65

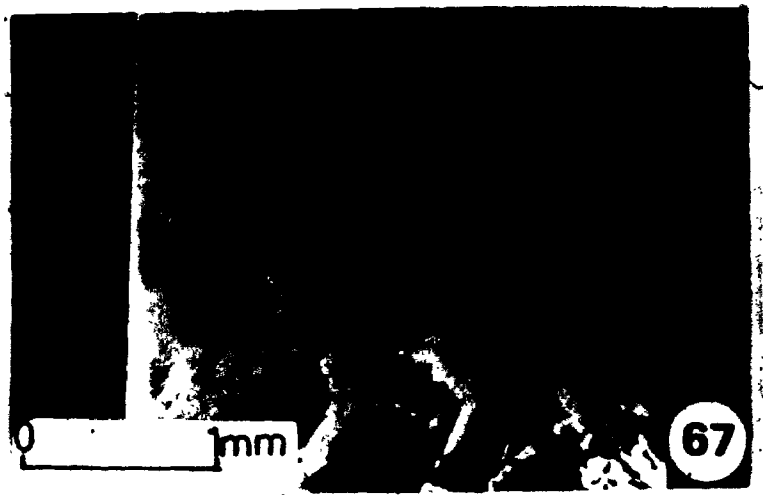
0
1mm
67

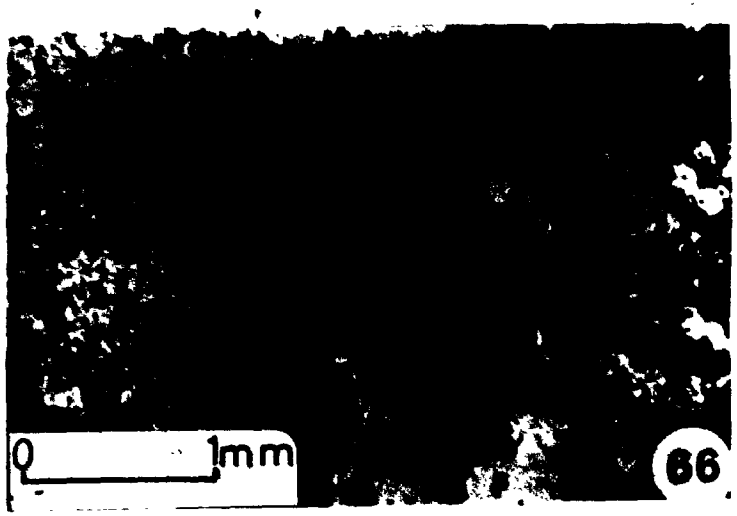
0
1mm
66

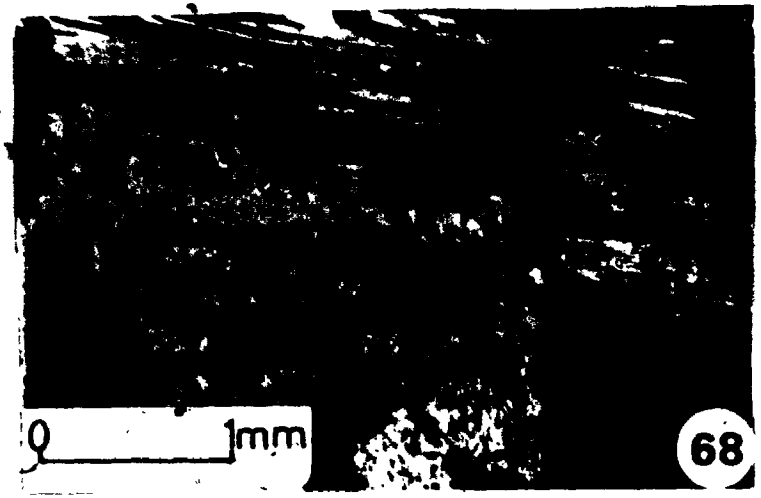
0
1mm
68

occurs mostly as inclusions in the hornblende.

4.5 Granodiorite:

Macroscopically this rock is light greyish in colour, medium to coarse grained and equigranular (Fig. 70). Plagioclase, potash feldspar and quartz are the major mineral phases, with biotite and hornblende as minor constituents. The principal petrographic features for this rock type are presented in Table 11. The modal analyses are given in Table 12.

Plagioclase:

Plagioclase (47%) is the most abundant mineral in these rocks: the average composition is oligoclase (An_{15}). The characteristic features of the plagioclase grains are albite, carlsbad and pericline twinning, along with normal zoning. The core of the plagioclase crystals are extensively altered, while fresh albite rims are formed (Fig. 71). The main alteration product is sericite and occasional epidote. Some of the plagioclase grains seem to be replaced by potash feldspar (Fig. 72, 73). Inclusions of biotite, zircon, apatite and vermicular quartz (=myrmkeites) are observed.

Potash feldspar:

Perthitic microcline (20%) is characterized by cross hatched twinning with thin strings of plagioclase

TABLE 11. A summary of the principal petrographic features of the Al Hadah granodiorite.

	%	Grain size	Colour	Remarks
Major Constituents				
Plagioclase (An_{15})	47%	0.5-2 mm in length 0.5 mm in width	colourless	subhedral to euhedral columnar and tabular crystals, twinned and zoned.
Potash feldspar (microcline perthite)	20%	1-3 mm	colourless	anhedral and interstial filling areas between relative euhedral plagioclase, occasionally twinned and zoned.
Quartz	23%	2 mm	colourless	anhedral and interstitial show undulatory extinction.
Minor Constituent				
Biotite	7%	0.5-1 mm	dark brown	subhedral to euhedral flaky crystals
Hornblende	3%	0.1-1 mm	green	subhedral to euhedral prismatic crystals
Accessory Minerals				
Sphene		0.2 mm	colourless	subhedral to euhedral
Apatite		0.1 mm	colourless	euhedral, prismatic
Zircon		0.1 mm	colourless	euhedral, prismatic
Magnetite		0.1- 0.2 mm	opaque	subhedral to euhedral

TABLE 12. Modal analyses (in percent) of the granodiorite

	FM150	FM134	FM133	FM129	FM131	FM122
Plagioclase	45	48	47	50	45	49
Perthite	20	21	19	16	15	17
Quartz	24	21	26	25	24	25
Biotite	10	9	7	8	10	7
Accessory	1	1	1	2	5	2
An. Content	14	14	10	12	10	12

Fig. 69. Hornblende prismatic crystals (H) containing remnants of pyroxene. Plagioclase (P) grains are partially to completely altered to sericite. (FM 64).

Fig. 70. A handspecimen of the granodiorite composed of plagioclase, microcline perthite, quartz, biotite and hornblende. (FM 50).

Fig. 71. Euhedral zoned plagioclase (P) having extensively altered cores and albitized rims. Microcline perthite and anhedral quartz (Q) are also observed. (FM 50).

Fig. 72. Microcline perthite replacing plagioclase (P). The plagioclase has albite twinning. The section also shows anhedral quartz (Q). (FM 133).

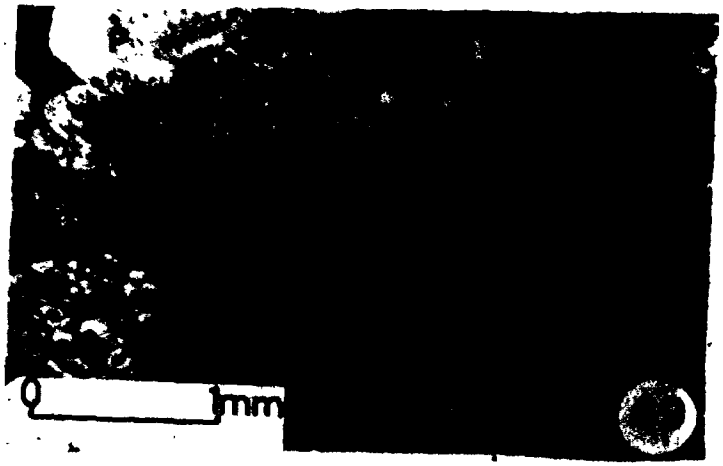
0
1mm

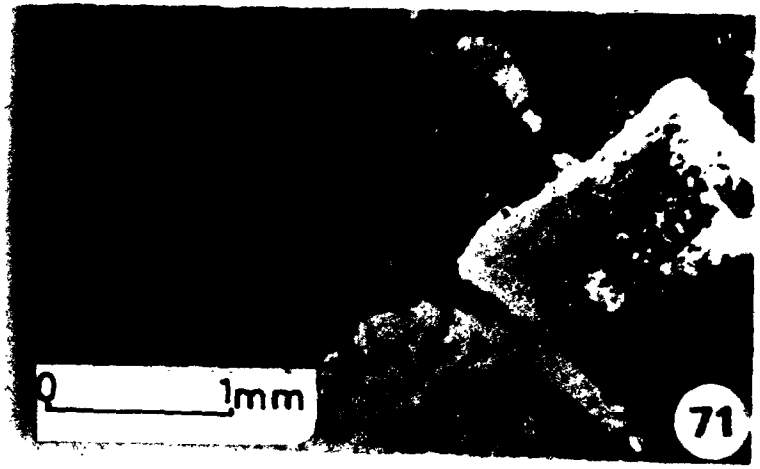
0
1mm
71

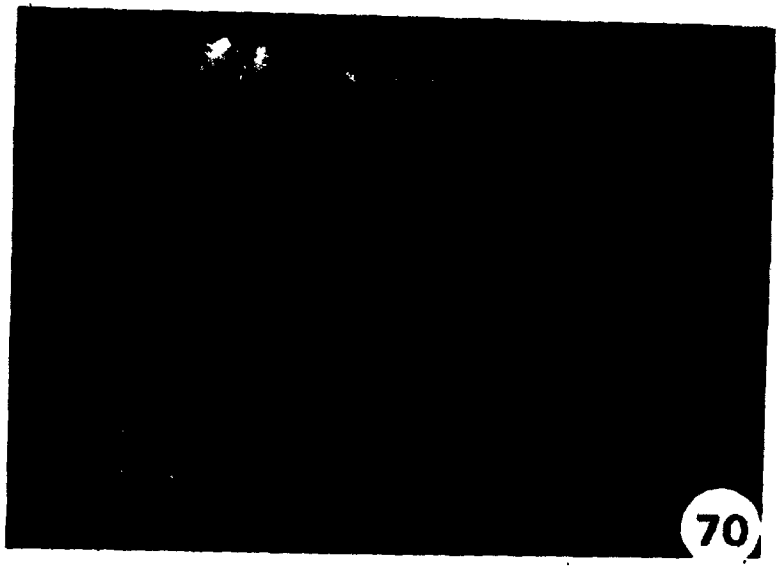
70

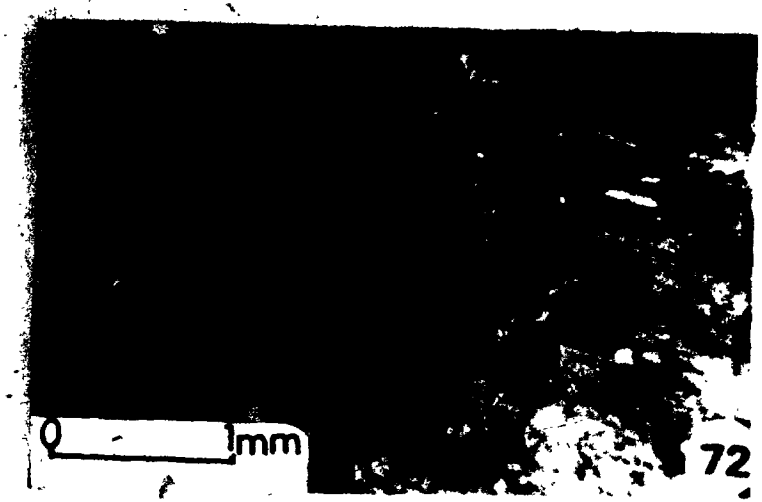
0
1mm
72

intergrowths (Fig. 75). Occasionally they show zoning and polysynthetic twinning (Fig. 74). Typically, biotite and quartz are present as inclusions.

Quartz:

Quartz (23%) grains are interstitial between the plagioclase and the potash feldspar. Inclusions of biotite, apatite and zircon are common.

Minor Constituents:

Biotite:

Biotite (7%) is the most abundant mafic mineral in these granodiorite rocks. Inclusions of zircon surrounded by pleochroic haloes, and magnetite are typical in the biotite grains.

Hornblende:

The hornblende (3%) grains contain inclusions of biotite, quartz, plagioclase, zircon and magnetite.

Accessory Minerals:

The main accessory minerals in this rock are sphene, apatite, zircon and magnetite.

Interpretation of Mineral Data:

From the description of the mineral constituents and the textural relationships it is possible to draw up a model of the paragenetic sequence of crystallization. Some of the textures could be interpreted as the result of crystallization from magma; examples are zoning in the

Fig. 73. Microcline perthite (MP) appears to be replacing plagioclase; plagioclase (P) grains are also altered to biotite (B). (FM 441).

Fig. 74. Microcline perthite (MP) has poly-synthetic twinning. Plagioclase (P) grains with extensively altered cores and albitized rims are observed too. The (MP) show very slight alteration to biotite (B). (FM 134).

Fig. 75. Zoned plagioclase (P) having extensively altered cores are observed along with anhedral microcline perthite (MP) and quartz (Q). (FM 133).

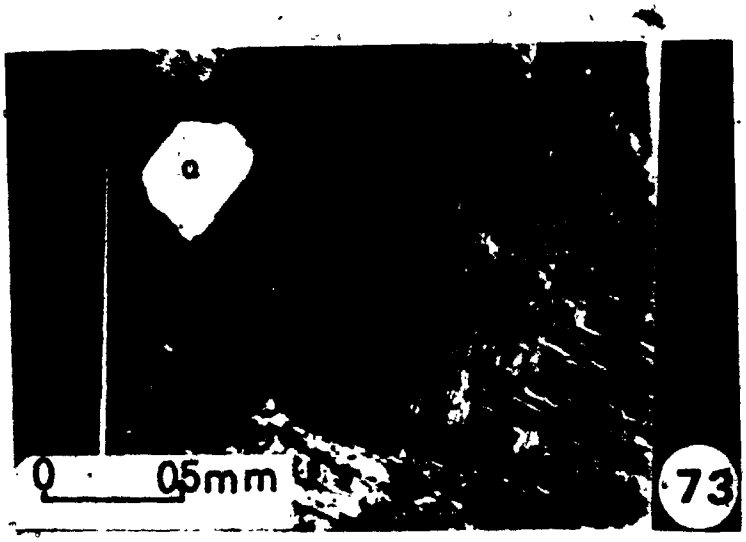
a
0 0,5mm
73

P
P
0 1mm
74

MP
P
0 1mm
75

plagioclase and simple twinning observed in both plagioclase and potash feldspar. On the other hand, some of the features described earlier, such as the replacement of plagioclase by K-feldspar could be interpreted as late stage replacement. A simplified model of crystallization shows that the plagioclase crystallized early from the liquid magma and it seems that there was continued growth of plagioclase at the expense of the mafic minerals hornblende and biotite. The bulk of quartz and potash feldspar seems to have crystallized last, filling the interstitial spaces between the relatively euhedral plagioclases. A late stage replacement process is indicated by the replacement of the early formed plagioclase by potash feldspar.

4.6 Biotite Monzogranite:

The biotite monzogranite is light pinkish in colour, coarse grained and slightly porphyritic with relatively large crystals of pinkish potash feldspar which are often rimmed by whitish plagioclase (Fig. 76). The major mineral constituents are plagioclase, potash feldspar and quartz, with biotite as a minor constituent. The principal petrographic features of this rock type are presented in Table 13; and the modal analyses are given in Tables 14 and 15.

TABLE 13. A summary of the principal petrographic features of the Al Hadah biotite monzogranite.

	%	grain size	colour	remarks
Major Constituents				
Plagioclase	40%	1-2.5 mm in length 0.3 mm in width	colour-less	subhedral to euhedral tabular and columnar grains, twinned and zoned.
Potash feldspar	29%	2-4 mm	colour-less	anhedral grains filling interstitial areas between enhedral plagioclase.
Quartz	25%	1-3 mm	colour-less	anhedral, interstitial, show strong undulatory extinction.
Minor Constituent				
Biotite	5%	0.5-1 mm	brown	subhedral to euhedral flaky crystals.
Accessory Minerals				
Sphene		0.2-1 mm	colour-less	subhedral to euhedral prismatic crystals
Apatite		<0.1 mm	colour-less	euhedral acicular or six-sided prismatic crystals.
Zircon		<0.1 mm	colour-less	euhedral prismatic crystals
Magnetite		0.1 mm	opaque	subhedral to euhedral crystals.

TABLE 14. Modal analyses (in percent) of biotite monzogranite

	FM13	FM14	FM15	FM16	FM94	FM18
Plagioclase	40	41	41	39	41	40
Perthite	28	36	29	27	29	27
Quartz	26	25	25	28	23	27
Biotite	6	5	5	6	6	5
Accessory	1					1
An. Content	12	10	10	12	11	12

TABLE 15. Thin section modal analysis (in percent) of samples from non-layered parts of the Al Hadah pluton. (After Hadley and Greenwood, 1976).

Samples	1	2	3	4	5
Quartz	30.3	20.5	20.1	24.9	26.7
Potassium feldspar	34.1	14.3	36.2	37.5	34.5
Plagioclase	30.6	45.2	33.5	37.1	29.4
Myrmekite	-	-	1.1	0.6	Tr*
Hornblende	-	5.4	0.6	Tr	1.9
Biotite	5.0	14.6	6.6	4.1	6.7
Chlorite	-	-	0.8	0.4	0.2
Sericite	-	-	0.2	Tr	Tr
Opaque minerals	-	Tr	Tr	Tr	0.4
Hematite	-	-	-	-	0.2
Sphene	Tr	Tr	0.8	0.6	Tr
Allanite	-	-	0.2	Tr	Tr
Zircon	Tr	Tr	Tr	Tr	Tr
Epidote	-	-	Tr	Tr	Tr
Calcite	-	-	Tr	0.6	Tr
Apatite	Tr	Tr	Tr	-	-
Total percent	100.0	100.0	100.0	99.8	100.0
No. point counts	600	600	636	469	565
Sample number	TFT-6	TFT-7	81573	81574	81575
Rock type	Qtz. monz.	Granodio.	Qtz. monz.	Qtz. monz.	Qtz. monz.

Tr* = Trace

Plagioclase:

Plagioclase (40%) has an average composition in the oligoclase range (An_{11}). Albite, carlsbad and pericline twinning together with normal zoning are common features in the plagioclase grains (Fig. 77). Various degrees of alteration are observed: the cores of the plagioclase grains, in particular, are extensively altered (Fig. 78) while albite rims are developed. The alteration product is mainly sericite and sometimes epidote. Furthermore, plagioclase grains are partially replaced by biotite and in some cases by potash feldspar (Figs. 78 and 82). Myrmeketic quartz inclusions are often observed on the rims of the plagioclase bordering the potash feldspar (Fig. 79).

Potash feldspar:

Microcline perthite grains (29%) are often seen rimmed by plagioclase (Fig. 81). Zoning and polysynthetic twinning are common (Fig. 80). Patches and stringers of well twinned exsolved plagioclase, together with inclusions of biotite, sphene and zircon are commonly observed in the potash feldspar grains.

Quartz:

Quartz is the third major mineral constituent: inclusions of biotite, apatite and sphene are common.

Fig. 76. A handspecimen of the monzogranite. It has a light pinkish color and it is composed of coarse-grained K-feldspar, plagioclase, quartz and biotite. The K-feldspar are rimmed by plagioclase.

Fig. 77. Albite and pericline twinning are observed in plagioclase (P). Plagioclase grains also have zoning and partial alteration to sericite. Anhedral quartz (Q), chlorite (CH) and accessory sphene (S) are observed too. (FM 13).

Fig. 78. Microcline perthite (MP) enclosing laths of plagioclase (P). (FM 18).

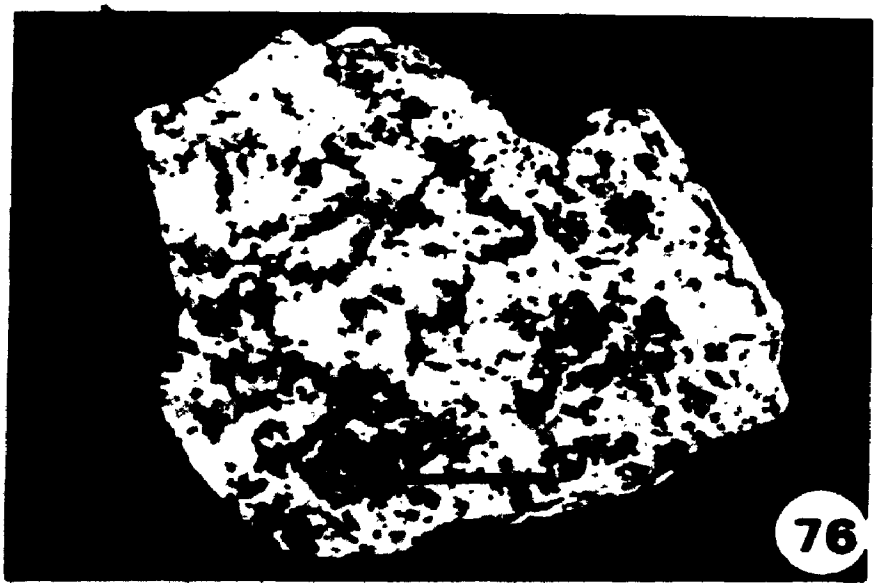
76

0
1mm
77

0
1mm
78

Fig. 79. Myrmekites developed on the border between plagioclase (P) and microcline perthite (dark grey). (FM 14).

Fig. 80. Polysynthetically twinned microcline perthite. (FM 94).

Fig. 81. Microcline perthite (MP) rimmed by plagioclase (P). (FM 94).

Fig. 82. Microcline perthite (MP) replacing plagioclase (P). (FM 541).

0 0.5mm

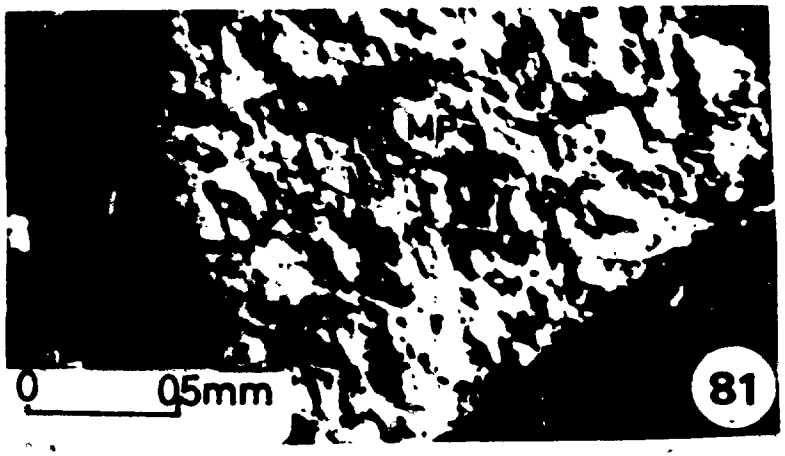
MP
0 0.5mm
81

0 0.5mm

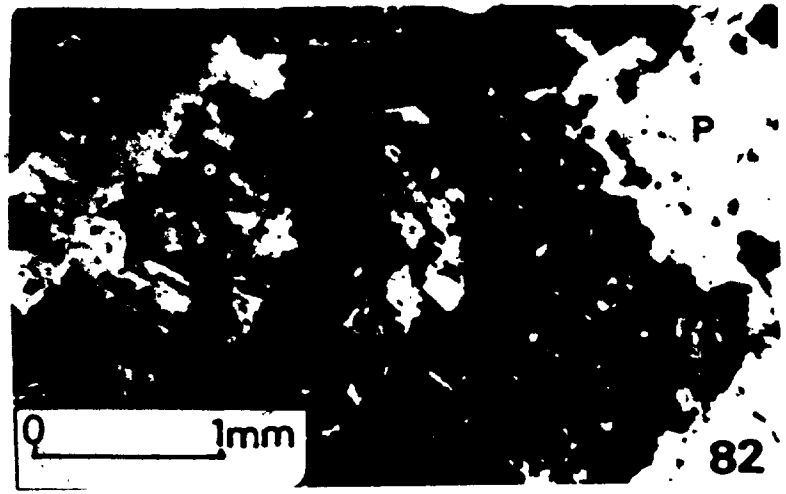
P
0 1mm
82

Minor Constituents:

Biotite:

Biotite is the only minor constituent and the most abundant mafic mineral in this rock type. Some grains show partial to complete alteration to chlorite (Fig. 77) and sometimes form an intergrowth with one another. Inclusions of magnetite and zircon surrounded by pleochroic haloes are common.

Accessory Minerals:

The principal accessory minerals in decreasing order of abundance are sphene, apatite, zircon and magnetite.

Interpretation of Mineral Data:

A simplified model of crystallization, based on the occurrence of the previously mentioned main mineral constituents and their textural relationship, may be drawn up to trace the paragenetic sequence of crystallization. It seems that plagioclase and biotite were the early crystals formed. The crystallization of the plagioclase continued over a wide range of temperatures and most probably at the expense of mafic minerals. The formation of the plagioclase could have been under conditions either of fractional crystallization or of equilibrium crystallization. Those formed under conditions of fractional crystallization would be zoned over a wide range, while those that were formed under equilibrium crystallization

conditions have reacted continuously with the magma to become more and more sodic and thus will not be zoned. The cores of the plagioclases which are highly sericitized, are not zoned at all, indicating equilibrium crystallization. Later plagioclase grains which were not formed by equilibrium crystallization are not sericitized. The quartz and potash feldspars were the last minerals to crystallize filling the interstitial areas between the relatively euhedral plagioclase crystals.

Myrmekite Origin in the Granodiorite and Monzogranite:

A short discussion on the presence of myrmekites which have been observed in the granodiorites and biotite monzogranite, occurring in the form of rims between plagioclases and the microcline perthite is presented here. It has been found that there is, usually, some correlation between Ca content of the rock and the amount of myrmekite present (Hubbard, 1966; Phillips, 1964). Beck (1908) concluded from his studies on myrmekites that the more calcic the plagioclase in myrmekite, the higher the quartz content. In fact, an accurate estimate of the abundance of quartz in myrmekite is difficult to obtain because of the fine-grained nature of the intergrowth.

Recently Ashworth (1972), Barker (1970), and Phillips and Ransom (1968) have concluded that they have found some evidence which suggests that a proportionality

relationship does exist. The situation however, is not yet clear, for myrmekites may have been formed in more than one way. Concerning the genesis of these myrmekites, Ashworth (1972) found that myrmekites, genetically, fall into two groups: the first group are those which are generated by metasomatic processes involving the replacement of potash feldspar by plagioclase, or visa versa. The second group are those which are formed by exsolution from potash feldspar. Phillips (1974) discussed the genesis of myrmekites under six broad headings:

1. Simultaneous or direct crystallization.
2. Replacement of potash feldspar by plagioclase.
3. Replacement of plagioclase by potash feldspar.
4. Solid state exsolution.
5. Recrystallizing quartz involved with basaltic plagioclase.
6. Miscellaneous hypothesis including combinations of some of the hypothesis listed under 1 to 5 above.

According to Phillips (1974), solid state exsolution is the most acceptable explanation of the genesis of myrmekites, and this hypothesis has been supported by experimental foundation.

4.7 Dikes

The dikes have been divided according to their composition into two groups: felsic dikes and mafic dikes. (For Chemical composition see Appendix B, Tables 5B, 6B.)

4.7.1 Felsic Dikes:

The felsic dikes can be subdivided according to their texture into two main subgroups: (1) aplitic to microgranitic, and (2), rhyolitic dikes. The aplitic and microgranitic subgroups are generally whitish in colour, fine to medium grained, and mostly equigranular. The rhyolitic subgroup are pinkish in colour, very fine grained, and mostly quartz porphyritic.

The microgranitic dikes are mainly composed of plagioclase, frequently showing albite and carlsbad twinning. Graphic and poikilitic texture are common features in some of the plagioclase grains. Their average size is 0.6 mm in length and about 0.5 mm in width. The average anorthite content is about An_{12} (oligoclase). Plagioclase grains are partially to completely altered to sericite with minor epidote. The second major mineral present is potash feldspar which occurs both as microcline and microcline perthite. These feldspars form anhedral grains, with a size ranging from 0.5-2 mm in diameter. Some polysynthetic

twinning and graphic texture are also observed in the potash feldspar grains. The third major mineral is quartz present as anhedral grains ranging in size from 0.5-1 mm in diameter. The minor constituents are mainly muscovite and/or biotite (0.5-1 mm). The volume percentage of these mafic constituents is 5-7 . The main accessory minerals are magnetite and apatite.

The rhyolitic dikes are very fine-grained to glassy, composed mainly of plagioclase, microcline and microcline perthite plus quartz. The dikes have a graphic or vitric texture.

4.7.2 Mafic Dikes:

The mafic dikes are compositionally similar to one another. These dikes are generally very dark greenish to blackish, fine to medium grained, and equigranular to porphyritic with plagioclase phenocrysts up to 1 cm in diameter. Microscopically, their major constituents are plagioclase and hornblende. The plagioclase occurs as fine-grained crystals (<0.5 mm) and as phenocrysts (1-4 mm). Plagioclase is strongly zoned and shows albite and carlsbad twinning. The composition of the plagioclase crystals varies between An_{36} to An_{48}, and in some dikes it is An_{60} (FM 4 db). Plagioclase is partially to completely altered

to sericite, and occasionally to epidote. The volume percent of plagioclase is about 50 . The second major constituent is hornblende occurring as prismatic crystals (0.5-1 mm in diameter). Some grains are polysynthetically twinned, and some show ophitic to subophitic texture. They are partially to completely altered to tremolite-actinolite, chlorite and magnetite. In some cases the hornblende pseudomorphously replace augite or may form a rim around it. The volume percent is 40 . There are two main minor constituents; biotite in some cases and augite in others. Biotite is mainly an alteration product from the hornblende and it is in turn partially altered to chlorite. The augite occurs as prismatic crystals. Their size is about 0.7 mm in diameter. They show ophitic to subophitic texture. Most of the augite crystals are completely replaced by hornblende.

The main accessory minerals in mafic dikes are magnetite, sphene, and quartz.

CHAPTER 5

PETROCHEMISTRY

5.1 Introduction:

The purpose of analysing rocks of the Al Hadah igneous complex is: 1) to classify the rocks using their normative and modal values, 2) to compare the abundances of major and minor elements and determine comagmatic relationships and if possible differentiation trends, and 3) to compare the chemical composition of Al Hadah plutonic rocks to those volcanic and plutonic rocks formed in subduction zones. The reason for this comparison is to evaluate recent hypotheses applying island arc models for the southern part of the Arabian Shield, which includes the area studied (Greenwood, et al., 1975; Nasseef and Gass, 1976).

Rocks of the Al Hadah complex have been classified after Streckeisen (1967) and Irvine and Baragar (1971). A number of variation diagrams have been constructed to portray fractionation processes that took place in the evolution of the pluton. Finally, absolute abundances of major element oxides and trace elements in both Al Hadah pluton and

Cascades, S.W. Pacific island arcs, Andes and Sierra Nevada have been compared. Sampling and analytical methods used are presented in Appendix A.

5.2 Classification:

Representative samples of the different rock types were chemically analysed and recalculated for CIPW norms (Appendix B, Tables, 1B, 2B, 3B and 4B). Normative values for quartz (Qz), Ab + An (Pl) and orthoclase (Or) were used to classify the plutonic rocks of Al Hadah complex. The Al Hadah plutonic rocks are mainly within three fields: 1) Field 10 (= diorite and gabbro), 2) Field 4 (= granodiorite), and 3) Field 3B (= Monzogranite) (Fig. 83). This chemical classification is in accordance with the modal classification of Fig. 84.
On the basis of plagioclase composition and alumina content the dioritic rocks of Al Hadah pluton fall within the calc-alkaline field (Fig. 85).

5.3 Comagmatic Relationships:

The Al Hadah plutonic rocks are, on the basis of element abundances, of two major rock groups: 1) the dioritic group, including both the diorites and the gabbroic enclaves enclosed within them, and 2) the granitic group including both the granodiorite and the monzogranite.

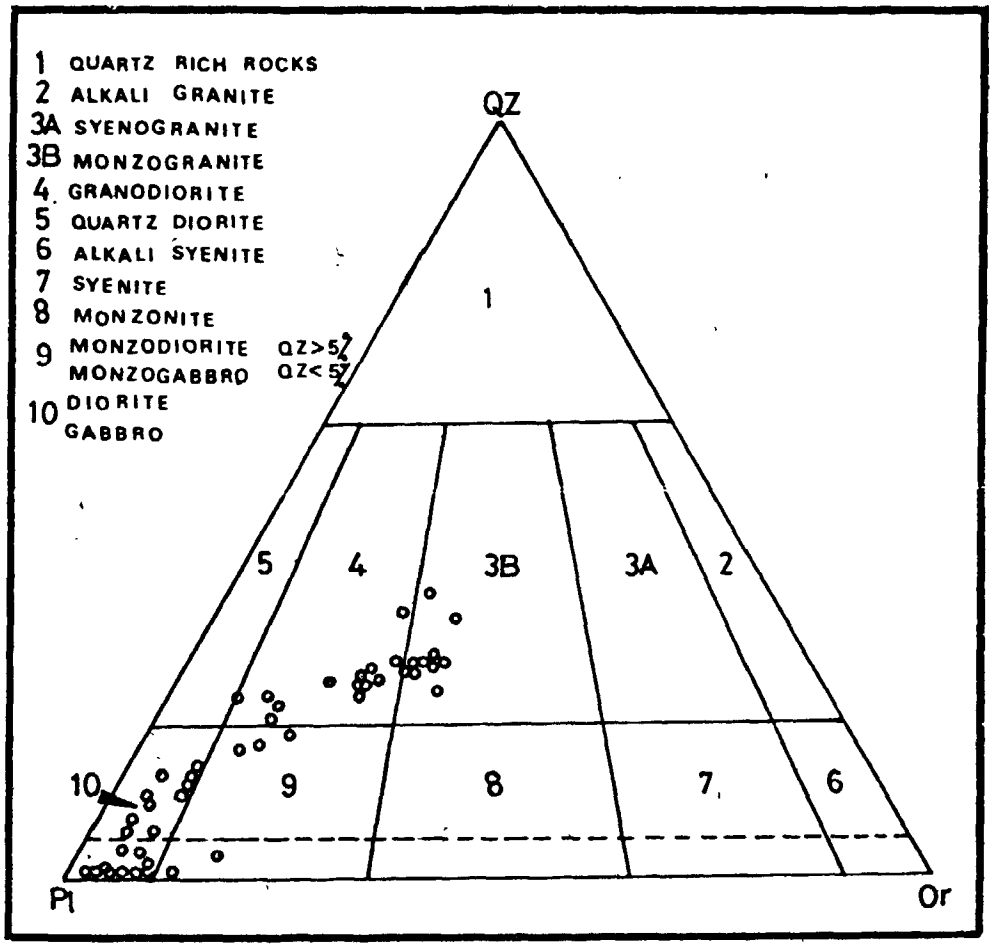

Fig. 83. Normative classification of rocks of Al Hadah Pluton (after Streckeisen, 1967).

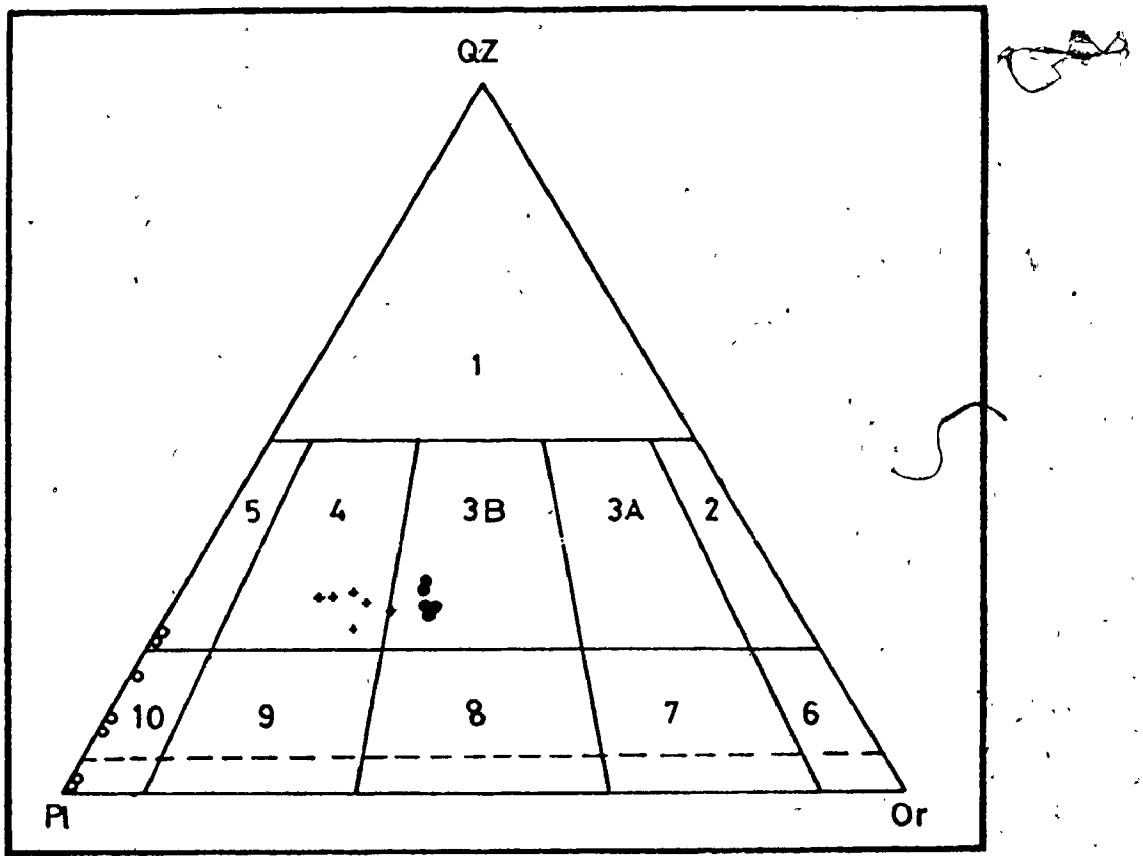

Fig. 84. Modal classification of rocks of Al Hadah Pluton (after Streckeisen, 1967).
o dioritic group (diorite and gabbro)
+ granodiorite
● monzogranite

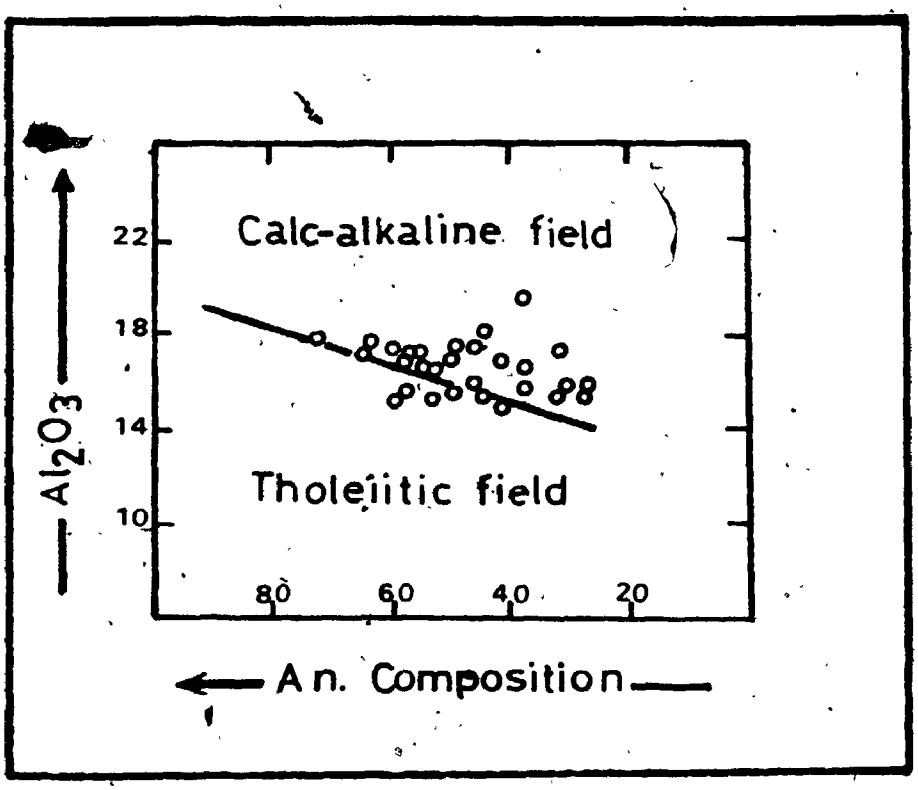

Fig. 85. The division between Tholeiitic and Calc-alkaline fields (After Irvine and Bargar, 1971).
Note = The dioritic rocks of Al Hadah Pluton fall within the calc-alkaline field.

5.3.1 Major Element Abundances:

(1) The Dioritic Group:

The major element oxide components of the dioritic group are presented in Appendix B, Tables 1B and 2B. Their averages are shown in Table 16. The variation in some major elements of the dioritic group is illustrated relative to: (1) silica content (Harker, 1909), (2) Mafic index, M, (Wager and Deer, 1939), and (3) Differentiation index, DI, (Thorton and Tuttle, 1960).

The averages of MgO and $Fe_2O_3t^*$ are about 6.5% and 9.5% respectively. The dioritic group is characterised by relatively large magnesium and total iron. The plots of MgO and Fe_2O_3t against the silica content (Fig. 86) have a distinct pattern, where MgO and Fe_2O_3t decrease with an increase in silica. Furthermore, the Mg content was plotted against the Mafic Index ($M = \frac{Fe \times 100}{Fe + Mg}$) (Fig. 87b). This diagram has a distinct trend in which Mg decreases progressively from the gabbroic to the dioritic rocks with respect to an increase in the Mafic Index. In addition, the Fe_2O_3t/MgO was plotted against Thorton and Tuttle's (1960) Differentiation Index (DI), (Fig. 87c). This diagram has a weak trend in which Fe_2O_3t/MgO ratio increase with an increase in the DI.

The Al Hadah dioritic group is characterized by large Al_2O_3 (average = 17.0%) content which is typical of calc-alkaline

$Fe_2O_3t^* = FeO + Fe_2O_3$

TABLE 16. The average and range of major element oxides of the gabbroic patches and the diorites of Al Hadah Pluton.

	GABBRO		DIORITE	
	Av.*	Range	Av.**	Range
SiO_2	48.59	45.8-50.2	55.53	50.9-64.5
TiO_2	1.22	0.4- 2.0	1.04	0.3- 1.9
Al_2O_3	16.28	14.7-17.6	17.56	14.5-20.6
Fe_2O_3	3.76	2.2- 5.1	3.35	1.6- 6.7
FeO	6.56	5.0- 9.7	5.52	3.4- 8.6
MnO	0.16	0.1- 0.2	0.15	0.1- 0.2
MgO	8.17	6.0-11.9	4.28	1.6- 8.0
CaO	9.13	7.5-10.5	7.12	3.5-10.4
Na_2O	2.57	1.6- 3.2	3.69	2.3- 4.9
K_2O	0.73	0.3- 1.7	1.09	0.5- 2.2
P_2O_5	0.28	0.1- 0.8	0.25	0.1- 0.5
Total	97.45		99.58	
Q	0.9	0.0- 4.0	8.2	0.0-20.8
or	4.6	1.8-10.3	6.5	2.9-13.1
ab	22.1	13.8-28.6	31.8	19.7-42.4
an	31.4	25.4-40.8	25.5	15.3-37.3
di	10.5	3.5-19.5	7.1	1.2-13.6
hy	18.2	9.7-26.3	13.0	6.2-19.5
ol	3.7	0.0-10.8	0.3	0.0- 5.7
mt	5.6	3.4- 7.5	4.9	2.4-10.0
il	2.3	0.9- 3.8	2.0	0.6- 3.7
ap	0.7	0.2- 1.9	0.6	0.2- 1.9

* Average of 12 analyses

** Average of 19 analyses

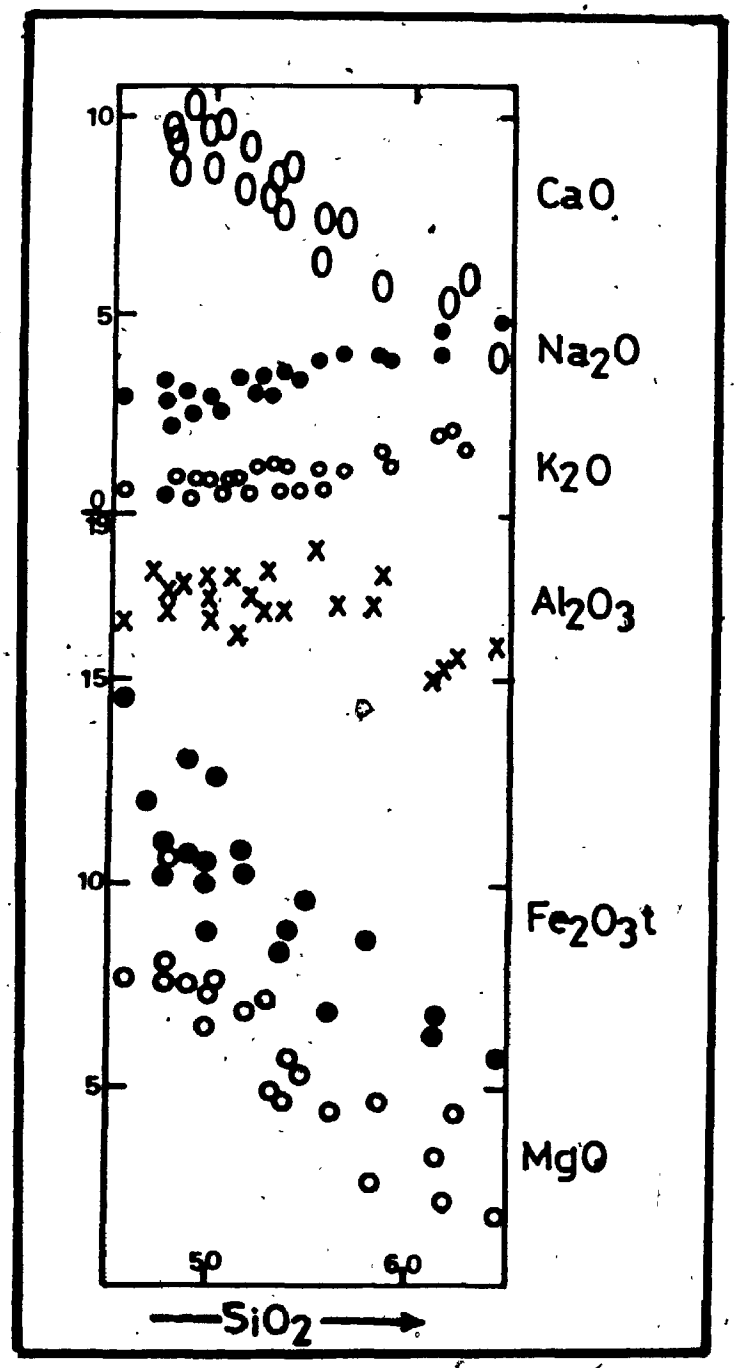

Fig. 86. Harker variation diagram for the dioritic group.

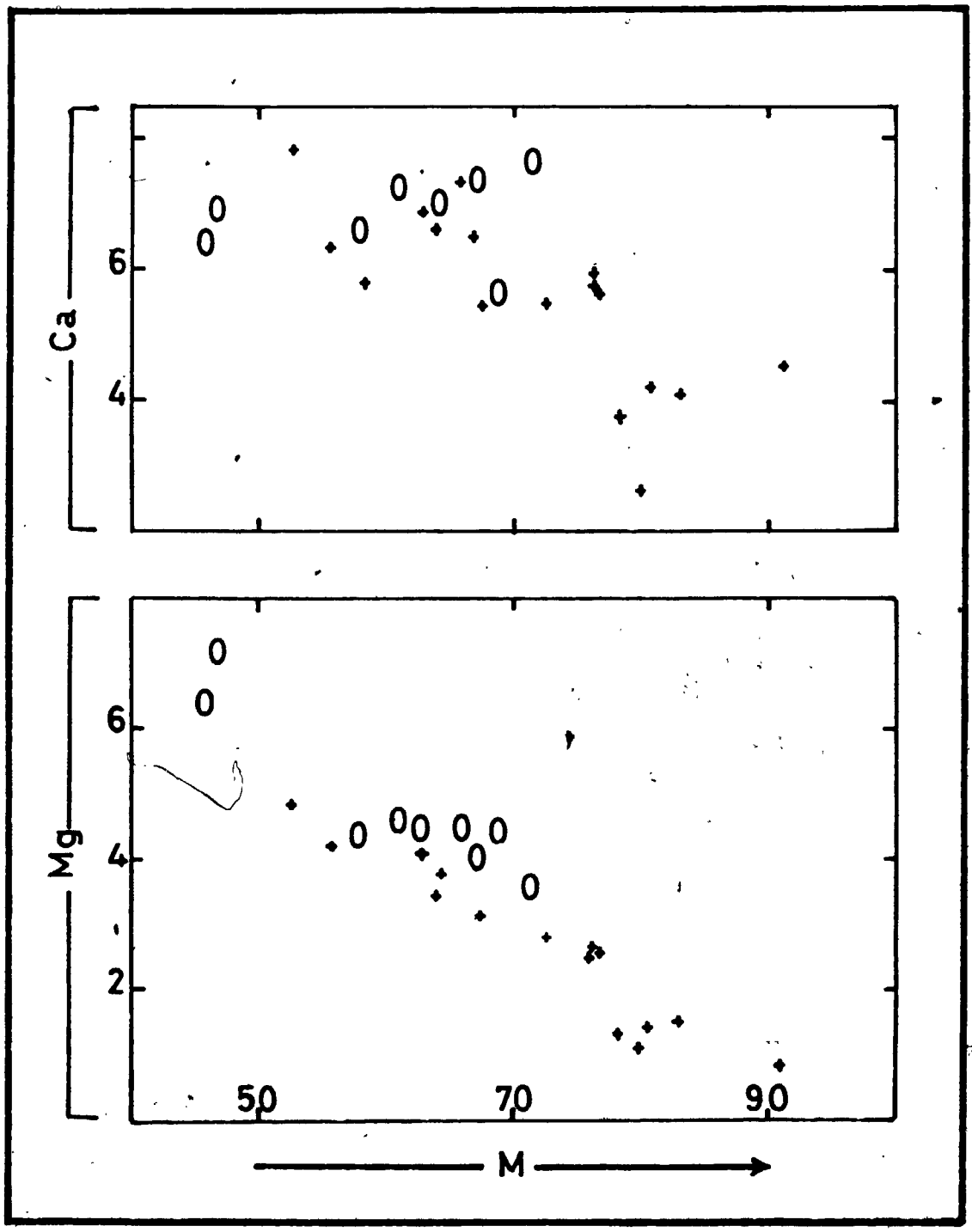

Fig. 87. The mafix index (M) plotted against Ca (a) and Mg (b).
0 gabbroic enclaves
+ diorite

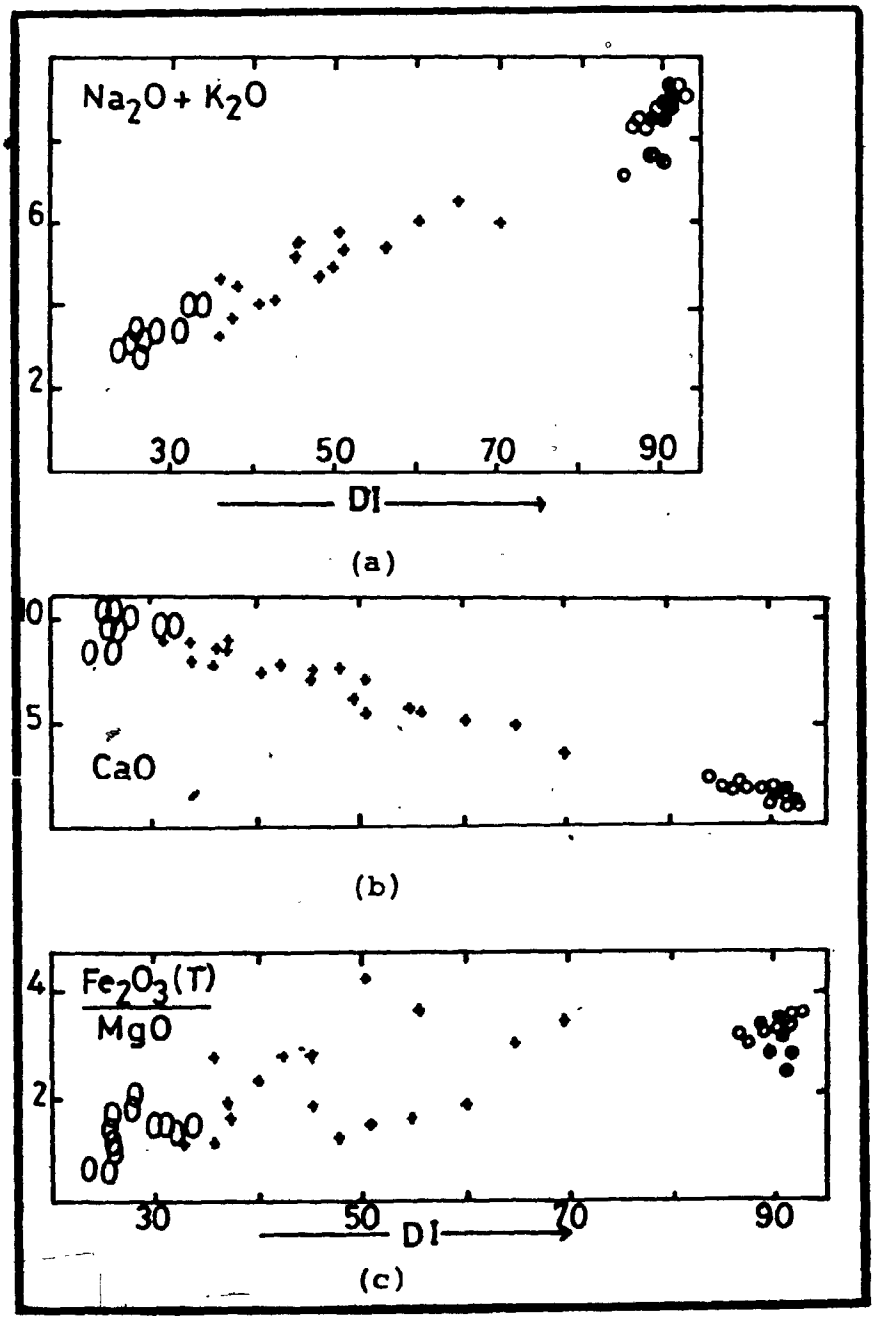

Fig. 88. The differentiation index (DI) plotted against total alkalies (wt.%) (a), CaO (wt.%), (b), and Fe_2O_3t/MgO (c).
0 gabbro
+ diorite
o granodiorite
● monzogranite

suites (Irvine and Baragar, 1971). Al_2O_3 plotted versus silica (Fig. 86) does not have a defined trend; although it seems that Al_2O_3 content decreases slightly with an increase of silica.

The dioritic group are characteristically low in K_2O (average = 0.9%) but relatively high in Na_2O (average = 3.1%). The plots of K_2O and Na_2O against silica (Fig. 86) have fairly defined trends in which both elements increase gradually as a function of increasing silica content. According to Bateman et al. (1970), Na_2O seems to be independent of silica and does not vary systematically with differentiation because of high normative quartz. Furthermore, total alkalies ($Na_2O + K_2O$) versus DI (Fig. 88a) has a defined trend in which total alkalies are increased relative to an increase in the differentiation index.

The average CaO content in the dioritic group is about 8.1%. Variation in CaO content has been illustrated by three different plots: against (1) silica (Fig. 86), (2) Differentiation Index (Fig. 88b), and (3) Mafic Index (Fig. 87a). In the first two plots defined trends are observed in which CaO decreases with the increase in silica and DI, while in the third plot, scattered points lacking a defined trend are observed.

The average silica content in the dioritic rocks is about 52.0%. This silica content is relatively low when compared to average diorites (Hyndman, 1972, p. 12). The variation in SiO_2 content versus the DI has a well marked trend in which silica content increases gradually with the increase in DI (Fig. 89). The dioritic rocks show one continuous differentiation trend.

(2) The Granitic Group:

The major element oxides of the granitic group are presented in Appendix B, Tables 3B and 4B and the averages and ranges are given in Table 17, The variation in some of the major elements are illustrated relative to: 1) silica content, and 2) Felsic Index (Simpson, 1954). Al_2O_3 (Av. 13.3%), Fe_2O_3t (Av. 2.1%), MgO (Av. 0.6%), and CaO (Av. 1.6%) plots versus silica content (Fig. 90g, f, e and d) have similar trends in which these elements decrease with the increase in silica. Furthermore, Ca and Mg were also plotted against the Felsic Index ($F = \frac{Na + K}{Na + K + Ca} \times 100$). Both plots (Fig. 91c, d) have also defined trends in which these two elements decrease with the increase in Felsic Index. The average contents of Na_2O and K_2O in the granitic group are 4.5% and 4.0%, respectively. The plots of Na_2O and K_2O against silica (Fig. 90 band c) and the Felsic Index (Fig. 91 a and b) have weak trends in which they increase with the increase in silica and Felsic Index.

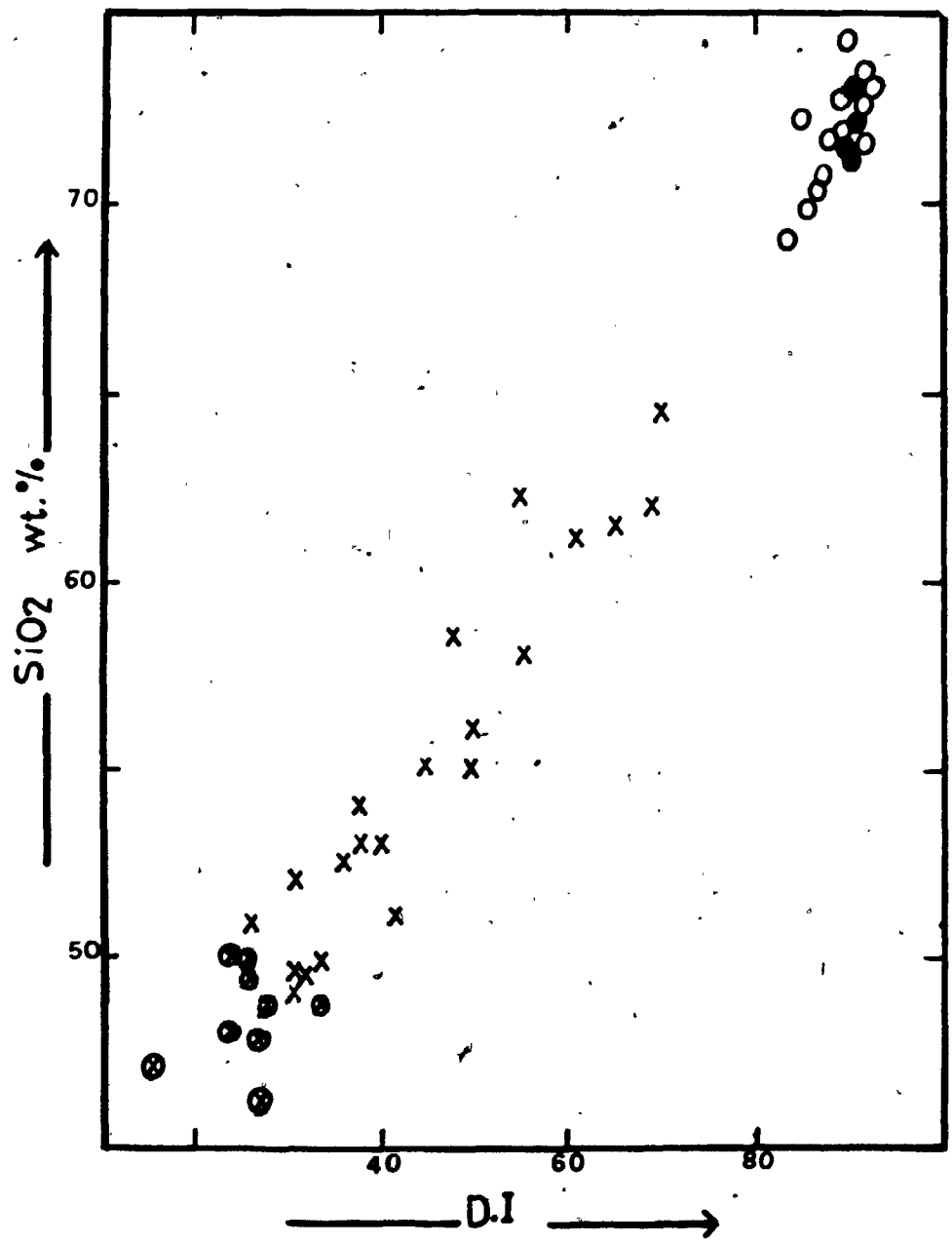

Fig. 89. Thorton and Tuttle (1960) differentiation index plotted against SiO_2 (wt.%).
●, gabbro
x, diorite
o, granodiorite
●, monzogranite

TABLE 17. The average and range of major element oxides of the granodiorite and the monzogranite of the Al Hadah Pluton.

	Monzogranite		Granodiorite	
	Av*	Range	Av**	Range
SiO_2	71.8	71.3-73.0	71.8	69.0-73.4
TiO_2	0.25	0.2- 0.3	0.27	0.2- 0.37
Al_2O_3	13.3	13.1-13.6	13.4	12.9-14.4
Fe_2O_3	0.9	0.8- 1.0	0.8	0.1- 1.2
FeO	1.1	0.9- 1.4	1.5	1.2- 2.1
MnO	0.04	0.0- 0.1	0.1	0.0- 0.1
MgO	0.6	0.6- 0.7	0.6	0.2- 0.8
CaO	1.5	1.3- 1.7	1.7	1.2- 2.2
Na_2O	4.4	4.3- 4.7	4.9	3.7- 5.7
K_2O	4.4	4.1- 4.8	3.5	2.7- 4.1
P_2O_5		0.0- 0.1		0.0- 0.1
Total	98.29		98.57	
Q	25.8	23.3-26.6	24.5	22.0-26.2
or	26.7	24.5-29.0	21.2	16.5-24.5
ab	38.1	36.5-39.7	43.5	37.9-49.0
an	3.4	2.5- 5.1	3.3	1.2- 8.8
di	3.2	1.8- 4.1	4.2	1.8- 5.9
hy	1.0	0.4- 1.6	1.5	0.4- 3.3
ol	-		-	
mt	1.3	1.1- 1.4	1.1	0.6- 1.8
il	0.5	0.4- 0.6	0.5	0.4- 0.7
ap	0.1	0.0- 0.2	0.1	0.1- 0.2

* Average of 6 analyses

** Average of 12 analyses

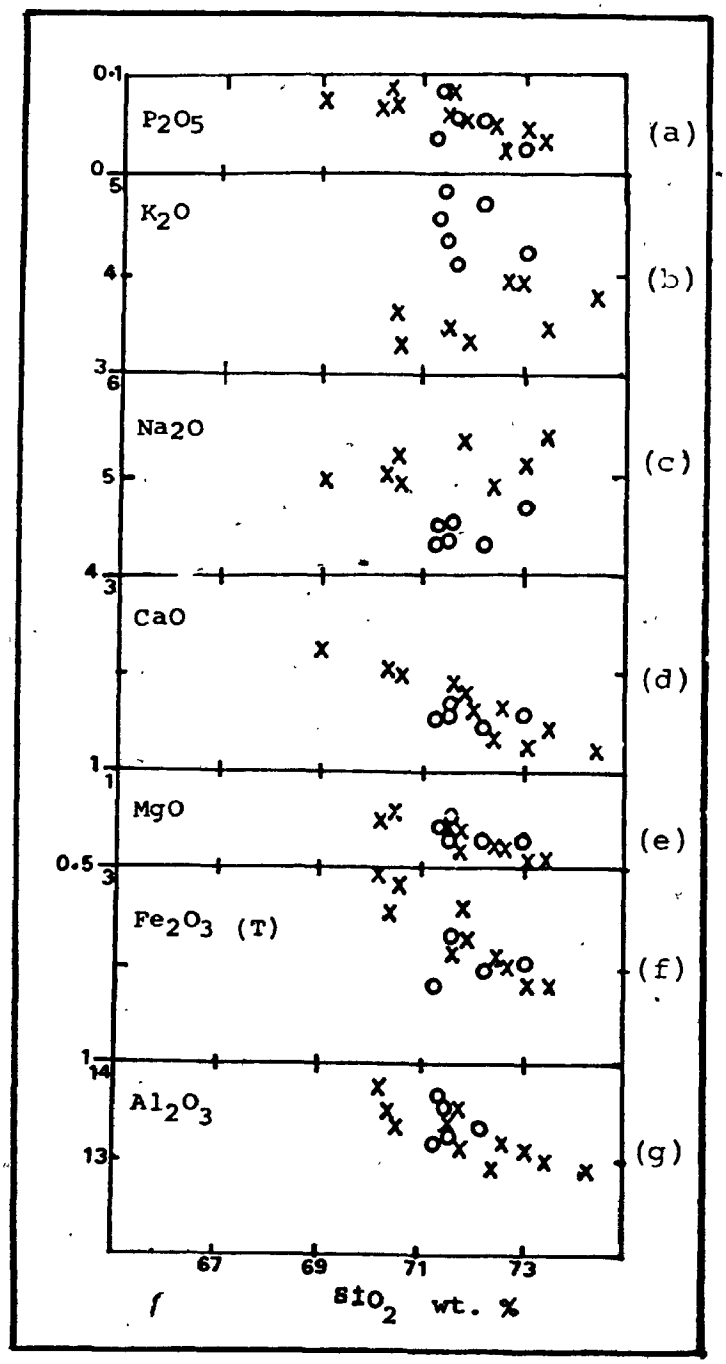

Fig. 90. Harker variation diagrams for the granitic group.
x granodiorite
o monzogranite

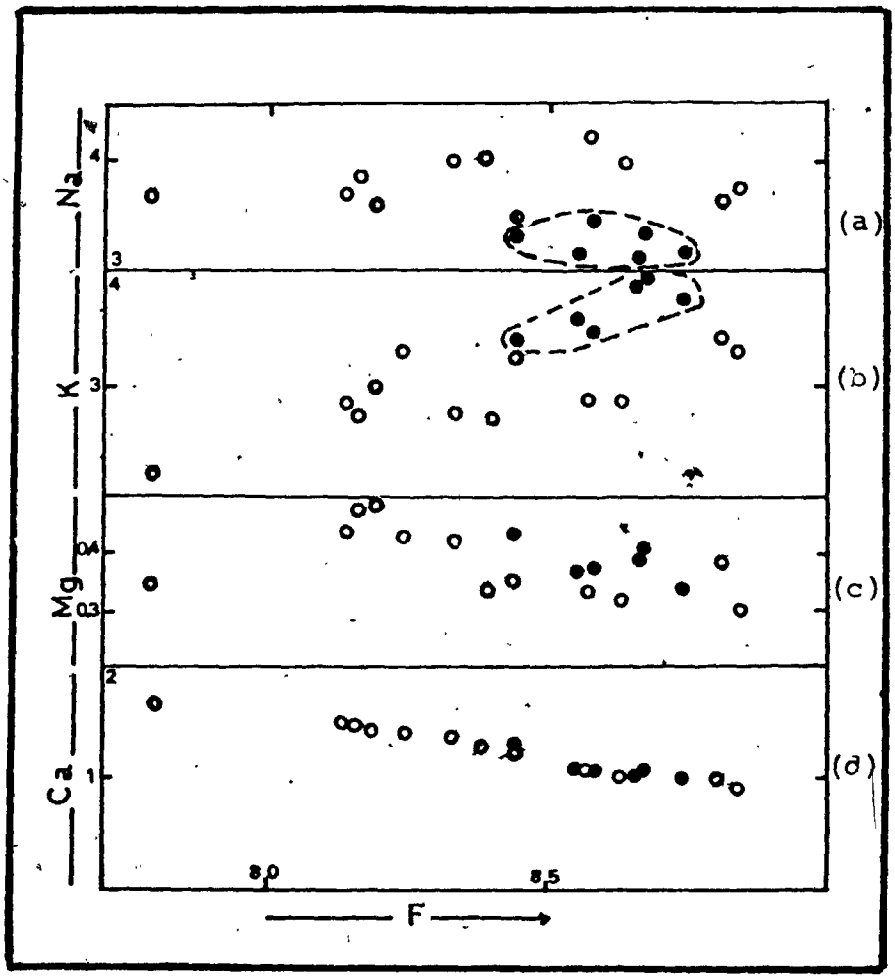

Fig. 91. The felsic index ($F = \frac{Na + K}{Na + K + Ca} \times 100$) plotted against Na(a), K(b), Mg(c), and Ca(d).
o granodioirte
● monzogranite

In both figures two distinct groups, at different levels, are observed. The granodiorite is enriched in sodium than potassium while the monzogranite is more potassic than the granodiorite for almost equal values of silica and Felsic Index.

The P_2O_5 plot versus silica (Fig. 90a) has a moderate trend in which it decreases with the increase in silica.

5.3.2 Trace-Element Abundances:

The trace-element analyses were determined on the same samples from which the major oxides were obtained. Eight elements were analysed: Cr, Ba, Ni, Pb, Zr, Y, Sr and Rb. The result of these analyses are presented in Appendix B, Tables 1B, 2B, 3B and 4B. The average and range of these traces in the dioritic and granitic groups are given in Tables 18 and 19 respectively. A comparison between the trace-element abundances in the Al Hadah complex and other similar igneous rocks is presented in Table 20. The variations in these traces are treated and illustrated in the same manner as those discussed for the major oxides.

(1) The Dioritic Group (= Gabbro + Diorite):

The average and range of the trace-element abundances for this group are presented in Table 18. These averages are compared to similar abundances in the crust, basalt,

TABLE 18. The average and range of trace element abundances in the gabbroic patches and in the diorites of the Al Hadah Pluton.

	GABBRO		DIORITE	
	Av.*	Range	Ave.**	Range
Cr	115	14-210	63	11- 177
Ba	287	155-809	501	198-1620
Ni	104	13-304	36	5- 127
Pb	10	8- 11	8	8- 11
Zr	80	47-116	134	54- 570
Y	22	11- 24	41	21- 64
Sr	408	306-477	486	303- 778
Rb	14	5- 37	19	5- 46
K/Rb	456	340-593	555	321- 996
Ba/Rb	23	9- 77	28	11- 114
Rb/Sr	0.026	0.02-.04	0.036	0.02-0.15
Ba/Sr	0.7	0.37-1.26	1.05	0.50-4.46

* Average of 12 analyses

** Average of 19 analyses

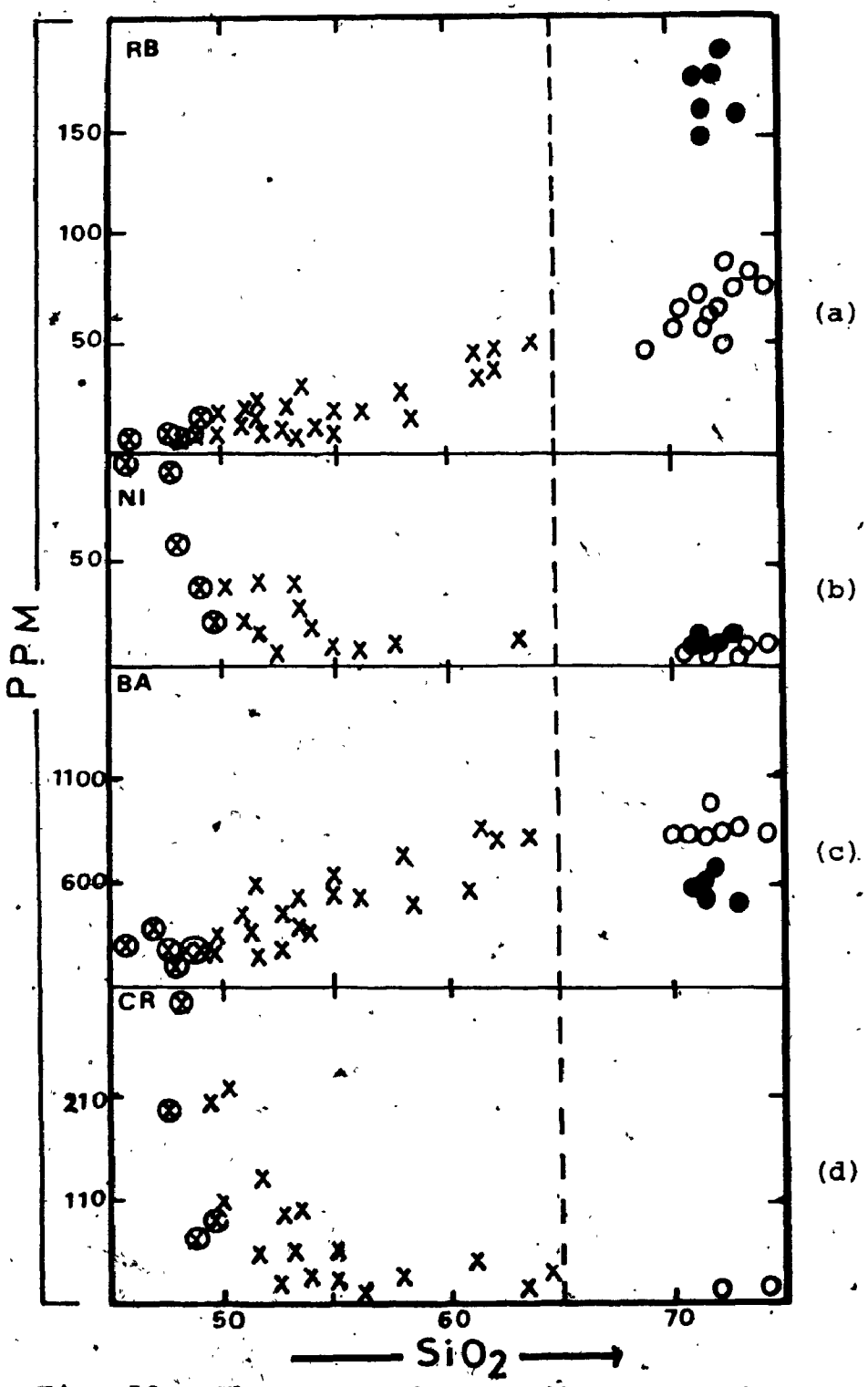

Fig. 92. The trace-element (in ppm) Rb(a), Ni(b), Ba(c) and Cr(d) are plotted against the silica content (wt.%).
■ gabbro
x diorite
o granodiorite
● monzogranite

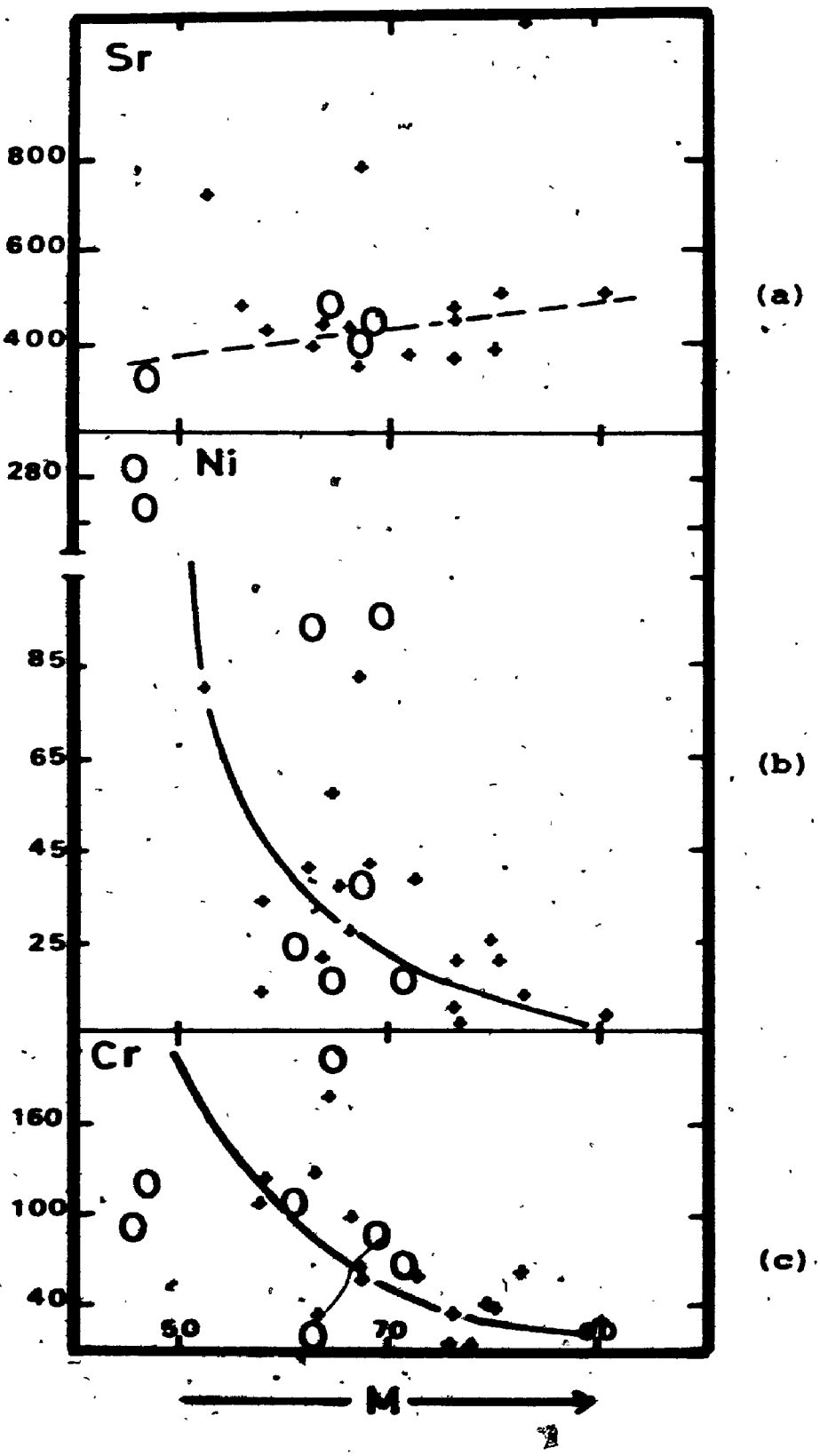

Fig. 93. The trace-elements Sr(a), Ni(b), and Cr(c) are plotted against the mafic index (M).
θ gabbro
+ diorite

calc-alkaline basalt associated with island arcs, Andean andesite and average andesite (see Table 20).

The plots of Cr and Ni against silica content (Fig. 92b and d) and the Mafic Index (Fig. 93b and c) have similar trends, in which the values of these two traces drop sharply relative to the increase in silica content on the Mafic Index.

The plot of Ba versus silica content (Fig. 92c) has a well defined trend in which Ba content increases gradually from the gabbros to the diorites. An increase in Ba content with silica confirms the fact that Ba, which occurs in plagioclase, is often enriched towards the end of a differentiation sequence and it is not depleted in the magma until very late in the differentiation process (Nockolds and Allen, 1953).

The Ba/Sr and Ba/Rb (see Table 18) have been found to provide a useful index of fractionation (Taylor, 1966). Both ratios have been plotted against the Differentiation Index (DI). The Ba/Sr plot (Fig. 94a) has a fairly marked trend in which this ratio increases with an increase in DI, while the Ba/Rb plot (Fig. 95) has scattered points, which seem to indicate a weak trend in which the Ba/Rb ratios seem to decrease with an increase in DI.

The Sr plot (Fig. 96a) has some scattered points, but a

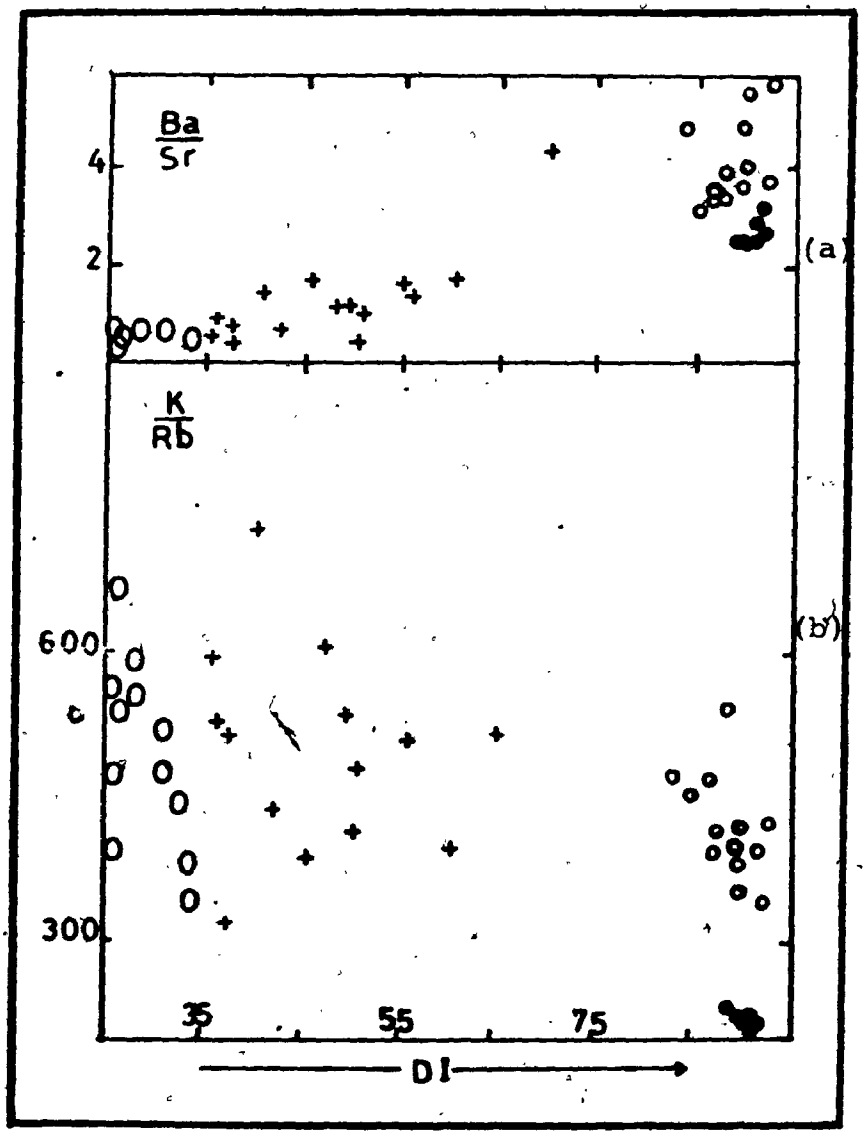

Fig. 94. Ba/Sr and K/Rb are plotted against the differentiation index (DI).
O gabbro
+ diorite
o granodiorite
● monzogranite

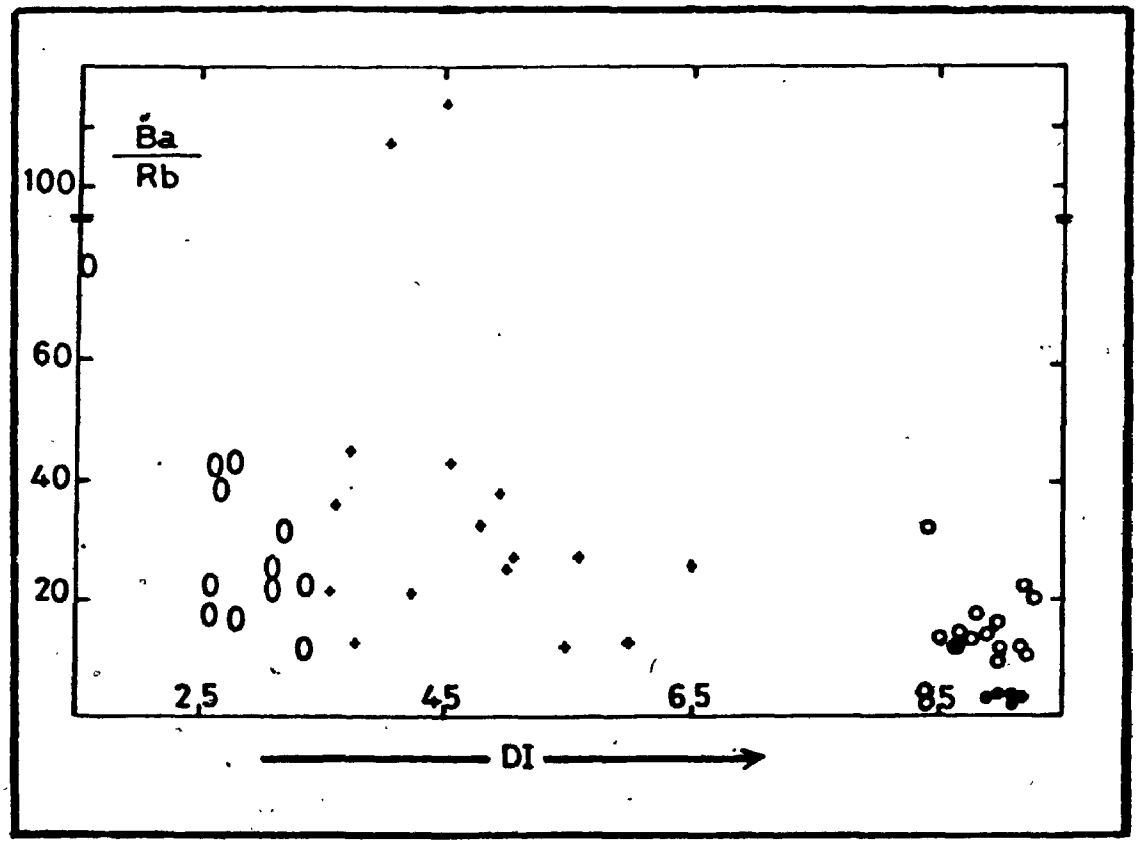

Fig. 95. Ba/Rb plotted against the differentiation index (DI).
0 gabbro
+ diorite
o granodiorite
● monzogranite

weak trend in which it decreases with the increase in silica, is still detected. Sr content seems to decrease with the increase in differentiation and this is due to the fact that the Sr ion is being admitted to calcium minerals and this admittance is the dominant process of removal of Sr from the magma (Mason, 1966).

The Rb plot versus silica content (Fig. 92a) has a marked trend in which Rb content increases with the increase in silica.

The K/Rb is considered by many petrologists as an important fractionation index. It has been shown by Jakes and White (1970) that fractionation or differentiation usually leads to a decrease in K/Rb and this fact is illustrated by Fig. 94b, where K/Rb seems to decrease with relative increase in the Differentiation Index. The dioritic group has a large K/Rb, ~500; it is also xenolithic. Hence, the large K/Rb may not be entirely the product of magmatic fractionation at a high level of emplacement but also a product of contamination as suggested by Erlank and Hofmeyr (1966), Gunn (1965, 1966), Compston (1968), Lambert and Heier (1969).

The Zr plot against silica content (Fig. 96b) has some scattered points but still a well defined trend can be observed in which Zr content increases sharply with the relative increase in silica.

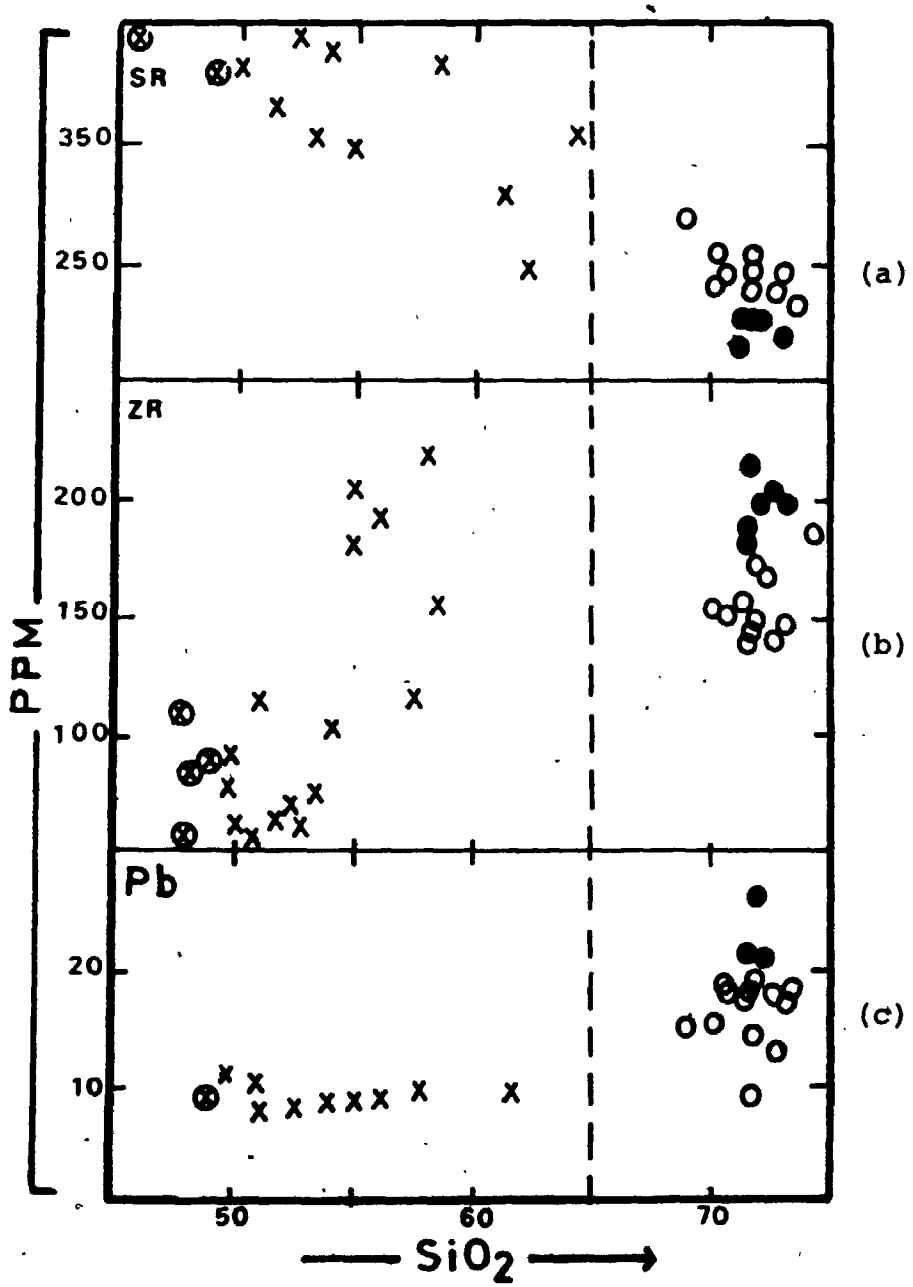

Fig. 96. The trace-elements (in ppm) Sr(a), Zr(b) and Pb(c) plotted against SiO_2 (wt.%).
⊗ gabbro
x diorite
o granodiorite
● monzogranite

The Pb plot versus silica (Fig. 96c) exhibits a weak smooth trend where the Pb content increases gradually with the increase in silica.

(2) The Granitic Group (= Granodiorite + Monzogranite):

The average and range of the trace-element abundances for this group is presented in Table 19. These averages are compared to similar abundances in other granitic rocks (see Table 20). The variations in the trace-element composition are plotted on the same diagrams with those of the dioritic group in order to examine if these two groups of rocks are genetically related.

The Ba plot (Fig. 92c) has two concentrations close to one another. Neither concentration shows a defined trend. The monzogranite cluster is depleted in Ba relative to the granodiorite. The depletion of Ba in the monzogranite indicates a very late stage in differentiation process (Taylor, 1966). Furthermore, in this diagram the granitic group forms a distinct differentiation trend different from that of the dioritic group.
The Ba/Sr has been plotted against both the Differentiation Index (Fig. 94a) and the Felsic Index (Fig. 94b). In both diagrams, the granodiorite and the monzogranite form two separate clusters having similar trends in which Ba/Sr increase relative to the increase in DI and F. Furthermore, Fig. 94a shows, too, that the granitic group has a different

TABLE 19. The average and range of trace element abundances in the monzogranite and in the granodiorite of the Al Hadah Pluton.

	Monzogranite		Granodiorite	
	Av*	Range	Av**	Range
Cr	4	2- 8	14	1- 35
Ba	585	503-639	989	806-1535
Ni	8	6- 13	10	5- 25
Pb	20	17- 26	16	9- 20
Zr	199	171-224	164	138- 202
Y	29	22- 39	40	30- 45
Sr	210	190-242	238	144- 307
Rb	168	147-185	69	46- 90
Nb	25	21- 28	9	6- 11
K/Rb	220	214-231	436	340- 740
Ba/Rb	3.5	3.1-3.9	16	10.8-32.4
Rb/Sr	0.8	0.6-0.9	0.28	0.15-0.37
Ba/Sr	2.8	2.6-3.2	4.3	3.2-6.5

* Average of 6 analyses

** Average of 12 analyses

TABLE 20. Trace element abundance in the Al Hadah plutonic rocks and other similar igneous rocks.

	Cr	Ni	Ba	Sr	Rb	Zr	Pb	Y	Rb/Sr	K/Rb	References
Crust	100	75	425	375	90	165	12.5	30		230	Taylor, 1966
Basalt	200	150	250	465	30	150	5	25			Taylor, 1966
Calc-alkaline Basalt	40	25	115	330	10	100		20			Jakes & White,1972
Andean Andesite	85	30	720	420	135	180		21			Siegers et al.,1969
Average Andesite	56	18	270	385	30	110					Taylor, 1964
Al Hadah Gabbro	115	104	287	408	14	80	10	22	0.03	456	This thesis
Al Hadah Diorites	63	36	501	486	19	134	8	41	0.04	555	This thesis
Granodiorites	20	20	500	450	120	140	15	30			Taylor, 1966
Granodiorites of Cent. E. Sierra Nevada	10	5	1000	700		100	20				Bateman et al.,1963
Granodiorites - Boulder Batholith					64				0.15	390	Doe, et al.,1968 Tillings et al., 1969
Andean Granodiorites					60						Aguirre et al., 1974
Granites	4	0.5	600	285	150	180	20	40			Taylor, 1966
Quartzmonzonite of Cent. E. Sierra Nevada	6		1000			500	20				Bateman et al., 1963
Quartzmonzonite Boulder Batholith					129				0.28	260	Doe et al., 1968; Tillings et al., 1969
Al Hadah Granodiorite	14	10	585	238	69	164	16	40	0.28	436	This thesis
Al Hadah Monzogranite	4	8	989	210	168	199	20	29	0.8	220	This thesis

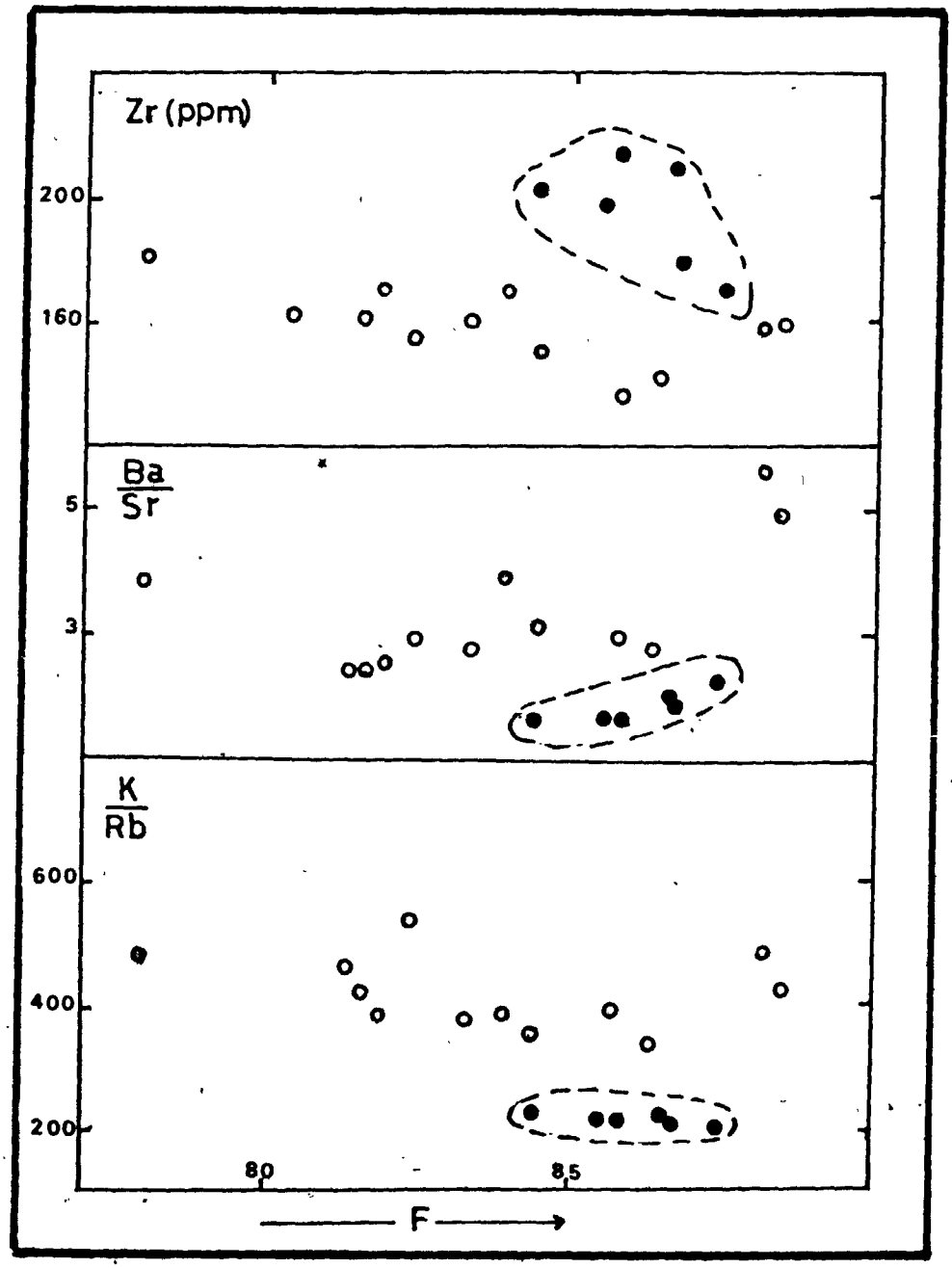

Fig. 97. Zr(ppm) (a) and Ba/Sr (b) and K/Rb in the granitic group are plotted against the felsic index (F).
o granodiorite
● monzogranite

differentiation trend from that of the dioritic group.

The Sr content is plotted versus silica (Fig. 96a) and potash content (Fig. 98). The Sr plot against silica has two distinct concentrations. The granodiorite is relatively richer in Sr than the monzogranite and shows a marked trend in which Sr decreases with the increase in silica, while the monzogranite lacks any trend. The Sr plot versus K_2O (Fig. 98) has a single discontinuous trend where the Sr content decreases going from the dioritic rocks which are relatively rich in plagioclase, towards the granitic group, which are relatively rich in K-feldspar. The Rb plot against silica (Fig. 92a) has two concentrations, occupied by the granodiorite and monzogranite. The granodiorite cluster has a marked trend in which Rb contents increase with the increase of silica, while the monzogranite group lacks any definite trend. The monzogranite is relatively enriched in Rb and K. The close relationship (in ionic size and chemical behavior) between Rb and K is illustrated in Fig. 99. This diagram shows Rb is enriched in rocks having a large proportion of K_2O (e.g. monzogranite) carried in K-feldspars. The K/Rb plot versus the Differentiation Index is shown in Fig. 94b. Two concentrations are also observed. The granodiorites have, relatively large K/Rb, while the monzogranite have small K/Rb ratios. The granodiorite exhibits a marked trend in which K/Rb decreases

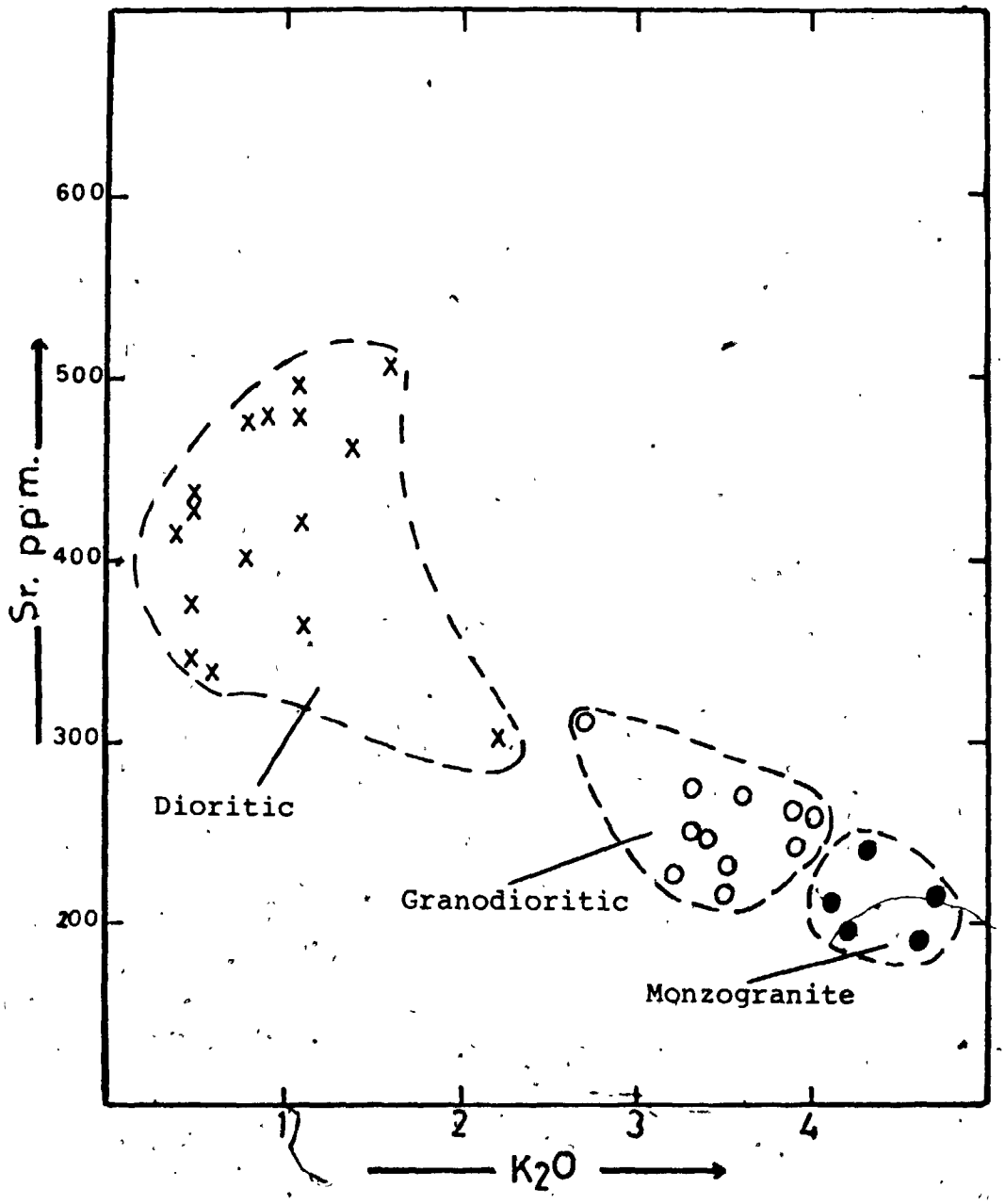

Fig. 98. Sr(in ppm) in the different rock types of Al Hadah Pluton is plotted against the K_2O content (in wt.%).

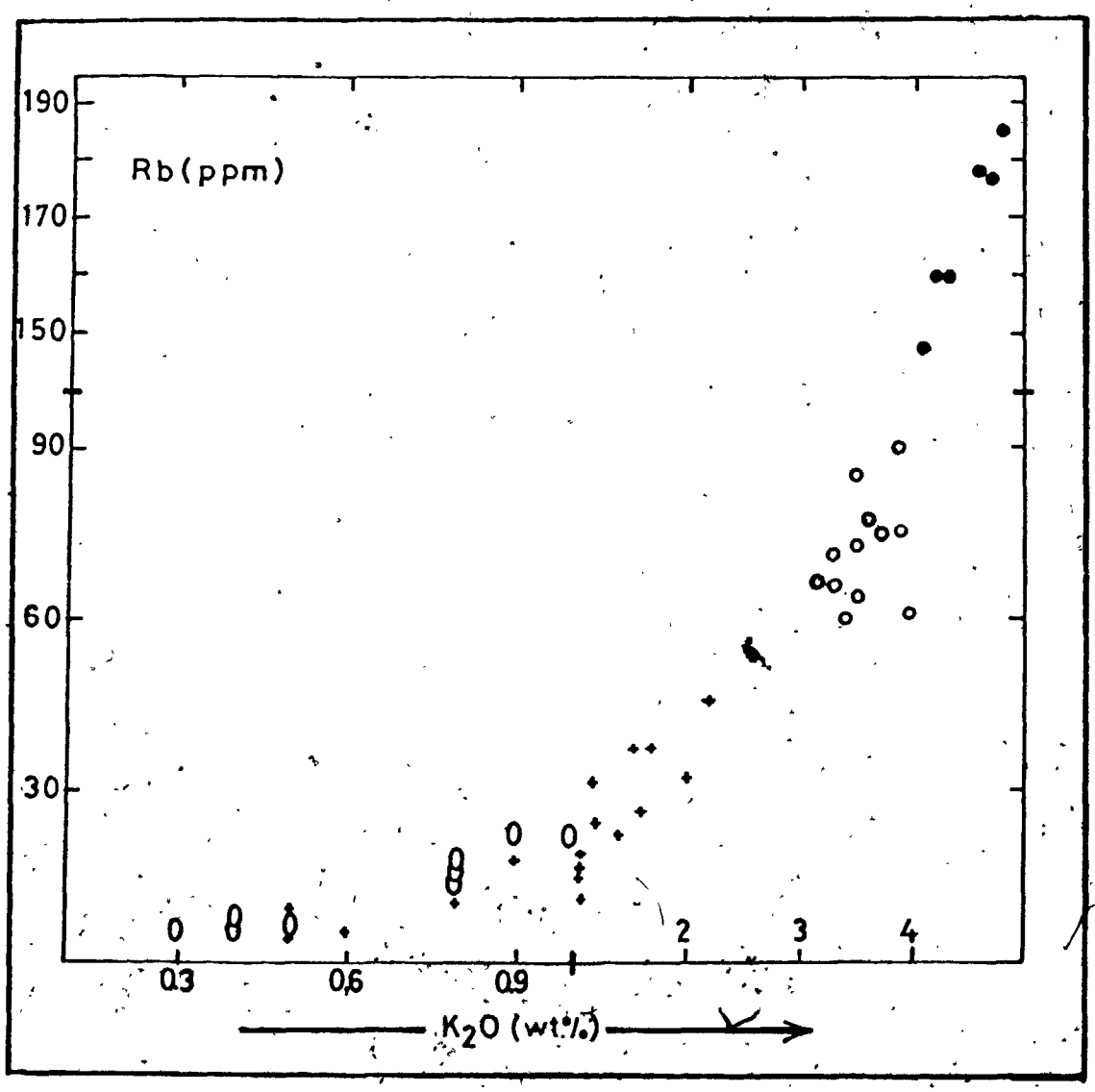

Fig. 99. Rb (ppm) is plotted against the K_2O (wt.%) content.
0 gabbro
+ diorite
o granodiorite
● monzogranite

with the increase in DI. The granitic group, in general, lies on a distinct and different differentiation trend from that of the dioritic group.

Zr is plotted against silica (Fig. 96b) and the Felsic Index (Fig. 97a). Zr seems to increase with the relative increase in silica (Fig. 96b), while decreasing with an increase in the Felsic Index (Fig. 97a). Furthermore, in Fig. 96b the dioritic group has a distinct and different trend from the granitic group. It has been shown by Taylor (1966) that Zr increases with fractionation. The Pb plot versus silica (Fig. 96c) exhibits two clusters: those of the granodiorite and those of the monzogranite. Both concentrations lack any defined trend. The monzogranite is relatively rich in Pb compared to the granodiorite because the monzogranite is relatively richer in K-feldspar in which Pb occurs substituting for potassium.

5.4 A Comparison of the Element Abundances in the Al Hadah Plutonic Rocks and Other Orogenic Suites:

The absolute abundances of the major oxides and trace elements of the Al Hadah diorites and andesites from different subduction environments are compared to one another (Tables 21, 22). Similarly the composition of the Al Hadah granitic rocks is compared to various granitic rocks located above subduction zones (Table 24). The

purpose of these comparisons is to examine the similarities and differences in major and minor element abundances in order to find out whether Al Hadah plutonic rocks were formed in similar tectonic environments. An AFM diagram plotted for both the dioritic and granitic rocks shows that both rock types trend more directly across the centre field of the diagram with gradual enrichment in iron (Fig. 100); this behavior is a characteristic feature of calc-alkaline suites which are most prominent in the circum Pacific region (Irvine and Baragar, 1971).

In Table 21 the major oxides of the Al Hadah diorites are very much similar to basaltic andesite of the S.W. Pacific island arcs, and Cascade andesite, but different from Andean andesites and continental margin andesite, mainly in SiO_2, Fe_2O_3t, MgO and K_2O. From inspection of the trace-element abundances presented in Table 22 most of the traces in both Al Hadah diorites and continental calc-alkaline series are reasonably similar with the exception of Rb. Furtheremore, the K/Rb and Rb/Sr in Al Hadah diorite are larger than those of continental calc-alkaline series. This may be due to the large difference in crustal thickness. The general differences between the calc-alkaline volcanic rocks of island arcs and those of continental margins are summerized by Jakes and White (1972) and compared to the dioritic rocks of Al Hadah pluton (Table 23). From inspection of this table it is possible to

TABLE 21. A Comparison between the composition of various andesitic rocks in orogenic suites and Al Hadah dioritic rocks.

	S.W. Pacific Island Arc Andesites	Andean Andesites	Cascade Andesites	Continental Margin Andesites	Average Andesites	Diorite (Coast Batholith B.C.)	Al Hadah Diorites
	1	2	3	4	5	6	7
SiO_2	54.8	57.9	54.05	58.7	58.2	49.75	55.5
TiO_2	0.8	0.97	1.4	0.8	0.8	1.06	1.04
Al_2O_3	16.0	17.2	17.0	17.4	17.2	17.4	17.5
Fe_2O_3	4.8	3.0	8.8	3.2	3.1	2.97	3.3
FeO	4.8	3.7		3.5	4.2	5.62	5.5
MnO	0.2	0.12	0.14	0.1	-	0.33	0.15
MgO	4.8	3.6	4.1	3.3	3.2	5.45	4.3
CaO	8.6	6.2	8.2	6.3	6.9	8.8	7.1
Na_2O	2.9	4.0	3.1	3.8	3.2	4.7	3.7
K_2O	0.9	2.0	1.3	2.0	1.6	1.1	1.1
P_2O_5	0.2	0.3	-	0.2	0.2	0.15	0.25
H_2O	1.3	1.0	-	-	-	1.47	-

1 = Average compiled from different sources (Ewart et al., 1973; Morgan, 1966; CTV, 1974; Stanton et al., 1969; Brothers et al., 1970; Steiner, 1958; Jakes and Gill, 1970; Gill, 1970).
2 = Average of 82 analyses of Andesite "Formation" in Chilean Andes (Pichler et al., 1972).
3 = Average of 7 analyses (Waters, 1955).
4 = Average of 29 analyses of calc-alkaline andesite (McBirney, 1969).
5 = Average of 1775 analyses compiled from world wide occurrences (Hyndman, 1972).
6 = Average of 13 diorites from Coast Batholith, British Columbia (Roddick, et al., 1974).
7 = Average of 20 analyses of dioritic rocks from Al Hadah Pluton (This Thesis).

TABLE 22. Trace element abundances in the dioritic rocks of Al Hadah Pluton and in other orogenic suites.

	Al Hadah Diorites	Andean Andesite	S.W. Pacific Island Arc	Calc-alk. Island Arc	Continental Calc-alk. Series (Andean)
	1	2	3	4	5
Cr	63	85	36	56	-
Ba	501	720	141	270	500-700
Ni	36	30	19	18	30
Pb	8	-	3	5	-
Zr	134	180	60	110	180
Y	41	-	25	-	-
Sr	486	420	266	380	600
Rb	19	135	14	30	45-100
K/Rb	555	-	870	450	100-200
Ba/Rb	28	8.5	21	-	-
Rb/Sr	0.036	0.11	0.024	0.05-0.1	0.07-0.2
Ba/Sr	1.05	0.97	-	-	-

1 = This thesis

2 = Siegers et al. (1969), found in Jakes and White (1971)

3 = Average compiled from various sources

4 = Jakes and Gill (1970)

5 = Siegers et al. (1969).

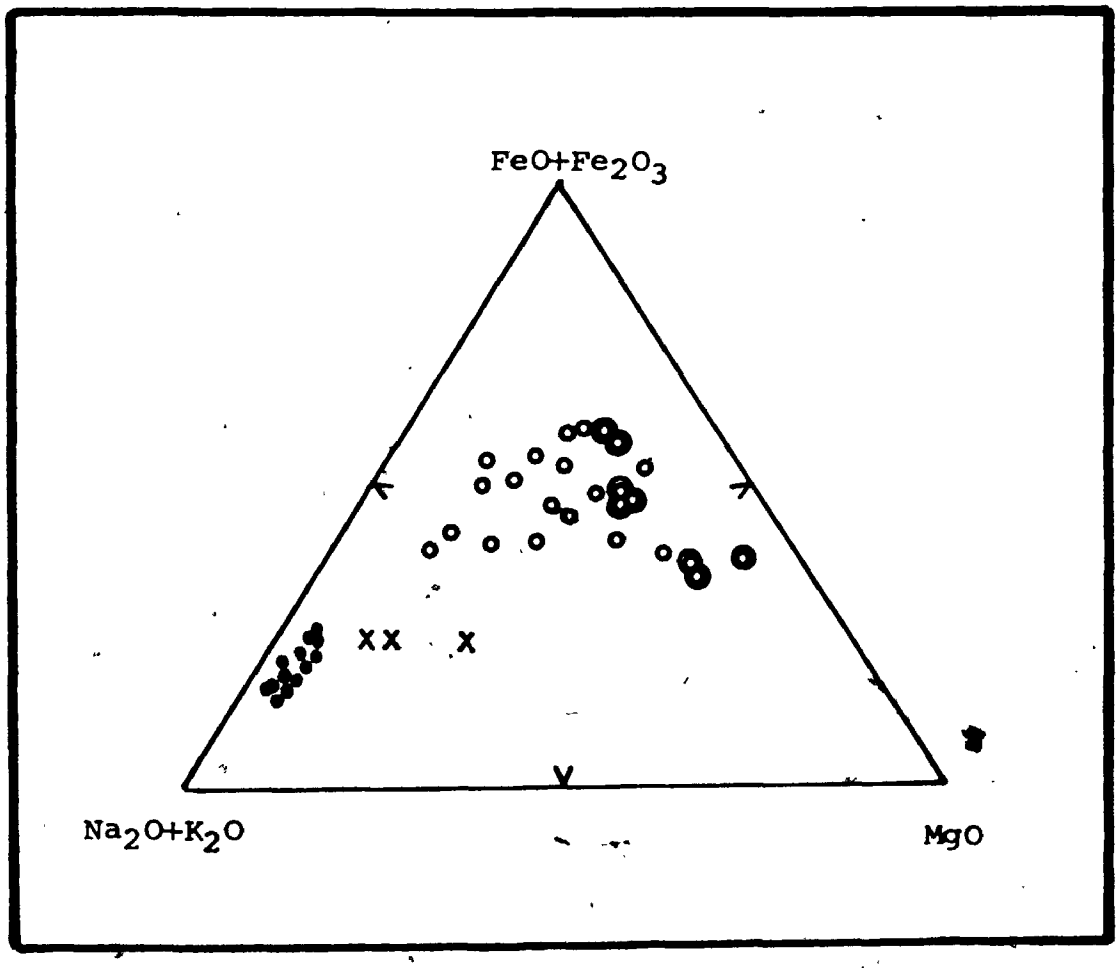

Fig. 100. An AFM diagram for the two major groups of Al Hadah Pluton.
◎ gabbro
o diorite
● granodiorite + monzogranite
x granites taken from Greenwood (1974)

TABLE 23. Generalized differences between calc-alkaline volcanic rocks of island arcs and those continental margins (after Jakes and White, 1972) compared to the dioritic rocks of Al Hadah Pluton.

	Continental Margin (Andean)	Island Arcs	Dioritic Rocks of Al Hadah Pluton
Range of SiO_2	56-75%	50-66%	50.9-65%
$\frac{FeO + Fe_2O_3}{MgO}$	>2.0	<2.0	2.07
$\frac{K_2O}{Na_2O}$	0.6-1.1	<0.8	0.29
Trace elements	Higher Rb, Ba, Sr and Zr. Lower K/Rb (≈230)	Lower Rb, Ba, Sr and Zr. Higher K/Rb (≈400)	Lower Rb, Zr, intermediate Ba, Sr. Higher K/Rb (≈555)

see some general similarities between the diorites of Al Hadah and those of Andean Continental margin. However, the range in silica content is greater in the Andean than those of the Al Hadah diorites, probably because the former are emplaced in thicker continental crust than the latter. The smaller K_2O/Na_2O in the Al Hadah diorites than in those of the Andean may be attributed to the fact that the former have been slightly metamorphosed and the mobile alkalies and related trace elements redistributed, whereas the Andean rocks are unmetamorphosed.

In summary, the Al Hadah dioritic rocks, which are situated on a continental basement, have general similarities in major and minor element abundances to calc-alkaline continental margin andesites. It should be noted, however, that all the dioritic rocks of Al Hadah have been subjected to some degree of metamorphism, and furthermore, this comparison is between extrusive and intrusive rocks.

In the same manner, the composition of the granitic group of the Al Hadah pluton is compared to various plutonic rocks of subduction zone areas. The normative plot of Al Hadah granitic rocks is similar to the plots of granitic rocks in the United States and Canada (Fig. 101). Furthermore, a comparison between the major oxides of the Al Hadah granitic group and those of other granitic rocks in orogenic suites is given in Table 24. This table shows that the

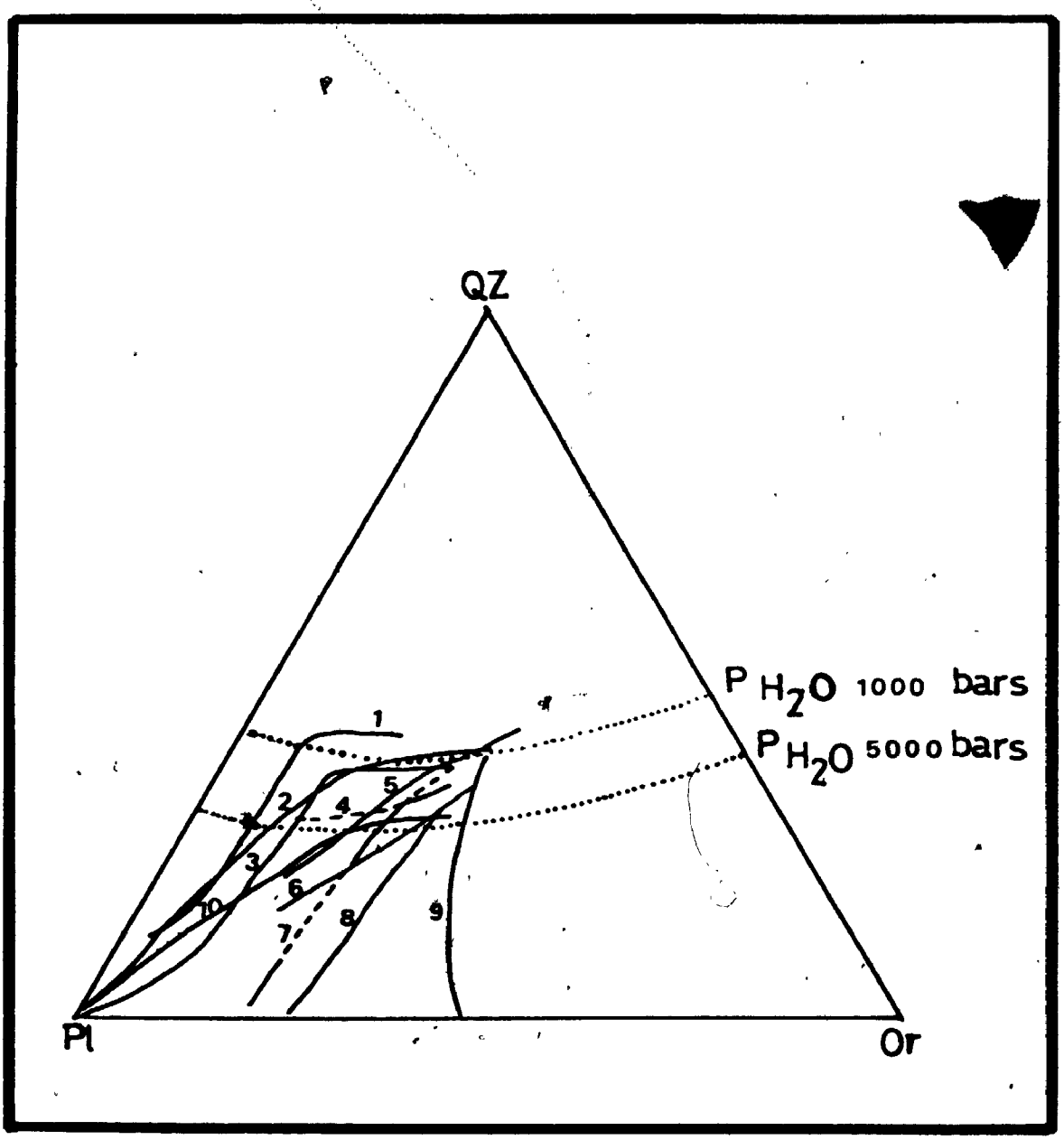

Fig. 101. Composite plots of norms for areas of granitic rocks in the United States and Canada compared to those of Al Hadah Pluton. (After Bateman, 1963). 1 = SW British Columbia, 2 = NW Oregon, 3 = Southern Calif. batholith, 4 = Idaho batholith, 5 = Vancouver Island, 6 = Sierra Nevada batholith, 7 = Boulder batholith, 8 = Stocks of Colorado and New Mexico, 9 = Alaska, 10 = Al Hadah granitic rocks.

TABLE 24. This table shows the chemical composition of various granitic and some rhyolitic rocks occurring over orogenic suites compared to Al Hadah granitic rocks.

	Al Hadah Granitic Rocks		Sierra Nevada			Cascade	Coast Batholith British Columbia		Plutonic Rocks Peru		Andean	New Zealand Rhyolite
	Monzo-granite	Grano-diorite	Ave.	Qtz. Monz.	Grano-diorite	Qtz. Monz.	Qtz. Monz.	Grano-diorite	Granite	Grano-diorite	Rhyolite	Rhyolite
	1	2	3	4	5	6	7	8	9	10	11	12
SiO_2	71.8	71.8	71.8	72.4	67.2	72.7	69.6	63.5	70.7	67.5	72.9	74.2
TiO_2	0.25	0.27	0.26	0.25	0.5	0.2	0.28	0.53	0.17	0.4	0.50	0.28
Al_2O_3	13.3	13.4	13.3	14.3	15.5	13.3	15.6	16.5	16.5	16.3	14.8	13.3
Fe_2O_3	0.9	0.8	0.85	0.75	1.6	2.2	0.8	1.3	0.5	1.3	1.6	0.9
FeO	1.1	1.5	1.3	1.2	2.2		1.5	2.7	1.1	1.5	0.3	0.9
MnO	0.04	0.1	0.07	0.1	0.1	-	0.12	2.0	0.04	0.06	0.13	0.05
MgO	0.6	0.6	0.6	0.7	1.5	0.8	0.9	2.0	0.55	1.5	0.1	0.3
CaO	1.5	1.7	1.6	1.7	3.3	2.0	2.8	4.5	2.5	3.6	1.1	1.6
Na_2O	4.4	4.9	4.6	3.4	3.3	3.6	4.4	4.5	4.7	3.8	3.5	4.2
K_2O	4.4	3.5	4.0	4.5	3.8	3.3	3.1	2.3	2.8	3.1	3.9	3.2
P_2O_5	-	-	-	0.1	0.16	-	0.06	0.09	0.08	0.18	0.01	0.05
H_2O	-	-	-	0.5	0.7	-	0.5	0.9	0.7	0.6	1.33	1.0

1 - Average of 6 analyses.
2 - Average of 17 analyses.
3 - Average of 1 + 2.
4-5 - Average compiled from different sources (Bateman et al., 1961, 1963, 1970).
6 - Average of 1 analysis (Erikson, 1969).
7 - Average of 12 analyses (Roddick, et al., 1974).
8 - Average of 63 analyses (Roddick, et al., 1974).
9 - Average of 2 analyses (Giogrgoio, 1963).
10 - Average of 3 analyses (Giogrgoio, 1963).
11 - Guirre, et al., (1974).
12 - Ewart and Stipp (1968).

average composition of the granitic group of Al Hadah pluton is closely comparable to the granitic rocks of Sierra Nevada batholith.

5.5 Summary and Discussion:

This chapter of rock classification, variation diagrams and comparisons to other rock suites leads to the following conclusions:

(1) The plutonic rocks of Al Hadah area belong to two major rock groups: (a) dioritic (diorite + gabbro), and (b) granitic (granodiorite + monzogranite).

(2) The dioritic group forms one continuous differentiation series (gabbro→diorite→quartz diorite) separate and different from that of the granitic group. Thus, magmatic differentiations were effective during the evolution of both rock groups.

(3) The presence of scatter values of some major and minor elements resulting in irregular variations, together with large K/Rb ratios might indicate that contamination was largely involved in the evolution of the dioritic magma.

(4) The chemical composition of the various rock types of the Al Hadah plutonic complex and the chemical variations indicate that the plutonic rocks of this region belong to at least two different magma sources. The first and older one is represented by the

dioritic group. The second and younger series is represented by the granitic group. This conclusion is similar to the conclusion reached by Greenwood and Brown (1973) that the dioritic and granitic rocks of the Arabian Shield belong to different magma series and they are not differeniates of the same magma. The monzogranite might belong to a third magma source but most probably it represents a final differentiate of the granodiorite giving a potassium rich monzogranite.

(5) On the basis of the various similarities in major and minor element abundances between Al Hadah plutonic rocks and those of the Cascades, continental calc-alkaline series and Sierra Nevada, formed above subduction zones, it seems possible that the plutonic rocks of Al Hadah were formed in a similar tectonic environment. Furthermore, besides similarities in composition, other general features are also comparable, such as: the predominance of basic to intermediate rocks over acidic rocks: the areal distribution of these rocks in the Arabian Shield are 72.3% diorite + quartz diorite + granodiorite, 27.6% quartz monzonite + granite (Greenwood et al., 1973), while this distribution in the Coastal batholith of Central Peru is as follows: 15.9% gabbro-

diorite, 57.9% tonalite, 25.6% adamellite and 0.6% granite (Myers, 1975; Cobbing and Pitcher, 1972); similarly the distribution in Southern California Batholith is as follows: 15.9% gabbro, 50% tonalite, 34% granodiorite and 2.5% granite (Bateman et al., 1963). Other features such as the order of emplacement from basic to acidic (gabbro→diorite→granodiorite→monzogranite) are also similar.

CHAPTER 6

THE EPIDOTIZATION PROCESS

6.1 General Statement

Special attention has been directed in this thesis to the epidotized diorites in terms of their occurrence, extent, chemistry and mode of formation. Their occurrence and extent have been described in detail in Chapter 3, and the petrography reported in Chapter 4. It is worthwhile to present here a brief summary of the occurrence and mineralogical composition of these epidotized rocks prior to discussing the chemistry and alteration processes. The occurrence of these rocks is restricted to a few localities within the diorites associated principally with felsic dikes. Their extent is variable, the largest outcrop is about 100 m^2. The characteristic feature of these rocks is the complete replacement of plagioclase by epidote. Mineralogically they are composed mainly of epidote, amphiboles (hornblende + tremolite-actinolite) and quartz. In this chapter the whole rock chemistry is reported and discussed; together with whole rock oxygen isotope analyses.

6.2 Whole Rock Chemistry

Representative samples of unepidotized, partially epidotized and completely epidotized rocks were selected and analysed in order to determine the chemical change which took place during the alteration process. The results of the chemical analyses are presented in Table 25. From inspection of Table 25 the changes in major element oxides between the unaltered and altered rocks may be summarised as follows: SiO_2, MgO, Na_2O and K_2O are depleted, while TiO_2, Fe_2O_3 and CaO are enriched. The FeO/Fe_2O_3t ratios are low in the completely altered rocks relative to the unaltered rocks (Table 26).

Similarly, the change in trace-element abundancies are as follows: Ba and Rb are depleted while Sr is enriched in the completely epidotized diorites (Table 25).

Discussion:

The general conditions of oxidation-reductions and their controls in rocks have been discussed by Eugster (1959) and Eugster and Wones (1962). The ratio $Fe^{2+}/\Sigma Fe$ is a geochemical parameter which describes the oxidation state of iron in rocks. The background $Fe^{2+}/\Sigma Fe$ in most primary igneous rocks is about 0.7 (Hyndman, 1972, p. 12). Oxidation may occur in response to the infiltration of oxidizing surface waters into the crust. Conversely, water in equilibrium with rocks at high temperature (QFM system)

Table 25. Chemical Analysis of Unepidotized, Partially Epidotized, and Epidotized Rocks Respectively.

	Unepidotized		Partially Epidotized		Epidotized		
Sample #	57	69	62	58C	68	67	58A
SiO_2	49.42	51.18	47.99	45.20	48.09	48.74	40.80
TiO_2	1.41	1.85	1.50	1.35	1.32	2.38	2.10
Al_2O_3	15.22	15.84	15.47	14.94	13.94	14.12	15.60
Fe_2O_3	5.06	3.6	4.88	7.29	10.22	9.06	10.75
FeO	5.09	8.3	5.12	3.48	2.16	5.23	2.16
MnO	0.22	0.2	0.18	0.18	0.16	0.19	0.20
MgO	7.53	4.20	7.21	5.87	2.91	4.15	4.53
CaO	9.64	7.62	10.69	14.61	16.59	16.55	19.74
Na_2O	3.16	4.74	2.99	2.22	0.27	0.15	0.15
K_2O	0.83	0.84	0.91	0.26	0.03	0.03	0.05
P_2O_5	0.39	0.44	0.37	0.62	0.38	0.30	1.03
L.O.I*	1.79	1.20	2.17	2.60	1.95	1.85	2.44
Total	99.76	99.9	99.48	98.62	98.02	97.75	99.55
Q	-	-	-	1.32	17.57	11.57	4.38
Or	5.00	8.1	5.52	1.60	0.18	0.18	0.30
Ab	27.28	28.3	25.99	19.56	2.38	1.32	1.31
An	25.40	29.1	26.81	31.27	38.23	39.37	42.96
di	16.50	10	19.98	31.15	16.27	23.24	25.04
hy	14.65	17.8	6.35	0.78	-	-	-
ol	-	0.6	4.25	-	-	-	-
wo	-	-	-	-	10.01	5.99	7.85
mt	7.49	3.8	7.27	8.21	3.81	11.03	1.57
il	2.73	1.3	2.93	2.67	2.61	4.71	4.10
ap	0.94	-	0.90	1.53	0.94	0.74	2.51
ht	-	-	-	1.92	8.01	1.84	9.98
Cr	108	98	185	35	9	34	12
Ba	448	127	55	2	-	25	-
Pb	9	8	11	9	12	11	9
Zr	103	69	166	194	194	89	215
Y	29	-	24	19	17	29	31
Sr	-	466	1089	2721	2173	895	3224
Rb	15	22	20	5	3	3	2

* L.O.I = weight percent loss on ignition at 1100°C.

TABLE 26. Determinations of total 'primary' iron, ΣFe, FeO and $Fe^{+2}/\Sigma Fe$ in the unepidotized, partially and completely epidotized rocks.

Sample description	Sample No.	FeO	ΣFe	$Fe^{2+}/\Sigma Fe$
Unepidotized Diorite	56	8.5	12.0	0.71
	69	8.3	11.9	0.70
	84	6.6	9.4	0.70
	89	6.2	8.7	0.71
Partially Epidotized Diorite	62	5.1	10.0	0.51
	58C	3.5	10.8	0.32
Completely Epidotized Diorite	68	2.2	12.4	0.17
	67	5.2	14.3	0.36
	58A	2.2	13.0	0.17
	5 A	2.3	11.3	0.20

becomes reduced by dissociation into O_2 and H and may act as a reducing agent during expulsion up through the crust. In general, rocks are resistant to such changes. Unless massive fluid volumes or "exotic reactants" (O_2, S_2) are involved, significant changes in $Fe^{2+}/\Sigma Fe$ are unlikely (Kerrich et al., 1977). As argued above, in a convecting system, one predicts oxidation in response to descending (heating) fluids and reduction in response to ascending (cooling) fluids (loc. cit.) and these relations have been confirmed in studies of submarine convectors, and meteoric geothermal systems, which form in response to shallow, cooling igneous intrusions. Inspection of Table 26 shows that significant oxidation of iron has occurred in the epidotized rocks ($Fe^{2+}/\Sigma Fe = 0.22 \pm 0.09$ one standard deviation) relative to the unepidotized rocks which have $Fe^{2+}/\Sigma Fe$ 0.7 equivalent to the background of $Fe^{2+}/\Sigma Fe$ for most unaltered igneous rocks. The shallow intrusions surrounding the epidotized diorites created fracture systems as has been observed in the field by the presence of numerous fractures and faults some of which are filled by granitic dikes. These fracture systems might have generated permeability and tapped large, near-surface, sources of water. These high level plutons may have provided both the energy source and conditions of high permeability to create the required conditions for

the generation of fluid convective cells. Hence, the observed oxidized state of iron in the epidotized diorites may be accounted for, most readily, by the interaction of oxidizing near-surface fluids set into convective motion by the plutons.

The water/rock ratio involved must have been large in order to oxidize the rocks because, as described above, rocks are generally resistant to changes of $Fe^{2+}/\Sigma Fe$. The shift in oxidation state of iron from background is a function of the integrated water/rock ratio passing through the system, inasmuch as it records the total mass of oxidising or reducing agent introduced into the system (Spooner, 1976). Therefore, the observed shift to high Fe^{3+} in epidotized rocks probably required high integrated water/rock ratios. The depletion in alkalies and the addition of Ca in the epidotized rocks confirms the fact that fluids have been circulating through these rocks.

6.3 Mineral Chemistry

The major mineral components in the unepidotized, partially epidotised, and completely epidotized diorites are plagioclase + hornblende, plagioclase + hornblende + tremolite-actinolite, and epidote + hornblende + tremolite-actinolite respectively. The chemical composition of the

principal mineral phases (plagioclase, amphiboles and epidote) were determined by the electron microprobe. The results of the microprobe analyses of these minerals are presented in Appendix C, Tables 1c, 2c and 3c. The average composition of these minerals are given in Tables 27, 28 and 29 respectively. A characteristic feature of the plagioclase in the partially epidotized diorite is its albitic composition (Ab 98.76) while its composition in the unepidotized diorites is andesine (Ab 66.6). The variations observed by comparing the structural formulas of plagioclase in both unepidotized and partially epidotized diorites, are the following: (a) Si and Na are increased with Al and Ca are decreased in the partially epidotized ones. The amphiboles show characteristic variations between those occurring in unaltered to completely altered diorites (see Table 28). The most important feature observed in this sequence of rocks is the occurrence of one amphibole (= hornblende) in the unepidotized rocks while there are two amphiboles (= hornblende + tremolite-actinolite) in both the partially and completely epidotized diorites.

Epidote is the principal mineral phase in these altered rocks. Its average composition and structural formula are presented in Table 29. The composition of epidote in both partially and completely altered rocks does

Table 27. Average Plagioclase Composition in Partially Epidotized Diorite and in Unepidotized Diorite.

	1	2
SiO_2	68.59	60.13
TiO_2	-	-
Al_2O_3	19.94	25.37
FeO	0.02	0.15
MnO	-	-
MgO	0.01	0.03
CaO	0.23	6.78
Na_2O	11.08	7.63
K_2O	0.02	0.11
BaO	0.04	0.11
H_2O		
SUM	99.88	100.20
Number of Ions on the Basis of 32(0)		
Si	11.963	10.688
Al	4.099	5.314
Fe	.003	0.022
Mg	.002	0.008
Na	3.745	2.628
Ca	.043	1.292
K	.004	0.026
Ab	98.76	66.60
An	1.24	33.40

1 - Plagioclase, average of 9 analyses (from partially epidotized Diorite).

2 - Plagioclase, average of 21 analyses (from unepidotized Diorite).

Analyst: R.L. Barnett.

Table 28. Average Amphibole Compositions in Unepidotized, Partially Epidotized and Completely Epidotized Dioritic Rocks.

	1	2	3	4	5
SiO_2	48.52	49.14	54.61	48.03	55.50
TiO_2	0.92	0.74	0.20	1.62	0.12
Al_2O_3	6.58	5.68	1.28	7.20	0.85
FeO	15.98	15.20	14.19	13.90	11.14
MnO	0.41	0.37	0.32	0.42	0.31
MgO	12.82	13.86	15.16	13.72	17.25
CaO	11.50	11.42	12.46	11.53	12.48
Na_2O	0.93	0.81	0.24	1.11	0.24
K_2O	0.32	0.27	0.01	0.54	0.07
H_2O	2.04	2.04	2.09	2.05	2.11
SUM	100.01	99.52	100.56	100.12	100.06
	Number of Ions on the Basis of 24(O, OH, F, Cl)				
Si	7.139	7.231	7.845	7.017	7.898
	8.000	8.000	8.000	8.000	8.000
Al	0.861	0.769	0.155	0.983	0.102
Al	0.280	0.215	0.062	0.256	0.041
Ti	0.101	0.082	0.022	0.178	0.012
Fe	1.967	1.871	1.704	1.698	1.326
	5.213	5.253	5.072	5.172	5.076
Mg	2.813	3.039	3.246	2.987	3.659
Mn	0.051	0.046	0.038	0.052	0.037
Na	0.266	0.231	0.067	0.315	0.067
Ca	1.813	1.800	1.918	1.804	1.902
	2.138	2.082	1.987	2.221	1.982
K	0.059	0.051	0.002	0.101	0.012

1. Hornblende, average of 19 analyses (from unepidotized Diorite)
2. Hornblende, average of 6 analyses from partially epidotized Diorite.
3. Actinolite-tremolite, average of 4 analyses from partially epidotized Diorite.
4. Hornblende, average of 7 analyses from wholly epidotized Diorite.
5. Actinolite-tremolite, average of 7 analyses from wholly epidotized Diorite.

Analyst R.L. Barnett.

Table 29. Average Composition of Epidotes Occurring in Partially Epidotized and in Completely Epidotized Dioritic Rocks.

	1		2	
SiO_2	38.04		38.04	
TiO_2	.04		0.69	
Al_2O_3	23.61		22.45	
Fe_2O_3	12.00		13.55	
MnO	0.08		0.15	
MgO	0.04		0.05	
CaO	23.25		22.75	
Na_2O	0.18		0.08	
K_2O	-		-	
H_2O	1.87		1.88	
SUM	98.93		99.56	
Number of Ions on the Basis of 13 (O,OH)				
Si	3.039	3.039	3.035	3.035
Al	-		-	
Al	2.222	2.944	2.110	2.924
Fe^{+3}	0.722		0.814	
Mn	0.005		0.010	
Mg	0.005		0.006	
Ti	.002	2.002	0.042	2.002
Ca	1.990		1.945	

1 Epidotes, average of 15 analyses (from partially epidotized Dioritic Rocks)

2. Epidotes, average of 18 analyses (from wholly epidotized Dioritic Rocks)

Analyst R.L. Barnett

not show remarkable differences with the exception of Fe^{+3} which seems to be enriched in the epidotes of the completely altered rocks. Furthermore, these epidotes show two types of zoning: (1) in the first type, the core is enriched in Fe^{+3} and depleted in Al, while the rims are depleted in Fe^{+3} and enriched in Al. (2) The second type of zoning is the converse of the first case.

6.4 Composition-Volume Changes

The actual gains and losses that take place in metasomatic alterations cannot be obtained without the knowledge of the relationship between the composition changes and the volume changes that accompany such processes (Gresens, 1967). A series of equations have been derived by Gresens (1967), allowing the calculations of gains and losses in terms of the chemical analyses and the specific gravities of the unaltered and altered rocks. The general mass balance equation derived by Gresens (1967), to calculate the actual gain or loss is:

$$100[fv\ (\frac{gB}{gA})\ C_n^B - C_n^A\ ] = X_n$$

The value of 100 is selected because chemical analyses add to 100 percent by weight; fv, is defined as the volume factor which is equal to the amount by which the volume of

solids on the left hand side of the equation is multiplied in order to obtain the volume occupied by the solids on the right side; when fv = 1, replacement is volume for volume, where fv >1, replacement takes place with a volume gain, when fv <1 replacement takes place with a volume loss; gB is the specific gravity of the altered rock, gA is the specific gravity of the unaltered rock; C_n^B is the weight percent of the different components in the altered rocks; C_n^A is the weight percent of the different components in the unaltered rocks; X_n is the actual gain or loss (in grams) of the different components. When comparing two rocks, it is necessary to know or assume a value for either the volume change or the geochemical behavior of one component in order to solve the equation (Gresens, 1967). Three examples of unaltered (= unepidotized rock) and altered (completely epidotized rock) were analysed in order to calculate the actual gains or losses in every set of these examples. Two sets of these examples (FM57→FM58A and FM69→FM68) were collected from the thesis area while the third set of examples (7536→7534) was collected by Dr W.S. Fyfe from the eastern part of the Arabian Shield. The chemical analyses and specific gravities of these sets of examples are given in Table 30. Using the chemical analyses and assuming different values for fv in the above equation, a set of data points are

Table 30. Major oxides of unepidotized (A) and epidotized (B) rock calculated to 100% anhydrous.

	A	B	A	B	A	B
	57	58A	69	68	7535	7534
SiO_2	50.44	42.01	51.78	50.06	60.65	61.39
TiO_2	1.44	2.16	1.87	1.37	0.54	0.46
Al_2O_3	15.54	16.06	16.03	14.51	17.14	15.42
Fe_2O_3t	10.35	13.29	12.06	12.89	6.48	7.48
MnO	0.22	0.21	0.21	0.17	0.11	0.09
MgO	7.69	4.67	4.25	3.03	3.22	0.60
CaO	9.84	20.33	7.71	17.27	6.19	14.45
Na_2O	3.23	0.16	4.80	0.28	3.71	-
K_2O	0.85	0.05	0.85	0.03	1.84	0.04
P_2O_5	0.40	1.06	0.44	0.39	0.12	0.07
L.O.I.*	1.79	2.44	1.20	1.95	1.50	1.80
S.G.**	2.90	3.03	2.98	3.21	2.83	3.09

L.O.I.* = weight percent loss on ignition at 1100°C.

S.G.** = specific gravity.

obtained. From these data points composition-volume diagrams were constructed (Figs. 102, 103, 104) by plotting gains and losses as a function of the volume factor. From the composition-volume diagrams it is possible to choose a value for fv where the curves for several components simultaneously intersect the isochemical axis (Gresens, 1967).

In the three examples of the composition-volume diagrams shown in Figs. 102, 103 and 104, it is noticed that Al_2O_3 intersects the isochemical axis at consistant values of fv (0.925, 1.03 and 1.025 respectively). Thus the values of Al_2O_3 fv, in the three individual examples, are assumed to be the most plausible estimate of the volume factor involved in this alteration process. In the first example (57→58A) shown in Fig. 102, the intersection of Al_2O_3 with the isochemical axis at fv value of 0.925 is assumed to be the volume factor. As a result of this assumption there would be little gain or loss in Al_2O_3 and TiO_2 and thus considered to be relatively immobile. Furthermore, this fv would require the addition of CaO and Fe_2O_3t and the removal of SiO_2, MgO, Na_2O and K_2O. The actual gains and losses calculated for this example are presented in Table 31.

In the second example (69→68) shown in Fig. 103, the intersection of Al_2O_3 with the isochemical axis at fv = 1.03, is also assumed to be the volume factor involved.

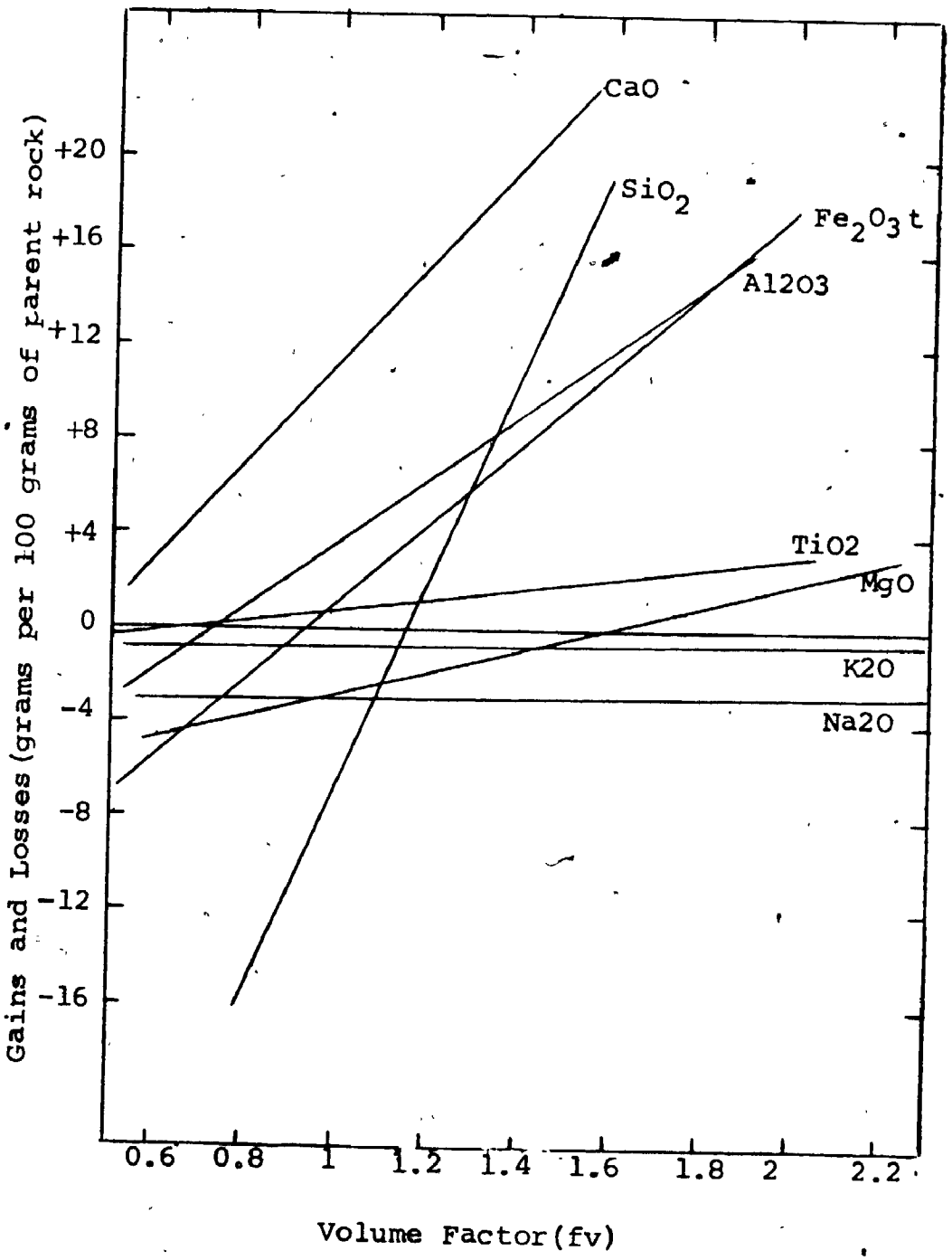

Fig. 102. Composition-volume diagram for samples # 57→58A.

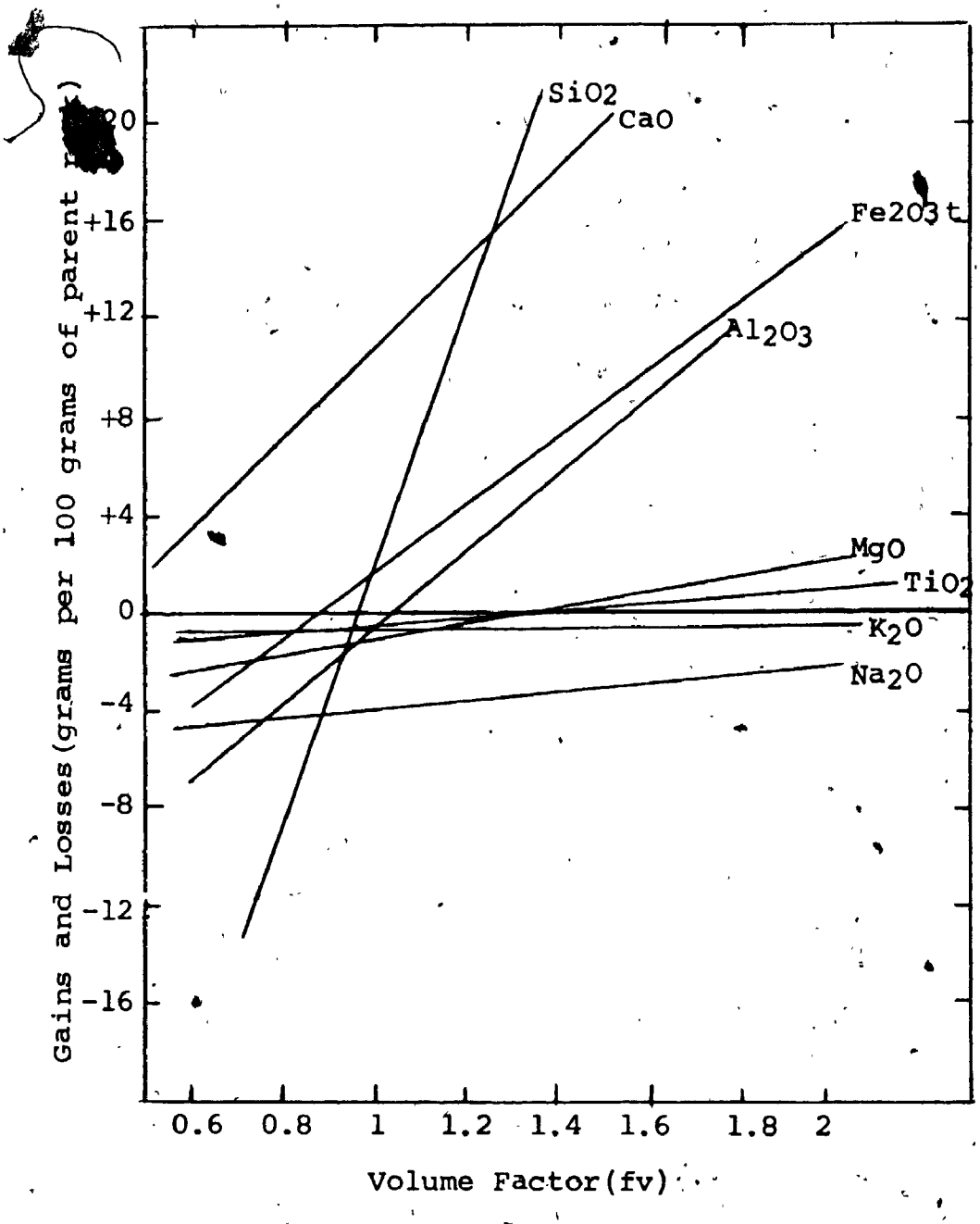

Fig. 103. Composition-volume diagram for samples #69→68.

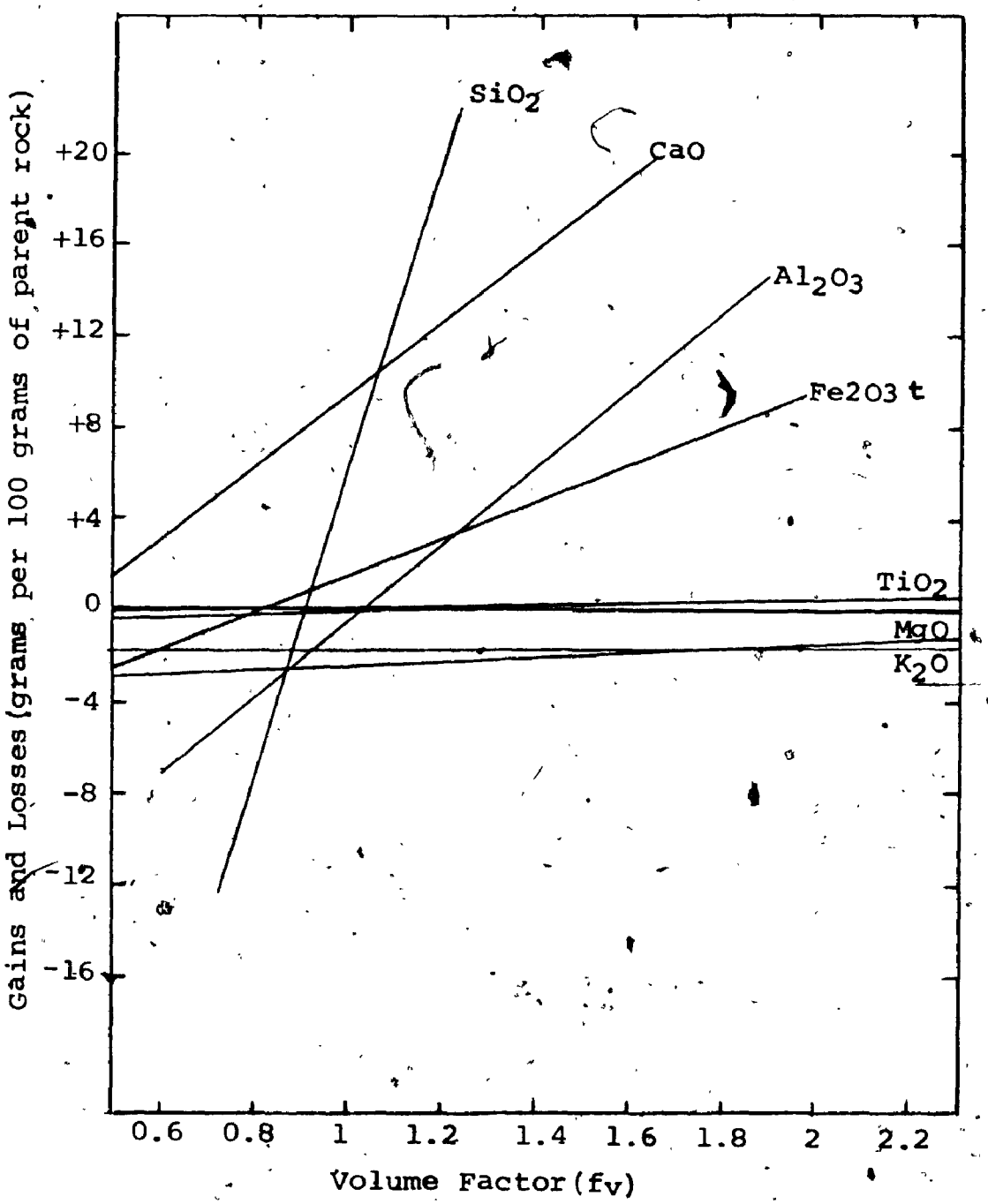

Fig. 104. Composition-volume diagram for samples #7535→7534.

3

TABLE 31. The gain and loss in grams per 100 grams of parent rock in the three examples and their average.

	1	2	3	4
SiO_2	-9.83	+3.78	+7.94	+0.63
TiO_2	+0.65	-0.35	-0.03	+0.09
Al_2O_3	-0.02	+0.07	+0.09	+0.04
Fe_2O_3t	+2.49	+2.25	+1.88	+2.21
MnO	-	-	-	-
MgO	-3.18	-0.89	-2.55	-2.21
CaO	+9.81	+11.46	+9.95	+10.41
Na_2O	-3.08	-4.49	-3.71	-3.76
K_2O	-0.80	-0.82	-1.80	-1.14

1 = The gains and losses in the first example (FM57→58A)

2 = The gains and losses in the second example (FM69→68)

3 = The gains and losses in the third example (7535→7534)

4 = Average gains and losses of the three previous examples.

As a result of this assumption of fv, Al_2O_3 and TiO_2 will be immobile; CaO, SiO_2 and Fe_2O_3t will be added while MgO, Na_2O and K_2O are removed. The actual gains and losses are given in Table 31. In the third example (7535→7534) shown in Fig. 104, the Al_2O_3 fv = 1.025 is also assumed. As a result, Al_2O_3 and TiO_2 will be immobile; CaO, SiO_2 and Fe_2O_3t are added, while MgO, Na_2O and K_2O are removed. The actual gains and losses in this example are presented in Table 31.

To summarise the discussion on these composition-volume diagrams, the following conclusions are drawn:

(1) The average volume factor (fv) is about 1, thus the alteration was approximately volume for volume.

(2) CaO and Fe_2O_3t were the principal components added. MgO was partially removed while Na_2O and K_2O were significantly depleted.

(3) Al_2O_3 and TiO_2 were relatively immobile.

6.5 Oxygen Isotope Relations:

Oxygen isotope analyses were performed on a suite of samples covering the range from primary igneous material, through partially epidotized, to the completely epidotized end product. Analyses were conducted on whole rock powders. The purpose of this stable isotope study was to test the hypothesis that the epidotization process and associated geochemical transport is the result of fluid-

rock interaction, and then to identify the fluid source. Oxygen isotope analysis is particularly suited to resolving this type of problem inasmuch as primary igneous rocks have a narrow and precisely established range of $\delta^{18}O$ values (+ 6 °/oo to + 8 °/oo SMOW, Taylor 1968, 1974) and any fluctuation from this value by isotopic exchange with an external oxygen reservoir, such as hydrothermal fluids may be readily detected.

(a) Results:

Whole rock $\delta^{18}O$ values are presented in Table 32. Inspection of the results reveals that the granites with primary igneous mineralogical and textural characteristics exhibit primary igneous $\delta^{18}O$ values (8.17 °/oo to 8.47 °/oo). However, the partially altered and epidotized rocks are depleted in $\delta^{18}O$ by up to 4 °/oo with respect to primary granitic rocks.

(b) Discussion:

During fluid-rock interaction, isotopic shifts from primary igneous $\delta^{18}O$ value are controlled essentially by the $\delta^{18}O$ of the external fluid reservoir, and by the temperature of oxygen isotope exchange. It is therefore pertinent to consider variations in the isotopic composition of natural waters in interpretation of the Al Hadah data. This subject has been extensively studied by Taylor and co-workers (1974). Natural waters fall into five

Table 32 Oxygen isotope analyses (in °/oo SMOW) of whole rock powders from primary and altered rocks of the Al Hadah igneous complex.

Sample description	Sample number	$\delta^{18}O$ °/oo
Primary	7535	8.47
	57	8.17
	26	8.26
Partially epidotized	62	4.78
Highly epidotized	7534	8.36
	68	6.21
	58A	4.71
	67A	5.04
	5A	5.79

distinct categories on the basis of oxygen and hydrogen isotope systematics; oceanic, meteoric, magmatic, metamorphic and evolved connate.

Ocean waters have a small range of isotopic composition, being defined as 0 °/oo, $\delta^{18}O$, δD. During evaporation of sea water and subsequent precipitation as meteoric water the light stable isotopes are progressively enriched by kinetic isotope effects, following the Rayleigh distribution equation. Such precipitated waters fall on a linear plot of δD against $\delta^{18}O$, where the depletion of heavy isotopes with respect to seawater is controlled essentially by climate.

Primary magmatic water exhibits a narrow range by $\delta^{18}O$ and δD values ($\delta^{18}O$ = 6 °/oo-9 °/oo SMOW). Metamorphic waters have a broad range of oxygen isotope values from 5 °/oo to 25 °/oo (Taylor, 1974). Connate or formation waters are generally seawater trapped in the pores of sediments, which may undergo enrichment of the heavy isotope by oxygen exchange with sedimentary minerals. However, Clayton et al.,(1966) obtained evidence that many formation waters contain a significant component of isotopically light meteoric water.

The oxygen isotope results for the Al Hadah granitic rocks may be evaluated in the light of the foregoing discussion. It is first necessary to assume a

temperature for the metasomatic process. The epidote, albite mineralogy is typical of a greenschist facies metamorphic assemblage, to which a reasonable temperature of 300°C may be assigned. If this value is assumed, then the observed $\delta^{18}O$ depletion in the epidotized rocks is consistent with transport of isotopically light meteoric waters through the system, or exchange with formation waters having a significant component of meteoric water. The recorded $\delta^{18}O$ values in epidotized granitic rocks are not compatible with exchange with magmatic or metamorphic fluids, which would yield isotopic enrichment in the alteration zone, at 300°C.

Oxygen isotope exchange with seawater at 500°C would yield depleted values relative to the primary igneous oxygen, but this temperature is considered to be too high in relation to the alteration mineralogy. In addition, field evidence implies that the Al Hadah plutons were not emplaced in a submarine environment.

Recent studies by Taylor and co-workers (1974) have emphasised the importance of the interaction of meteoric water with epizonal intrusions emplaced in proximity to the terrestrial surface. The igneous bodies act as energy sources to drive convective circulation of meteoric groundwater resulting in $\delta^{18}O$ depletion of the igneous rocks.

Oxygen isotope data for altered rocks of Al Hadah are most consistent with this model. Further evidence to support this interpretation is provided by data on the oxidation state of iron, which implies transport of oxidising surface waters through the system at elevated temperature.

Without a precise knowledge of the primary $\delta^{18}O$ value of the meteoric fluids, and the temperature of epidotization it is not possible to compute a water/rock ratio for the alteration process.

6.6 Conclusion on the Process:

As discussed above, the oxygen isotope data strongly suggests that meteoric water is involved in the epidotization process; magmatic water is virtually ruled out as a possible fluid source.

Inspection of the raw chemical data (Table 30), and the results of Gresens analysis of these data, clearly indicates:

(a) that there is large calcium enrichment.

(b) sodium and potassium are heavily leached.

(c) iron is oxidized.

(d) magnesium is leached

(e) that silica suffers either considerable loss or smaller gains.

Returning to the question of the alteration fluid source, it should be noted:

1 - fluids coming from an igneous source must be reducing and contain significant partial pressures of hydrogen (Carmichael et al., 1974).

2 - fluids from the granitic rocks must be saturated with quartz - alkali feldspar (of pegmatitites) and must precipitate these components along a path of falling temperature.

Thus such a fluid could not lead to Na-K or SiO_2 leaching. Again, magmatic fluids appear to be excluded. What is required appears to be a source of fluids with oxidizing components (SO_4^{2-}, O_2) and a high ratio of $Ca^{2+}/Na^{+} + K^{+}$. Marine fluids are known to oxidize and albitize rocks (spilitization). Inspection of typical ground and river water analyses, clearly show that, in these systems Ca^{2+} is the dominant cation and SO_4^{2-} exceeds chlorine. Much of the data could thus be rationalized by massive flow of high calcium ground waters along paths of increasing temperature; that is motion towards the granite as has been well documented by Taylor (1974). The only data found here which is ambiguous is that related to silica content. Water moving up temperature should leach SiO_2 and alkali elements: Sample 58A clearly shows this effect but the other pairs appear to show enrichment on the composition-volume diagrams which is less obvious in the raw data. Further work is needed to clarify this

aspect of the problem. The bulk of chemical data presented and the oxygen isotopes indicate that epidotization may be related to fluid migration from near the surface into the dry high-level intrusives. Concentration of the process near late rhyolite dike walls may indicate that such sites acted as good channels for such motion. This could be related to extension fractures filled by the dikes followed by volume contractions as the magma crystallizes. If this is sound, then extensive zones of epidotization around plutons may serve as an indication of the direction and extent of fluid flow into high-level granitic plutons. Fyfe (personal communication) has frequently noted extensive epidotization of andesites around the granites of the Sierra Nevada batholith. Some workers have attributed epidote concentrations to local calcareous patches in the contact rocks. At Al Hadah, the distribution of epidote rich rocks is not in accord with such a model.

CHAPTER 7

PETROGENESIS AND TECTONICS

7.1 General Statement

The two major groups of rocks that compose the Al Hadah Pluton are the dioritic group (diorite + gabbro) and the granitic group (granodiorite and monzogranite). In Chapter 5 the geochemistry of these two groups has been discussed in detail. The dioritic group exhibits some similarities of chemistry to the Cascade andesites and also to the basaltic andesite of S.W. Pacific island arcs. The granitic group shows some similarities of chemistry to the Sierra Nevada batholith. It has been concluded that the dioritic group is equivalent in composition to the Cascade andesite and also to S.W. Pacific island arc basaltic andesite, and it thus seems possible that the petrogenesis of the dioritic group is quite similar to the petrogenesis of these rock suites. Similarly, the petrogenesis of the granitic group may be equivalent to the petrogenesis of the Sierra Nevada batholith. In this chapter the origin of andesites (=diorite) and granites are reviewed, and the recent applications of plate tectonic models to the Arabian Shield is discussed in light of the

Al Hadah petrochemistry.

7.2 Origin of Calc-Alkaline Andesites (=Diorite)

It is difficult to give a general model for the origin of calc-alkaline andesites, for there is no universally accepted model which satisfies all of the restrictions of composition which have been determined to date. The principal hypotheses for the origin of andesites are as follows:

(a) Fractional Crystallization of Basaltic Magma

Bowen (1928) suggested that andesites were derived by fractional crystallization of basaltic magma, but this explanation requires tremendous volumes of parent basalts to yield the huge volumes of derived andesites exposed on the surface. Osborn (1959, 1962, 1969a) also suggested, on the basis of experimental studies, that andesite could be produced by fractional crystallization of basaltic magma under conditions of constant oxygen fugacity. An objection to this hypothesis was raised by Carmichael (1967), who concluded from experimental work that oxygen fugacity does not remain constant during fractional crystallization. Kuno (1966, 1968, 1969) also proposed that andesitic magma may form by fractionation of basaltic magma on the basis of field associations and the frequency of eruption of basaltic andesite associated with

basalt and andesite. The hypothesis of crystal fractionation has fallen to disfavor, and yet it is the only model which can be treated with any rigor at this time. Perhaps the eruption of andesite magmas, which are often accompanied by large volumes of pyroclastic material, requires a substantial amount of water, whereas the relatively anhydrous more basic magma beneath it lacks the propellant to achieve eruption; if it can be shown in future that the failure to erupt large volumes of basaltic magma in these andesitic arcs is due to some property of the magma, then much of the current criticism of the crystal fractionation hypotheses (in low pressure environment) will be void (Carmichael et al., 1974, p. 560).

(b) Contamination of Basaltic Magma by Sialic Material

Daly (1933) advanced a hypothesis to account for the predominance of andesite, saying that andesites represent basaltic magma with the addition of sialic crustal material. This suggestion has been subsequently developed, and is supported by a number of petrologic studies conducted by Tilly (1950), Kuno (1950, 1968), Waters (1955a), Dickinson (1962), Hamilton and Myers (1967), Ewart and Stipp (1968), and Peterman et al. (1970). However, this hypothesis has been refuted for the following reasons: i) Andesites are found in volcanic island arcs

which are built on oceanic crust, and geophysical and chemical data imply that there is no underlying crustal material (Gorshkov, 1965). ii) The trace element content of andesites are not compatible with assimilation of large quantities of crustal materials (Taylor, 1969; Hedge, 1969; Hedge and Peterman, 1969) and iii) The strontium isotope ratios are lower than they should be if basaltic magma were contaminated by crustal material. Moreover, the Sr^{87}/Sr^{86} ratios are not much different from ratios for tholeiites of Hawaiian Islands where sialic crust is generally believed to be absent. Furthermore, a detailed study carried out by Brooks, et al. (1976), to find the cause of the high Sr^{87}/Sr^{86} ratios in Cenozoic andesites and dacites of southern Peru, led them to reject crustal contamination as a plausible mechanism for the large recorded value.

(c) Partial Melting of Mantle Material

Kushiro, et al. (1968) and Kushiro (1969), showed that andesitic liquids could be obtained directly by partial melting of the upper mantle in the presence of sufficient amounts of water. Green and Ringwood (1968) suggested on the basis of their high-pressure experimental studies that calc-alkaline andesites were formed at depths of 80 to 150 km by partial melting of quartz eclogite, or, at depths of 30 to 40 km by partial melting of amphibolite

and gabbro. On the other hand, on the basis of experimental work, Yoder (1968) pointed out that calc-alkaline andesite magma can be derived directly from the mantle peridotite under hydrous conditions; and he emphasised the specific characterisitcs of andesitic rocks such as over-all high alumina content, the common presence of hydrous phenocrysts of hornblende which indicate the importance of high water content at high pressures. McBirney (1969b) has suggested that abundant water might enter the mantle deep beneath eruptive arcs. The water might readily flux the hot mantle which is already near its liquidus temperature. If these speculations are correct, according to McBirney (1969b), basaltic parentage for andesitic magma is not required. Recently, Brooks et al. (1976) concluded from their study on isotopic pseudoisochrons of various magma products that the source for these magmas might have been an ancient sub-continental lithosphere which is isotopically enriched and grossly heterogeneous. If this ancient lithosphere participates in younger magmatism, then the volcanic products will contain isotopic evidence of the "prehistory" of the source region.

(d) Melting of the Descending Oceanic Lithosphere

The intimate association of calc-alkaline andesites with descending oceanic plates (i.e. subduction zones) is

so well established (Isack et al., 1969; Barazangi et al., 1970; Dickinson and Hatherton, 1967; Dickinson, 1970), that there is a tendency to assume the presence, or recent occurrence of a subduction zone under andesitic volcanic chains that are not associated with deep seismic activity (Carmichael et al., 1974, p. 530). The oceanic plates are believed to begin their descent where they meet either a continental plate (e.g. the Andes of South America) or another oceanic plate (e.g. Marianas arc). This close association between the formation of calc-alkaline andesites and subduction zones led to a number of recent hypotheses for the origin of these magmas above subduction zones. Some of these hypotheses are supported by experimental evidence. The idea of the genesis of andesite magma from the partial melting of the downgoing oceanic plate has been developed in recent years and has become accepted by many workers (Sykes, 1969; Gilluly, 1969, 1971; Press, 1969; Hamilton, 1969; Green and Ringwood, 1969; Souther, 1970; Dickinson, 1969, 1970a; Fyfe and McBirney, 1975). Ringwood (1974), on the basis of recent studies in experimental petrology has suggested three mechanisms for the genesis of orogenic volcanic series: i) partial melting of amphibolite. ii) Partial melting of quartz eclogite. iii) Direct partial melting of unfractionated primary mantle (pyrolite) under conditions of high

load pressure and high water pressure. According to Ringwood (1974) all these three processes are important and play complementary roles. The common feature for all three processes is the neccessity of high load pressures and high water vapour pressure. Moreover, he suggested that the generation of high water pressure in the mantle source regions was caused by the introduction of water into the mantle by the subducted lithosphere. Ringwood (1974), proposed two idealized models to explain the two phases (tholeiitic and calc-alkaline) in relation to the location of volcanoes with respect to the Benioff zone. In the first model (Fig. 105a) the subducted lithosphere descends and starts to heat up, at the stage where the crust reached a depth of 100 km. A large amount of the water produced by the dehydration of amphibolite in the slab rises into the mantle above causing a drastic decrease in the viscosity and initiating the uprise of pyrolite from the Benioff zone. Partial melting occurs in the rising magma diapirs in the presence of high water vapour pressure, leading to the separation of hydrous tholeiitic magmas and this represents the early tholeiitic stage of island arc development. The second model (Fig. 105b), at greater depths most of the oceanic crust will have been converted into quartz eclogite. The dehydration of serpentinite and its high pressure derivatives maintains a

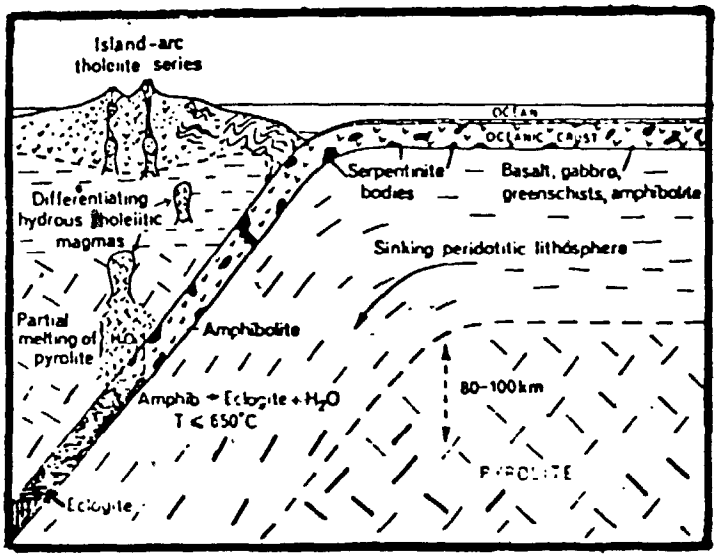

(a)

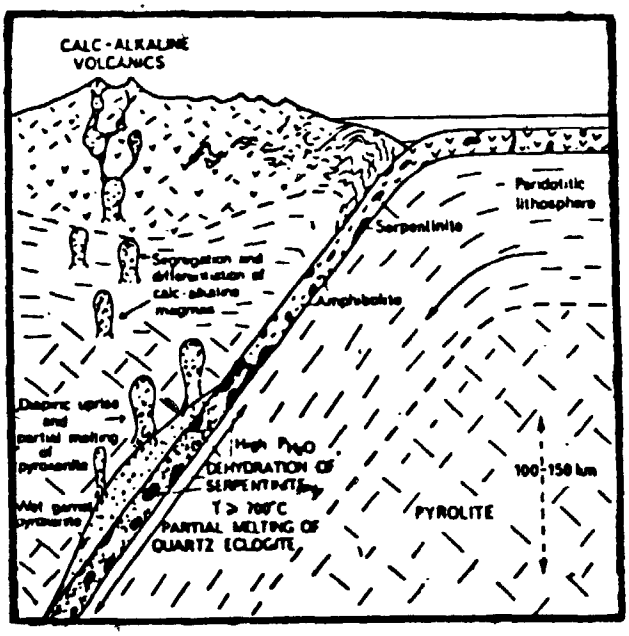

(b)

Fig. 105 . Early(a) and late(b) phases in the development of island arcs(after Ringwood,1974).

high P_{H_2O} throughout the crust in the depth range 100-300 km. As the temperature in the crust rises above 750°C, partial melting of quartz eclogite occurs, leading to the development of rhyodacite-rhyolite magmas, particularly in the 100-150 km depth interval. These liquids will rarely reach the surface, but will more likely react with overlying mantle pyrolite, converting it into a garnet pyroxenite. The pyroxenite bodies will possess a slightly lower density than surrounding pyrolite. Moreover, the addition of water makes these pyroxenite bodies highly mobile. As a result, diapirs of hydrous pyroxenite are detached from the Benioff zone and undergo partial melting as they rise. During their ascent, these magmas will fractionate giving a wide range of orogenic-type magmas possessing calc-alkaline characteristics. Thus according to this model, calc-alkaline magmas are derived from two distinct sources - by partial melting of the subducted oceanic crust and by partial melting of the pyrolite wedge overlying the Benioff zone.

Another possibility is generation of andesitic magma by fusion of oceanic crust and some of its veneer of pelagic sediment in a subduction zone (Carmichael, et al., 1974, p. 562). If chemically unaltered abyssal tholeiite retaining its typical Sr^{87}/Sr^{86} ratio of 0.7026 is the main component of the crust, the value of 0.704 typical of island

arc andesites could be achieved by incorporation of the overlying sediment (Sr^{87}/Sr^{86} = 0.709 [Armstrong, 1968]). There are no unequivocal data to support or refute the possibility that pelagic sediments are involved in the process of magma generation (as suggested by Coates, 1962). Church (1973) concluded from experimental studies that very minor amounts (less than 2 percent) of pelagic sediment are involved in the genesis of andesitic magma of the High Cascade. A similar conclusion, concerning the minor contribution of pelagic sediment to the generation of magma in the Tonga Arc, was reached by Oversby and Ewart (1972). A quite different point of view has been stated by Sibley and Vogel (1976): "Pelagic sediments in contrast to other sediments, are not usually recycled; most are subducted and therefore act as a geochemical sink."

Fyfe and McBirney (1975) argued that the amount of water carried to greater depths is largely a function of the amount of potassium in the rocks, and the dehydration process occurs in two main zones: a shallow one where amphibole, muscovite, talc and serpentine become unstable and a deeper one where phlogopite breaks down and the proportion of water released in the two zones is largely related to the potassium content of the system. Furthermore, the dehydration process is strongly endothermic and

will tend to prolong the stability interval of hydrous phases to greater depths. They also concluded that the rate of magma generation must be a direct function of the amount of phlogopite and in turn the amount of potassium originally in the sediments and alkali-rich basalt of the descending slab.

7.3 Origin of Granite

This discussion on the origin of granites is not intended to be a comprehensive review because the subject has been dealt with in detail (Gilluly, 1948; Read, 1957; Mehnert, 1959, 1968; Winkler, 1967). Its purpose is to present a short review of recent hypotheses on the possible sources for granitic magma. At the present time, there is little support for the once popular genetic model which derived great volumes of granitic magma by fractionation of parental basaltic magma (Bowen, 1928), nor for the alternative hypothesis that postulated metasomatic granitization on a large scale without the participation of granite melts (Perrin and Roubault, 1949; Perrin, 1954, 1956; Read, 1957; Barth, 1948; Raguin, 1965). Recent hypotheses for the origin of granitic magmas are:

(a) Partial Melting of Sialic Crust (including Geosynclinal Sediments):

This model argues that granitic magmas are derived

from partial fusion of the lower part of the crust including the thick accumulations of geosynclinal sediments and volcanic rocks. During burial, these rocks become metamorphosed and partially dehydrated, and will be subsequently heated and start to yield liquid fractions of granitic composition. This model is widely accepted by many workers (Bateman and Wahrhaftig, 1966; Hydnman, 1969; Bateman and Dodge, 1970; Wollenberg and Smith, 1970). Pitcher and Berger (1972) concluded from studies of the Donegal Granites, that these granites were produced by remelting of the sial, and during ascent the composition was diversified by processes of contamination.

The processes involved in generation of granitic magmas as envisaged by Fyfe (1970) and Brown and Fyfe (1970) are as follows: before melting starts the sedimentary rocks must be depressed into domains of high grade metamorphism and these rocks must reach the amphibolite or granulite facies. Water in these rocks is present in hydrous minerals such as biotite, hornblende or muscovite. "As these metamorphic rocks become progressively buried and heated, an initial liquid fraction would be produced depending on the amount of muscovite present followed by a biotite fraction and finally a hornblende fraction." The shaded area in Fig. 106 shows the major production area of large masses of granitic liquids. If these

liquids formed are sufficient they will start to invade the crust; if not, they will accumulate until they are able to overcome the forces resistant to upward motion (Brown and Fyfe, 1970). It is important to note that the melting of hydrates occurs on curves having a positive slope ($\frac{dP}{dT}$).

Pitcher (1974) concluded that the Mesozoic and Cenozoic batholiths of Peru were produced by remelting of the crustal material by the heat and volatile input of rising magmas generated in the Benioff zone, and such a process can lead to the production of a normal calc-alkaline sequence, in the order of diorite → quartz diorite → tonalite → granodiorite. This model is also accepted by Cobbing and Pitcher (1972a) for the generation of the Coastal Batholith.

Chapell and White (1974) have distinguished two types of batholiths that they interpreted as being derived by partial melting of either sedimentary (S-type) material or mantle-derived igneous (I-type) material. Green (1976) tested the proposal that specific S-type granites were derived by partial melting of pelitic rocks. He confirmed that the fusion of pelitic rocks with 2 and 5% H_2O at pressures of 4, 7 and 10 Kb, produces granitic liquids.

Wyllie (1977) reviewed the experimental studies in the synthetic systems An-Ab-Or-Qz-H_2O and K_2O-Al_2O_3-

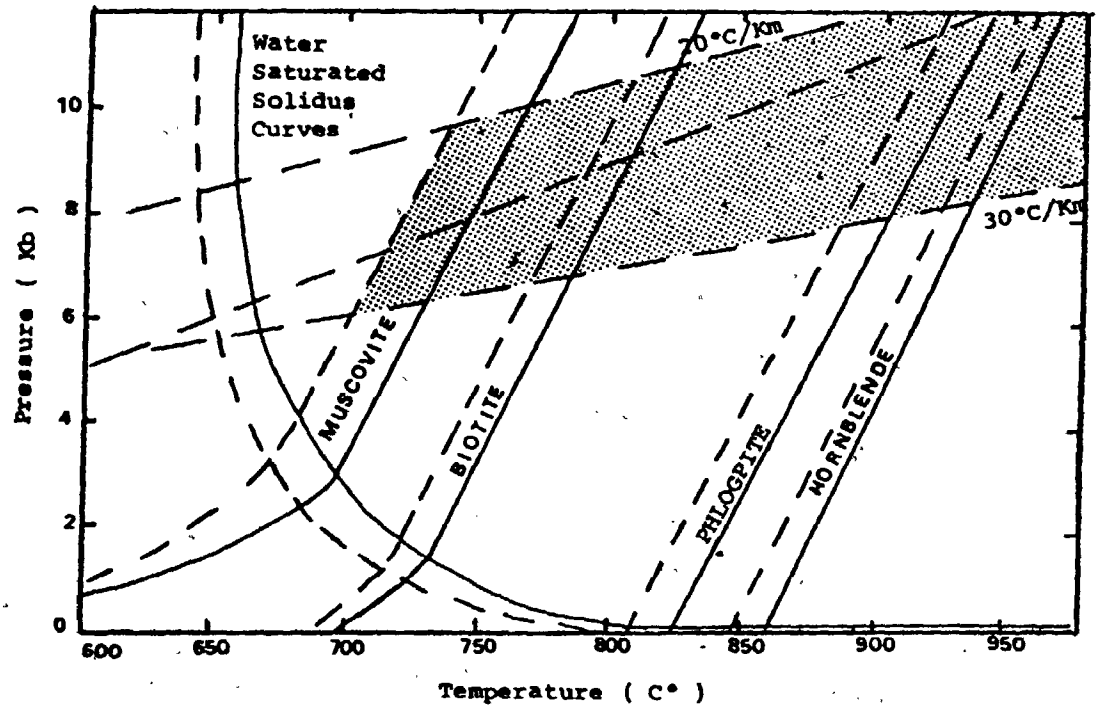

Fig. 106. This diagram shows the beginning of melting in granitic (dashed lines) and dioritic (solid lines) compositions. The shaded area shows the probable region for maximum magma generation. (After Brown and Fyfe, 1970).

SiO_2-H_2O and concluded that these studies showed the dominance of feldspar and quartz assemblages in crustal anatectic processes, and the role of hydrous materials such as muscovite. The normal product of regional metamorphism is H_2O-undersaturated granitic liquid. Liquids of granite composition trend towards a granodiorite composition with increasing temperature or pressure (loc. cit.). Liquids of tonalitic and dioritic composition cannot be generated by crustal anatexis under conditions of normal regional metamorphism (contrast to Fyfe, 1973) and these magmas must represent crystal mushes, unless there has been significant contribution of heat and material from less silicious magmas generated in subducted ocean crust and mantle peridotite (Wyllie et al., 1976; Wyllie, 1977). More basic magmas rising from the mantle could differentiate into tonalite by the time they enter the crust or within the crust.

(b) Partial Melting of the Oceanic Crust:

Partial melting of ocean basaltic crust or upper mantle-lower crust has been suggested by Hamilton and Myers (1967) as another possible source for granitic magma. Partial melting of the upper mantle occurs above a subduction zone where the oceanic plate descends below a continental margin (Hamilton, 1969; Gilluly, 1967; Dickinson, 1970). Hietenen (1973) concluded that the

granitic magmas of the Sierra Nevada, California, were generated by mixing magmas formed by anatexis of lower crust and magmas formed by partial melting of the mantle and the subducted oceanic crust below. This hypothesis of partial melting of the mantle is favoured by a number of workers, and very recently Brown (1977) suggested a mantle origin for the Cordilleran granites, based on strontium isotope data. Sr isotopes have been utilized by many workers as a helpful guide to solve the problem of [illegible]mas. However it may be misleading to rely completely on Sr isotope data in the interpretation of the source rocks for granite, as argued by Carmichael et al. (1974): "The isotopic composition of lead and strontium in granitic rocks cannot be used alone to identify source rocks nor to locate these at specific levels within the mantle or deep crust." Armstrong (1977) confirmed this fact by saying that the Sr ratios of many rocks are better indicators of the nature of the enclosing crust than of the magma source at depth, and this restriction may also apply to all isotopic and trace-element characteristics. Fyfe (1977) argued against Brown's hypothesis, saying that the Cordilleran granites are possibly best described as "the product of mixing of the fusion products of contaminated mantle and crust."

Collection and Ascent of Granitic Liquids:

The problem of collection and ascent of these granitic liquids are considered by Elsasser, 1963; Ramberg, 1967, 1970; Fyfe, 1970; Brown and Fyfe, 1972; and Fyfe, 1973. If small volumes of material are to collect and move, either the viscosity of the lower crust must decrease or generation of a permeable system is necessary (Fyfe and Brown, 1972). The melting process itself will lead to the necessary lowering of viscosity. The lowering of the viscosity will lead to the separation of molten lower crust from the solid and less dense liquid and as a result a clean melt layer bounded by high viscosity upper crust will be formed. The fluid dynamic theory discussed and illustrated by Ramberg (1967) showed that such a gravitationally unstable layer will spontaneously develop perturbations. These perturbations amplify to the point where they detach off and move upwards. Small masses would move slowly and cool rapidly and their chances of high level intrusion would be small (Fyfe and Brown, 1972). In the lower crust a liquid drop rises by plastic deformation of the surroundings, while near the surface, brittle processes become dominant accompanied by stoping and fracture (Fig. 107).

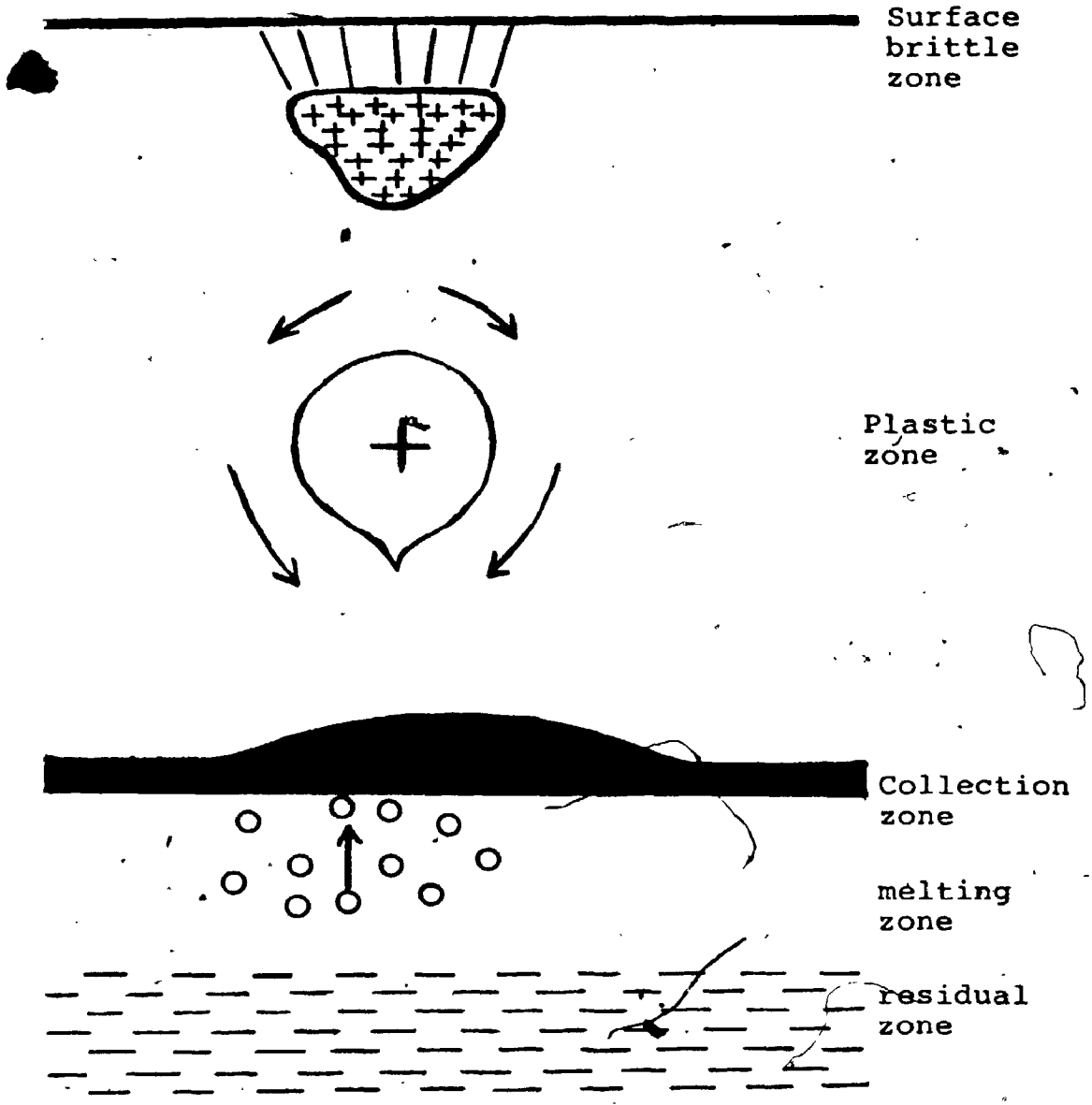

Fig. 107 . Schematic diagram of the formation of a pluton. (After Fyfe, 1970.)

7.4 Al-Hadah Granite in the Light of Granite Hypotheses:

To conclude this short discussion on the possible origin of granites it seems that the granitic rocks of Al Hadah Pluton possibly fit within the model which invokes anatexis of the lower crust (Fyfe, 1970; Brown and Fyfe, 1970; Fyfe and Brown, 1972; Fyfe, 1973). A similar conclusion was reached by Nasseef (1971), and Nasseef and Gass (1976) from their studies on At Taif Granites in which they concluded that these granites were produced by partial fusion (anatexis) of the lower crust. Furthermore, emplacement of Al Hadah and At Taif granites in an area of high regional metamorphism support the concept of anatexis.

7.5 Some Quantitative Aspects of Granitic Magmas:

The granitic rocks of Al-Hadah region have been affected by assimilation. Secondly, igneous layering has been observed in the monzogranite. These features are discussed and explained in the following quantitative examples:

(a) Assimilation:

It has been concluded in Chapter 5 that contamination has played an important role in the evolution of the dioritic and granodiorite rocks of Al Hadah Pluton, thus it is relevant to discuss the ability of granitic magma

(in general) to assimilate a country rock. The assimilation process involves heating the country rock from its initial temperature T_i to the temperature where it melts T_m. For most country rocks the melting temperature will be near the melting temperature of the granite itself. To heat the country rock the energy required is equal to the heat capacity, Cp, times the difference in temperature between the initial and melting temperatures of the country rock (T_m-T_i). We must also take into consideration the latent heat of fusion which to a first approximation could be ignored, for it could be compensated for by an equal amount of latent heat of crystallization of the initial granite-melt. The ability of a granite magma to assimilate depends primarily on its superheat which is equal to the difference between the freezing temperature and the temperature of ascent (T_m-T_A), (Fig. 108). The superheat is dependent on the ascent velocity; if the ascent was fast, the melt formed at the melting region (X) will hardly cool down and it will arrive at the surface close to its maximum temperature T_{max} or to the same temperature where it starts to melt, T_x. The slope of the melting curve for granites, $\frac{dp}{dt}$, is positive (Fyfe, 1973) and is about 100°C for 10 Kb or 30 km (See Fig. 106). Thus, if a melt rises from say 40 km having a temperature T≈ 800°C and rises rapidly towards the surface (10 km) its freezing

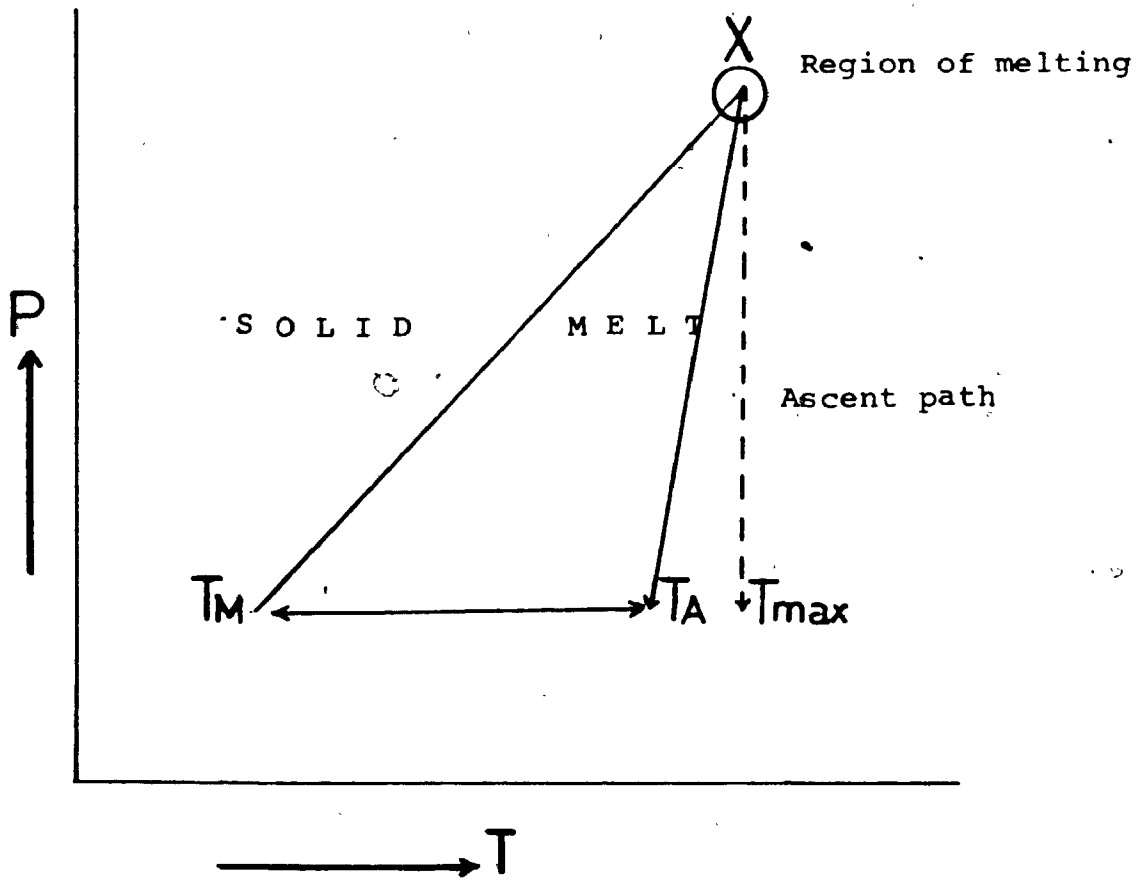

Fig.108 . Schematic diagram showing that the amount of superheat ($T_M - T_A$) of a granitic melt is dependent on its velocity of ascent.

temperature will be about 700°C. It then has a maximum superheat of 100°C or a heating ability of Cp x 100. Assuming that Cp (liquid) is similar to Cp (solid) (Carmichael, et al., 1974, p. 126), then we can write the assimilation equation:

Q (quantity assimilated) α Cp x 100 --- Therefore

M_{cr} (mass of country rock) x $(T_m - T_i)$ = $M_{liq.}$ (mass of granitic liquid) x 100. Let us assume that the melting temperature of the country rock $T_m \simeq$ 800°C and its initial temperature $T_i \simeq$ 400°C (at a depth of 12 km), then:

$$M_{cr} \times (800-400) = M_{liq.} \times 100 \text{ --- or}$$

$$M_{cr} = 1/4\ M_{liq.} \text{ --- that is 25\% assimilation}$$

or contamination.

Under these conditions the granitic liquid could assimilate 25% of the country rock by the time 25% of the granite liquid is frozen, to compensate for the latent heat of fusion. Let us take another example where the initial temperature is $T_i \simeq$ 200°C (at a depth of 7 km), then $M_{cr} = 1/6\ M_{liq.}$ or 17% contamination.

It is noteworthy that because rising granites must be rather dry (Fyfe, 1973), most country rocks will contribute water to the melt and this will lower the real freezing

temperature. Therefore, the assumption of very rapid rise leads to overestimation, but the addition of H_2O leads to underestimation. The maximum figure could be conservative.

Thus, we have seen from the quantitative examples given above that a granite liquid could readily assimilate the country rock to various degrees, depending on the superheat and the depth at which assimilation occurs.

(b) Settling Rates of Xenoliths in Granitic Liquids:

Since numerous xenoliths were observed in the granitic rocks of Al Hadah Pluton, it is worthwhile here, to discuss the rate of sinking of xenoliths in granitic magmas in general.

This rate could be obtained by applying Stoke's law:

$$V = \frac{2.g.r^2.(\Delta\rho)}{9.\eta}$$

where V is the rate of sinking; g, acceleration of gravity (= 10^3 cm sec^{-2}); r, the radius of the object or inclusion (let us assume a value of 10 cm); $\Delta\rho$, the difference in densities between that of the inclusion ($\simeq$ 2.8 g cm^{-3}) and that of the granitic melt ($\simeq$ 2.4 g cm^{-3}); η, the viscosity of granitic liquid which varies between 10^6 (for wet melt) to 10^{10} poises (=g s^{-1} cm^{-1}) (for dry melt) (Carmichael, et al., 1974, p. 144).

In the first case where the viscosity of the granite is 10^{10} poises (dry granite) the velocity of sinking (V) will be 300 cm year^{-1}; while in the other case where the viscosity is 10^{6} poises (wet granite) the rate of sinking (V) will be faster (3 km year^{-1}). These calculated examples show that xenoliths sink very fast in granitic melt and it is very possible that large blocks of the country rock could be assimilated during sinking through the granitic magma.

(c) Convection of Granitic Liquids:

The chemical and mineralogical data for the granodiorite and monzogranite of Al Hadah Pluton, show that these rocks were relatively homogenous in composition, secondly the monzogranite showed some local graded layering. (The origin and description of these layering have been studied in full detail by Hadley and Greenwood, 1976.) These features could be explained in terms of the ability of granitic magma to convect and mix. Could a granite magma convect? The ability of any fluid to convect depends on its Rayleigh number* (Elder, 1976), a dimensionless parameter which is defined by by the following formula:

---

* Rayleigh number: is a measure of the effectiveness of the buoyancy forces acting against the combined resistance to motion of viscosity and the diffusion of temperature variations by thermal conductivity (Elder, 1976 p. 53).

$$Ra = \frac{\gamma . g . \Delta T . h^3}{K . \eta}$$

where γ is the coefficient of expansion ($= 10^{-5}/C°$); g, the acceleration of gravity ($= 10^3$ cm sec^{-2}); ΔT, the temperature difference across the body (let us say 10°); h, the dimension of the body; K, the thermal diffusivity ($= 10^{-3}$ cm^2 sec^{-1}); η, the kinematic viscosity ($= 10^6$-10^{10} stokes). If we take an example of a granitic mass 1 km in diameter (10^5 cm), substituting the assumed values in this formula will give a Rayleigh number (Ra) of 10^{11}-10^7. This value for Ra coincides with Elder's (1976) third category which is defined by Rayleigh number (Ra)> 10^5 in which case we get "vigorous non-steady convection dominated by an apparently chaotic eddying motion with eddies of a wide range of sizes." Thus, this calculation shows that granitic magma can vigrously convect under the assumed conditions. Therefore, it is no wonder that granitic plutons are contaminated and show evidence of flow structures (e.g. the layering in the monzogranite).

7.6 Tectonics of the Arabian Shield

One of the dominant problems of modern earth science involves the search for evidence concerning the time span of modern-type plate motions. All major tectonism is closely associated with thermal structures

and patterns in the upper mantle and hence with igneous activity. Hargraves (1976) has put forward a convincing case for different tectonic styles in the Archean (see also Kroner, 1976); tectonics as discussed by Ramberg involving vertical and horizontal motions of comparable scale and wavelength. The modern style is one of large scale horizontal motions resulting from vertical motions (at ocean ridges and subduction zones) at restricted regions. At the present time a great deal of information is accumulating from regions influenced by Pan-African structures. These structures formed at a time which straddles the Proterozoic-Phanerozoic time periods, appear to represent a period when modern styles were initiated. Part of the discussion is well summerised by Shackleton (1976): "A large proportion of the African crust yields Pan-African radiometric ages (650-450 Ma). The Pan-African domains (Fig. 109) form a network of mobile belts surrounding cratons which remained relatively stable, cool and undeformed. The crust in the Pan-African domains had a similar previous history to that in the cratons. There is no process of cratonization and no progressive increase in cratonic dimensions, only a progressive reduction in the area unaffected by successive deformations. No tectonic, structural, stratigraphic or paleomagnetic data suggest large-scale plate motions. No convincing ophiolites or

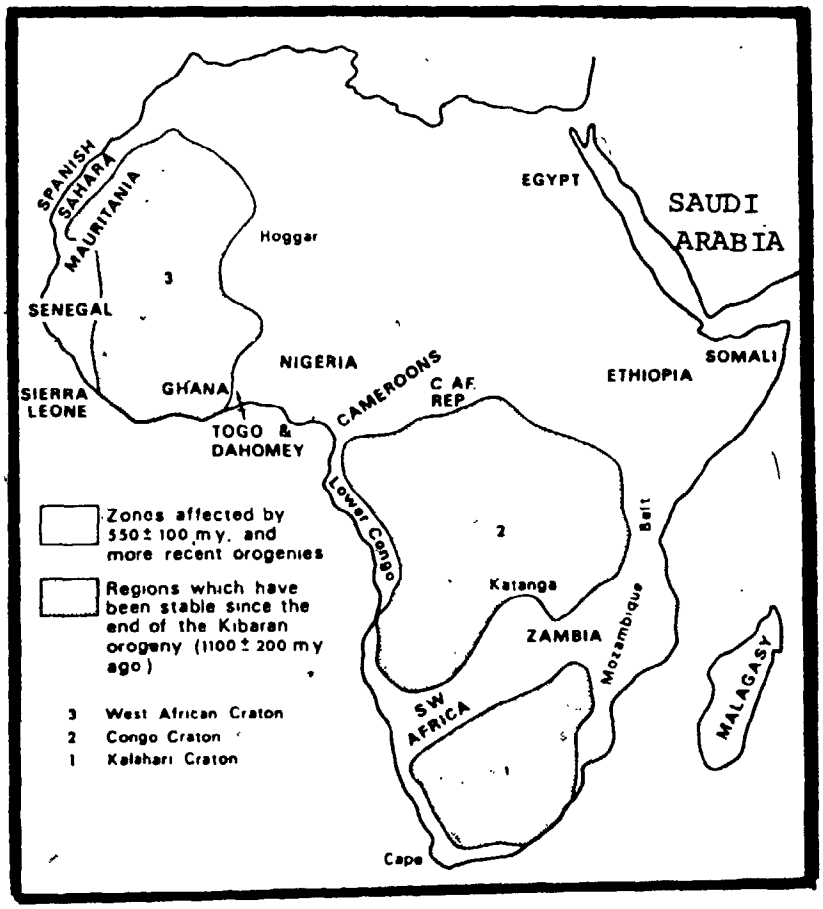

Fig. 109. Zones affected by Pan African Orogeny (500 ± 100 my) surrounding stable cratons.

sutures have been recognised within Pan-African domains. "In situ' deformation rather than collision orogeny seems probable."

The application of modern-type motions to the Arabian Shield has been taken into consideration very recently, and in fact, the interpretation of the tectonics of the Arabian Shield in terms of the modern theories developed during the last four years by a number of workers (Greenwood and Brown, 1973; Greenwood et al., 1975; Al-Shanti and Mitchell, 1975; Bakor and Gass, 1976; Nasseef and Gass, 1976; Marzouki and Fyfe, 1977).

The Arabian Shield and NE Africa are characterised by a marked abundance of granitic rocks (Nasseef and Gass, 1976). As one of the primary locations of acid magmatism in the present day tectonic environments is above subduction zones, thus speculations and hypothesis of a possible island arc model were envisaged for parts of the Arabian Shield (Greenwood and others, 1975; Baker and others, 1976; Nasseef and Gass, 1976; Marzouki and Fyfe, 1977).

Greenwood and Brown (1973) related their findings of an increase in the ratio $K_2O/K_2O + Na_2O$, accompanied by an increase in the proportion of granite to diorite exposure, from the southwest to the northwest, to a possible eastward dipping subduction zone. Though the rock types of

the Arabian Shield are similar to those found in areas of subduction zones, still, this hypothesis needs a lot more chemical and structural data (loc. cit.). Later, this hypothesis was developed by further studies carried out by Greenwood and others (1975) in which the southern part of the Arabian Shield was identified as a cratonized intraoceanic island arc (loc. cit.). This represents a different point of view of the situation as seen by Shackleton (1976). This cratonization process was episodic and evolved, as envisaged by Greenwood and others (loc. cit.) through "extensive volcanism and cannibalistic sedimentation accompanied and interrupted by the intrusion of large volumes of plutonic rocks and associated tectonism and metamorphism". They (Greenwood and others, loc. cit.) confirmed the northwest trend and eastward dipping Benioff zone for the proposed island arc suggested by Greenwood and Brown (1973). The episodic character in the Arabian Shield orogeny suggests that subduction of the oceanic plate was also episodic and such episodic activity is common in subduction zones associated with modern island arcs. Similar conclusions have been reached by further studies carried out in the northern part of the Arabian Shield (Rexworthy, 1971; Bakor, 1973; Neary, 1974), the eastern desert of Egypt

(Garson and Shalaby, 1974) and in the NE Sudan (Gass and Neary, 1976). All these studies called for the cratonization of oceanic island arc systems. Recent work on outer arcs and collision belts provided possible models for the evolution of parts of the Arabian Shield. This type of model led Al Shanti and Mitchell (1975) to propose that "the thick volcanic, volcaniclastic and sedimentary succession of the Proterozoic Halaban Group in the east of the Shield is intruded by syn- to late-tectonic plutons and resembles Cenozoic subduction-related magmatic areas". On the other hand, and along with this type of investigation, other workers were looking for basic-ultrabasic and possibly ophiolitic suites, if present, associations in the region (Bakor, 1973; Neary, 1974; Bakor and others, 1976; Garson and Shalaby, 1974). Bakor and others (1976), on the basis of petrographic and geochemical data identified the mafic and ultramafic complex of Jabal Al-Wask (NE of the Arabian Shield) as an ophiolite formed in a back-arc environment. Furthermore, several ultramafic zones lying in a NW-SE zone across Western Arabia and northeast Africa separated by a granite basement (Fig. 110) believed to be formed by cratonization of island arcs (Bakor and others, 1976). These ultramafic zones are sutures between these arcs and they represent lithosphere remnant of back-arc seas (loc. cit.). A possible model explaining the

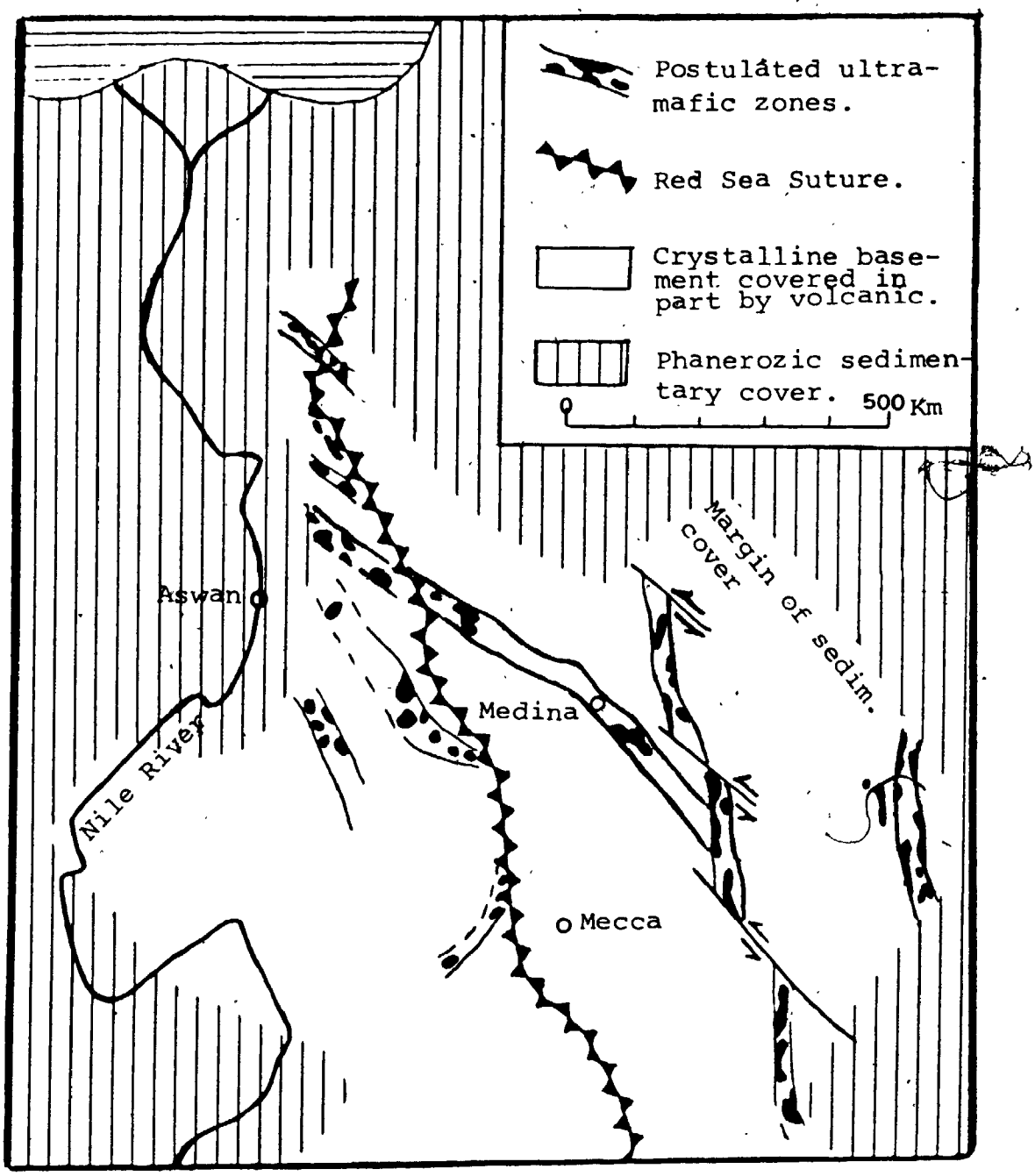

Fig. 110. Distribution of mafic-ultafmafic complexes and zones in western Arabia and northeast Africa. (After Bakor, et al., 1976).

presence of these suture zones is given in Fig. 111.

The lack of any paleomagnetic data which suggest large scale plate motions (Shackleton, 1976) suggests that a paleogeogeographic situations similar to that of present day south-west Pacific might have existed (Bakor and others, 1976; Marzouki and Fyfe, 1977).

7.7 Discussion:

On the basis of similarities in composition, rock distribution and order of emplacement between the plutonic rocks of Al Hadah region and rocks emplaced in subduction zones, it appears that the Al Hadah plutonic rocks are typical of a subduction environment under a continental crust. The source for the magmas that produced these rocks involved both partial melting of the subducted material and partial melting of the continental crust. The sequence of the rocks present in Al Hadah pluton could be explained by the model given in Fig. 112. In the first stage, when the ocean crust descends with its pelagic sediments to deeper levels it starts to melt producing andesitic liquids which rise to the surface. Parts of these andesites were trapped in the crust and formed the dioritic rocks. In the second stage, as a consequence of the huge deposition of andesites, the continental crust will be loaded and gets thicker. In the

(1) Micro continental plates separated by oceanic crust.

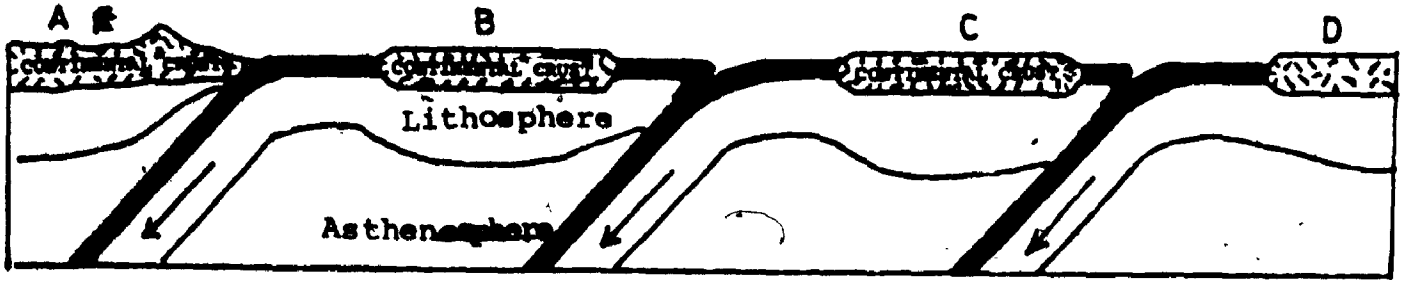

(2) Several subduction zones start to develop.

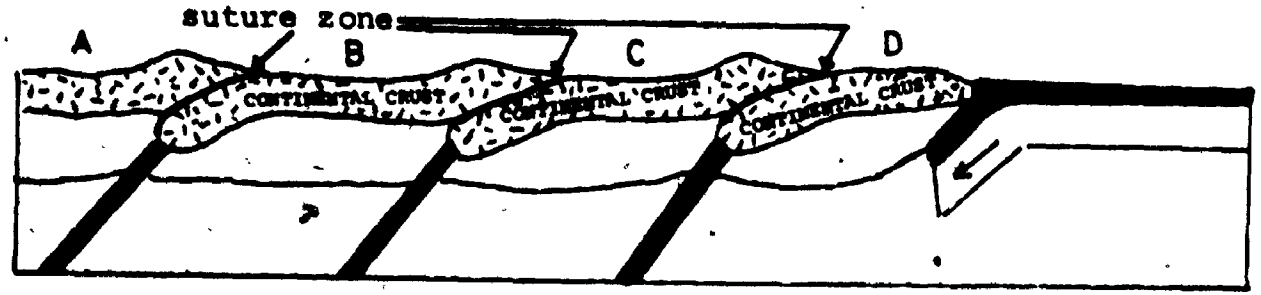

(3) When the subducted layers are consumed the microcontinents, which are too buoyant to be carried down, will collide with one another. The sutures are sites of former oceans.

Fig. 111 . Plate tectonic models for possible subduction and collision in the Arabian Shield.

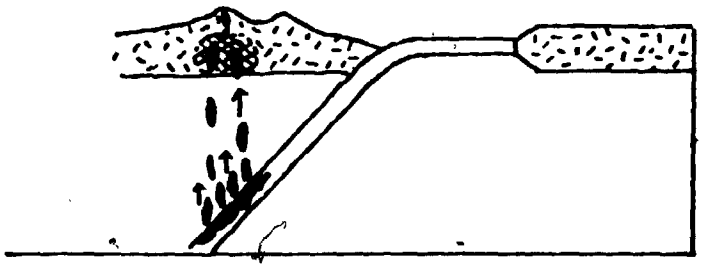

(1) Andesitic magma starts to form from the descending ocean slab. The traped andesite (cross-hatched area) produced the dioritic rocks.

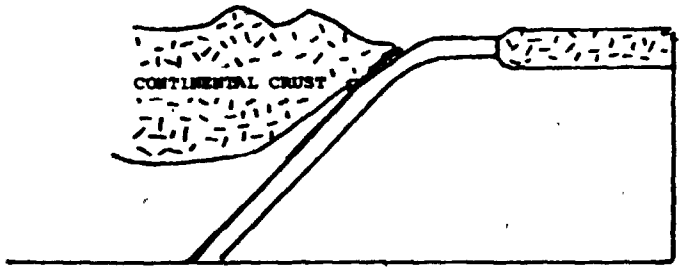

(2) Crustal loading and thickening.

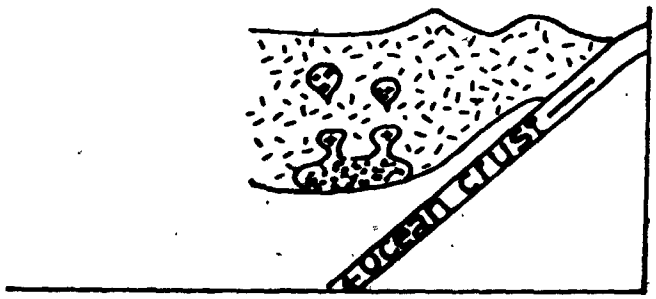

(3) Due to heavy loading and high heat flow, the base of the crust starts to melt to give granodiorite and later on the granodiorite will differentiate to give monzogranite.

Fig.12. A schematic model illustrating the tectonic environment and the generation of the different magmas.

third stage, as a result of crustal loading and the high heat flow produced below, the base of the crust will partially melt producing the granodiorite and finally its differentiate, the monzogranite. These magmas will collect and start to ascend according to the model presented in Fig. 107. During their ascent these magmas were partially contaminated. Similar conclusions have been reached by Nasseef and Gass (1976) for the origin of At Taif granites. The repetition of similar sequences across the entire Arabian Shield and the presence of three parallel N-S suture zones established by Bakor and Gass (1976) suggest a process involving minor continental collisions involving closely spaced ocean basins.

CHAPTER 8

CONCLUSIONS

(1) Al Hadah igneous complex was formed during the Pan African orogenic events (600 my) and consist of a series of andesitic to rhyolitic dikes and intrusive rocks, which are emplaced in an amphibolite and quartz feldspathic gneiss country rock. The intrusive rocks appear in the following sequence (from oldest to youngest): gabbro → diorite → granodiorite → biotite monzogranite.

(2) Chemically, these plutonic rocks were divided into two groups: the dioritic group (diorite + gabbro) and the granitic group (granodiorite + biotite monzogranite). These two groups showed different differentiation trends thus indicating separate magma sources.

(3) The Al Hadah plutonic rocks are comparable to those of Sierra Nevada and some of the continental subduction environments.

(4) The study of the metasomatic alterations, which involved the replacement of plagioclase by epidotes, indicates that large amounts of oxidizing surface waters set into convective motion by the cooling plutons below were involved. The alteration process was approximately volume for volume. Ca and Fe were the main elements added whereas Na and K were depleted from the system.

(5) The plutonic rocks of Al Hadah seem to fit to a modern subduction model with the exception that the scale of both plates and motion were smaller than that of present time. The magma source involves both partial melting of the subducted material and partial melting of the continental crust.

APPENDICES

APPENDIX A - METHODS

APPENDIX B - ELEMENT ABUNDANCE S

APPENDIX C - MICROPROBE ANALYSES

APPENDIX A

METHODS

(1) SAMPLING:

Fresh samples were collected mainly along the highway cutting across the different rock units of Al Madah area. Samples were collected at an interval of about 100 m.

(2) ANALYTICAL METHODS:

(a) X-Ray Fluorescence Analyses:

Fresh representative samples (about 500 g) from the different rock types were selected, crushed and grounded in a Bleuler Mill to about 200 mesh. Powder and fused pellets were made from the powder of each sample according to the method of Norrish and Chappell (1967) and Norrish and Hutton (1969), respectively.

All analyses were done on a Philips PW1450 AHP automated X-ray fluorescence spectrometer. The standards used were: FS72 (for all major elements except Na), GA (for Na), AGV-1 (for Ba, Sr and Zr), GSP (for Rb) and VSN (for Y). The chemical composition (in wt% oxides) was determined from the absorption values using a computer program obtained from Dr H. Hunter, University of Western Ontario. The analyses are accurate to within 1% of the amount present for major elements except Na and to within 10% of the amount present for trace elements and Na.

(b) Determination of FeO:

FeO was volumetrically determined by the method of Wilson (1955). The analyses are accurate within 5% of the amount of FeO present.

(c) Determination of Volatiles:

The total volatiles for all the chemically analysed samples were determined using the method of loss on ignition (LOI). About 2 g of sample was weighed, ignited at about 1100°C in a porcelain crucible, cooled in a dessicater and reweighed. The weight loss was assumed to be due to volatile loss (= LOI).

APPENDIX B

ELEMENT ABUNDANCES

TABLE 1B

Gabbroic Rocks

Sample #	2	55	57	60	74	24
SiO_2	47.8	49.7	49.4	50.2	47.1	49.8
TiO_2	1.3	1.22	1.4	1.4	0.7	1.2
Al_2O_3	17.1	17.2	15.2	15.3	17.6	16.3
Fe_2O_3	10.1	4.8	5.1	5.0	3.7	3.5
FeO		5.0	5.1	7.6	5.4	5.1
MnO	0.2	0.2	0.2	0.2	0.1	0.1
MgO	8.1	6.3	7.5	7.5	11.9	7.2
CaO	9.6	9.5	9.6	9.7	9.3	8.8
Na_2O	2.8	2.6	3.2	2.3	1.6	2.5
K_2O	0.4	0.8	0.8	0.4	0.3	1.7
P_2O_5	0.2	0.2	0.4	0.3	0.1	0.8
L.O.I	1.22	1.79	1.79		2.9	2.91
Total	98.88	99.19	99.69	99.9	100.70	99.91
		NORMS (CIPW)				
Q		3.57	-	4.02	-	1.53
Or		4.85	5.0	2.37	1.81	10.35
ab		22.56	27.3	19.47	13.84	21.80
an		33.74	25.4	30.26	40.85	29.10
di		10.56	16.5	12.87	4.50	8.43
hy		14.77	14.7	20.38	26.27	19.28
ol		-	-	-	5.65	-
mt		7.14	7.5	7.25	5.48	5.23
il		2.34	2.7	2.66	1.36	2.35
ap		0.50	0.9	0.71	0.24	1.95
		TRACE-ELEMENTS (PPM)				
Cr	195	203	108	210	118	105
Ba	236	311	470	155	387	809
Ni	91	16	24	38	244	13
Pb	11	-	9	-	-	nd
Zr	109	78	103	57	47	92
Y	nd	24	nd	37	18	11
Sr	-	477	-	414	306	1453
Rb	6	14	15	7	5	37

TABLE 1B (cont.)

Sample #	56	53	64	31	41	111
SiO_2	49.0	48.7	45.8	47.8	49.8	48.0
TiO_2	1.57	2.0	1.74	1.14	0.54	0.4
Al_2O_3	14.70	14.8	16.4	16.5	17.3	17.0
Fe_2O_3	3.3	3.9	4.7	3.4	2.3	2.2
FeO	7.1	9.0	9.7	7.4	5.4	5.2
MnO	0.2	0.2	0.2	0.2	0.1	0.1
MgO	7.5	6.0	7.5	7.4	10.5	10.7
CaO	10.5	10.2	7.5	7.9	8.5	8.5
Na_2O	2.3	3.0	2.9	3.2	2.5	2.0
K_2O	0.8	0.4	0.5	0.9	0.8	1.0
P_2O_5	0.2	0.5	0.4	0.1	0.1	0.1
L.O.I	1.87	0.89	0.84	2.1	2.6	3.14
Total	98.77	99.59	98.14	98.01	100.4	98.34
			NORMS (CIPW)			
Q	0.62	0.2	-	-	-	-
or	4.88	2.6	3.0	5.3	4.7	6.0
ab	20.07	25.4	25.1	28.6	21.2	17.8
an	28.29	26.2	31.2	29.2	34.7	36.4
di	19.51	18.3	3.3	8.8	6.5	5.8
hy	18.66	16.8	16.6	9.7	21.0	21.7
ol	-	-	9.3	10.8	7.3	7.8
mt	4.94	5.7	7.0	5.2	3.5	3.4
il	2.55	3.8	3.4	2.3	1.1	0.9
ap	0.49	1.1	1.1	0.3	0.2	0.2
			TRACE-ELEMENTS (PPM)			
Cr	-	68	86	14	91	70
Ba	290	283	302	247	278	200
Ni	37	16	96	94	283	304
Pb	9	-	-	-	11	-
Zr	88	85	116	82	55	53
Y	nd	nd	nd	nd	nd	nd
Sr	404	-	437	-	-	-
Rb	17	6	7	22	17	22

TABLE 2 B

DIORITES

Sample #	77	69	70	87	80	65
SiO_2	50.9	51.2	51.6	52.6	53.2	53.5
TiO_2	0.7	1.85	1.4	1.7	1.2	0.85
Al_2O_3	17.5	15.8	19.4	16.4	16.4	20.6
Fe_2O_3	3.1	3.6	4.3	3.5	4.4	3.3
FeO	4.6	8.3	6.5	8.6	6.5	4.9
MnO	0.2	0.2	0.1	0.2	0.2	0.1
MgO	8.2	4.2	2.5	4.3	4.7	4.6
CaO	10.4	7.6	5.5	7.8	7.4	8.7
Na_2O	2.3	4.7	4.5	2.8	3.5	3.3
K_2O	0.8	0.8	1.2	0.5	0.5	1.2
P_2O_5	0.2	0.4	0.5	0.4	0.2	0.3
L.O.I	1.67	1.2	1.88	0.77	0.5	-
Total	100.37	99.9	99.38	99.57	98.7	101.3
			NORMS (CIPW)			
Q	1.80	-	4.00	8.90	7.40	3.00
or	4.80	5.0	7.27	3.00	3.01	7.00
ab	19.71	40.6	39.0	24.00	30.15	27.71
an	35.52	19.7	24.66	31.07	28.06	37.30
di	12.31	13.0	-	4.53	6.51	2.69
hy	19.50	6.2	12.8	19.18	15.57	15.27
ol	-	5.7	-	-	-	-
mt	4.55	5.3	6.39	5.13	6.50	4.70
il	1.35	3.6	2.73	3.27	2.32	1.60
ap	0.48	1.1	1.21	0.96	0.48	0.77
cor	-	-	1.93	-	-	-
			TRACE ELEMENTS (PPM)			
Cr	464	11	61	30	61	99
Ba	429	737	604	252	535	389
Ni	81	21	14	5	39	28
Pb	nd	10	nd	nd	nd	nd
Zr	54	-	860	61	230	74
Y	20	nd	46	34	60	21
Sr	709	-	1094	436	345	778
Rb	10	17	24	7	5	31

TABLE 2B (cont.)

Sample #	89	84	96	33	103	115	26
SiO_2	54.1	54.9	55.0	51.4	51.7	52.7	56.3
TiO_2	1.1	1.28	0.83	1.91	1.06	0.7	0.7
Al_2O_3	15.7	15.6	18.1	14.6	18.9	17.4	16.5
Fe_2O_3	2.5	2.8	5.0	6.7	5.1	2.6	3.2
FeO	6.2	6.6	7.5	6.0	6.0	5.1	3.4
MnO	0.2	0.2	0.2	0.2	0.2	0.1	0.2
MgO	5.6	5.2	1.4	4.5	6.8	7.0	4.3
CaO	8.9	7.3	6.1	7.9	9.2	8.5	7.3
Na_2O	3.2	4.6	3.8	3.3	2.9	3.3	4.2
K_2O	0.5	0.6	1.1	0.9	0.5	1.4	1.1
P_2O_5	0.2	0.2	0.4	0.3	0.2	-	0.1
L.O.I	0.72	0.42	0.65	0.66	1.3	1.9	1.45
Total	98.92	99.72	100.05	98.36	100.8	100.7	98.75
			NORMS (CIPW)				
Q	6.5	2.4	10.75	7.9	3.84	-	7.7
or	3.3	3.4	6.54	5.7	2.94	8.1	6.7
ab	27.8	39.5	32.34	28.8	24.41	28.3	36.3
an	27.2	20.3	27.88	22.5	31.45	29.1	23.8
di	13.6	12.4	-	12.5	10.15	10.9	9.9
hy	15.5	15.1	12.25	8.2	17.50	17.8	9.1
ol	-	-	-	-	-	0.6	-
mt	3.7	4.1	7.30	10.0	7.36	3.8	4.8
il	2.1	2.5	1.53	3.7	1.90	1.3	1.3
ap	0.4	0.4	0.95	0.7	0.47	-	0.3
			TRACE ELEMENTS (PPM)				
Cr	33	65	30	-	127	95	14
Ba	358	570	611	369	198	465	511
Ni	21	72	9	11	41	127	6
Pb	8	8	nd	8	nd	8	8
Zr	100	203	178	116	62	69	191
Y	nd	nd	48	nd	23	nd	nd
Sr	432	340	495	478	377	466	482
Rb	8	5	17	17	8	22	19

TABLE 2B (cont.)

Sample #	35	116	48	32	107	114
SiO_2	57.9	58.5	61.3	61.5	62.3	64.5
TiO_2	1.0	0.31	0.74	1.06	0.6	0.72
Al_2O_3	16.7	17.5	14.8	15.1	15.3	15.7
Fe_2O_3	3.5	1.9	1.6	2.1	2.7	1.9
FeO	5.1	3.6	4.5	4.6	3.9	3.6
MnO	0.1	0.1	0.1	0.1	0.1	0.1
MgO	2.4	4.5	3.3	2.2	4.2	1.6
CaO	5.6	7.6	5.2	4.9	5.8	3.5
Na_2O	3.8	3.6	3.8	4.5	3.2	4.9
K_2O	1.6	1.1	2.2	2.0	1.6	1.1
P_2O_5	0.4	0.1	0.1	0.4	0.1	0.1
L.O.I	0.34	0.77	0.57	0.46	0.3	1.44
Total	98.44	99.57	98.17	98.96	100.1	99.14
			NORMS (CIPW)			
Q	13.50	10.50	14.7	14.1	18.50	20.80
Or	9.64	6.58	13.1	11.8	9.47	6.65
ab	32.77	30.83	32.6	39.0	27.13	42.44
an	24.24	28.68	17.4	15.3	22.70	17.11
di	1.18	7.12	6.9	6.0	4.41	-
hy	10.61	12.70	11.2	7.9	12.50	8.24
ol	-	-	-	-	-	-
mt	5.17	2.79	2.4	3.1	3.92	2.82
il	1.94	0.58	1.4	2.1	1.14	1.36
ap	0.97	0.24	0.3	0.9	0.24	0.24
			TRACE ELEMENTS (PPM)			
Cr	38	123	54	11	177	41
Ba	708	483	555	853	395	1620
Ni	21	34	41	-	57	25
Pb	nd	nd	8	9	nd	nd
Zr	219	153	115	212	112	570
Y	52	49	nd	nd	29	64
Sr	505	418	303	-	238	363
Rb	26	15	46	32	37	10

TABLE 3B

GRANODIORITE

	104	127	129	50	130	132	133	134	22*	29*	34*	37*	39*	100*
SiO_2	71.6	73.0	72.3	70.2	70.6	71.8	73.4	71.5	74.4	72.4	70.4	72.6	71.8	69.0
TiO_2	0.27	0.22	0.27	0.31	0.31	0.26	0.21	0.20	0.2	0.3	0.3	0.25	0.30	0.37
Al_2O_3	13.3	13.1	14.4	13.8	13.4	13.6	13.0	13.4	12.9	12.9	13.5	13.1	13.1	14.2
Fe_2O_3	0.7	0.6	3.0	1.2	1.0	0.9	0.6	0.4	2.3	0.6	0.8	0.6	0.8	0.9
FeO	1.4	1.2		1.7	1.9	1.4	1.2	1.4		1.4	1.8	1.4	1.8	2.1
MnO	0.1	0.1	0.1	0.1	0.1	0.1	0.1	0.1	0.1	0.0	0.1	0.1	0.1	0.1
MgO	0.7	0.5	0.4	0.7	0.8	0.7	0.5	0.6	0.2	0.6	0.8	0.6	0.6	0.6
CaO	1.9	1.2	1.9	2.0	2.0	1.8	1.5	1.6	1.2	1.3	2.0	1.7	1.7	2.2
Na_2O	4.4	5.1	3.7	5.0	5.2	5.4	5.4	5.7	3.7	4.9	4.8	4.7	5.4	4.9
K_2O	4.0	3.9	3.5	3.4	3.3	3.3	3.5	3.5	3.8	4.1	3.6	3.9	3.2	2.7
P_2O_5	0.1	0.1	0.1	0.1	0.1	0.1	0.0	0.1	0.1	0.1	0.1	0.0	0.1	0.1
Total	98.5	99.0	99.7	98.5	98.7	99.4	99.4	98.5	98.9	98.6	98.2	99.0	98.9	97.2
NORMS (CIPW)														
Q	26.2	25.7		23.5	23.1	23.8	25.8	22.0		25.6	23.7	26.2	24.3	24.4
or	24.1	23.5		20.5	19.7	19.7	20.5	20.9		24.5	21.7	23.5	19.2	16.5
ab	37.9	43.4		42.7	44.6	45.8	45.8	49.0		41.8	41.8	40.2	46.0	42.9
an	4.8	1.3		5.3	3.6	3.2	1.3	0.7		1.2	4.5	3.1	2.1	0.8
di	3.5	3.8		3.6	5.0	4.7	4.9	5.9		4.1	4.0	4.3	5.2	1.8
hy	1.7	0.8		1.9	1.8	1.0	0.4	0.5		1.3	2.4	1.2	1.3	3.3
ol	-	-		-	-	-	-	-		-	-	-	-	-
mt	1.1	0.9		1.8	1.4	1.2	0.9	0.6		0.9	1.1	0.9	1.2	1.4
il	0.5	0.4		0.6	0.6	0.5	0.4	0.4		0.5	0.6	0.5	0.6	0.7
ap	0.2	0.1		0.1	0.2	0.1	0.1	0.1		0.1	0.2	0.1	0.1	0.2
TRACE ELEMENTS (PPM)														
Cr	1.0	-	28	-	-	1.0	-	-	35	-	1.0	1.0	-	-
Ba	1012	1535	838	853	855	1006	878	824	815	1037	947	984	1103	1522
Ni	7	6	25	5	7	5	10	-	12	-	6	10	5	8
Pb	14	19	nd	15	18	20	18	9	nd	13	19	18	19	15
Sr	155	156	167	162	161	160	144	138	182	302	167	153	172	181
Y	41	36	39	42	40	36	43	nd	45	nd	39	30	nd	-
Sr	258	259	258	247	249	272	232	215	144	159	269	243	226	307
Rb	61	76	64	60	66	72	85	73	75	46	77	90	67	47
Nb	10	6	11	7	9	11	9	nd	11	nd	-	7	nd	7

* small separate granodioritic intrusions.

TABLE 4B

BIOTITE-MONZOGRANITE

Sample #	13	14	15	16	93	94
SiO_2	71.3	73.0	71.4	72.2	71.5	71.6
TiO_2	0.2	0.3	0.20	0.3	0.23	0.31
Al_2O_3	13.1	13.1	13.6	13.3	13.6	13.2
Fe_2O_3	0.8	1.0	0.8	1.0	0.8	0.9
FeO	0.9	1.1	0.9	0.9	0.9	1.4
MnO	0.0	0.1	0.0	0.0	0.0	0.1
MgO	0.6	0.6	0.7	0.6	0.6	0.7
CaO	1.3	1.6	1.5	1.5	1.6	1.7
Na_2O	4.3	4.7	4.5	4.3	4.3	4.5
K_2O	4.6	4.2	4.8	4.7	4.3	4.1
P_2O_5	0.0	0.0	0.0	0.1	0.1	0.1
L.O.I	0.80	0.33	0.62	0.43	0.83	0.36
Total	98.00	100.03	99.12	99.33	98.73	98.96
NORMS (CIPW)						
Q	26.4	26.4	23.3	26.3	26.6	25.8
or	27.7	24.9	29.0	28.1	26.2	24.5
ab	37.3	39.7	38.9	36.6	37.1	38.8
an	3.3	2.5	2.6	3.3	5.1	3.8
di	2.8	4.1	4.0	3.0	1.8	3.5
hy	1.0	0.4	0.6	0.7	1.4	1.6
ol	-	-	-	-	-	-
mt	1.2	1.4	1.1	1.4	1.2	1.3
il	0.4	0.5	0.4	0.5	0.5	0.6
ap	0.1	0.1	-	0.1	0.2	0.1
TRACE ELEMENTS (PPM)						
Cr	8.0	5.0	3.0	3.0	4.0	2.0
Ba	605.0	503.0	594.0	628.0	639.0	544.0
Ni	7.0	13.0	7.0	9.0	6.0	12.0
Pb	18.0	17.0	18.0	21.0	21.0	26.0
Zr	171.0	215.0	180.0	210.0	195.0	224.0
Y	26.0	31.0	27.0	29.0	22.0	39.0
Sr	190.0	194.0	213.0	214.0	242.0	211.0
Rb	178.0	160.0	185.0	177.0	160.0	147.0
Nb	27.0	27.0	21.0	26.0	22.0	28.0

TABLE 5B

FELSIC DIKES

Sample #	26	64	129	50	84
SiO_2	76.12	75.95	74.31	75.44	74.8
TiO_2	.08	.04	.05	.05	.1
Al_2O_3	12.79	12.55	12.24	12.06	13.7
Fe_2O_3(T)	0.62	.46	.46	.75	1.1
MnO	.02	.02	.03	.01	.02
MgO	.41	.33	.38	.27	.2
CaO	.31	.61	.66	1.07	4.9
Na_2O	4.75	5.37	5.75	7.77	5.7
K_2O	4.28	4.39	3.70	1.73	.1
P_2O_5	-	.01	-	-	.02
Total	99.38	99.73	97.56	99.15	98.62
		TRACE ELEMENTS (PPM)			
Cr	-	-	-	-	32
Ba	238	156	70	430	1005
Ni	3	-	5	-	20
Pb	18	22	20	10	-
Zr	89	56	60	53	52
Sr	76	57	37	202	169
Rb	129	93	184	20	2

TABLE 6 B

MAFIC DIKES

Sample #	123	101	103	58	114
SiO_2	45.88	46.05	52.36	50.77	47.70
TiO_2	1.43	1.76	2.53	1.16	1.50
Al_2O_3	16.38	15.23	13.13	14.48	15.93
Fe_2O_3 FeO	12.12	12.06	13.82	9.26	13.60
MnO	0.27	0.21	0.26	0.16	0.25
MgO	7.60	7.77	3.52	7.80	6.46
CaO	8.39	10.58	7.24	8.32	8.38
Na_2O	2.86	2.52	3.59	4.54	3.06
K_2O	0.36	0.49	0.96	0.33	0.86
P_2O_5	0.11	0.22	0.75	0.27	0.34
Total	95.40	96.89	98.16	97.09	98.08
TRACE ELEMENTS (PPM)					
Cr	49	125	21	586	57
Ba	181	222	474	264	403
Ni	91	75	-	175	10
Pb	18	16	-	16	-
Zr	77	97	152	92	54
Sr	328	321	334	-	344
Rb	13	9	17	3	9

APPENDIX C

MICROPROBE ANALYSES

TABLE 1C

PLAGIOCLASES

Sample #26 (Unepidotized diorite)

	1	2	3	4	5	6	7
SiO_2	59.70	59.89	60.21	61.53	61.16	60.57	59.46
Al_2O_3	25.02	25.51	25.90	24.65	25.22	25.33	25.86
FeO	.22	.11	.70	.14	.11	.17	.12
MgO	.03	.02	.02	.04	.02	.05	.07
CaO	6.73	6.66	7.26	6.43	6.75	7.08	7.24
Na_2O	7.46	7.66	7.46	7.47	7.57	7.76	6.91
K_2O	.16	.12	.21	.17	.15	.13	.12
BaO	.11	.12	.10	.16	.14	.14	.16
Total	99.32	99.97	101.76	100.43	100.98	101.09	99.78
	Number of Ions on the Basis of 32 (0)						
Si	10.708	10.668	10.588	10.875	10.771	10.689	10.607
Al	5.288	5.355	5.367	5.134	5.234	5.267	5.436
Fe	.033	.016	.103	.021	.016	.025	.018
Mg	.008	.005	.005	.011	.005	.013	.019
Na	2.594	2.645	2.543	2.560	2.585	2.655	2.390
Ca	1.293	1.271	1.368	1.218	1.274	1.339	1.384
K	.037	.027	.047	.038	.034	.029	.027
O	32.000	32.000	32.000	32.000	32.000	32.000	32.000
Ab	66.11	67.08	64.25	67.08	66.41	66.00	62.88
An	33.89	32.92	35.75	32.92	33.59	34.00	37.12

Analyst R.L. Barnett

TABLE 1C (cont.)

Sample #54 (Unepidotized)

	1	2	3	4	5
SiO_2	61.80	58.24	58.49	56.74	60.24
Al_2O_3	22.46	27.34	26.37	27.16	25.09
FeO	.08	.10	.14	.09	.13
MgO	.04	-	.04	.07	.02
CaO	4.88	8.42	7.14	9.05	5.95
Na_2O	8.66	6.81	7.61	6.34	8.36
K_2O	.19	.04	.08	.03	.06
BaO	.05	.13	.16	.16	.09
Total	98.11	100.95	99.87	99.48	99.85
Number of Ions on the Basis of 32 (O)					
Si	11.161	10.322	10.464	10.227	10.739
Al	4.780	5.710	5.559	5.768	5.271
Fe	.012	.015	.021	.014	.091
Mg	.011	-	.011	.019	.005
Na	3.032	2.340	2.640	2.215	2.890
Ca	.944	1.599	1.369	1.748	1.136
K	.044	.009	.018	.007	.014
O	32.000	32.000	32.000	32.000	32.000
Ab	75.42	59.27	65.56	55.81	71.53
An	24.58	40.73	34.44	44.19	28.47

Analyst R.L. Barnett

TABLE 1C (cont.)

Sample #62 (Partially epidotized diorite)

	1	2	3	4	5
SiO_2	68.39	68.53	67.30	69.20	69.67
Al_2O_3	20.03	20.04	20.15	19.87	20.02
FeO	.02	.01	-	-	-
MgO	.01	-	.02	.01	-
CaO	.04	.13	.10	.10	.07
Na_2O	9.72	11.73	11.54	10.66	10.81
K_2O	.01	.04	.03	.03	.03
BaO	.07	.04	.09	.07	.05
Total	98.22	100.48	99.14	99.87	100.60
	Number of Ions on the Basis of 32 (0)				
Si	12.044	11.916	11.811	12.034	12.031
Al	4.157	4.106	4.185	4.072	4.074
Fe	.003	.001	-	-	-
Mg	.003	-	.005	.003	-
Na	3.319	3.954	3.943	3.594	3.619
Ca	.008	.024	.019	.019	.013
K	.002	.009	.007	.007	.007
O	32.000	32.000	32.000	32.000	32.000
Ab	99.71	99.17	99.35	99.30	99.46
An	.29	.83	.65	.70	.54

Analyst R.L. Barnett

TABLE 1C (cont.)

Sample #56

	1	2	3
SiO_2	67.58	69.17	68.87
Al_2O_3	19.53	20.11	19.79
FeO	.03	.02	.10
MgO	-	-	.01
CaO	.50	.57	.34
Na_2O	11.23	11.39	11.52
K_2O	-	-	-
BaO	.02	-	-
Total	98.87	101.26	100.63
Si	11.939	11.928	11.954
Al	4.066	4.086	4.048
Fe	.004	.003	.015
Mg	-	-	.003
Na	3.846	3.808	3.877
Ca	.095	.105	.063
K	-	-	-
O	32.000	32.000	32.000
Ab	97.60	97.31	98.40
An	2.40	2.69	1.60

Analyst R.L. Barnett

TABLE 2C

AMPHIBOLES

Sample #26 (Unepidotized diorite)

	1	2	3	4
SiO_2	52.43	49.29	47.72	47.67
TiO_2	.20	1.41	1.51	1.22
Al_2O_3	2.44	5.86	6.99	6.72
FeO	15.36	15.41	16.40	16.26
MnO	.56	.45	.50	.50
MgO	14.86	13.11	12.02	12.09
CaO	12.02	11.12	11.42	11.77
Na_2O	.48	1.23	1.33	1.16
K_2O	.07	.32	.43	.46
H_2O	2.06	2.05	2.03	2.02
Total	100.48	100.25	100.35	99.97

Number of Ions on the Basis of 24 (O, OH)

Si	7.616	7.212	7.039	7.061
Al	.384 (8.000)	.788 (8.000)	.961 (8.000)	.939 (8.000)
Al	.034	.223	.254	.234
Ti	.022	.155	.167	.136
Fe	1.866 (5.208)	1.886 (5.179)	2.023 (5.150)	2.014 (5.138)
Mg	3.217	2.859	2.643	2.691
Mn	.069	.056	.062	.036
Na	.135	.349	.380	.333
Ca	1.871 (2.019)	1.743 (2.152)	1.805 (2.266)	1.868 (2.288)
K	.031	.060	.081	.087
H	2.000	2.000	2.000	2.000
O	24.000	24.000	24.000	24.000

Analyst R.L. Barnett

TABLE 2C (cont.)

Sample #54 (Unepidotized diorite)

	1	2	Center	Edge	3
SiO_2	47.64	45.13	45.26	43.61	47.75
TiO_2	1.32	2.36	.34	.19	.59
Al_2O_3	6.24	8.20	10.36	11.52	7.62
FeO	16.51	17.76	18.27	18.81	17.65
MnO	.37	.43	.41	.37	.43
MgO	12.55	11.11	10.48	9.74	11.84
CaO	11.24	10.88	11.70	10.83	10.77
Na_2O	.77	1.23	1.34	1.50	.93
K_2O	.38	.51	.29	.39	.23
H_2O	2.01	2.00	2.01	1.98	2.02
Total	99.03	99.61	100.46	98.94	99.83

Number of Ions on the Basis of 24 (O, OH)

Si	7.108	6.773	6.733	6.610	7.075
Al	.892 8.000	1.227 8.000	1.267 8.000	1.390 8.000	.925 8.000
Al	.205	.223	.549	.668	.406
Ti	.148	.266	.038	.022	.066
Fe	2.060	2.229	2.273	2.384	2.187
Mg	2.791 5.251	2.485 5.258	2.324 5.235	2.200 5.322	2.615 5.328
Mn	.047	.055	.052	.048	.054
Na	.223	.358	.358	.441	.267
Ca	1.797	1.749	1.865	1.759	1.710
K	.072 2.092	.098 2.205	.055 2.306	.075 2.275	.043 2.020
H	2.000	2.000	2.000	2.000	2.000
O	24.000	24.000	24.000	24.000	24.000

Analyst R.L. Barnett

TABLE 2C (cont.)

Sample #65 (Unepidotized diorite)

	1	2	3
SiO_2	50.32	50.63	49.55
TiO_2	.74	.53	1.35
Al_2O_3	5.96	6.34	6.80
FeO	13.02	12.54	13.77
MnO	.38	.27	.39
MgO	14.99	15.55	14.48
CaO	11.74	11.91	11.71
Na_2O	.74	.62	.93
K_2O	.21	.29	.40
H_2O	2.07	2.09	2.09
Total	100.17	100.77	101.47
Number of Ions on the Basis of 24 (O, OH)			
Si	7.266	7.246	7.110
Al	.734 (8.000)	.754 (8.000)	.890 (8.000)
Al	.281	.315	.260
Ti	.080	.057	.146
Fe	1.572 (5.206)	1.501 (5.223)	1.652 (5.202)
Mg	3.226	3.317	3.097
Mn	.046	.033	.047
Na	.207	.172	.259
Ca	1.816 (2.062)	1.826 (2.051)	1.800 (2.132)
K	.039	.053	.073
H	2.000	2.000	2.000
O	24.000	24.000	24.000

Analyst R.L. Barnett

TABLE 2C (cont.)

Sample #62 (Partially epidotized diorite)

	1	2	3	4
SiO_2	49.89	49.66	54.78	54.92
TiO_2	1.12	.85	.61	.08
Al_2O_3	6.19	6.36	1.34	.57
FeO	12.73	11.37	13.84	13.55
MnO	.45	.34	.58	.32
MgO	15.02	15.70	15.11	15.86
CaO	11.48	11.66	12.93	12.79
Na_2O	.91	.86	.31	.11
K_2O	.33	.25	.02	.02
H_2O	2.07	2.06	2.10	2.08
Total	100.19	99.11	101.62	100.30

Number of Ions on the Basis of 24 (O, OH)

Si	$7.207_{8.000}$	$7.205_{8.000}$	$7.797_{8.000}$	$7.893_{8.000}$
Al	.793	.795	.203	.097
Al	.261	.292	.021	-
Ti	.122	.093	.065	.009
Fe	$1.538^{5.209}$	$1.380^{5.201}$	$1.647^{5.009}$	$1.629^{5.074}$
Mg	3.234	3.395	3.205	3.397
Mn	.055	.042	.070	.039
Na	.255	.242	.086	.031
Ca	$1.777^{2.092}$	$1.813^{2.101}$	$1.972^{2.061}$	$1.969^{2.004}$
K	.061	.046	.004	.004
H	2.000	2.000	2.000	2.000
O	24.000	24.000	24.000	24.000

Analyst R.L. Barnett

TABLE 2C (cont.)

Sample f56 (Partially epidotized diorite)

	1	2	3	4	5
SiO_2	50.80	46.61	46.65	54.72	54.02
TiO_2	.11	1.55	.46	-	.12
Al_2O_3	2.81	6.28	7.64	1.64	1.57
FeO	17.94	18.44	18.93	14.06	15.30
MnO	.32	.40	.36	-	.36
MgO	13.82	11.86	10.60	14.94	14.73
CaO	11.86	10.45	11.36	12.49	11.64
Na_2O	.44	.94	.96	.21	.33
K_2O	.07	.51	.31	-	.01
H_2O	2.03	1.99	1.99	2.08	2.07
Total					

Number of Ions on the Basis of 24 (O, OH)

Si	7.500	7.989	7.029	8.000	7.025	8.000	7.868	8.000	7.822	8.000
Al	.489		.971		.975		.132		.178	
Al	-		.144		.381		.146		.089	
Ti	.012		.176		.052		-		.013	
Fe	2.215	5.308	2.325	5.362	2.384	5.242	1.691	5.039	1.853	5.178
Mg	3.041		2.666		2.379		3.202		3.179	
Mn	.040		.051		.046		-		.044	
Na	.126		.275		.280		.059		.093	
Ca	1.876	2.015	1.688	2.061	1.833	2.173	1.924	1.983	1.806	1.900
K	.013		.098		.060		-		.002	
H	2.000		2.000		2.000		2.000		2.000	
O	24.000		24.000		24.000		24.000		24.000	

Analyst R.L. Barnett

TABLE 2C (cont.)

	Sample #58A (Epidotized Diorite)		Sample #68 (Epidotized Diorite)			
	1	2	1	2	3	4
SiO_2	47.42	55.89	47.13	48.10	54.91	55.54
TiO_2	1.14	.01	1.73	1.26	.07	.08
Al_2O_3	7.14	.52	7.42	6.71	1.11	.55
FeO	13.13	9.17	14.30	15.07	14.24	14.86
MnO	.46	.27	.54	.48	.25	.26
MgO	13.64	18.65	12.97	12.61	13.74	14.26
CaO	11.91	12.86	11.37	11.86	12.57	12.26
Na_2O	1.39	.07	1.19	1.05	.28	.07
K_2O	.36	.01	.57	.52	.06	-
H_2O	2.02	2.11	2.02	2.03	2.06	2.07
Total	98.61	99.56	99.24	99.69	99.29	99.95
	Number of Ions on the Basis of 24 (O, OH)					
Si	7.027	7.922	6.974	7.100	7.980	8.020
Al	.973 8.000	.078 8.000	1.026 8.000	.900 8.000	.020 8.000	8.020
Al	.273	.009	.268	.267	.170	.094
Ti	.127	.001	.193	.140	.008	.009
Fe	1.627	1.087	1.770	1.860	1.731	1.795
Mg	3.013 5.098	3.940 5.070	2.861 5.159	2.774 5.101	2.976 4.915	3.069 4.998
Mn	.058	.032	.068	.060	.031	.032
Na	.399	.019	.341	.300	.079	.020
Ca	1.891 2.358	.953 .974	1.803 2.252	1.876 2.274	1.957 2.047	1.897 1.916
K	.068	.002	.108	.098	.011	-
H	2.000	2.000	2.000	2.000	2.000	2.000
O	24.000	24.000	24.000	24.000	24.000	24.000

Analyst R.L. Barnett

TABLE 2C (cont.)

Sample #5 (Epidotized Diorite)

	1	2	3	4	5	6
SiO_2	48.30	48.60	48.85	47.80	55.98	54.70
TiO_2	1.59	1.89	1.69	2.06	.14	.13
Al_2O_3	6.87	7.51	6.76	7.98	.88	1.41
FeO	14.20	13.32	13.54	13.73	8.99	10.32
MnO	.36	.36	.32	.41	.31	.36
MgO	14.23	14.24	14.74	13.58	9.07	17.23
CaO	11.21	11.74	11.39	11.20	12.52	12.76
Na_2O	1.05	.91	1.07	1.13	.18	.26
K_2O	.51	.64	.60	.61	.01	.04
H_2O	2.06	2.08	2.08	2.06	2.13	2.09
Total	100.38	101.29	101.04	100.56	100.21	99.30

Number of Ions on the Basis of 24 (O, OH)

Si	7.036	8.000	6.992	8.000	7.049	8.000	6.942	8.000	7.874	8.000	7.831	8.000
Al	.964		1.008		.951		1.058		.126		.169	
Al	.216		.266		.199		.308		.019		.069	
Ti	.174		.204		.183		.225		.015		.014	
Fe	1.730	5.254	1.603	5.170	1.634	5.226	1.668	5.191	1.057	5.126	1.236	5.039
Mg	3.090		3.054		3.170		2.940		3.998		3.677	
Mn	.044		.044		.039		.050		.037		.044	
Na	.300		.297		.254		.299		.049		.072	
Ca	1.876	2.247	1.750	2.141	1.810	2.181	1.761	2.171	1.887	1.938	1.957	2.037
K	.098		.095		.117		.110		.002		.007	
H	2.000		2.000		2.000		2.000		2.000		2.000	
O	24.000		24.000		24.000		24.000		24.000		24.000	

Analyst R.L. Barnett

TABLE 3C

EPIDOTES

Sample #62 (From partially epidotized diorite)

	Core	Rim	Core	Rim
SiO_2	37.47	37.26	38.60	37.45
TiO_2	.04	.06	.08	.05
Al_2O_3	21.79	22.11	24.20	21.31
Fe_2O_3	14.79	14.25	11.54	15.28
MnO	.07	.08	.06	.05
MgO	.04	.05	.05	.09
CaO	23.20	22.65	22.88	23.50
Na_2O	.01	.07	-	.07
H_2O	1.86	1.85	1.89	1.86
Total	99.26	98.31	99.30	99.59

Number of Ions on the Basis of 13 (O, OH)

Si	3.018	3.020	3.058	3.015
Al	- 3.018	- 3.020	- 3.058	- 3.015
Al	2.068	2.112	2.259	2.022
Fe^{+3}	.896 2.964	.869 2.981	.688 2.947	.926 2.947
Mn	.005	.005	.004	.003
Mg	.005 2.014	.006 1.982	.006 1.957	.011 2.044
Ti	.002	.004	.005	.003
Ca	2.002	1.967	1.942	2.027
H	1.000	1.000	1.000	1.000
O	13.000	13.000	13.000	13.000

Analyst R.L. Barnett

TABLE 3C (cont.)

Sample #56 (From partially epidotized diorite)

	Rim	Core	Rim	Intermed.	Core
SiO_2	38.36	38.64	37.61	37.06	38.61
TiO_2	.05	.02	.06	.03	.01
Al_2O_3	21.47	25.30	23.67	26.17	25.54
Fe_2O_3	13.46	6.50	12.17	11.01	5.63
MnO	-	.11	.10	.06	.17
MgO	.02	.03	.02	.02	-
CaO	23.33	23.59	23.73	23.44	23.94
Na_2O	2.44	-	-	-	-
H_2O	1.86	1.85	1.87	1.89	1.85
Total	98.55	96.04	99.23	99.68	95.74

Number of Ions on the Basis of 13 (O, OH)

Si	3.094	3.120	3.005	2.931	3.123
Al	- 3.094	- 3.120	- 3.005	.069 3.000	- 3.123
Al	2.041	2.407	2.229	2.370	2.434
Fe^{+3}	.817 2.858	.395 2.802	.732 2.960	.655 3.025	.343 2.777
Mn	-	.008	.007	.004	.012
Mg	.002	.004	.002	.002	-
Ti	.003 2.022	.001 2.053	.004 2.044	.002 1.994	.001 2.086
Ca	2.016	2.041	2.032	1.986	2.074
H	1.000	1.000	1.000	1.000	1.000
O	13.000	13.000	13.000	13.000	13.000

Analyst R.L. Barnett

TABLE 3C(cont.)

Sample #68 (From wholly epidotized diorite)

	Core	Rim	Core	Interm.	Rim
SiO_2	37.39	37.97	38.07	38.08	37.37
TiO_2	.11	.07	.18	.13	10.35
Al_2O_3	21.20	21.51	22.52	20.65	16.56
Fe_2O_3	16.17	15.67	14.23	16.83	11.91
MnO	.32	.09	.13	.23	.07
MgO	.04	.05	.05	.06	.04
CaO	22.15	23.15	22.73	22.53	22.42
Na_2O	-	.11	-	.09	.01
H_2O	1.85	1.88	1.88	1.87	1.88
Total	100.23	100.39	99.79	100.38	100.60

Number of Ions on the Basis of 13 (O, OH)

Si	3.020	3.028	3.034	3.046	2.972
Al	- 3.020	- 3.028	- 3.034	- 3.046	- 2.972
Al	2.018	2.022	2.115	1.946	1.524
Fe^{+3}	.983 3.001	.940 2.962	.853 2.969	1.013 2.959	.713 2.237
Mn	.022	.006	.009	.016	.005
Mg	.005	.006	.006	.007	.005
Ti	.007 1.950	.004 1.995	.011 1.967	.008 1.961	.619 2.539
Ca	1.917	1.978	1.941	1.931	1.910
H	1.000	1.000	1.000	1.000	1.000
O	13.000	13.000	13.000	13.000	13.000

Analyst R.L. Barnett

TABLE 3C (cont.)

Sample #58A (From wholly epidotized diorite)

	1	2	Core	Rim
SiO_2	37.54	37.95	37.52	36.89
TiO_2	.02	.03	.13	.08
Al_2O_3	21.54	21.92	22.85	20.89
Fe_2O_3	15.58	15.03	13.69	17.27
MnO	.07	.06	.05	.14
MgO	.01	.04	-	-
CaO	23.01	22.63	23.19	22.09
Na_2O	.16	-	-	-
H_2O	1.86	1.87	1.87	1.85
Total	99.63	99.53	99.30	99.85

Number of Ions on the Basis of 13 (O, OH)

Si	3.017	3.040	3.007	2.992
Al	- 3.017	- 3.040	- 3.007	.008 3.000
Al	2.040	2.069	2.158	1.989
Fe^{+3}	.942 2.983	.906 2.975	.826 2.983	1.054 3.043
Mn	.005	.004	.003	.010
Mg	.001	.005	-	-
Ti	.001 1.989	.002 1.953	.008 2.002	.005 1.934
Ca	1.982	1.942	1.991	1.920
H	1.000	1.000	1.000	1.000
O	13.000	13.000	13.000	13.000

Analyst R.L. Barnett

TABLE 3C(cont.)

Sample #5 (From wholly epidotized diorite)

	1	2	Core	Rim
SiO_2	37.80	38.34	38.46	37.98
TiO_2	.22	.23	.21	.09
Al_2O_3	25.61	25.73	23.08	22.15
Fe_2O_3	9.88	9.11	12.55	14.96
MnO	.53	.21	.05	.09
MgO	.05	.07	.04	.02
CaO	22.86	23.55	23.78	23.48
Na_2O	.04	.13	.04	.08
H_2O	1.89	1.90	1.89	1.89
Total	98.84	99.14	100.06	100.66

Number of Ions on the Basis of 13 (O, OH)

Si	3.002	3.027	3.047	3.016
Al	3.002	3.027	3.047	3.016
Al	2.397	2.394	2.154	2.073
	2.987	2.935	2.903	2.967
Fe^{+3}	.590	.541	.748	.894
Mn	.036	.014	.003	.006
Mg	.006	.008	.005	.002
	2.000	2.028	2.039	2.012
Ti	.013	.014	.013	.005
Ca	1.945	1.992	2.018	1.998
H	1.000	1.000	1.000	1.000
O	13.000	13.000	13.000	13.000

Analyst R.L. Barnett

REFERENCES

Aguirre, L., R. Charrier, J. Davidson, A. Mpodozis, S. Rivano, R. Thiele, E. Tidy, M. Vergara and J.C. Vicente, 1974: Andean magmatism: its paleogeographic and structural setting in the central part (30°-35°) of the Southern Andes; Pacific Geology, v. 8, pp. 1-38.

Al Shanti, A.M.S., and A.H.G. Mitchell, 1976: Late Precambrian subduction and collision in the Al Amar-Idsas region, Arabian Shield, Kingdom of Saudi Arabia; Tectonophysics, 30, T41-T43.

Armstrong, R.L., Taubeneck, W.H., Hales, P.O., 1977: Rb-Sr and K-Ar geochronometry of Mesozoic granitic rocks and their Sr isotopic composition, Oregon, Washington and Idaho; Geol. Soc. America Bull., v. 88, pp. 397-411.

Ashworth, J.R., 1972: Myrmekites of exsolution and replacement origins; Geol. Mag. 109, pp. 45-62.

_____, 1973: Myrmekites of exsolution and replacement origins - a discussion. Geol. Mag. 110, pp. 77-80.

Bakor, A.R., I.G. Gass, and C.R. Neary, 1976: Jabal Al Wask, Northwest Saudi Arabia: An eocambrian back-arc ophiolite; Earth Planetary Sci. Letters 30, pp.1-9.

Barazangi, M., Isacks, B., Oliver, J., 1970: Propagation of Seismic Waves through and beneath the lithosphere that descends under the Tonga Island arc; Geol. Soc. America Bull., v. 2, pp. 488-489.

Barker, D.S., 1970: Compositions of granophyre, myrmekite, and graphic granite; Geol. Soc. America Bull. v. 81., pp. 3339-3350.

Barth, T.F.W., 1962: Theoretical Petrology; Wiley, New York.

Bateman, P.C., 1961: Granitic formations in the East-Central Sierra Nevada, near Bishop, Calif.; Geol. Soc. America Bull., v. 72, pp. 1521-1538.

_____, L.D, Clark, N.K. Huber, J.C. Moore and C.D. Rinehart, 1963: The Sierra Nevada Batholith; U.S.G.S. Prof. Paper 414-D.

_____, and J.P. Eaton, 1967: Sierra Nevada Batholith; Science, v. 158, pp. 1407-1417.

_____, and F.C.W. Dodge, 1970: Variations of major chemical constituents across the Central Sierra Nevada Batholith; Geol. Soc. America Bull., v. 81, pp. 409-420.

_____, and C. Wahrhaftig, 1966: Geology of the Sierra Nevada, in Baily, E.H., ed., Geology of northern California: California Div. Mines and Geology Bull. 190, pp. 107-172.

Beck, F., 1908: Uber Myrmekit; Min. Pet. Mitt., 27, pp. 377-390.

Bowen, N.L., 1928: The evolution of Ignean Rocks; Princeton University Press, Princeton, N.J.

Brooks, C., D.E. James, and S.R. Hart, 1976: Ancient Lithosphere - Its role in young continental volcanism; Science, v. 193, pp. 1086-1094.

Brothers, R.N. and E.J. Searle, 1970: The Geology of Raoul Islands, Kermadec Group, Southwest Pacific, Bull. Volc., v. 34, pp. 7-37.

Brown, G.C., 1977: Mantle origin of Cordilleran granites, Nature, v. 265, pp. 21-24.

_____, and W.S. Fyfe, 1970: The production of granitic melt during ultrametamorphism; Cont. to Min. and Petrol., v. 28, pp. 31-318.

_____, 1973: Evolution of granite magmas at destruction plate margins; Nature Physical Science, v. 241, pp. 26-28.

Brown, G.F., and R.O. Jackson, 1960: The Arabian Shield; Proc. Internat. Geol. Cong., 21st., Copenhagen, Rept. pt. 9, pp. 69-77.

_____, R.G. Bouge and W.H. Maclean, 1962: Geologic map of the southern Hijaz quadrangle, Kingdom of Saudi Arabia; U.S. Geol. Surv. Misc. Geol. Inv. Map I-210A.

Brown, G.F. and R.G. Coleman, 1972: The tectonic framework of the Arabian peninsula; Internat. Geol. Cong., 24th, Montreal, Rept. 3, pp. 300-305.

Buddington, A.F., 1959: Granite emplacement with special reference to North America; Geol. Soc. America Bull., v. 70, pp. 671-747.

Carmichael, I.S.E., and Nicholls, 1967: Iron-Titanium oxides and oxygen fugacities in volcanic rocks; Jour. Geophys. Res., v. 72, pp. 4665-4687.

_____, F.J. Turner and J. Verhoogen, 1974: Igneous Petrology; McGraw Hill, New York, 739 p.

Chappell, B.W. and A.J.R. White, 1974: Two contrasting granite types; Pacific Geology, v. 8, pp. 173-174.

Christie, O.H.J., 1959: Note on the equilibrium between plagiocase and epidote: Norsk Geol. Tidsker 39, pp. 268-271.

Clayton, R.N., L.J.P. Muffler, and D.E. White, 1968: Oxygen isotope study of calcite and silicates of the River Ranch No. 1 Well, Salton Sea geothermal field, California; Am. Jour. Sci., v. 266, pp. 968-979.

Cobbing, E.J. and W.S. Pitcher, 1972: The coastal batholith of Central Peru; Jour. Geol. Soc. London, v. 128, pp. 421-460.

Compston, W., I. McDougall, and K.S. Heier, 1968: Geochemical comparison of the Mesozoic basaltic rocks of Antarctica, South Africa, South America and Tasmania; Geochim. Cosmochim. Acta, v. 32, pp. 129-149.

Dal Piaz, G.V. and De Vecchi, G., 1963: Il chimismo di alcune rocce rapppresentative del plutone granodioritico della Cordillera Blanca (Peru); La Ricerca Scinetifica, series 2, part II-A, v. 3, n. 5, pp. 573-578.

Daly, R.A., 1933: Igneous Rocks and the Depths of the Earth; McGraw-Hill, New York. 598 p.

Deer, W.A., R.A. Howie, and J. Zussman, 1966: An introduction to the rock forming minerals; Longman, 528 pp.

Dickinson, W.R., 1962: petrogenic significance of geosynclinal andesitic volcanism along the Pacific margin of North America; Geol. Soc. America Bull., v. 73, pp. 1241-1256.

_____, 1968: Circum-Pacific andesite types; Jour. Geophys. Res., v. 73, pp. 2261-2269.

_____, 1969: Evolution of calc-alkaline rocks in the geosynclinal system of California and Oregon; Oreg. Dept. Geol. Miner. Ind. Bull. 65, pp. 151-156.

_____, 1970: Relation of andesite, granites and derivative sandstone to arch-trench tectonics; Rev. Geophys., v. 8, pp. 813-860.

_____, and T. Hatherton, 1967: Andesitic volcanism and seismicity around the Pacific; Science, v. 157, pp. 801-803.

Doe, B.R., R.I. Tilling, C.E. Hedge and M.R. Kleppes, 1968: Lead and strontium isotype studies of the Boulder batholith, southwest Montana; Econ. Geol., v. 63, pp. 884-906.

Elder, J., 1976: The Bowels of the Earth; Oxford University Press, London, 222 pp.

Elsasser, W.M., 1963: Early history of the earth. In Earth Science and Meteoritics (Ed. J. Geiss and E.D. Goldberg); North-Holland Publ. Co. Amsterdam, p. 1.

Erikson, E.H., Jr., 1969: Petrology of the Composite Snoqualamie batholith, central Cascade Mountains, Washington; Geol. Soc. America Bull., v. 80, pp. 2213-2236.

Erlank, A.J., and P.K. Hofmeyr, 1966: K/Rb and K/Cs ratios in Karro dolerite from South Africa; Jour. Geophys. Res., v. 71, pp. 5439-5445.

Eugster, H.P., 1959: Reduction and oxidation in metamorphism; in Abelson, P.H., ed. Researches in geochemistry, v. 1., New York, McGraw Hill Co., 739 p.

———————, and D.R. Wones, 1962: Stability relations of the ferruginous biotite, annite; Jour. Petrol., v. 3, pp. 82-115.

Ewart, A., and J.J. Stipp, 1968: Petrogenesis of the volcanic rocks of the Central North Island, New Zealand, as indicated by a study of Sr^{87}/Sr^{86} ratios, and Sr, Rb, K, U and Th abundances; Geochim. Cosmochim. Acta, v. 32, pp. 699-735.

_____, W.B. Bryan, and J.B. Gill, 1973: Mineralogy and geochemistry of the younger volcanic islands of Tonga, S.W. Pacific; Jour. of Petrol., v. 14, pp. 429-465.

_____, 1976: A petrological study of the Younger Tongan andesites and dacites, and the olivine tholeiites of Niua Fo'ou Islands, S.W. Pacific; Cont. Min. Petrol., v. 58, pp. 1-21.

Fleck, R.J., R.G. Coleman, H.R. Cornwall, W.R. Greenwood, D.G. Hadley, W.C. Prinz, J.C. Ratte and D.L. Schmidt, 1976: Potassium-argon geochronology of the Arabian Shield, Kingdom of Saudi Arabia; Geol. Soc. America Bull., v. 87, pp. 9-21.

Fyfe, W.S., 1970: Some thoughts on granitic magmas, in G. Newall and N. Rast (eds.), "Mechanics of Igneous Intrusion" Gallery Press, Liverpool, pp. 201-216.

_____, 1973: The generation of batholiths; Tectonophysics, v. 17, pp. 273-283.

Fyfe, W.S., 1977: Cordilleran granites: Production of geosphere mixing. Comment on G.C. Brown's "Mantle Origin of Cordilleran granite"; Nature (in press).

_____, and G.C. Brown, 1972: Granites past and present; Jour. of Earth Sci., v. 8, pp. 249-260.

_____, and A.R. McBirney, 1975: Subduction and the structure of andesitic volcanic belts; Am. Journ. of Sci., v. 275A, pp. 285-297.

Garson, M.S., and I.M. Shalaby, 1974: Precambrian-Lower Paleozoic plate tectonics and metallogenesis in the Red Sea region; In Symposium on Metallogy and Plate Tectonics, GAC/MAC meeting 1974, St. John's Newfoundland.

Gass, I.G. and C.R. Neary, 1976: The granitic association of the N.E. Sudan; Geol. Surv. America Bull., v. 87, pp. 1501-

Gavelin, S., 1952: Lime metasomatism and metamorphic differentiation in the Adak Area; Sveriges Geol. Undersok., Ser. C, no. 521, 52 p.

Gill, J., 1970: Geochemistry of Vitu Leon, Fiji and its evolution as an island arc; Contr. Min. Pet., v. 27, pp. 179-203.

Gilluly, J., 1948: Origin of granite; Geol. Soc. America Mem. 28, 139 p.

Gilluly, J., 1965: Volcanism, tectonism and plutonism in the western United States; Geol. Soc. America, Spec. Pap. 80, 69 p.

_____, 1969: Oceanic sediment volumes and continental drift; Science, v. 166, pp. 992-994.

_____, 1971: Plate tectonics and magmatic evolution; Geol. Soc. America Bull., v. 82, pp. 2383-2396.

Goldschmidt, V.M., 1954: Geochemistry; Clarendon Press, Oxford.

Goldsmith, R., 1971: Mineral resources of the southern Hijaz quadrangle, Kingdom of Saudi Arabia, Saudi Arabian Dir. Gen. Mineral Resources Bull. n. 5, 62 pp.

Gorshkov, G.S., 1965: On the relations of volcanism and the upper mantle; Bull. volcancl., v. 23, pp. 159-168.

Green, T.H., 1976: Experimental generation of cordierite- or garnet-bearing granitic liquids from a pelitic composition; Geology, v. 4, pp. 85-88.

Green, T.H., and A.E. Ringwood, 1968: Genesis of the calc-alkaline igneous rock suite; Cont. Min. Petrol., v. 18, pp. 105-162.

_____, 1969: High pressure experimental studies on the origin of andesites, in "Proceedings of the Andesite Conference," A.R. McBirney, editor; Oregon Dept. Geol. Mineral Ind. Bull., v. 65, pp. 21-32.

Greenwood, W.R., and G.F. Brown, 1973: Petrology and chemical analysis of selected plutonic rocks from the Arabian Shield, Kingdom of Saudi Arabia; Saudi Arabian Dir. Gen. Mineral Resources Bull. no. 9, pp. 9.

_____, D.G. Hadley and D.C. Schmidt, 1973: Tectonstratigraphic subdivision of Precambrian rocks in the southern part of the Arabian Shield (abs.); Geol. Soc. America Abstracts with Programs, v. 5, p. 643.

_____, D.G. Hadley, R.E. Anderson, R.J. Fleck and D.L. Schmidt, 1975: Late Proterozoic cratonization in Southwestern Saudi Arabia; U.S. Geol. Survey Saudi Arabian Project Report 196, 22 pp.

Gresense, R.L., 1967: Composition-volume relationships of metasomatism; Chem. Geol., v. 2, pp. 47-65.

Gunn, B.M., 1965: K/Rb and K/Ba ratios in Antarctic and New Zealand tholeiites and alkali basalts; Jour. Geophys. Res., v. 70, pp. 6241-6247.

_____, 1966: Modal and element variation in Antarctic tholeiites; Geochim. Cosmochim. Acta, v. 30, pp. 881-920.

_____, 1974: Systematic petrochemical differences in Andesite suites; Bull. Volcon., V. 38, pp. 481-490

Hadley, D.G. and W.R. Greenwood (in press): Graded layering in Al-Hadah Pluton, At Taif region, Kingdom of Saudi Arabia; U.S. Geol. Survey, Saudi Arabian Project Report.

Hamilton, W., 1969: The volcanic central Andes - A modern model for the Cretaceous batholiths and tectonics of Western North America; Proc. Andesite Conf., Oregon Dept. Geol. and Min. Ind. Bull., v. 65, pp. 175-184.

Hamilton, W. , 1969: Mesozoic California and the underflow of Pacific mantle; Geol. Soc. America Bull., v. 80, pp. 2409-2430.

Hamilton, W., and W.B. Myers, 1967: The nature of batholiths, U.S. Geol. Survey, Prof. Pap. 554-C, 30 p.

Hargraves, R.B., 1976: Precambrian geologic history: continents grew and emerged from beneath the primordial sea; Science, v. 193, pp. 363-371.

Harpum, J.R., 1964: Formation of epidote in Tanganyika; Geol. Soc. America Bull., v. 65, pp. 1075-1092.

Hedge, C.E., 1969: The sources of calc-alkaline magmas as indicated by Sr isotopes [abs.], in McBirney, A.R., ed., Proceedings of the andesite conference; Oregon Dept. Geol. Min. Ind. Bull., v. 65, p. 191.

Hedge, C.E., and Z.E. Peterman, 1969: Sr^{87}/Sr^{86} of circum-Pacific andesites; Geol. Soc. America, Abs. with Programs for 1969, pt. 7, p. 96.

Hietanen, A., 1973: Origin of andesitic and granitic magmas in the northern Sierra Nevada, Calif., Geol. Soc. America Bull., v. 84, pp. 2111-2118.

Hubbard, F.H., 1966: Myrmekite in charnockite from southwest Nigeria; Am. Mineral., v. 51, pp. 762-773.

Hyndman, D.W., 1969: The development of granitic plutons through anatexis in the northern Cordillera, British Columbia; Geol. Soc. America Spec. Paper 121, 146 pp.

_____, 1972: Petrology of Igneous and Metamorphic Rocks; International Series in the Earth and Planetary Sciences, New York; McGraw-Hill, 533 p.

Irvine, T.N. and W.R.A. Baragar, 1971: A guide to the chemical classification of the common volcanic rocks; Canadian Jour. of Earth Sci., v. 8, pp. 523-548.

Isacks, B., J. Oliver, and L.R. Sykes, 1969: Focal mechanisms of deep and shallow earthquakes in the Tonga-Kermadec region and the tectonics of island arcs; Geol. Soc. America Bull., v. 80, pp. 1443-1469.

Jakes, P., and J. Gill, 1970: Rare earth elements and the island arc tholeiitic series; Earth Planet. Sci. Letters, 9, pp. 17-28.

Jakes, P., and A.J.R. White, 1970: K/Rb ratios of rocks from island arcs; Geochim. Cosmochim. Acta 34, pp. 849-856.

_____, 1971: Composition of island arcs and continental growth; Earth Planet. Sci. Letters, 12, pp. 224-230.

_____, 1972: Major and trace element abundances in volcanic rocks of orogenic areas; Geol. Soc. America Bull., v. 83, pp. 29-40.

Kerrich, R., W.S. Fyfe and I. Allison, 1977: Iron reduction around gold-quartz veins, Yellowknife District, NW Territories, Canada; Econ. Geology, v. 72, pp. 657-663.

Kröner, A., 1976: Proterozoic crustal evolution in parts of southern Africa and evidence for extensive sialic crust since the end of the Archean; Phil. Trans. Roy. Soc. London, Ser. A280, pp. 541-553.

Kuno, H., 1950: Petrology of Hakone Volcano and the adjacent areas, Japan; Geol. Soc. America Bull. v. 61, pp. 957-1020.

_____, 1966: Lateral variation of basalt magma across continental margins and island arcs; Can. Geol. Surv. Paper 66-15, pp. 317-336.

_____, 1968: Origin of andesite and its bearing on the island arc structure; Bull. Volc., v. 32, pp. 141-176.

Kuno, H., 1969: Andesite in time and space, in "Proceedings of the Andesite Conference," A.R. McBirney (ed.); Oregon Dept. Geol. Min. Ind. Bull., v. 65, pp. 13-20.

Kushiro, I., 1969: Effects of water on the composition of magmas formed in the upper mantle [abs.]; EOS, Trans. AGU, 50, p. 355.

_____, H.S. Yoder, Jr., and M. Nishikawa, 1968: Effect of water on the melting of enstatite; Geol. Soc. America Bull., v. 79, pp. 1685-1692.

Marmo, V., 1967: On the granite problem; Earth Sci. Rev., 3, pp. 7-29.

Marzouki, F. and W.S. Fyfe, 1977: Pan-African plates: additional evidence from igneous events in Saudi Arabia; Cont. Min. Petrol., v, 60, pp. 219-224.

Mason, B., 1966: Principles of Geochemistry; 34rd ed., Toppan Co. Ltd., Japan, 329 pp.

McBirney, A.R., 1969a: Compositional variations in Cenozoic calc-alkaline suites of Central America, in "Proceedings of the Andesite Conference', A.R. McBirney, (ed.), Oregon Dept. Geol. Min. Ind. Bull., v. 65, pp. 185-189.

_____, 1969b: Andesitic and rhyolitic volcanism of orogenic belts; in "The Earth's Crust and Upper Mantle", P.J. Hart, (ed.), Am. Geophys. Union, Geophys. Monograph 13.

Mehnert, K.R., 1959: Der Gegenwartige stand des granit-problems; Fortschr. Mineral., v. 37, pp. 117-206.

_____, 1969: Migmatites and the origin of granitic rocks; Elsevier, Amsterdam, 403 pp.

Mitchell, A.H., and H.G. Reading, 1971: Evolution of island arcs; Jour. Geology, v. 79, pp. 253-284.

Moore, J.G., and J.P. Lockwood, 1973: origin of comb layering and obicular structure, Sierra Nevada batholith, Calif.; Geol. Soc. America Bull., v. 84, pp. 1-20.

Morgan, W.R., 1966: A note on the Petrology of some lava types from east New Guinea; Jour. Geol. Soc. Australia, v. 13, pp. 583-591.

Nasseef, A.O., 1971: The geology of the northeastern At-Taif area, Saudi Arabia; Unpubl. Ph.D. Thesis, University of Leeds.

_____, and I.G. Gass (in press): Granites and related rocks of the Taif area, Western Saudi Arabia;

Neary, C.R., 1974: Chromitiferous ultrabasic rocks in the northern Hijaz of Saudi Arabia; Unpub. Ph.D. Thesis, University of Leeds.

Nockolds, S.R. and R. Allen, 1953: The geochemistry of some igneous rock series; Geochim. Cosmochim. Acta, v. 4, pp. 105-142.

Norrish, K. and B.W. Chappell, 1967: X-ray fluorescence spectrography, In: Zussman, J., Ed., Physical Methods in Determinative Mineralogy, Academic Press, London, pp. 161-214.

_____, and J.T. Hutton, 1969: An accurate X-ray spectrographic method for the ananlysis of a wide range of geological samples; Geochim. et Cosmochim. Acta, v. 33, pp. 431-453.

O'Connor, J.T., 1966: A classification for quartz-rich igneous rocks based on feldspar ratios; in Geological Surv. Res. 1965; U.S. Geol. Surv. Prof. Paper 525-B, pp. 79-84.

Osborn, E.F., 1959: Role of oxygen pressure in the crystallization and differentiation of basaltic magma; Am. Jour. Sci. v. 257, pp. 609-647.

_____, 1962: Reaction series for subalkaline igneous rocks based on different oxygen pressure conditions; Am. Mineral., v. 47, pp. 211-226.

_____, 1969a: Experimental aspects of calc-alkaline differentiation in "Proceedings of the Andesite Conference", A.R. McBirney, (ed.); Oregon Dept. Geol. Min. Ind. Bull., v. 65, pp. 33-42.

Peacock, M.A., 1931: Classification of igneous rocks; Jour. Geology, v. 39, pp. 54-67.

Perrin, R., 1954: Granitization, metamorphism and volcanism; Am. Jour. Sci., v. 252, pp. 449-465.

_____, 1956: Granite again; Am. Jour. Sci., v. 254, pp. 1-18.

_____, and M. Roubault, 1949: On the granite probl[illegible] Jour. Geol., v. 57, pp. 357-379.

Peterman, Z.E., I.S.E. Carmichael and A.L. Smith, 1970: Sr^{87}/Sr^{86} ratios of quaternary lavas of the Cascade Range, northern Calif.; Geol. Soc. America Bull., v. 81, pp. 311-318.

Phillips, E.R., 1964: Myrmekite and albite in some granites of the New England batholith, New South Wales; Jour. Geol. Soc. Australia 11, pp. 49-60.

_____, 1974: Myrmekite - one hundred years later; Lithos, v. 7, pp. 181-193.

_____, and D.M. Ransom, 1968: The proportionality of quartz in myrmekite; Am. Mineral., v. 53, pp. 1411-1413.

Pitcher, W.S., 1972: The coast batholith of Peru: Some structural aspects; Internat. Geol. Cong. (24th), Canada, Soc. 2, pp. 156-163.

_____, 1974: The Mesozoic and Cenozoic batholiths of Peru; Pacific Geology, v. 8, pp. 51-62.

Pitcher, W.S., and A.R. Berger, 1972: The geology of Donegal: A study of granite emplacement and unroofing, L.U. De Sitter, editor, New York, John Wiley and Sons, Inc., 435 p.

Presnall, D.C., and B.C. Bateman, 1973: Fusion relations in the system $NaAlSi_3O_8$-$CaAl_2Si_2O_8$-$KAlSi_3O_8$-SiO_2-H_2O and generation of granitic magmas in the Sierra Nevada batholith; Geol. Soc. America Bull., v. 84, pp. 3181-3202.

Press, F., 1969: The suboceanic mantle; Science, v. 165, pp. 174-176.

Raguin, E., 1965: Geology of granite (translated from French by E.H. Kranck and P.R. Eakins), Interscience (Wiley) New York.

Ramberg, H., 1967: Gravity, deformation and earth's crust as studied by centrifuged models; New York, Academic Press, 214 p.

_____, 1970: Model studies in relation to intrusion of plutonic bodies, in "Mechanism of Igneous Intrusion" ed., Newall, G. and Rast, N., Geol. Jour. Spec. Issue 2, Liverpool, Gallery Press, pp. 261-286.

Read, H.H., 1957: The granite controversy - Geological Addresses Illustrating the Evolution of a Disputant; Hertsford, Thomas Murby, 430 p.

Rexworthy, S.R., 1972: Geology and mineralogy of the Precambrian metavolcanic and intrusions of the Jabal Samran-Wadi Hanara region - southern Hijaz, Saudi Arabia; Unpubl. Thesis, London University.

Ringwood, A.E., 1974: The petrological evolution of island arc systems; Jour. Geol. Soc. London, v. 130, pp. 183-204.

Roddick, J.A., and W.W. Hutchinson, 1974: Setting of the coast plutonic complex, British Columbia; Pacific Geology, v. 8, pp. 91-108.

Schmidt, D.L., D.G. Hadley, W.R. Greenwood, R.G. Coleman, L. Gonzalez, and G.F. Brown, 1973: Stratigraphy and tectonism of the southern part of the Precambrian Shield of Saudi Arabia; Saudi Arabian Dir. Gen. Mineral Resources Bull. n. 8, 13 p.

Shackleton, R.M. 1976: Pan-African structures; Phil. Trans. Roy. Soc. London, Ser. A 280, pp. 491-497.

Sibley, D.F. and T.A. Vogel, 1976: Chemical mass balance of the Earth's crust: The calcium dilemma and the role of pelagic sediments; Science, v. 192, pp. 551-553.

Siegers, A., H. Pichler and W. Zeil, 1969: Trace element abundances in the "andesite" formation of northern Chile; Geochim. et Cosmochim Acta, v. 33, pp. 882-887.

Simpson, E.S.W., 1954: On the graphical representation of differentiation trends in igneous rocks; Geol. Mag., v. 91, pp. 238-244.

Souther, J.G., 1970: Volcanism and its relationship to recent crustal movements in the Canadian cordillera; Can. Jour. Earth Sci., v. 7, pp. 553-568.

Spooner, E.T.C., 1976: Isotopic evidence for the origin of mineralisation associated with the Troodos Massif; Institution of Mining and Metallurgy, London (in press).

Stanton, R.L., and J.D. Bell, 1969: Volcanic and associated rocks of the New Georgia Group, British Islands Protectorate; Overseas Geol. Min. Res. (G.B.), v. 10, pp. 113-145.

Steiner, A., 1958: Petrogenetic implications of the 1954 Ngauruhoe lava and its xenoliths; New Zealand Jour. Geol. Geophys., v. 1, pp. 325-363.

Streckeisen, A.L., 1967: Classification and nomenclature of igneous rocks (final report of inquiry); N. Jahrb. Mineral. Abh., v. 107, pp. 144-240.

Sykes, L.R., 1969: The new global tectonics (abs.); EOS, Trans. AGU, 50, p. 113.

Taylor, H.P., Jr., 1968: The oxygen isotope geochemistry of igneous rocks; Contr. Mineral. Petrol., v. 19, pp. 1-17.

_____, 1974: The application of oxygen and hydrogen isotope studies to problems of hydrothermal alteration and ore deposition; Econ. Geol., v. 69, pp. 843-883.

4 4

OF/DE

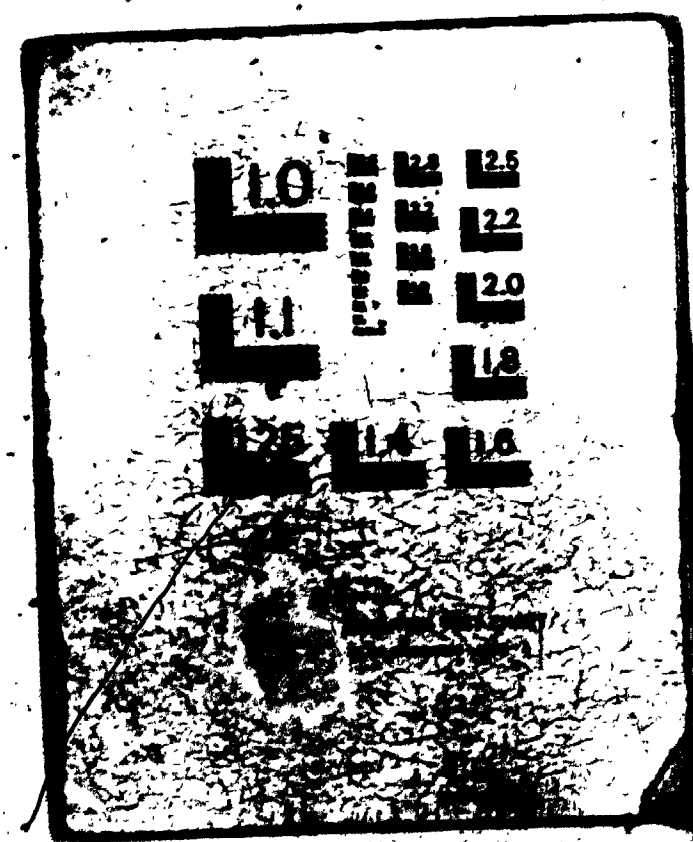

Taylor, S.R., 1964: Trace element abundances and the chondritic earth model; Geochim. Cosmochim Acta, v. 28, p. 1989.

_____ , 1966: The application of trace element data to problems in petrology; Physics and Chemistry of the Earth, v. 6, pp. 133-213.

_____ , 1969: Trace element chemistry of andesites and associated calc-alkaline rocks; Oregon Geol. Dept. Mineral. Ind. Bull., v. 65, pp. 43-63.

_____ , C.H. Emeleus, and C.S. Exley, 1956: Some anomalous K/Rb ratios in igneous rocks and their petrological significance; Geochim. Cosmochim. Acta, v. 10, 224-229.

_____ , and A.J.R. White, 1966: Trace-element abundances in andesite; Bull. Volcanol., v. 29, pp. 174-194.

Tilley, C.E., 1950: Some aspects of magmatic evolution; Geol. Soc. London Quartz Jour., v. 106, pp. 37-61.

Tilling, R.I., and D. Gottfired, 1969: Distribution of thorium, uranium and potassium in igneous rocks of Boulder Batholith region, Montana; U.S. Geol. Surv. Prof. Paper 641-E.

Thorpe, R.J., P.J. Potts, and P.W. Francies, 1976: Rare earth data and petrogenesis of andesite from the north Chilean Andes; Cont. Mineral. Petrol., v. 54, pp. 65-78.

Thorton, C.P., and O.F. Tuttle, 1960: Chemistry of igneous rocks, part 1: Differentiation Index; Am. Jour. Sci., v. 258, pp. 664-684.

U.S. Geological Survey and Arabian American Oil Co., 1963: Geologic map of the Arabian peninsula; U.S. Geol. Surv. Misc. Geol. Inv. Map I-270A.

Wager, L.R., and W.A. Deer, 1939: Geological investigations in the east Greenland, Part III: The petrology of the Skaergaard Intrusion, Kangerdlugssuag, East Greenland; Medd. Greenland, v. 105, pp. 1-352.

Waters, A.C., 1955a: Volcanic rocks and the tectonic cycle; Geol. Soc. America Spec. Papers 62, pp. 703-722.

Williams, H., F.J. Turner, and C.M. Gilbert, 1954: Petrography - An Introduction to the Study of Rocks in Thin Section; San Francisco, W.H. Freeman and Co., 406 p.

Wilson, A.D., 1955: A new method for the determination of ferrous iron in rocks and minerals; Great Britain Geol. Survey Bull., v. 9, pp. 56-58.

Winkler, H.G.F., 1967: Petrogenesis of metamorphic rocks, 2nd ed.; Springer-Verlag, New York, 237 pp.

Wollenberg, H.A. and A.R. Smith, 1970: Radiogenic heat production in prebatholithic rocks of the central Sierra Nevada; Jour. Geophys. Res., v. 75, pp. 431-438.

Wyllie, P.J., 1977: Crustal annatexis - An experimental review; Tectonophysics (in press).

_____, W.L. Huang, C.R. Stern, and S. Maaløe, 1976: Granitic magmas - possible and impossible sources, water contents and crystallization sequences, Can. Jour. Earth Sci., v. 13, pp. 1007-1019.

Yoder, H.S., Jr., 1968: Experimental studies bearing on the origin of anorthosite; N.Y. State Mus. Sci. Serv. Mem. 18, pp. 13-22.